Formulation of natural cyclodecapeptides for surface sterilisation

by

Christopher Borrageiro

BScHons (Biochemistry)

March 2023

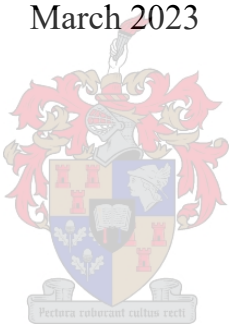

Thesis presented for the degree

Master of Science (Biochemistry)

in the
Faculty of Science
at the
University of Stellenbosch

Supervisor: Prof. Marina Rautenbach

Co-supervisor: Dr. Wilma van Rensburg

Department of Biochemistry

University of Stellenbosch

Declaration

By submitting this thesis electronically, I ***Christopher Borrageiro*** declare that the entirety of the work contained therein is my own, original work, that I am the sole author thereof (save to the content explicitly stated otherwise), that reproduction and publication thereof by Stellenbosch University will not infringe any third-party rights and that I have not previously in its entirety or in part submitted it for obtaining any qualification.

Christopher Borrageiro
Name

March 2023
Date

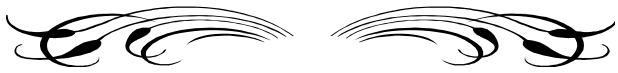

Faith is taking the first step

Even when you don't see the whole staircase.

Martin Luther King

Summary

Bacterial adhesion to various surfaces leading to the formation of biofilms is a serious and persisting problem within various industries. Furthermore, once a biofilm reaches its mature stage, its mechanical removal becomes increasingly difficult and expensive. Additional to this rising problem of antimicrobial-resistant bacteria, another concern is further resistance development towards current surface sterilisation and disinfection techniques. This would be attributed to the chemical agents influencing the bacterial microenvironment imposing a constant selective pressure on the bacteria that promote tolerance over time. To circumvent this, the research focus has moved into developing active surfaces/ materials by changing the approach to preventing bacterial adhesion or killing bacterial cells that are in contact with the surface. Antimicrobial peptides (AMPs) serve as viable active ingredients due to their broad range and rapid activity towards various targets, limited resistance and multiple modes of action. A group of AMPs of interest are the tyrocidines (Trcs) and analogues, produced by the soil bacterium *Brevibacillus parabrevis*. The Trcs have a broad range of activity towards bacterial targets, various pathogenic and filamentous fungi, the malaria parasite *Plasmodium falciparum* and viruses. Recently it was shown that the peptides have potent activity in various materials and on surfaces towards the bacterial pathogens *Listeria monocytogenes* and *Staphylococcus aureus*.

As limited solvent and formulation studies have been performed on the Trcs for the treatment of materials and depositing on surfaces, the aim of this study was to investigate the influence varying formulations had on the Trcs surface activity and biophysical properties. The Trcs were formulated in six different solvents, acetonitrile (ACN), ethanol (EtOH), methanol (MeOH), iso-propanol (IPA), tertiary butanol (TBA) and propylene glycol (PG) with or without co-formulants namely zinc chloride ($ZnCl_2$), calcium chloride ($CaCl_2$) or glycerol (Glr). Activity studies revealed that when assessed against both targets (*L. monocytogenes* and *S. aureus*), EtOH serves as the best general solvent to be used without any additives compared to the other five solvents, The addition of 1% Glr resulted in significantly lower activity in the more polar solvents when compared to formulation in the solvents alone. However, PG and TBA in formulation with 1% Glr + 100 µM $CaCl_2$ were found to be the two best formulations. TBA as solvent was marginally better due to a higher activity against both targets compared to PG.

How the surface activity links with the formulant influence on the peptide structure was assessed by mapping activity versus chemical parameters, changes in Trp environments (fluorescence) and

oligomerisation (ion mobility mass spectrometry). The relative dielectric constant (ε) and relative molar mass (M_r) values for all solvents, with and without 1% Glr, revealed a distinct breakpoint of ε = 65 and relative M_r = 32-33 for activity towards both bacterial targets. This suggests that when the solvent or additives are within the defined M_r range, they are able to disrupt or destabilise inactive oligomers whereas outside of the defined M_r range (M_r < 33) could result in stabilising inactive oligomers and obscuring active structures. Evaluation of the Trp fluorescence versus activity revealed that the Trp environment in solution does not have an overt link with the Trc surface activity. Although Trp may have an important conformational and activity role when the Trcs are organised on the surface, the cationic residues, Orn^9 and Lys^9 are known to have major importance in recognising negatively charged cellular targets and in the peptide's activity. Ion mobility mass spectrometric analysis of Trc oligomerisation indicated 1% Glr as additive resulted in a higher total ion signal for dimers than in the solvent alone. Glr may be acting as a chaotropic agent disrupting larger oligomers by competing for hydrogen bonds and thereby releasing stabile dimers. Amphipathic dimers are regarded as active structures. Therefore, in light of the detection of lower activity in the presence of Glr, this higher dimer signal may not be due to the availability of active amphipathic dimers, but rather inactive non-amphipathic dimers. The addition of $CaCl_2$ showed a lower than expected dimer contribution, but no change in activity. However, 1% Glr + 100 µM $CaCl_2$ as Trc co-formulants resulted in a substantially increased total ion signal for Trc dimers combined with the highest activity compared to other formulations.

There is a weak link between active Trc dimers detected *in vacuo*, but elucidation of the surface structure-activity relationship is clearly complex and demands an in-depth study of the peptide structure on surfaces, as well as the release of active structures.

Opsomming

Bakteriese adhesie aan verskeie oppervlaktes kan lei tot die vorming van biofilms en is 'n ernstige en volgehoue probleem binne verskeie industrieë. Verder, sodra 'n biofilm sy volwasse stadium bereik, word die meganiese verwydering daarvan al hoe moeiliker en duurder. Bykomend tot hierdie toenemende probleem van antimikrobiese weerstandbiedende bakterieë, is kommer oor verdere potensiële weerstandsontwikkeling teenoor huidige oppervlaksterilisasie en ontsmettingstegnieke. Dit kan toegeskryf word aan die chemiese middels wat die bakteriese mikro-omgewing beïnvloed en 'n konstante selektiewe druk op die bakterieë plaas wat toleransie oor tyd bevorder. Om dit te omseil, het die navorsingsfokus verskuif na die ontwikkeling van aktiewe oppervlaktes/materiale waardeur die benadering verander is om bakteriese adhesie te voorkom of bakteriese selle wat in kontak met die oppervlak is, dood te maak. Antimikrobiese peptiede (AMP's) dien as lewensvatbare aktiewe bestanddele as gevolg van hul wye reeks en vinnige aktiwiteit teenoor verskeie teikens, beperkte weerstand en veelvuldige modusse van aktiwiteit. 'n Groep AMP's van belang is die tirosidiene (Trcs) en analoë wat deur die grondbakterie *Brevibacillus parabrevis* geproduseer word. Die Trcs het 'n wye reeks aktiwiteit teenoor bakteriese teikens, verskeie patogeniese en filamentagtige swamme, die malariaparasiet *Plasmodium flaciparum* en virusse. Onlangs is getoon dat die peptiede kragtige aktiwiteit het in verskeie materiale en op oppervlaktes teenoor die bakteriële patogene *Listeria monocytogenes* en *Staphylococcus aureus*.

Aangesien beperkte oplosmiddel- en formuleringstudies op die Trcs uitgevoer is vir die behandeling van materiale en afsetting op oppervlaktes, was die doel van hierdie studie om die invloed wat verskillende formulerings op die Trc oppervlaksaktiwiteit en biofisiese eienskappe het, te ondersoek. Die Trcs is geformuleer in ses verskillende oplosmiddels, asetonitriel (ACN), etanol (EtOH), metanol (MeOH), isopropanol (IPA), tersiêre butanol (TBA) en propileenglikol (PG) met of sonder ko-formulante naamlik sinkchloried ($ZnCl_2$), kalsiumchloried ($CaCl_2$) of gliserol (Glr). Aktiwiteitstudies het aan die lig gebring dat wanneer dit teen beide teikens (*L. monocytogenes* en *S. aureus*) geassesseer word, EtOH dien as die beste algemene oplosmiddel wat gebruik kan word sonder enige ko-formulante in vergelyking met die ander vyf oplosmiddels. Die byvoeging van 1% Glr het ‘n aansienlike laer aktiwiteit tot gevolg gehad vir formulering in die meer polêre oplosmiddels in vergelyking met in die oplosmiddels alleen. Daar is wel gevind dat PG en TBA in formulering met 1% Glr + 100 µM $CaCl_2$ die twee beste formulerings is. TBA as oplosmiddel was effens beter as gevolg van 'n hoër aktiwiteit teen beide teikens in vergelyking met PG.

Hoe die oppervlaksaktiwiteit verband hou met die formulering se invloed op die peptiedstruktuur is geassesseer deur aktiwiteit teenoor chemiese parameters, veranderinge in Trp-omgewings (fluoressensie) en oligomerisasie (ioonmobiliteit-massaspektrometrie) te karteer. Die relatiewe diëlektriese konstante (ε) en relatiewe molêre massa (Mr) waardes vir alle oplosmiddels, met en sonder 1% Glr, het 'n duidelike breekpunt van ε = 65 en relatiewe M_r = 32-33 getoon vir aktiwiteit teenoor beide bakteriese teikens. Dit dui daarop dat wanneer die oplosmiddel of ko-formulante binne die gedefinieerde M_r-reeks is, hulle in staat is om onaktiewe oligomere te ontwrig of te destabiliseer, terwyl buite die gedefinieerde M_r -reeks (M_r <33) kan lei tot stabilisering van onaktiewe oligomere en die afskerming van aktiewe strukture. Evaluering van die Trp-fluoressensie teenoor aktiwiteit het uitgewys dat die Trp-omgewing in oplossing nie 'n duidelike skakeling met die Trc-oppervlaksaktiwiteit het nie. Alhoewel Trp 'n belangrike konformasie- en aktiwiteitsrol kan speel wanneer die Trcs op die oppervlak georganiseer is, is dit bekend dat die kationiese residue, Orn^9 en Lys^9 'n groot belang het in die herkenning van negatiewe gelaaide sellulêre teiken en in die peptied se aktiwiteit. Ioon-mobiliteit massaspektrometriese analises van Trc oligomerisasie het aangedui dat 1% Glr as ko-formulat lei tot 'n hoër totale ioonsein vir dimere as in die oplosmiddel alleen. Dit is ‘n indikasie dat Glr as 'n chaotropiese middel kan optree en groter oligomere ontwrig deur met waterstofbindings te kompeteer en sosoende stabiele dimere vry te stel amfipatiese dimere word as aktiewe strukture beskou. In die lig van laer aktiwiteit waarnemings in die teenwoordigheid van Glr, is hierdie hoër dimeer sein moontlik nie te wyte aan die beskikbaarheid van amfipatiese dimere nie, maar wel onnaktiewe nie-afipatiese dimere. Die byvoeging van $CaCl_2$ het 'n laer as verwagte dimeer bydrae getoon, maar geen verandering in aktiwiteit nie. Die 1% Glr + 100 µM $CaCl_2$ as Trc ko-formulante het egter gelei tot aansienlike verhoogde totale ioonsein vir Trc dimere, gekombineer met die hoogste aktiwiteit in vergelyking met ander formulerings.

Daar is slegs 'n swak verband tussen aktiewe Trc dimere wat *in vacuo* opgespoor word, maar ontrafelling van die oppervlakstruktuur-aktiwiteit-verwantskap is duidelik kompleks en slegs aangespreek word met 'n in-diepte studie van die peptiedstruktuur op oppervlaktes, sowel as die vrysteling van aktiewe strukture.

Acknowledgements

I would like to thank and appreciate the following persons and institutions:

- Prof Marina Rautenbach, for her immense support, encouragement, wisdom and guidance through my research and writing and teaching me how to believe in myself as a scientist and a man.
- The Central Analytical Facility (CAF) staff specifically Dr. Marietjie Stander and Mr. Malcom Taylor for setting up and assisting with mass spectrometry.
- The significant financial support via the BIOPEP Peptide Fund in funding my studies.
- The BIOPEP peptide group for the support, extensive and random discussions and for always being helpful when I was stuck.
- To, AJ, Dylan, Brent, Jesse and Ntsiki, for loving and believing in me without question and for always being real with me like brothers I never had.
- My friends and family, for constantly encouraging me through my studies and always asking when I would be done.
- My parents, Vasco and Filomena Borrageiro, who I am forever grateful to for pushing me in my studies, unconditional love and support and for never doubting my abilities.
- My Heavenly Father for His grace that carried me through this season of my studies.

Table of Contents

Abbreviations and Acronyms

$[M+H]^+$	singly charged monomeric molecular ion
$[M+2H]^{2+}$	doubly charged monomeric molecular ion
$[2M+2H]^{2+}$	doubly charged dimeric molecular ion
$[M+Ca+H]^{3+}$	triply charged peptide-calcium complex
ACN	acetonitrile
AMPs	antimicrobial peptide(s)
Asn	asparagine
ATCC	American type culture collection
BHI	brain heart infusion
Br. parabrevis	*Brevibacillus parabrevis*
$CaCl_2$	calcium chloride
Ca^{2+}	calcium (2+) cation
CCS	cross collational section
CDP(s)	cyclodecapeptide(s)
CMC	critical micellular concentration
DC	direct current
DEE	diethyl ether
DSMZ	Deutsche Sammlung von Mikrooganismen und Zelkulturen
DTIM-MS	drift time ion mobility linked to mass spectroscopy
ε	relative dielectric constant
Ems	emission
ESMS	electrospray ionisation mass spectrometry
EtOH	ethanol
Ex	excitation
FRET	fluorescence resonance energy transfer
Gln	glutamine
Glr	glycerol
Grm(s)	linear gramicidin(s)
GRAS	generally regarded as safe
GS	gramicidin S
HPLC	high performance liquid chromatography

HR-ESMS	high-resolution electrospray mass spectrometry
IC_{50}	peptide concentration leading to 50 % microbial growth inhibition
IM-MS	ion mobility mass spectrometry
IPA	iso-propanol
KCL	potassium chloride
LB	Luria Betrani
Leu	leucine
L. monocytogenes	*Listeria monocytogenes*
Lys	lysine
MeOH	methanol
MDR	multidrug resistance
MIC	minimum inhibitory concentration
M_r	relative molar mass
MRSA	Methicillin-resistant *Staphylococcus aureus*
MS	mass spectrometry
m/z	mass over charge ratio
m/m	mass/mass
m/v	mass/volume
$NaCl_2$	sodium chloride
NRPS	non-ribosomal peptide synthetases
OD	optical density
Orn	ornithine
OH groups	hydroxyl group
PBS	phosphate buffered saline
PG	propylene glycol
PhcA	phenycidine A
Phcs	phenycidines
Phe	phenylalanine
Pro	proline
RFU	relative fluorescence units
ROS	reactive oxygen species
RP-HPLC	reverse phase high performance liquid chromatography

R_t	retention time of analyte in column chromatography
R^2	coefficient of determination
S. aureus	*Staphylococcus aureus*
SD	standard deviation
SEM	standard error of mean
TBA	tertiary butanol
TFA	trifluoroacetic acid
TGS	tryptone glucose and salts culture medium
TOF	time of flight
TOF-MS	time-of-flight mass spectroscopy
TpcA	tryptocidine A
TpcB	tryptocidine B
$TpcB_1$	tryptocidine B_1
TpcC	tryptocidine C
$TpcC_1$	tryptocidine C_1
Tpc(s)	tryptocidines(s)
TrcA	tyrocidine A
TrcA1	tyrocidine A_1
TrcB/B’	tyrocidine B/B’
$TrcB_1$	tyrocidine B_1
TrcC	tyrocidine C
$TrcC_1$	tyrocidine C_1
Trc(s)	tyrocidine(s)
Trc mix	tyrocidine mixture (tyrocidines purified from commercial tyrothricin)
Trp	tryptophan
TSB	tryptone soy broth
TSA	tryptone-soy agar
TWIM-MS	travelling wave ion mobility linked to mass spectroscopy
Tyr	tyrosine
UPLC	ultra-performance liquid chromatography
UPLC-MS	ultra-performance liquid chromatography linked to mass spectroscopy
Val	valine

VGA	linear gramicidins
v/v	volume/volume
QAC	quaternary ammonium compounds
$ZnCl_2$	zinc chloride
Zn(II)	zinc (2+) cation

Standard 3-letter and 1-letter abbreviations were used for the natural amino acids, with uppercase 1-letter abbreviations for L-amino acid residues and lower case 1-letter abbreviations for D-amino acid residues in peptide sequences

Preface

Surface contamination by micro-organisms is an ever-present issue within the industrial, medical and food industries, specifically exacerbated by biofilm formation and difficulty in the prevention of biofilms. Furthermore, antimicrobial resistance (AMR) development is becoming an ever more serious problem due to the abuse of certain antibiotics rendering them ineffective in the removal of microbial contamination and biofilms from surfaces. Parallel to this is the increased ineffectiveness of current cleaning and disinfecting chemicals due to the COVID pandemic-driven excessive routine usage leading to a potential new route of antimicrobial resistance. This accelerated the investigation, development, and implementation of alternative and effective antimicrobial active surface coatings to either prevent microbial attachment (anti-adhesive) or kill the microorganisms before or after contact with the surface.

A prime antimicrobial group of compounds for active surface development are the large array of natural antimicrobial peptides (AMPs) due to their potent and broad-spectrum activity towards bacteria, fungi and viruses. More important, AMPs display a limited potential to elicit resistance development due to rapid action and multiple modes of action. A specific group of AMPs that hold potential are the tyrocidines (Trcs) and their analogues from the tyrothricin complex. Produced by the soil bacterium *Brevibacillus parabrevis*, and having a highly conserved sequence, the Trcs are very active against a wide array of Gram-positive bacteria, various pathogenic and filamentous fungi, the malaria parasite *Plasmodium falciparum,* and have been shown to be active against viruses. Furthermore, the Trcs exhibit multiple modes of action on their targets, thereby ensuring a limited degree of resistance development towards them. Successful formulation studies using the Trcs with cellulose and soluble carbohydrates have illustrated the potential of Trc-based formulations for multiple target-based applications. However, the sticky nature of the Trcs not only benefits active surface formulation development but also peptide oligomerisation.

The ultimate goal of this project is in developing a Trc-based formulation that can have limited oligomerisation on a surface while having a high degree of activity to prevent contamination and biofilm formation. This will be achieved by assessing the role of different solvents and additives towards the bioactivity of the peptide, while simultaneously investigating the influence on the biophysical properties in developing a formulation for sterile surface applications. In order to reach the aforementioned objective, the following aims and objectives were developed and described below:

Aims and objectives

Aim 1: Bacterial production, isolation and characterisation of tyrocidines and analogues from the tyrothricin complex

In order to reach the first aim the following objectives were met in this study:

- Culturing the producer organism *Brevibacillus parabrevis* ATCC 10068, ATCC 8185 and DSMZ 5618 (Chapter 2).
- Profiling the variability of tyrocidine analogue and linear gramicidins production with HR-ESMS (High resolution electrospray mass spectrometry) (Chapter 2).
- Extraction of the tyrocidines and analogues (commercial and crude extract) and removal of the linear gramicidins (Chapter 2).
- Analysis of successfully purified extract using electrospray mass spectrometry linked to ultra-performance liquid chromatography (Chapter 2).

Aim 2: Formulation and bioactivity assessment of the tyrocidines within various solvent and additive formulations.

In order to reach the second aim, the following objectives were met in this study:

- Preparations of tyrocidine formulations in six solvents namely, acetonitrile (ACN), ethanol (EtOH), methanol (MeOH), tert-butanol (TBA), iso-propanol (IPA) and propylene-glycerol (PG) alone (Chapter 3).
- Combination of the tyrocidines in the six solvents with various co-formulants, namely glycerol (Glr), zinc chloride ($ZnCl_2$) and calcium chloride ($CaCl_2$) (Chapters 3).
- Determination of the antibacterial activity of the various tyrocidine formulations after deposition on polystyrene surfaces towards *Listeria monocytogenes* and *Staphylococcus aureus* (Chapter 3).

Aim 3: Biophysical analysis of the tyrocidine formulations.

In order to reach the third aim, the following objectives were met in this study:

- Analysis of higher order oligomerisation and tyrocidine self-assembly by assessing the changes in tryptophan environment(s) in peptide formulations via fluorescence spectroscopy (Chapter 4).

- Analysis of higher order aggregation and tyrocidine self-assembly by assessing the changes in the oligomer profile using travelling-wave ion mobility mass spectrometry (Chapter 5).

Thesis content summary

This thesis is comprised of six chapters, wherein Chapter 1 provides a literature review on antimicrobial resistance, microbial surface contamination, antimicrobial peptides and current developments in surface sterilisation. The experimental results are given in Chapters 2 to 5, which were written as independent units in article formatting for ease in future publications, but potential repetition was kept to a minimum. Finally, Chapter 6 provides a concluding summary and future studies of all the work in this study.

Outputs of MSc study

Borrageiro, CM.*, (2020) Formulation of natural cyclodecapeptide for sterility applications, Biochemistry forum, University of Stellenbosch, Oral presentation

Borrageiro, CM.*, (2022) Development and formulation of the tyrocidines, a natural cyclodecapeptide, for surface sterilisation applications, Biochemistry forum, University of Stellenbosch, Oral presentation, MSc defence.

Borrageiro, CM.*, Rautenbach, M. (2022) Formulation of natural cyclopeptides for surface sterilisation. Poster, AC21 Workshop on antimicrobial peptides, University of Strasbourg, Strasbourg, France

Borrageiro, CM.*, Rautenbach, M. (2022) Development and formulation of the tyrocidines, a natural cyclodecapeptide, for surface sterilisation applications. Oral presentation, World Antimicrobial Awareness Week (WAAW), Stellenbosch, Western Cape, South Africa. (Winner: Oral presentation)

Kumar, V.; van Rensburg, W.; Snoep, J. L.; Paradies, H. H.; Borrageiro, C.; de Villiers, C.; Singh, R.; Joshi, K. B.; Rautenbach, M*. Antimicrobial nano-assemblies of tryptocidine C, a tryptophan-rich cyclic decapeptide, from ethanolic solutions. *Biochimie* **2023**, 204, 22–32. (https://doi.org/10.1016/j.biochi.2022.08.017)

Borrageiro, C., Van Rensburg, W., Rautenbach, M*. The influence of solvent focused formulations on bioactivity of tyrocidines and tyrocidine-materials. (Manuscript prepared from Chapters 3 and 4 for submission to Antibiotics, special issue in Feb 2023: Biosynthesis, Antimicrobial Activity, and Therapeutics Development of Novel Peptides)

*Presenter/Corresponding author.

Chapter 1: Literature review

Overview of microbial resistance to current surface sterilisation and antimicrobial peptides as alternative for active surface sterilisation development.

1.1 Introduction

The rise in bacterial resistance towards conventional antimicrobial compounds is becoming ever more prevalent and has been extensively reviewed [1-3]. The ability of microbial pathogens to adhere to and colonize various surfaces resulting in microbial contamination and/or biofilm formation has been observed in both the agricultural and medical industry alike [4,5]. The effects caused by these bacterial pathogens are seen with food spoilage resulting in large post-harvest losses, thereby decreasing the annual food availability [4]. Furthermore, microbial contamination within the medical sector via infection or surface colonization influences the medical equipment sterility that results in patient infections [5]. The main culprit aiding this problem is the extensive utilization of antimicrobial compounds, namely antibiotics and biocides, which are not always fully effective in the removal and elimination of microbial infections and contamination on surfaces, respectively [6]. This allows for selective pressure on the target pathogens by these antimicrobial compounds, which encourage resistance development. Parallel to the selective pressure on microbial organisms via antibiotics used in agriculture and medicine, is the rising concern of a similar selective pressure placed by biocides and sanitizing agents used in the food and medical industry alike [7,8].

Therefore, the discovery and development of novel antimicrobial compounds in formulations may be the required approach to alleviate the rising concerns in preventing the colonization and biofilms of resistant pathogenic organisms, no matter the industry they are applied in [9-11].

1.2 Brief overview of microbial resistance and tolerance

1.2.1 Antibiotic resistance

The development and misuse of antibiotics has led to increased resistance to antibiotic combinations in many bacterial species [12,13]. This allows bacterial species to adapt to the point where infections previously cured with antibiotics are no longer curable because these antibiotics are said to be ineffective [12,13]. This evolving antibiotic resistance has led to the definition of bacterial species as multi-drug resistant (MDR) species that exhibit high levels of resistance to antibiotics. This inability of antibiotics to effectively kill these MDR species has resulted in increased rates of mortality in MDR infected individuals [6].

The increased degree of antibiotic resistance and the realisation that the current antibiotics are becoming ineffective is linked to mankind's failure to understand that antibiotic resistance is an effect of evolution by bacteria. The production and over exploitation of antibiotics usage has now resulted in mankind reverting to the age defined as the post antibiotic era [14]. The vast range of niches which have acquired the ability to be resistant to antibiotics has increased and the realisation that the contributors to this problem come from the microbes in the environment [14]. The environment and the microbial communities within these environmental habitats have been ignored and were not monitored over the antibiotic era. The problem is that only now is it realised that the microbial communities within the environment play a crucial role in antibiotic resistance and the distribution of these antibiotic resistant characteristics [14].

There are two forms of microbial antibiotic resistance which confer microbes the ability to negate the effect of antibiotics, namely, intrinsic and acquired resistance. Intrinsic resistance refers to the existence of genes within the bacterial specie which confers it the ability to produce a resistant phenotype toward certain antibiotics such as multidrug resistant *Acinetobacter* species, fluconazole-resistant *Candida* species, vancomycin-resistant *Enterococci* species and methicillin-resistant *Staphylococcus aureus* [6,15]. These evolved mechanisms of defence include SOS responses to DNA replication inhibition, genes encoding inactivation enzymes such as β-lactamases, limited uptake of the drug, modification of the drug target, active efflux of the drug and in activation of the drug [16].

The problem posed by intrinsic resistance is that the bacterial specie containing the genetic code for resistance can pass this on which in turn causes future generations to contain this degree of resistance. Acquired resistance comprises of a mechanism in which the evolution of a specific antibiotic resistance is built upon a scaffold which is transferred via a mechanism defined as horizontal gene transfer (HGT) [14]. The significant issue which is created via HGT is that it violates the passage of gene flow down generations which would not normally be present via normal reproduction and replication processes [17]. This provides microbial species the ability to transfer genetic code from one species to the next which are known to confer advantageous capabilities therefore making the recipient have a better survival advantage against a specific "attack", which in this case is antibiotics [17]. The issue this introduces within the antibiotic realm is that bacterial species which were previously not resistant now can obtain resistance due to the high exploitation of antibiotics in the environment therefore making it a selective pressure for the bacterial species to evolve against.

1.2.2 Biocide tolerance by bacteria

The excessive usage of chemical agents in disinfectants and sterilisers allows for a direct influence on the microenvironment of the bacterial target but simultaneously promotes a selective pressure

leading to increased tolerance [18]. Bacterial biocide-tolerance is not a new phenomenon with multiple studies from various industries, such as food processing industry [19,20], livestock and agriculture [21,22], healthcare [23] and domestic environments [24], indicating the prevalence of biocide-tolerant bacteria. Furthermore, as mentioned earlier there is a lack of diverse active ingredients in the currently approved and used disinfectant and sterilising chemicals with 81% of the products using either quaternary ammonium compounds (QACs), hydrogen peroxide, ethyl alcohol and sodium hypochlorite, shown by Chen *et al.* [25]. Additionally, it was found that QACs are the most utilized active ingredient making up 40% of the total 81% posing a significant problem with exposure to bacteria by the same biocidal agent [25]. Although there are varying generations of QACs that are used, the mode of action is similar between the different generations [26] suggesting that if bacteria have intrinsic or acquired tolerance to a QAC, they will potentially display tolerance to the other QACs [26]. Studies by He *et al*. showed surfaces frequently treated with QAC containing wipes or sprays resulted in 24% of community isolated surface bacteria having tolerance to the QACs, specifically BACs (first generation QAC) [27]. Various studies investigated the influence of chlorine-based disinfectants in drinking water systems and identified multiple chlorine-tolerant bacteria species specifically those of *Pseudomonas* [28], *Bacillus* [29], *Legionella* [30] and *Mycobacterium* [31].

1.2.3 Mechanisms of biocide resistance/tolerance development

As in the case with antimicrobial resistance, bacterial tolerance and resistance can be grouped under intrinsic or acquired in which intrinsic tolerance is a natural change or mutation in the bacterial chromosomal properties whereas acquired tolerance is the acquisition or uptake of external mobile genetic material that carry the biocide-tolerant/resistant genes (Figure 1.1) [18,29,32]. The negative effect of this is that mechanisms of tolerance results in bacteria being influenced less by certain biocides compared to other bacterial species [18]. Furthermore, physiological adaptations can further enhance bacterial tolerance to biocides, especially cells that are within a biofilm, leading to lower susceptibility to biocides compared to planktonic cells [29,32]. Selective pressure placed on bacterial cells by biocide agents, especially when ineffective, can lead to increased tolerance through genetic mutations [18,33]. This was observed in a study by Kim *et al.* [34] in which mutations were observed in *Pseudomonas aeruginosa* (*P. aeruginosa*) *pmrB* gene after constant exposure to BAC (type of QAC) leading to changes in the outer membrane charge decreasing bacterial susceptibility. Assessing the influence on mutation probability when exposed to varying concentration of alcohols, Horinouchi *et al.* [35] observed that mutations in the *relA, marC, proQ* and *rraA* genes conferred increased tolerance by *Escherichia coli* to isopropanol but also ethanol and butanol.

The role of horizontal gene transfer (HGT) provides another avenue in which bacteria can obtain mobile genetic elements (MGEs) that contain biocide-tolerant/resistant genes allowing for the development of tolerance and resistance to biocides by the recipient bacteria [18]. These MGEs can either be in the form of insertion sequences, genetic cassettes or plasmids with the overall objective of carrying biocide-tolerant/resistant genes ultimately to be incorporated and replicated in the new host cell [18,36-38]. The rising problem MGEs pose is that the ability of bacteria to obtain, integrate and stockpile these tolerant genes will allow the rapid evolution and subsequent rise in biocide tolerant bacteria [18].

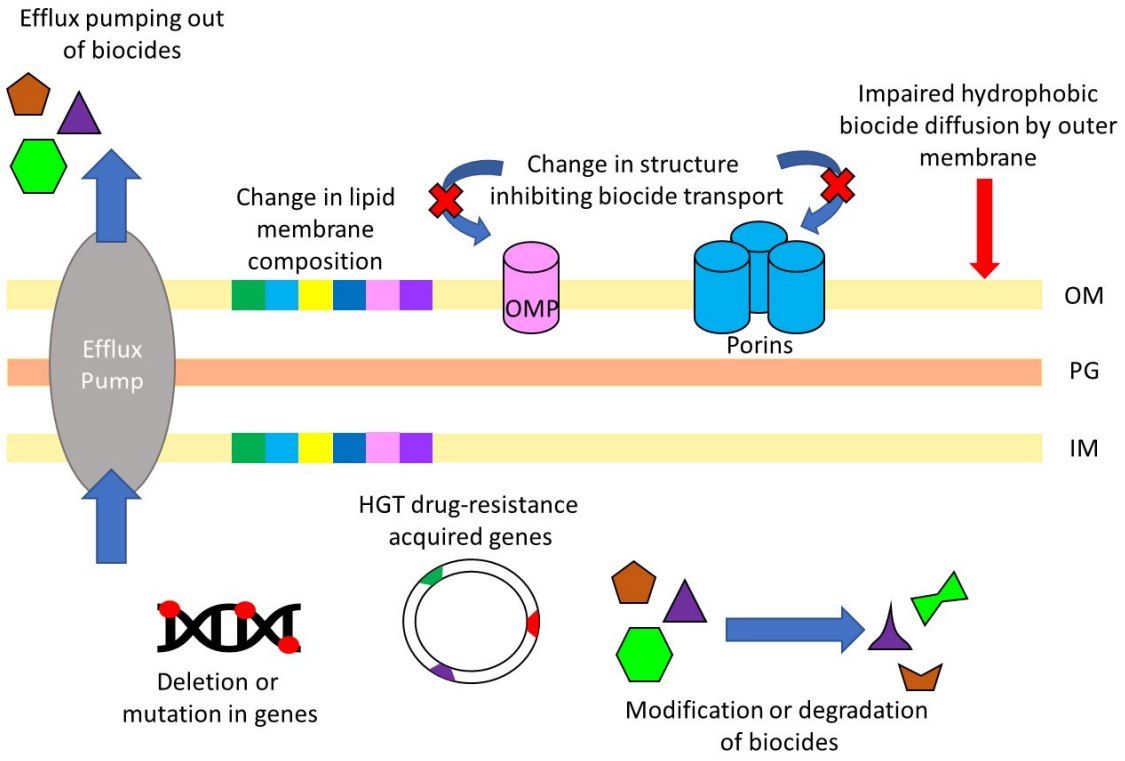

Figure 1.1 Visual summary of the various resistance strategies developed and employed by bacteria to overcome biocide exposure. Graphics adapted from [39] (OM = outer membrane, PG = peptidoglycan layer; IM = Inner membrane; OMP = Outer membrane protein; HGT = horizontal gene transfer)

The ability of biocide-tolerance related to the function MGEs specifically plasmids containing biocide-tolerant genes have been explored specifically using BACs. Studies on *Listeria monocytogenes* (*L. monocytogenes*) H7550 when exposed to BACs resulted in an increase in the expression of pLM80 genes located on the plasmid gene cassette, which contain two efflux pump related genes (bcrB and bcrC) as well as bcrA which is controls the transcription of known multidrug efflux pumps leading to increased tolerance by the microbial cells [40]. Furthermore, studies on

biofilm formation by *E. coli* showed that there was an increased ability in biofilm formation along with increased expression of multidrug efflux pumps with both effects related to the MDR pOLA52 plasmid, encoding the efflux pump (*oqxAB*) and the type 3 fimbriae (*markABCDF*), sequence of the conserved conjugated LncX1-type backbone, when exposed to BACs [41].

Other mechanisms that may be employed by bacteria for biocide tolerance can be physical changes to the membrane, such as compositional changes to the fatty acids, phospholipid bilayer and proteins [33]. Membrane protein studies towards BAC-tolerant *P. aeruginosa* showed that when exposed to BAC, there was an increased expression in the OprR outer membrane protein leading to a decreased susceptibility to BAC, whereas when the bacteria had the OprR gene knocked out, the cells recovered high susceptibility to BAC [42]. Changes in bacterial membrane potential were observed towards *P. aeruginosa* [33], with findings by Kim *et al.* [34] showing that when the overall negative charge of the membrane was reduced, there was decrease in the degree of positively charged BAC attachment and adsorption.

As described earlier, biofilm formation within various industries is a significant issue especially due to the nature of biofilms being able to colonise and contaminate various types of surfaces leading to substantial problems [43-45]. Bacterial cells within biofilms are fully capable of withstanding high biocide concentrations due to the advantageous nature of the biofilms [46,47]. A study performed by Smith and Hunter assessed the effectiveness of three hospital used disinfectants on various relevant hospital surfaces towards two grown biofilms, methicillin resistant *S. aureus* (MRSA) and *P. aeruginosa* [48]. Findings revealed that the treatment at recommended concentrations did not result in complete killing of the bacteria with, 11% of MRSA and 80% of *P. aeruginosa* still being viable within their respective biofilms [48]. Furthermore, the minimum inhibitory concentration (MIC) of the tested biofilms in the biofilm were found to be between 10 to 1000 times higher compared to the same cells not within a biofilm [48]. Another biocide tolerant factor offered by biofilms to bacteria is the physical properties of the biofilm that confer various mechanisms such as reduced biocide penetration and diffusion leading to sub lethal concentration exposure [49,50], enhanced bacterial mutation and increased frequencies of horizontal gene transfer [49,50]. Two studies performed on HGT frequencies within biofilms of *P. aeruginosa* showed that when the cells were in a biofilm, there was a 100-fold to 1000-fold increase in HGT frequencies when compared to the planktonic cells [51,52]. Additionally, Ehlers and Bouwer in the same study, demonstrated that when present within a biofilm, the close physical proximity between those bacteria facilitated a higher degree of HGT compared to free planktonic cells [52].

Biofilm forming bacteria possess the ability to colonize any surface and are extremely problematic not only within the healthcare system but also with the industrial, food and public sectors [43-45].

Furthermore, multiple performed studies by Cooper and Hanlon [46], Shen *et al*. [47], Smith and Hunter [48] and Wong *et al.* [53] have shown that biofilms further enhance and provide bacteria with a means to overcome biocide exposure, even at high biocide concentrations with the downstream impact being suboptimal concentration exposure leading to increase tolerance development [49,50]. The link between biofilms, resistance and bacterial surface attachment strategies will be explored further below.

1.2.4 Biofilms

A biofilm, as described by Flemming [54], is a structure that is formed because of a microorganism's initial attachment and subsequent colonization of abiotic or biotic surfaces, followed by the production of the extracellular polysaccharide matrix (EPS). Biofilm formation is a common and problematic phenomenon within multiple industries such as the dairy [55], wine [56], medical [57], water [58], food [59] and power [60] industries leading to substantial negative effects such as product loss and spoilage, equipment failure and infections [55-60]. The reasoning in their lack of prevention can being attributed to either poor or insufficient disinfection methods for the equipment or working surfaces [61].This has resulted in a profound need in the development of an alternative state-of-the-art wide range applications and techniques for biofilm prevention and eradication [62,63].

The essential requirements for the formation of a biofilm by bacteria is reliant on two major factors namely the microbes themselves and a substrate on which to bind [64]. If there is a lack of either of the two factors, no biofilm formation will occur, which is expected [64]. Additionally, the formation of a biofilm provides many advantages for the bacteria for example protection from antibiotics [65], cleaning and disinfection agents [66], various environmental and mechanical changes [67] and the ability to adapt and survive in nutrient poor conditions via potential upregulation or downregulation of various bacterial genes [68]. Furthermore, it has been documented that bacteria present within biofilms exhibit a degree of resistance to antibiotic treatment [69-71], with the mechanisms being due to the biofilm's barrier protection and function, the presence of dormant persister cells and the ability for horizontal gene transfer and upregulation of various antibiotic resistant genes being enhanced in the biofilms [69-71]. Additionally, experiments performed by John *et al.* [72] revealed that bacterial surface adhesion causes changes to the bacterial membrane which further enhance antibiotic resistance namely the reduction in the negative surface charge and membrane enhancement.

1.3 Overview of microbial surface adhesion and colonisation

1.3.1 Mechanisms of surface attachment

Prior to the attachment to a surface bacteria are suspended within a solution from which there are three areas that motile bacteria occupy being the bulk liquid, near surface bulk liquid and lastly the near surface constrained liquid [73]. Depending on the liquid phase the bacteria are present in, the effect from the surface on the bacteria varies, thereby influencing their interaction with the surface or not, with the near surface bulk liquid having hydrodynamic effects while the near surface constrained has both hydrodynamic and physicochemical effects on the cells [73,74]. The surface on which attachment will occur provides the conditional layer which serves as the foundation for attachment and is the first step to surface attachment. It is important that the surface characteristics such as the surface charge, surface tension and surface potential are favourable for attachment [75,76]. When exposed to favourable, binding surface conditions bacteria undergo two attachment phases namely reversible and irreversible attachment. Reversible attachment occurs when bulk liquid cells interact with the conditional layer, and it is a very rapid and quick onset that is driven by hydrodynamic and electrostatic interactions [77,78]. Studies performed by Busscher *et al.* [79] attributed the rapid surface attachment by bacterial cells to physicochemical effects rather than biological effects in which multiple events such as loss of interfacial water, cellular repositioning for increased surface area for attachment and surface structural changes occur leading to stable surface attachment. Additionally, due to the net negative charge on the surface of bacteria, there is a higher degree of interaction with a positively charged surface, especially during the early development in cellular growth [80]. This has been shown in studies performed on *E. coli* which revealed that structural changes induced by quorum sensing resulted in an increased net negative charge on the cell surface leading to improved surface binding [81]. Irreversible attachment occurs when cells absorbed to the surface via reversable attachment now become fixed against that surface [76]. This is driven by van Der Waals interactions that occur between the outer cellular wall (hydrophobic region) and the attached surface [82]. Furthermore, as the cells become immobilized on the surface, studies have shown that physical changes of the bacterial appendages such as flagella, fimbria and/or pili occur to as further anchoring of the cells to the surface by overcoming the physical repulsion by the surfaces [83,84]. When binding occurs between the bacterial cells and molecules presented on the surface, these organelles are terminated and replaced with adhesins [85]. Early studies on *E. coli* revealed that although bacteria may be present within the same niche and may present adhesins, they will not interact with the same surfaces, which was shown for their type I and type II pili [85]. Once the irreversible attachment has occurred, cellular proliferation and the production of the extracellular polysaccharide (EPS) matrix

[86] followed by mature biofilm formation [87] ultimately to then lead to detachment of individual bacterial cells or clumps leading to the dispersion and colonization of other surfaces [88,89].

As described earlier, the ability of microbes to attach and colonize various surfaces leading to detrimental effects is very problematic [55-60] with multiple strategies being investigated to control surface chemistry [90], controlling the surface structural properties [91] or the development of seeded surfaces with antibacterial compounds [92,93]. Multiple material studies have been performed and reviewed [94-97] assessing surface characteristics that have different impacts on bacterial attachment. Attachment to hydrophilic surfaces (high surface energy materials) occurs when the surface energy of the bacteria is larger than the surface energy of the liquid they are within (bulk liquid). Furthermore, attachment to hydrophobic surfaces (low surface energy materials) occurs when the surface energy of the bacteria is less that the surface energy of the liquid they are suspended in [98].

To prevent or develop technologies in preventing surface attachment, understanding the how to manipulate the different surface properties and the role they have on attachment is vital. These can be split into two different groups namely physiochemical surface properties and environmental factors that influence bacterial adhesion to a surface [82,96,97]. Surface charge density has been attributed to be a vital surface property that facilitates bacterial binding, with van der Waal forces and electrostatic interactions being the major forces [82,97]. Furthermore, as bacteria possess a net negative surface charge, they are expected to have a higher attachment affinity for positive surfaces compared to negative surfaces [99]. Various studies on *P. aeruginosa* reported more adhesion to positive surfaces of poly(methcrylates) [100] and poly(acrylic acid) [101] compared to negatively charged surfaces respectively. Interestingly, although a trend between bacterial negative charge and positive surfaces charges are observed, some studies have reported the ability of some bacteria to overcome the electrostatic repulsion by their surface organelles (fimbriae) [102]. Seen in *E. coli* and *P. aeruginosa*, Rzhepishevska *et al.* [103] observed that the bacterial LPS assisted in adhesion to a negatively charged surface, suggesting that surface charge density manipulation is not a single factor to consider when attempting to prevent bacterial adhesion. Surface roughness is another factor to be considered when assessing the viability of a surface to promote or discourage bacterial adhesion. It is considered that as there is a direct relationship between surface roughness and bacterial adhesion, with an increase in surface roughness leading to an increase in bacterial attachment and biofilm formation [104,105]. This is because there is an increase in surface area for bacterial attachment thereby providing a scaffold allowing bacterial attachment [104,105] leading to bacterial protection from sheer forces preventing bacterial removal [106].

Studies performed by James *et al.* [107] observed that for *Staphylococcus epidermidis* (*S. epidermidis*) and *P. aeruginosa*, bacterial adhesion was significantly higher on rough surfaces

whereas the opposite was observed for smooth surfaces [107]. Surface material adhesion studies further observed that there was a direct correlation between surface roughness and bacterial adhesion, with *S. epidermidis* showing much higher adhesion to course biomaterial groups compared to fine groups [106]. It is evident that surface characteristic and properties have an important role in dictating if adhesion will be achieved or not. Furthermore, another factor assessed and able to be exploited by bacteria is surface topology and layout, in which bacteria interpret surface mechanical information in which the microscale and nanoscale features will influence binding differently [95]. Surfaces that are larger than the bacterium will allow for greater contact area and shielding leading to better attachment [108], whereas the opposite is observed in surfaces smaller than the bacterial cells [108]. Interestingly, studies on the superhydrophobic physical surface characteristics as an alternative in prevention of bacterial attachment have been explored as a new antifouling concept. Studies performed on shark skins revealed that bacterial adhesion was impaired on protruding surfaces compared to smooth surfaces [109], while gecko skin studies displayed superhydrophobic traits in acting as an anti-wetting barrier, leading to very low bacterial adhesion [110]. Additionally, the development of micro- and nano surface structures with specific height and spacing have allowed for self-cleaning and killing anti fouling surfaces towards adhering bacteria [110,111]. Successful studies testing cones [112], varying silicon heights [113] and various hemispheres [114] resulted in successful prevention of bacterial adhesion and bactericidal effects towards *S. aureus* and *P. aeruginosa* for the smaller and more densely packed structures. Although studies tend to look at individual physiochemical parameters to assess biofilm formation or prevention, limitation in studying the effects of multiple surface parameters being merged requires much more investigation to enhance the surfaces' ability in preventing biofilm formation.

Parallel to physiochemical factors that can influence bacterial adhesion to surfaces, environmental factors may also contribute to enhancing or preventing surface adhesion. Factors such as pH, temperature and fluid dynamics all have been shown to influence the ability of surface adhesion for bacteria. Due to the presence of proton pumps situated within the membrane of bacteria, changes to external pH will result in an influx of protons from resulting in an inbalance of the cytoplasmic pH resulting in a biocidal effect [115]. Studies by Stepanović *et al.* [116] have shown that successful biofilm formation can be linked to nutrient intake which can be influenced by altering the temperature the microorganisms are exposed to [116]. Therefore, as nutrient uptake and utilization can be linked to enzymes, with many enzymatic reactions driving physiological and biological processes, changing the temperature will result in reaction rate changes leading to optimal or inhibition of cells development [76]. Lastly, fluid dynamics have been suggested to have a role in either promoting or preventing biofilm formation of various surfaces, with biofilm formation and growth occurring when

exposed to fluid conditions [117]. Interestingly, it was observed that when *S. aureus* was exposed to shear flow fluid conditions that an increase in EPS production and strengthening of the EPS matrix occurred, serving as a protective role [118], enhancing the biofilm formation [119]. Additionally, a study by Rodesney *et al.* [120] observed that when *P. aeruginosa* was under sheer fluid stress, an upregulation of *c-di-GMP* signals were observed which function in promoting biofilm development. Therefore, when biofilms develop under sheer stress fluid conditions occurring, the result is the increased expression of proteins favouring bacterial growth [120].

1.4 Sterilisation and disinfection: Current approaches and issues

1.4.1 Current understanding of sterilisation

The ability of harmful microorganisms to adhere and colonize various inanimate surfaces, followed by subsequent biofilm formation, is a substantial problem in multiple industries. Furthermore, prolonged surface and biofilm adhesion by the harmful microorganisms allows for the surfaces to become secondary reservoirs for indirect bacterial transmission leading to the dispersion from one contaminated surface to many others [121,122]. To circumvent this issue, current approaches rely on intensive and indiscriminate usage of cleaning and disinfectant agents, however, limited insight and understanding of the selective pressure and efficacy of these agents on microorganisms have been overlooked [18,25]. Furthermore, highlighted by the recent COVID pandemic, there has been a significant increased usage of many cleaning and disinfecting chemicals [25] leading to the concern of antibiotic co-resistance phenotype with biocides or AMR bacterial gene selection conferring biocide resistance [16,123,126]. As the focus has shifted from limiting antibiotic usage as a means of control, alternative effective approaches are required [124].

The function of disinfectants, cleaning, and sanitizing agents, or combinedly known as biocides, is the effective removal of biological contaminants, microbial cells, or life, from a product or surface by either inhibiting cellular growth or killing the target organisms by rendering them to levels that are justified as “safe” by industry standards [123,125,126]. Although defined under the same banner of biocides, the role of a disinfectants differs considerably to that of a sanitizer with both being part of the biocontamination procedure [127]. This is namely that disinfectants inactivate microorganisms to appropriately defined levels while sanitizers function to completely remove and microorganisms from a product or surface, rending it sterile [125]. Although the primary focus of disinfecting and sterilization is towards the consumer and the consumers product, the goals differ between industries and should be considered when developing or using disinfection or sterilisation methods as there is no uniform standard definition on the market for all industries [128,129]. Furthermore, factors that need to be considered when either using or designing sterilizing or disinfecting agents are the type of

biocontaminants, the surrounding environmental conditions and the time of exposure of the sterilant to the target [128,130,131]. Understanding the bioburden of the target microorganisms is paramount in effective development and usage as understanding the influence of the sterilant on target's growth and proliferation once exposed and the distribution of the microorganisms on the surface will affect the efficacy of the sterilizing agent [132]. Factors that are important to understand are the method of sterilization, the type of applied sterilizing agent and how this will impact the overall quality and final sterilized surface [133]. Moreover, operations and working environmental safety of the sterilisation agent needs to be considered and the impact of sterilant toxicity and negative environmental impact and risks need to be determined [134]. Lastly, for the successful development and implementation of a sterilisation method, the sterilant needs to be in contact for a specific "dwell time" with the target allowing for effective decontamination and/or sterilisation of the product or surface [125]. Factors that need to be considered for an effective decontamination of a product is 1) the sterilant needs to be evenly and homogenous distributed on the surface and towards the target, 2) the concentration of the sterilant is constant throughout the entire process, 3) the sterilant must be capable in penetrating through porous materials indicating good penetration strength, 4) long enough and constant contact time between the sterilant and microbial target [125]. To achieve this, three categories of sterilisation techniques namely, radiation sterilisation (X-ray, gamma, ultra-violet and E-beam irradiation [135]), thermal sterilisation (dry heat [125] and moist heat [125]) and chemical sterilization (liquid phase, gas phase and mixed phase) [125], in combination or singular use, have been developed and applied to the respective application. For the purposes of this literature review, only chemical sterilization will be briefly defined as this project and research falls under this category.

A chemical sterilant can be defined as a compound or substance that has microbicidal properties such as DNA and/or RNA synthesis inhibition, interfering or inhibition cellular function, protein and enzymatic inhibition or directly interacting with the cellular membrane and wall, will all these factors resulting in microbial cell death [125]. As highlighted by the 2020/21 COVID pandemic, there was a substantial spike in the employment and treatment of surfaces using "liquid phase" chemical sterilant with the primary function in decreasing microbial surface contamination achieved via spraying of surfaces [25,125]. Although there were many disinfectants and sterilization products developed and released, a significant drawback is the lack of diversity of the active ingredient, with two thirds of the common active ingredients being either quaternary ammonium compounds, hydrogen peroxide, chlorine, iodine, chlorohexidine, ethanol, ethylene oxide and sodium hypochlorite [25,136]. The problem this creates is due to their significant role in various industries, the public and private domains, the creation of selective pressures and the potential oversight into the presumed

insignificance of resistance to disinfectants is the overall lack of attention for it being a rising concern [137,138].

1.4.2 Drawbacks of excessive sterilisation

As described earlier, antimicrobial resistance has gained significant attention over the years because of the inappropriate and excessive misuse of antibiotics. Increased antibiotic resistance las led to significant economic pressures in various industries such as medical/heath [139], agricultural [140], food [141] industries [142]. However, minimal interest and attention has been placed on the excessive exposure of disinfectants and sterilizing agents that may promote resistance to biocides and give rise to further antibiotic multidrug resistant bacteria [26,34]. This is brought about because excessive and chronic exposure of biocides to microbial targets in the wide array of applications may allow for a selective pressure to arise of subeffective concentrations leading to resistance development as reviewed in detail by Malani *et al.* [143], Merchel Piovesan Pereira *et al*. [144] and Mulder *et al.* [145]. Furthermore, increased concerns have arisen regarding the adverse effects of the chemical agents towards various environments and ecosystems such as urban wildlife [146], natural microbiota, aquatic environments and ecosystems as in general [147]. This collateral damage is because of the injudicious usage that inevitably will lead to antimicrobial resistance and dysbiosis once it is discharged, dispersed or disposed in the environment [25,148]. Coupled with environmental concerns is the overlooked direct risk placed on community and public settings, in which the massive amounts of chemical disinfectants and sanitizer usage in regular surface cleaning may allow for the emergence of biocide-tolerant and drug-resistant antimicrobial pathogens leading to direct transfer to and between humans via surface contact [148,149].

The utilization of disinfectants and sterilizing agents are paramount in reducing and preventing microbial spread and contamination [150] and infection prevention and spread [151], even more so when they are used correctly. However, as described earlier, the selective pressure applied to microorganisms may contribute to the development of biocide tolerance and drug-resistant resistance within various community and industry orientated environments enhancing bacterial transfer and spread. Furthermore, multiple studies have identified and reported on the acquisition of antimicrobial-resistant bacterial pathogens were associated with high touch surfaces in public and indoor environments [152,153]. He *et al*. [154] found that when assessing high contact areas, door handles, dumbbells, toilet handles and bathroom faucet handles, within four gyms and two school observed that 9.6% of the isolated bacterial strains were BAC-tolerant, with identified BAC-tolerant Staphylococci strains having resistance towards antibiotics penicillin and ampicillin [154]. Furthermore, all the BAC-tolerant strains were isolated from frequently cleaned, wiped, or sprayed surfaces whereas bacterial strains isolated from non-BAC cleaned surfaces displayed no BAC

tolerance but were all susceptible [154]. In a 244 double-blind study performed Carson *et al.* BAC-insensitive bacteria were identified in the homes assigned to using biocide cleaning agents and these isolates further displayed resistance to various antibiotics [155]. Additionally, incorrect use of disinfectants and sterilising agents is a highly common issue, specifically related to human error and misuse [156], inappropriate dilutions, insufficient contact time and external interference with the disinfectant during the disinfection process which may all result in bacterial exposure to sub-lethal concentrations [157,158]. The significance these studies highlight is that the excessive usage of the current chemical disinfectants in the different settings has resulted in undesirable consequences, specifically the increased tolerance and resistance development to antibiotics by bacteria due to the selective pressure. Therefore, there is a urgent need to develop and implement new, effective methods with limited-tolerance and resistance development for surface applications.

1.5 Alternatives to conventional sterilisation and disinfection

1.5.1 Strategies to create self-sterilising surfaces

The ability of microorganisms to colonise and subsequently contaminate a wide array of different surfaces has placed an increased intensity in developing new fabricated active surfaces [159] with surfaces serving as a medium of transmission and spreading of the microorganisms especially in high contact areas thereby representing a source of infection spreading [160]. At presently used extensively are the various types of cleaning and disinfecting methods as an agreed process in maintaining effective infection prevention and microbial transfer on surfaces, especially since microbes have been shown to be able to survive on surfaces using biofilms within the healthcare and community-orientated environments [161]. Alternative approaches in preventing biofilm formation by either creating surfaces or materials that disrupting/preventing adhesion or by the direct of killing the bacteria have become paramount [159,162]. One developmental approach which hold great promise is the development of active antimicrobial coatings in which surface of the materials is coated or dried with an active antibacterial compound that can elicit active when exposed to a target [152,163]. Active surfaces can be divided into two groups namely, antibacterial (bactericidal) and antibiofouling, with the developments and applications of various active surfaces have extensively been reviewed by Hasan *et al*. [152], Yang *et al.* [124] and Campoccia *et al.* [164]. Antibacterial surfaces can be defined as surfaces which exhibit antibiofouling traits or are able to kill the bacterial cells when in contact with the surface [165]. Antibiofouling surfaces are surfaces which prevent and resist bacterial cellular attachment by having the surfaces provide undesirable and unfavourable binding conditions either via topological or surface chemical modifications [166]. Table 1.1 provides a brief summary of the two different approaches along with effects elicited on the microbial targets.

Table 1.1 Brief overview of current antimicrobial surface design strategies

Design approach		Antimicrobial effect		References
		Antimicrobial	Anti-adhesive	
Surface coating		QACs, AMPs, Nanoparticles, polymers	Titanium coating, zwitterions	[184], [187]
Surface modification	Chemical modification	covalent bonding QACs, nanotubes	Polyanionic surface, surface wettability, polyethylene glycol	[188]
	Physical modification	surface nanopatterns, nanowires, nanopillars	Surface charge, Surface stiffness	[173]

1.5.2 Chemically functionalised antimicrobial surfaces

Described earlier in this chapter, bacteria possess various mechanisms in which they can attach and adhere to various surfaces specifically when assessing the surface characteristics. To overcome these advantages, present by bacteria, various self-cleaning nature bio-inspired surfaces have been studied from natural surfaces such as leaves, shark skin, fish scales and insect wings [124] promoting the development of bio-mimicked surfaces [124]. Factors that have been shown to influence bacterial surface attachment include the wettability, surface charge, surface topography and surface stiffness as well as their combinations (Figure 1.2) [124]. Assessing the wettability, one approach is the development of super-hydrophobic and super-hydrophilic surfaces in which the surfaces are coated or grafted with polymers leading to the reduction of microbial adhesion [121]. A study performed on the biofilm attachment of *S. aureus* by grafting polyurethane with a tyramine-conjugated polymer resulted in the reduction of bacterial attachment and subsequent biofilm formation to the surface [167]. Additionally, development of super-hydrophilic surfaces allows for the decrease in bacterial protein attachment to the surfaces of which various studies have successful tested coating with hydrophilic polymers and zwitterions [167,168]. A study assessing the effectiveness of zwitterions was performed by coating cotton surfaces it was observed that the surfaces was able to resist bacterial adhesion, as well as being successful in killing attached bacteria [169].

Modifications to the surface topography in which the surface can be structured to provide a more direct physical means in decreasing and preventing bacterial attachment specifically pattern usage has more recently gained traction [170,171]. As expanded on earlier, surface roughness studies observed a direct correlation between smooth surfaces and bacterial adhesion, therefore effective changes on the surface micro and nanostructures can influence bacterial adhesion and subsequent

surface colonisation [161]. Structures that have gained attention in reducing the surface area for bacterial adhesion and colonisation are superficial nanostructures such as nanotubes, nanoparticles and nanofibers as shown by Yang *et al.* [172], showing successful anti-adhesion, growth and colonisation by *E. coli* and *S. aureus* when using a submicron scale pillar patterns [172]. An alternative surface modification is related to contact killing in which the bacterial surfaces are ruptured by the surface structures specifically nanopillars [173] and nanowires [174]. Although this can be defined as antibacterial due to killing the bacteria, these are grouped here due to not containing any active compounds that illicit the killing of the target cell.

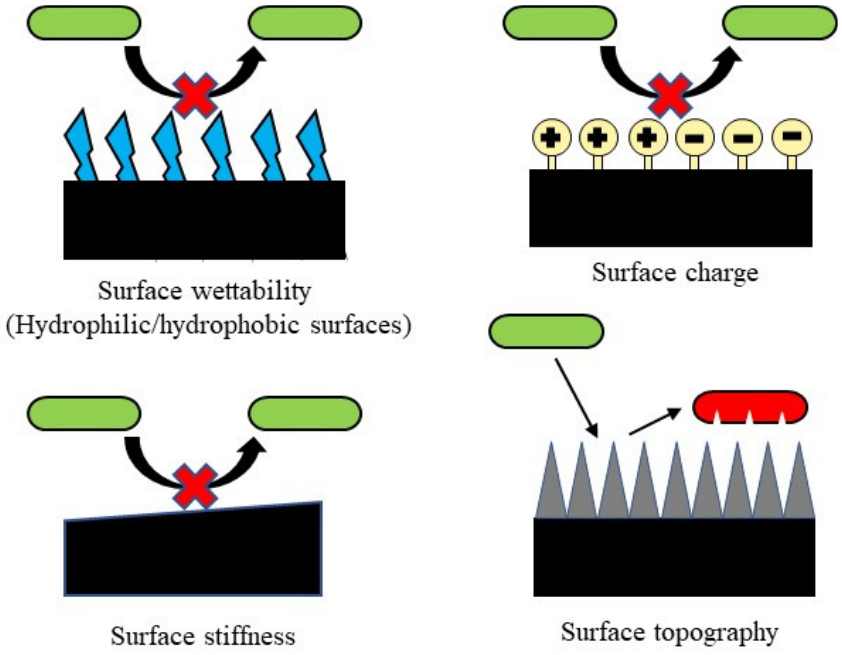

Figure 1.2 Non-active antimicrobial containing surface strategies to limit microbial adhesion representing surface wettability, surface charge, surface stiffness and surface topography approaches. Adapted from [124].

Another such development takes inspiration from the dragon-fly wing was tested by Ivanova *et al.* [165] in which black silicon surface nanopillars mechanically disrupted the cell integrity of tested Gram-negative and Gram-positive bacteria.

1.5.3 Active compound containing antimicrobial surfaces

Although physical surface modifications listed above provide the approach in preventing bacterial adhesion, however they cannot always successfully prevent adhesion thereby rendering them ineffective for their designed purpose. Therefore, an alternative design approach is the development of active compound containing surfaces in which the bacterial targets are directly killed when encountering the surface (Figure 1.3). Active antimicrobial surfaces treatments can be broadly categorised as being developed using surface polymerisation, coatings, surface functionalisation or

as natural materials which possess intrinsic antimicrobial activity [124,159,161,175] (Table 1.1). Briefly, surface polymerisation involves modifying a surface using covalent bonding or atom radical transfer of the antimicrobial agent to the surface [175,176]. These include and are not limited to antimicrobial metals, which also display intrinsic activity, such as Zn^{2+}, Ag^{+}, Ca^{2+}, polymers ,with the most notable and widely used being chitosan, and antimicrobial peptides [161,177] (Table 1.2). Silver for example, possesses substantial antimicrobial activity and therefore has an extensive record in being used in medical applications [178] with applications of silver nanoparticles having been vastly explored in biomaterials for implants, namely catheters [179]. The activity of the metals is proposed to be linked to two methods, namely the generation of oxidative stress resulting in the formation of reactive oxygen species (ROS), as observed in studies performed by Richards *et al.* [180] and Xiao *et al.* [181] in which the addition of gold (Au) resulted in an increase of ROS resulting in increased biofilm inhibition and killing activity when compared to H_2O_2 alone. The second method of activity may be attributed to the binding of the free metal ions to the bacterial membrane leading to overall bacterial membrane disruption and ultimately cellular death [182] as was observed in a study using Zn^{2+} in which bacterial cells underwent cellular shrinking, twisting and then cellular death [183].

The loading or immobilisation of an antimicrobial compounds, such as polymers, on a material (physiochemical absorption) is another method in which active surface can used in active material development (Table 1.2). This is achieved by covalently bonding a surface material with the polymer, such as QACs, due to their high degree of activity but also long-term stability and activity [124]. As described earlier, QACs are the primary active ingredient in current disinfectants, with compounds such as chlorohexidine, nitric acid and benzalkonium chloride [25,161], and are useful due to their strong bacterial contact killing by destroying the bacterial membrane [183].

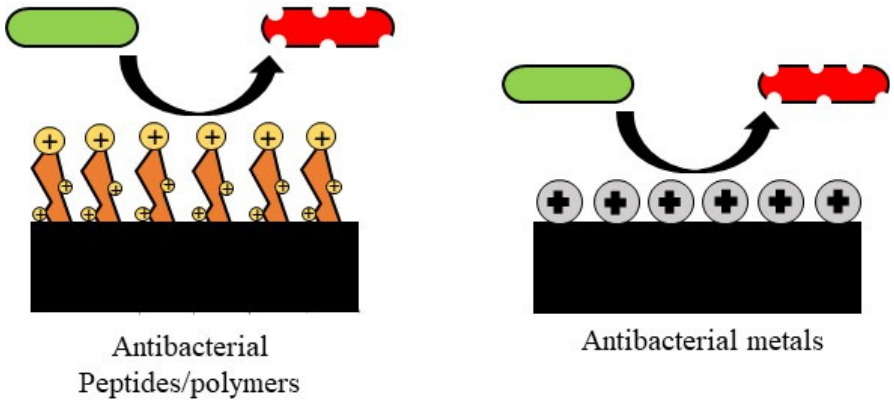

Figure 1.3 Summary of described active compound containing antimicrobial surfaces with the schematics representing the antibacterial peptides/polymers and the antibacterial metals. Adapted from [124].

Table 1.2 Different antimicrobial groups and material applications

Group	Active agent	Application	References
Polymer	Polyvinyl pyridine polymers (QACs)	Disinfectants, water treatment, healthcare, pharmaceutical applications	[184]
	DDA bromide	Medicine	[193]
Nanoparticles	Silver	Medicine, wound dressing, cosmetics, plastics	[194]
	TiO_2	Medical, water purification	[188]
Natural	AMPs	Biomaterials, pharmaceuticals	[195]
	Plant leaves and animal skin inspired surfaces	Medicine, industry vessels and pipes, ship hulls	[165]

Surface studies using hydrophobic polycation QACs were observed to display activity when covalently bonded to the surfaces [175]. Additionally, studies using N-alkylated poly(ethyleneimines) (PEIs) by being covalently bonded to cotton, wool and various polyester surfaces displayed varying degrees of activity which was linked to variation in the size and weight of the PEIs [184]. This is achieved due to the positive charge carried on the nitrogen in the ammonium group that interacts with the negative bacterial lipid membrane leading to lipid disruption [185]. Interestingly, antimicrobial enzymes have also displayed great potential when applied to materials with examples such as hydrolysing enzymes (subtilins) [186] and various polysaccharide degrading enzymes (amylases and lysozymes) showing significant activity against bacteria when assessing the active surfaces [186].

Another method in developing active surfaces is photo activated surfaces with titanium oxide (TiO_2) being the most well documented and studies material with it not only exhibiting activity to a wide range of targets such a bacteria, fungi and viruses but it also being applied in various applications (skincare, water treatment and wall coatings) [189,190]. Activity of TiO_2 is maintained for a long period of time and this can be linked to the surfaces only being activated once exposed and subsequently irradiated by a specific light energy (photon) [191,192]. Once activated, the generation of ROS occurs due to a photo-oxidative reaction between O_2 and H_2O_2 taking place on the surface. The generated ROS will bind to the cell membrane leading to cellular leaked and later lysis [191,192].

The application of active compounds to materials can be performed using the coatings approach in which surface coatings is the most used method for the fabrication of antibacterial materials and surfaces [159,196]. This method can be defined as either the incorporation or build-up of an antibacterial compound into or onto the material, from which the activity of the antimicrobial compound is either due to coming into direct contact with the microbial target or being by releasing itself from the surface [175]. Incorporation of the antimicrobial compound occurs at the beginning of

material development in which the compound is added to the ingredients during production leading to a mixture of material and antimicrobial. The advantage this provides is that not only is the surface protected from bacterial attachment and colonisation but also deeper layers in the material possess antibacterial activity resulting in much longer prolonged activity even when the material is severely worn out and degraded [197]. This approach was successfully tested using textile fibres against *S. aureus* by Li *et al*. [198] in which the produced bandages containing ciprofloxacin resulted in decreased wound infection when exposed to *E. coli* and *S. aureus* species in animal rat trials [198]. Han *et al*. [199] were able to successfully develop dental adhesive by incorporating methacrylates (QACs). When testing the biofilm formation of *Streptococcus mutans* (*S. mutans*), *Streptococcus gordonii* (*S. gordonii*) and *Streptococcus sanguins* (*S. sanguins*) they observed significantly decreased biofilm formation compared to dental adhesive without QACs [199].

Alternative to incorporation is the coating of a material with the active compound is achieved by either adsorption (non-covalent modification) of the compound onto the material surface, covalently binding it to the material or via compound immobilisation to the material using self-assembly layers onto the surface (non-covalent) [161]. Although antibiotics are not favoured to be used for coatings, the application of antibiotic coatings was shown to be successful in a study performed by Neut *et al*. [200]. The authors coated gentamycin onto a prosthetic hip and this coating resulted to limiting *S. aureus* biofilm growing and adhesion on the prosthetic hip surface. Studies by Iyamba *et al.* [201] using QACs showed that when the compounds were immobilised onto catheters, there was a significant reduction in *S. aureus* adhesion, whereas in the second study of Zanini *et al.* [202] observed increased activity towards *E. coli* leading to decreased surface adhesion when compared to the control surfaces was observed.

The development of active surfaces has gained traction with the focus moving from antibiotics, due to the ability of resistance development, to alternative compounds such as QACs. However, as elaborated on earlier in this chapter, bacteria have started developing resistance and tolerance towards currently utilised disinfectants and sterilising agents such as QACs with an additional drawback of QAC surfaces being their ability to induce irritation and inflammation [203]. A group of compounds that have gained much attention and hold great potential in solving QAC drawback, as well as reduce resistance development are antimicrobial peptides (AMPs). AMPs are a class of peptides with broad spectrum of activity, multiple modes of action (Figure 1.4) and low susceptibility to induce resistance with recent studies showing the significant advantages that AMPs have resulting in them being desirable active compound for loading onto materials [204,205]. Ma *et al.* [204]. successfully loaded the HHC-36 AMP onto TiO_2 nanotubes and observed significant anti-biofilm and anti-microbial activity when assessed against *S. aureus* (activity was > 99%). Additionally, Cassin *et al*. [206] was

able to develop anti-infection films for injured tissues when using LL-37 in combination with collagen.

1.5.4 Antimicrobial peptides as actives in coatings

As described above, AMPs show great promise and have gained significant interest due to the various advantageous characteristics they possess. Therefore, as they hold such great promise, AMPs can be used as the active ingredient in the coatings. Factors that need to be considered when developing an ideal antimicrobial coating when using a antimicrobial polymer can also be applied when selecting for a antimicrobial peptide. These factors are that the active compound 1) is easy and inexpensive to produce, 2) has long-term stability, 3) is not soluble in water when used for water-disinfection 4). does not produce any toxins when broken down, 5) does not cause skin irritation or have toxic effects towards people working with it and most importantly 6) possess antimicrobial/biocidal activity towards a large broad spectrum of pathogenic microorganisms, 7) without eliciting resistance.

Antimicrobial peptides are characterised as small peptides that display a broad range of activity towards a wide array of microorganisms such as bacteria, fungi, viruses and parasites [207-209]. Additionally, the rapid multi-mode of action antimicrobial activity possessed by AMPs is another advantage [208,209]. Furthermore, many of the host AMPs have various roles in biological functions such as immune regulation [210], wound healing [211] and antitumor activity [212]. AMPs serve as the first line host defence to clear infections due to drug resistant bacteria, the latter being the consequence of overuse of antibiotics [213]. This is because AMPs show substantial advantageous due to their broad range of activity and multi-modes of action such as eliciting activity on the bacterial membrane, inducing cellular leakage, exert intracellular actions, binding to DNA, RNA or preventing cellular processes [209,214] (Figure 1.4). These actions explain their potent antimicrobial activity towards antibiotic resistant bacteria [209,214].

AMPs have been isolated from a wide array of organisms such as microorganisms [215], reptiles [216], birds [217], mammals [218], and plants [219]. Nisin, a very well-known AMP isolated from lactic acid bacteria, has been shown to disrupt and destroy the bacterial membranes and inhibits bacterial cellular function by disrupting the bacterial DNA against a wide array of Gram-positive and Gram-negative bacteria [220]. Furthermore, nisin is generally regarded as safe (GRAS) and possesses antiseptic properties that has been extensively utilised as a natural preservative in various food products [220]. Plant AMPs such as the thionins, defensins and cyclotides have an important role in protection by protecting plants from pathogenic microorganisms from the air and soil environments [221]. In mammals, AMPs have a vital role in the innate immune system from which two classes of AMPs have been derived namely, cathelicidines and defensins [222]. The first class of AMPs the

cathelicidines exhibit broad antimicrobial activity towards multiple Gram-positive and Gram-negative bacteria [223] and have been isolated from fish [223], rabbits [224 and goats [225] with humans only having one cathelicidin, LL-37 [226]. Cathelicidins are broad spectrum but selective with cathelicidin-PV having activity towards Gram-positive and Gram -negative bacteria, various fungi, multiple antibiotic-resistant bacteria all the while having low haemolytic activity [227]. The second AMP group, defensins, can be divided based on the arrangement of the disulphide bonds resulting in α- , β- and θ-defensins [228] with α- and β- defensins only being present in humans, β-defensins in reptiles and birds and θ-defensins in lower primates [222].

Variation in AMP amino acid composition, charge and structure gives rise to variation in peptide structure and properties, further limiting the resistance development possibilities. From this vertebrate AMPs can be subdivided into four distinct groups namely, anionic AMPs [208,209,229], cationic α-helical AMPs [208,209,229], β-sheet AMPs [208,209,229] and lastly extended cationic AMPs [208,209,229,231]. Briefly, anionic AMPs are comprised of α-helical peptides and cyclic cystine knots [229] and can interact with microbes via salt bridges formed by utilising metal ions and the negative membrane charge [230]. Cationic α-helical AMPs are disordered when in an aqueous solution but in the presence of liposomes, phospholipids and micelles are transformed into a amphiphilic α-helical structures as 50% of the amino acids are hydrophobic [231]. Cationic β-sheet AMPs, mostly comprised of defensins [229], which are comprised of 2-8 cysteine amino acid residues leading to the formation of 1-4 intramolecular disulphide bonds that are essential in structural stabilisation and eliciting biological activity of the peptides [229]. Lastly extended cationic AMPs are comprised of specific amino acids such as proline, tryptophan, glycine, arginine and histidine, however, they lack secondary structures [229,231] with their structures relying on only hydrogen bonds and Van der Waal forces in order to interact with the target membrane [232].

The interest in developing surfaces that are able in preventing bacterial adhesion and subsequent biofilm formation that in turn prevents or decreases infection and disease transmission has increased drastically in recent years. Investigation into various materials and surfaces using AMPs has been performed as shown in Table 1.3, with their success further driving a wider array of AMPs to be used and applied to surfaces for the goal of application. Using the non-ribosomal synthesised peptide , vancomycin, Zhang *et al.* [234] showed that the coating was able to inhibit *S. aureus* bacterial growth [234].

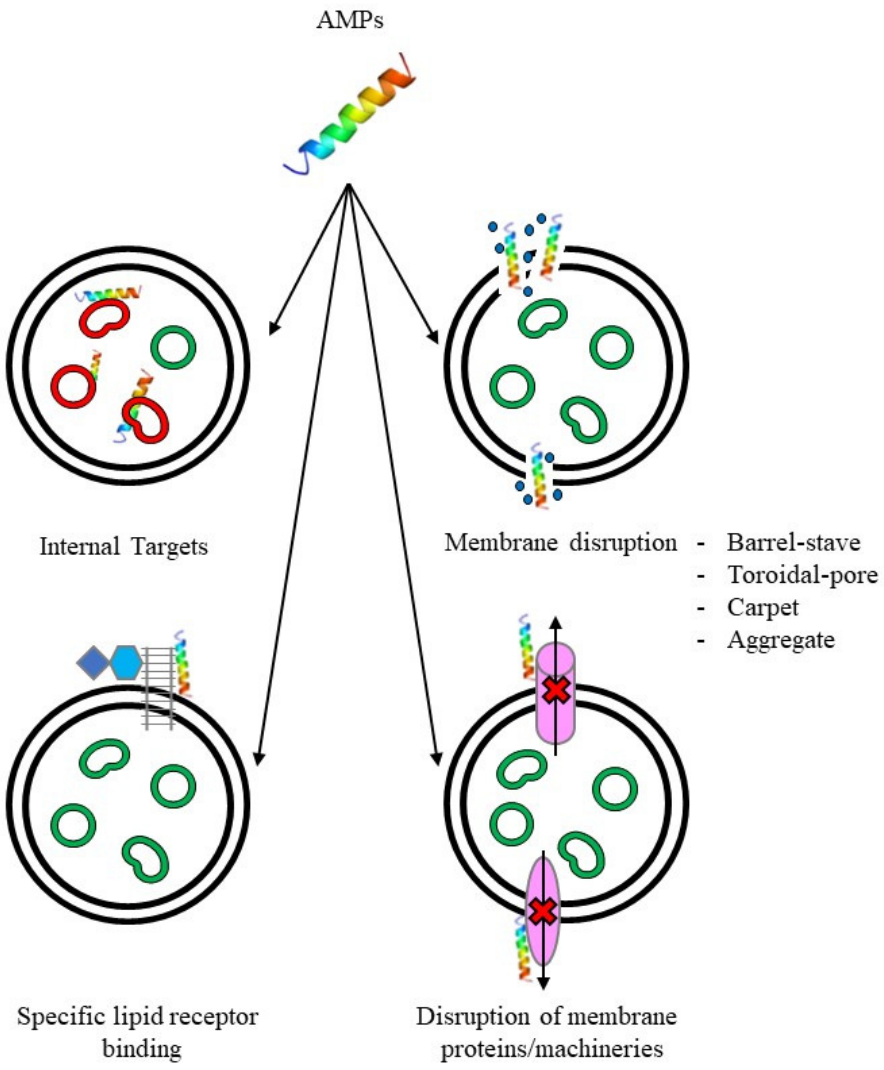

Figure 1.4 General summary of proposed modes of action and cellular targets of antimicrobial peptides. Adapted from [233].

Material studies looking at latex gloves and glass slides were performed by Jeong *et al.* [235] in which the AMP SHAP1 was immobilised onto the latex gloves and glass slide with the activity assessment towards *E*. coli and *S. aureus* having killed > 96% of the cells when in contact with the surface of the tested materials [235]. Studies using wool fibres immobilised with cecropin-B from the giant silk moth and a synthetic analogue [Ala^5]-$triTrp^7$ were found to be extremely stable when exposed to harsh heating and wash cycles and were found to have maintained activity towards S. *aureus* and *Klebsiella pneumoniae* [236].

Table 1.3 Various antimicrobial peptides used in the successful creation of active materials/surfaces assessed towards different microbial targets

Antimicrobial peptide	Material/ Surface	Microbial Target	Mode of action	Reference
KLR	Polystyrene*	*E. coli* and *S. aureus*	Cellular inhibition (100% inhibition)	237
Nisin-Z	High density polyethylene*	*S. epidermidis*	Inhibition of adhesion and cellular inhibition	238
SHAP1-GS-Cys	Slide glass* Latex glove*	*E. coli* and *S. aureus*	>99% cellular inhibition	235
GL13K	Collagen*	*E. coli* and *S. epidermidis*	Surface contact inhibition	239
β-peptide	Polyethylene*	*Candida albicans*	Reduced biofilm adhesion and growth	240
Caspofungin	Titanium*	*C. albicans*	Cellular adhesion and proliferation inhibition	241
LL-37	Cotton*	*S. aureus* and *K. pneumoniae*	Cellular membrane lysis	242
Magainin II	Stainless steel*	*E. coli* and *S. aureus*	Cellular membrane lysis	243
Tyrocidines	Various materials and surfaces#	*L. monocytogenes* and *Micrococcus luteus*	Cellular membrane lysis	244,245

*Covalent attachment between material and peptide, #-Adsorption of peptide to material

A specific AMP group of great interest are the tyrocidines and analogues (Trcs) (Table 1.4), specifically because they have been previously shown to stick to surfaces with a Trc-cellulose based material having maintained activity after being exposed to a wide array of harsh conditions [244,245]. These peptides are therefore the focus of this study specifically in developing highly active formulations for surface applications (reported in this study in Chapter 3- 5) and will be discussed in more detail below.

1.6 The tyrocidines and analogues

The challenges posed by AMR bacteria has shifted the focus from using antibiotics to alternative, effective and low-resistance development profiled compounds, from which AMPs are a very suitable and undervalued option. The Trcs and their analogues, a group of cationic cyclic β-sheet decapeptides, are isolated from the soil bacterium *Brevibacillus parabrevis* from the tyrothricin complex [246,247].

Although shown to be very haemolytic [248] thereby limiting application to only topical [249,250] and oral applications [251], the Trcs were the first antibiotic to be used in the medical industry [249]. The tyrothricin complex is comprised of two peptide groups namely the linear gramicidins and the cationic cyclic β-decapeptides the tyrocidines (Trcs) [252]. Although the Trcs are limited in application, the Trcs have been shown to exhibit a broad range of activity towards an array of different microorganisms, such as various Gram-positive bacteria [246,247,253], the malaria parasite *Plasmodium falciparum* (*P. falciparum*) [254], pathogenic yeast *C. albicans* [255] and various filamentous fungi [256,257]. Furthermore, studies performed by Van Rensburg and Rautenbach [245] found that the Trcs readily associate and bind to various material types, with main selectivity towards cellulose making them of specific interest for surface related applications. Additionally, it was recently shown by Kumar *et al.* [258] that changes to the solvent concentrations influence the Trcs polymorphic surface morphologies which in turn influenced the activity of the peptide towards it target. Therefore, as limited understanding into the role of various solvents and additives on the Trcs was present, the focus of this research is investigating how the Trcs and Trc analogues can be manipulated for optimal antimicrobial surface application.

1.6.1 Tyrocidines structural characteristics

The Trcs and Trc analogues from the tyrothricin complex are comprised of 28 different analogues as described by Tang *et al.* [259], with the primary amino acid sequence being highly conserved. The Trcs and Trc analogues are comprised of a highly conserved amino acid sequence, (*cyclo*-[f^{1}-P^{2}-X^{3}-x^{4}-N^{5}-Q^{6}-X^{7}-V^{8}-X^{9}-L^{10}]), with variation at position three, four, and nine giving rise to different analogues (Figure 1.5). The tyrocidine mixture used in this study is comprised of six major analogues namely TrcA, $TrcA_1$, TrcB, $TrcB_1$, TrcC and $TrcC_1$ with variability of the dipeptide amino acid moiety position three and four ($Phe^{3,4}$ or $Trp^{3,4}$) giving rise to the different analogues A, B and C whereas variation of position nine (Orn^{9} or Lys^{9}) giving rise to the A_1, B_1 and C_1 analogues [260]. Furthermore, substituting the amino acid at position seven defines the Trc analogue produced in which Tyr^{7} gives rise to the tyrocidines, Phe^{7} the phenycidines and Trp^{7} the tryptocidines (refer to Chapter 2 Table 2.1 for details on the Trc and analogues).

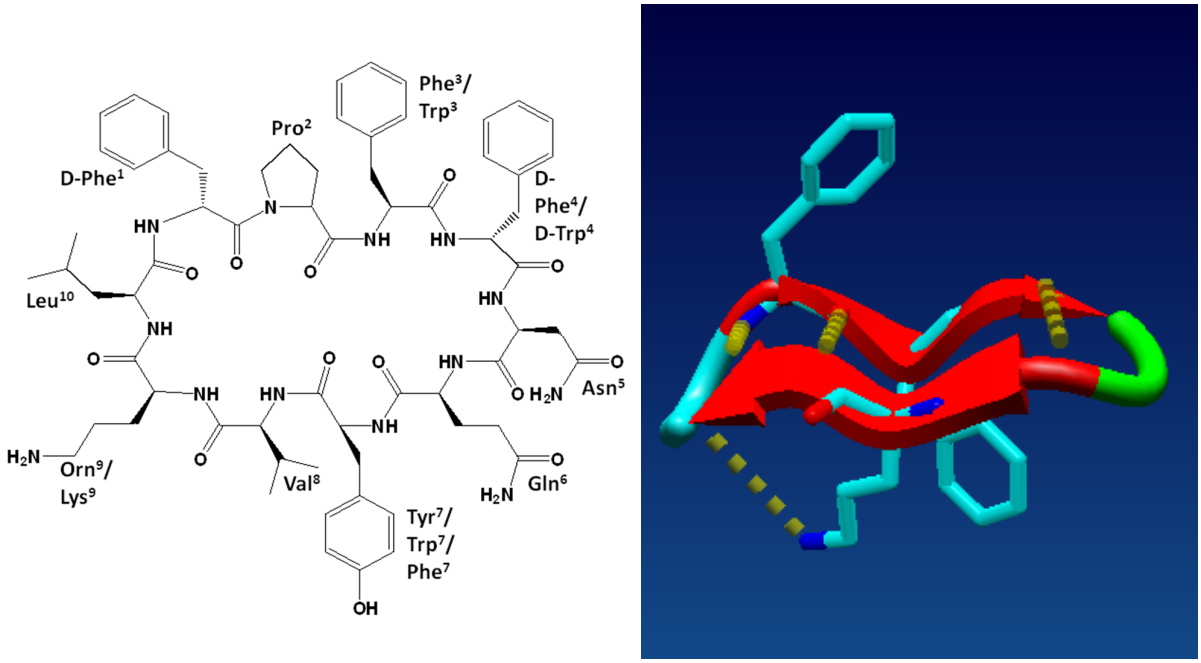

Figure 1.5 The primary structure of the tyrocidine A (left) showing the variable amino acid residues given by their three letter abbreviations with Phe[3] D-Phe[4] designating tyrocidine B, Trp[3] D-Trp[4] denoting tyrocidine C and substitution of Orn[9] to Lys[9] giving rise to the tyrocidine A_1, tyrocidine B_1 and tyrocidine C_1 analogues. Amino acid substitution of Tyr[7] with Trp[7] and Phe[7] produces the tryptocidines and phenycidines, respectively. The low energy 3-D model structure of tyrocidine A (right) of Munyuki *et al.* [261] represents the secondary structures of two antiparallel β-sheets connected via type I and type II β-turns, with the intramolecular hydrogen bonds between the peptide backbone amides and the orientation of the aromatic residues also represented. Figure reproduced with permission from M. Rautenbach (unpublished data).

Structural studies performed on the Trcs have shown that the Trcs when in an aqueous solution develops into a two-stranded antiparallel β-sheet connected by tight turns at either end, type I (slightly distorted turn) and type II' [261,262]. The antiparallel β-sheets are formed between Trp[3]-Asn[5] and Val[8]-Leu[10] with the Type I turn being between Gln[6]-Tyr[7] and the Type II' being between Phe[1]-Pro[2] [261,262]. Peptide stabilisation of the two strains are connected by three intramolecular hydrogen bonds between the amide and carbonyl groups (Phe[3]-Leu[10], Asn[5]-Val[8] and Leu[10]-Phe[3] amide to carbonyl respectively) [262]. A fourth hydrogen bond is present between Val[8] and the side chain of Asn[5], whereas the strand-to-strand stabilisation within the monomer is driven by hydrophobic interactions between the Phe[4], Val[8] and Leu[10] [262]. Studies related to the polarity and structure formation of the Trcs have shown that when the Trcs are in their monomeric state the peptides amphipathicity is minimal due to there being no separation of the hydrophobic and hydrophilic amino acid residues [261]. Trcs dimer studies the formation of backbone-backbone hydrogens bonds between two Trc monomers by either sideways hydrogen bond interaction or via aromatic stacking [261,262]. The formed dimer is highly amphipathic in which the concave face of the dimer is polar

in character whereas the convex or opposite face adopts a strong apolar nature [262]. As the dimer conformation is assumed to be the active moiety state of the peptide, the amphipathic dimer structure suggests membrane association and disruption with the hydrophobic face inserting into the membrane whereas the polar concave facer would orientate towards the polar outer environment [262]. This would be brought about as the cationic amino acid residues would be interactive with the negatively charged bacterial membrane leading to the D-Trp4/Phe^4 anchoring the dimer [262]. This would result in the hydrophobic effect driving the hydrophobic cluster to be pushed into the membrane leading to pore formation [262].

1.6.2 Tyrocidine antimicrobial activity

The Trcs have been shown in multiple studies to have broad spectrum activity to a wide range of microbial targets such as the Gram-positive bacteria *L. monocytogenes* [253], *S. aureus* [263] and *M. luteus* [253]. It also exhibits activity against various fungal species namely filamentous plant fungi such as *Fusarium solani, Botrytis cinerea, Neurospora crassa* and *Aspergillus fumigatus* [256,258]. Furthermore, the Trcs possess anti-malaria activity as shown by Rautenbach *et al.* [254] demonstrating anti-malaria activity of by the Trcs on the human malaria pathogen *P. falciparum* by disruption of the parasitic cell-cycle development. The Trcs have been observed to be active against the pathogenic yeast *C. albicans* against the planktonic and biofilm cells, with TpcC showing the least activity of all the analogues assessed, as well as displaying biofilm eradiation for TrcA, TrcB and TrcC [255].

Mode of action studies performed on the Trcs have shown they are able to illicit both membrane related activity as well as non-lytic alternative modes of action [260]. Trc interaction has been shown to be related to interaction between the peptide and lipid in the cellular membrane [264] leading to cellular death due to the disruption imposed on the membrane [244]. Membrane association and orientation has been proposed by Loll *et al*. [262] in which the convex hydrophobic face of the Trcs dimer would be inserted into the cellular peptidoglycan bilayer whereas the polar concave face would orientate outwards, which is potentially indicative of a barrel-stave or toroidal-pore mode of action [262]. Furthermore, multiple alternative modes of action have been suggested to be performed by the Trcs ranging from binding to DNA leading to transcriptional inhibition in *Br. parabrevis* [265,266], cell cycle regulation [267] as well as inactivation of the glucose metabolism as a secondary process [246]. Non-lytic modes of action have been shown to be further enhanced or improved in the presence of metal ions specifically as shown by Spathelf [260] and Leussa [268] in which Ca^{2+} induced a non-lytic mode of action of the Trcs assessed toward *L. monocytogenes*.

The utilisation of Trcs as the active ingredient in the development of surface sterilisation applications hold significant promise. As has been shown, the Trcs readily associate with surfaces and that changes to their activity can be influenced by their solvent environment [258]. However, as they readily oligomerise leading to a potential loss of activity [258,261,262], screening for optimised Trc formulations is paramount due to the great promise and potential the Trcs hold, since it fulfils all six of the earlier mentioned requirements of an active antimicrobial coating/surface. Therefore, this study focussed on further optimising the Trcs in formulations, as the active compounds, specifically for surface sterilisation by maintaining or improving the antimicrobial activity while limiting peptide oligomerisation. This was achieved by using six different solvent systems namely, acetonitrile (ACN), ethanol (EtOH), iso-propanol (IPA), propylene-glycol (PG), tertiary-butanol (TBA) and methanol (MeOH) alone or in formulation with three different additives being glycerol (Glr), zinc chloride ($ZnCl_2$) and calcium chloride ($CaCl_2$) at specific concentrations.

1.7 References

1. C Reygaert, W. An overview of the antimicrobial resistance mechanisms of bacteria. *AIMS Microbiology* 2018, *4* (3), 482–501.
2. Munita, J. M.; Arias, C. A. Mechanisms of antibiotic resistance. *Microbiology Spectrum* 2016, *4* (2), 1–37.
3. Pulingam, T.; Parumasivam, T.; Gazzali, A. M.; Sulaiman, A. M.; Chee, J. Y.; Lakshmanan, M.; Chin, C. F.; Sudesh, K. Antimicrobial resistance: Prevalence, economic burden, mechanisms of resistance and strategies to overcome. *European Journal of Pharmaceutical Sciences* 2022, *170*, 106103.
4. Carrascosa, C.; Raheem, D.; Ramos, F.; Saraiva, A.; Raposo, A. Microbial biofilms in the food industry—a comprehensive review. *International Journal of Environmental Research and Public Health* 2021, *18* (4), 2014-2045.
5. Russotto, V.; Cortegiani, A.; Raineri, S. M.; Giarratano, A. Bacterial contamination of inanimate surfaces and equipment in the Intensive Care Unit. *Journal of Intensive Care* 2015, *3* (1), 1-8.
6. Davies, J.; Davies, D. Origins and Evolution of Antibiotic Resistance. *Microbiology and Molecular Biology Reviews* 2010, *74* (3), 417–433.
7. Condell, O.; Iversen, C.; Cooney, S.; Power, K. A.; Walsh, C.; Burgess, C.; Fanning, S. Efficacy of biocides used in the modern food industry to control *Salmonella enterica*, and links between biocide tolerance and resistance to clinically relevant antimicrobial compounds. *Applied and Environmental Microbiology* 2012, *78* (9), 3087–3097.
8. Curiao, T.; Marchi, E.; Grandgirard, D.; León-Sampedro, R.; Viti, C.; Leib, S. L.; Baquero, F.; Oggioni, M. R.; Martinez, J. L.; Coque, T. M. Multiple adaptive routes of *Salmonella enterica Typhimurium* to biocide and antibiotic exposure. *BMC Genomics* 2016, *17* (1), 1–16.
9. Fair, R. J.; Tor, Y. Antibiotics and bacterial resistance in the 21st century. *Perspectives in Medicinal Chemistry* 2014, *6*, 25–64.
10. Murugaiyan, J.; Kumar, P. A.; Rao, G. S.; Iskandar, K.; Hawser, S.; Hays, J. P.; Mohsen, Y.; Adukkadukkam, S.; Awuah, W. A.; Jose, R. A.; Sylvia, N.; Nansubuga, E. P.; Tilocca, B.; Roncada, P.; Roson-Calero, N.; Moreno-Morales, J.; Amin, R.; Kumar, B. K.; Kumar, A.; Toufik, A.-R.; Zaw, T. N.; Akinwotu, O. O.; Satyaseela, M. P.; van Dongen, M. B. Progress in alternative strategies to combat antimicrobial resistance: Focus on antibiotics. *Antibiotics* 2022, *11* (2), 1–37.
11. Wang, L.; Hu, C.; Shao, L. The antimicrobial activity of nanoparticles: Present situation and prospects for the future. *International Journal of Nanomedicine* 2017, *Volume 12*, 1227–1249.
12. Andersson, D. I. The biological cost of mutational antibiotic resistance: Any practical conclusions? *Current Opinion in Microbiology* 2006, *9* (5), 461–465.
13. Andersson, D. I.; Hughes, D. Persistence of antibiotic resistance in bacterial populations. *FEMS Microbiology Reviews* 2011, *35* (5), 901–911.
14. Surette, M. D.; Wright, G. D. Lessons from the environmental antibiotic resistome. *Annual Review of Microbiology* 2017, *71* (1), 309–329.
15. Centre for Disease Control and Prevention. 2019 antibiotic resistance threats report. Available at: https://www.cdc.gov/drugresistance/biggest-threats.html (accessed Nov 28, 2022).

16. C Reygaert, W. An overview of the antimicrobial resistance mechanisms of bacteria. *AIMS Microbiology* 2018, *4* (3), 482–501.
17. Zhaxybayeva, O.; Doolittle, W. F. Lateral Gene Transfer. *Current Biology* 2011, *21* (7), 1–5.
18. Mc Carlie, S.; Boucher, C. E.; Bragg, R. R. Molecular basis of bacterial disinfectant resistance. *Drug Resistance Updates* 2020, *48*, 1–9.
19. Marino, M.; Frigo, F.; Bartolomeoli, I.; Maifreni, M. Safety-related properties of *Staphylococci* isolated from food and food environments. *Journal of Applied Microbiology* 2010, *110* (2), 550–561.
20. Langsrud, S.; Sidhu, M. S.; Heir, E.; Holck, A. L. Bacterial disinfectant resistance—a challenge for the food industry. *International Biodeterioration & Biodegradation* 2003, *51* (4), 283–290.
21. Bjorland, J.; Steinum, T.; Kvitle, B.; Waage, S.; Sunde, M.; Heir, E. Widespread distribution of disinfectant resistance genes among *Staphylococci* of bovine and caprine origin in Norway. *Journal of Clinical Microbiology* 2005, *43* (9), 4363–4368.
22. Long, M.; Lai, H.; Deng, W.; Zhou, K.; Li, B.; Liu, S.; Fan, L.; Wang, H.; Zou, L. Disinfectant susceptibility of different *Salmonella* serotypes isolated from chicken and egg production chains. *Journal of Applied Microbiology* 2016, *121* (3), 672–681.
23. Gebel, J.; Gemein, S.; Kampf, G.; Pidot, S. J.; Buetti, N.; Exner, M. Isopropanol at 60% and at 70% are effective against 'isopropanol-tolerant' *Enterococcus faecium*. *Journal of Hospital Infection* 2019, *103* (1), 1–4.
24. Cooper, I. R.; White, J.; Mahenthiralingam, E.; Hanlon, G. W. Long-term persistence of a single *Legionella pneumophila* strain possessing the mip gene in a municipal shower despite repeated cycles of chlorination. *Journal of Hospital Infection* 2008, *70* (2), 154–159.
25. Chen, B.; Han, J.; Dai, H.; Jia, P. Biocide-tolerance and antibiotic-resistance in community environments and risk of direct transfers to humans: unintended consequences of community-wide surface disinfecting during COVID-19? *Environmental Pollution* 2021, *283*, 1–15.
26. Buffet-Bataillon, S.; Tattevin, P.; Bonnaure-Mallet, M.; Jolivet-Gougeon, A. Emergence of resistance to antibacterial agents: The role of quaternary ammonium compounds—a critical review. *International Journal of Antimicrobial Agents* 2012, *39* (5), 381–389.
27. He, G.-X.; Landry, M.; Chen, H.; Thorpe, C.; Walsh, D.; Varela, M. F.; Pan, H. Detection of benzalkonium chloride resistance in community environmental isolates of *Staphylococci*. *Journal of Medical Microbiology* 2014, *63* (5), 735–741.
28. Jia, S.; Jia, R.; Zhang, K.; Sun, S.; Lu, N.; Wang, M.; Zhao, Q. Disinfection characteristics of *Pseudomonas peli,* a chlorine-resistant bacterium isolated from a water supply network. *Environmental Research* 2020, *185*, 1–8.
29. Ortega Morente, E.; Fernández-Fuentes, M. A.; Grande Burgos, M. J.; Abriouel, H.; Pérez Pulido, R.; Gálvez, A. Biocide tolerance in bacteria. *International Journal of Food Microbiology* 2013, *162* (1), 13–25.
30. Falkinham, J. O.; Hilborn, E. D.; Arduino, M. J.; Pruden, A.; Edwards, M. A. Epidemiology and ecology of opportunistic premise plumbing pathogens: *Legionella pneumophila*, *Mycobacterium avium*, and *Pseudomonas aeruginosa*. *Environmental Health Perspectives* 2015, *123* (8), 749–758.
31. Jia, S.; Bian, K.; Shi, P.; Ye, L.; Liu, C.-H. Metagenomic profiling of antibiotic resistance genes and their associations with bacterial community during multiple disinfection regimes in a full-scale drinking water treatment plant. *Water Research* 2020, *176*, 1–11.
32. Sheldon, A. T. Antiseptic "resistance": real or perceived threat? *Clinical Infectious Diseases* 2005, *40* (11), 1650–1656.
33. Maillard, J.-Y. Resistance of bacteria to biocides. *Microbiology Spectrum* 2018, *6* (2), 1–17.
34. Kim, M.; Hatt, J. K.; Weigand, M. R.; Krishnan, R.; Pavlostathis, S. G.; Konstantinidis, K. T. Genomic and transcriptomic insights into how bacteria withstand high concentrations of benzalkonium chloride biocides. *Applied and Environmental Microbiology* 2018, *84* (12), 1–15.
35. Horinouchi, T.; Sakai, A.; Kotani, H.; Tanabe, K.; Furusawa, C. Improvement of isopropanol tolerance of *Escherichia coli* using adaptive laboratory evolution and OMICS technologies. *Journal of Biotechnology* 2017, *255*, 47–56.
36. Carraro, N.; Burrus, V. The dualistic nature of integrative and conjugative elements. *Mobile Genetic Elements* 2015, *5* (6), 98–102.
37. Johnson, C. M.; Grossman, A. D. Integrative and conjugative elements (ICES): What they do and how they work. *Annual Review of Genetics* 2015, *49* (1), 577–601.
38. Shintani, M.; Sanchez, Z. K.; Kimbara, K. Genomics of microbial plasmids: Classification and identification based on replication and transfer systems and host taxonomy. *Frontiers in Microbiology* 2015, *6*, 1–16.
39. Milani, E. S.; Hasani, A.; Varschochi, M.; Sadeghi, J.; Memar, M. Y.; Hasani, A. Biocide resistance in *Acinetobacter baumannii*: Appraising the mechanisms. *Journal of Hospital Infection* 2021, *117*, 135–146.
40. Elhanafi, D.; Dutta, V.; Kathariou, S. Genetic Characterization of plasmid-associated benzalkonium chloride resistance determinants in a *Listeria monocytogenes* strain from the 1998-1999 outbreak. *Applied and Environmental Microbiology* **2010**, *76* (24), 8231–8238.
41. Norman, A.; Hansen, L. H.; She, Q.; Sørensen, S. J. Nucleotide Sequence of pola52: A conjugative incx1 plasmid from *Escherichia eoli* which enables biofilm formation and multidrug efflux. *Plasmid* 2008, *60* (1), 59–74.

42. Tabata, A.; Nagamune, H.; Maeda, T.; Murakami, K.; Miyake, Y.; Kourai, H. Correlation between resistance of *Pseudomonas aeruginosa* to quaternary ammonium compounds and expression of outer membrane protein OPRR. *Antimicrobial Agents and Chemotherapy* 2003, *47* (7), 2093–2099.
43. Hu, H.; Johani, K.; Gosbell, I. B.; Jacombs, A. S. W.; Almatroudi, A.; Whiteley, G. S.; Deva, A. K.; Jensen, S.; Vickery, K. Intensive care unit environmental surfaces are contaminated by multidrug-resistant bacteria in biofilms: Combined results of conventional culture, pyrosequencing, scanning electron microscopy, and confocal laser microscopy. *Journal of Hospital Infection* 2015, *91* (1), 35–44.
44. Rayner, J.; Veeh, R.; Flood, J. Prevalence of microbial biofilms on selected fresh produce and household surfaces. *International Journal of Food Microbiology* 2004, *95* (1), 29–39.
45. Ledwoch, K.; Dancer, S. J.; Otter, J. A.; Kerr, K.; Roposte, D.; Rushton, L.; Weiser, R.; Mahenthiralingam, E.; Muir, D. D.; Maillard, J.-Y. Beware biofilm! Dry biofilms containing bacterial pathogens on multiple healthcare surfaces; a multi-centre Study. *Journal of Hospital Infection* 2018, *100* (3), 1–24.
46. Cooper, I. R.; Hanlon, G. W. Resistance of *Legionella pneumophila* Serotype 1 biofilms to chlorine-based disinfection. *Journal of Hospital Infection* 2010, *74* (2), 152–159.
47. Shen, Y.; Huang, C.; Lin, J.; Wu, W.; Ashbolt, N. J.; Liu, W.-T.; Nguyen, T. H. Effect of disinfectant exposure on *Legionella pneumophila* associated with simulated drinking water biofilms: release, inactivation, and infectivity. *Environmental Science & Technology* 2017, *51* (4), 2087–2095.
48. Smith, K.; Hunter, I. S. Efficacy of common hospital biocides with biofilms of multi-drug resistant clinical isolates. *Journal of Medical Microbiology* 2008, *57* (8), 966–973.
49. Bridier, A.; Briandet, R.; Thomas, V.; Dubois-Brissonnet, F. Resistance of bacterial biofilms to disinfectants: A review. *Biofouling* 2011, *27* (9), 1017–1032.
50. Chapman, J. S. Disinfectant resistance mechanisms, cross-resistance, and co-resistance. *International Biodeterioration & Biodegradation* 2003, *51* (4), 271–276.
51. Conibear, T. C.; Collins, S. L.; Webb, J. S. Role of mutation in *Pseudomonas aeruginosa* biofilm development. *PLoS ONE* 2009, *4* (7), 1–8.
52. Ehlers, L. J.; Bouwer, E. J. Rp4 plasmid transfer among species of *Pseudomonas* in a Biofilm reactor. *Water Science and Technology* 1999, *39* (7), 163–171.
53. Wong, H. S.; Townsend, K. M.; Fenwick, S. G.; Trengove, R. D.; O'Handley, R. M. Comparative susceptibility of planktonic and 3-day-old *Salmonella typhimurium* biofilms to disinfectants. *Journal of Applied Microbiology* 2009, 1–7.
54. Flemming, H.-C.; Wingender, J.; Szewzyk, U.; Steinberg, P.; Rice, S. A.; Kjelleberg, S. Biofilms: An emergent form of bacterial life. *Nature Reviews Microbiology* 2016, *14* (9), 563–575.
55. Latorre, A. A.; Van Kessel, J. S.; Karns, J. S.; Zurakowski, M. J.; Pradhan, A. K.; Boor, K. J.; Jayarao, B. M.; Houser, B. A.; Daugherty, C. S.; Schukken, Y. H. Biofilm in milking equipment on a dairy farm as a potential source of bulk tank milk contamination with *Listeria monocytogene*s. *Journal of Dairy Science* 2010, *93* (6), 2792–2802.
56. Storgårds, E.; Tapani, K.; Hartwall, P.; Saleva, R.; Suihko, M.-L. Microbial attachment and biofilm formation in brewery bottling plants. *Journal of the American Society of Brewing Chemists* 2006, *64* (1), 8–15.
57. Bryers, J. D. Medical biofilms. *Biotechnology and Bioengineering* 2008, *100* (1), 1–18.
58. Lewandowski, Z.; Avci, R.; Geiser, M.; Shi, X.; Braughton, K.; Yurt, N. Biofouling and corrosion of stainless steels in natural waters. *Water Supply* 2002, *2* (4), 65–72.
59. Awad, T. S.; Asker, D.; Hatton, B. D. Food-safe modification of stainless steel food-processing surfaces to reduce bacterial biofilms. *ACS Applied Materials & Interfaces* 2018, *10* (27), 22902–22912.
60. Reis, M. de; de Paula, R. S.; Reis, A. L.; Souza, C. C.; Júnior, R. B.; Ferreira, J. A.; Mota, H. R.; de Carvalho, M. D.; Jorge, E. C.; Cardoso, A. V.; Nascimento, A. M. Microbial composition of a hydropower cooling water system reveals thermophilic bacteria with a possible role in primary biofilm formation. *Biofouling* 2021, *37* (2), 246–256.
61. Carpentier, B.; Cerf, O. Biofilms and their consequences, with particular reference to hygiene in the food industry. *Journal of Applied Bacteriology* 1993, *75* (6), 499–511.
62. Mishra, R.; Panda, A. K.; De Mandal, S.; Shakeel, M.; Bisht, S. S.; Khan, J. Natural anti-biofilm agents: Strategies to control biofilm-forming pathogens. *Frontiers in Microbiology* 2020, 11, 1–23.
63. Roy, R.; Tiwari, M.; Donelli, G.; Tiwari, V. Strategies for combating bacterial biofilms: A focus on anti-biofilm agents and their mechanisms of action. *Virulence* 2018, 9 (1), 522–554.
64. Dunne, W. M. Bacterial adhesion: Seen any good biofilms lately? *Clinical Microbiology Reviews* 2002, *15* (2), 155–166.
65. Goldberg, J. Biofilms and antibiotic resistance: A genetic linkage. *Trends in Microbiology* 2002, *10* (6), 264.
66. Peng, J.-S.; Tsai, W.-C.; Chou, C.-C. Inactivation and removal of *Bacillus cereus* by sanitizer and detergent. *International Journal of Food Microbiology* 2002, *77* (1-2), 11–18.
67. Chen, M. J.; Zhang, Z.; Bott, T. R. Direct measurement of the adhesive strength of biofilms in pipes by micromanipulation. *Biotechnology Techniques* 1998, *12* (12), 875–880.

68. Koch, B.; Worm, J.; Jensen, L. E.; Højberg, O.; Nybroe, O. Carbon limitation induces s-dependent gene expression in *Pseudomonas fluorescens* in Soil. *Applied and Environmental Microbiology* 2001, *67* (8), 3363–3370.
69. Madsen, J. S.; Burmølle, M.; Hansen, L. H.; Sørensen, S. J. The interconnection between biofilm formation and horizontal gene transfer. *FEMS Immunology & Medical Microbiology* 2012, *65* (2), 183–195.
70. Mah, T.-F. Biofilm-specific antibiotic resistance. *Future Microbiology* 2012, *7* (9), 1061–1072.
71. Mah, T.-F. C.; O'Toole, G. A. Mechanisms of biofilm resistance to antimicrobial agents. *Trends in Microbiology* 2001, *9* (1), 34–39.
72. John, A.-K.; Schmaler, M.; Khanna, N.; Landmann, R. Reversible daptomycin tolerance of adherent S*taphylococci* in an implant infection model. *Antimicrobial Agents and Chemotherapy* 2011, *55* (7), 3510–3516.
73. Vigeant, M. A.-S.; Ford, R. M.; Wagner, M.; Tamm, L. K. Reversible and irreversible adhesion of motile E*scherichia coli* cells analysed by total internal reflection aqueous fluorescence microscopy. *Applied and Environmental Microbiology* 2002, *68* (6), 2794–2801.
74. Carniello, V.; Peterson, B. W.; van der Mei, H. C.; Busscher, H. J. Physico-chemistry from initial bacterial adhesion to surface-programmed biofilm growth. *Advances in Colloid and Interface Science* 2018, *261*, 1–14.
75. Yuan, Y.; Hays, M. P.; Hardwidge, P. R.; Kim, J. Surface characteristics influencing bacterial adhesion to polymeric substrates. *RSC Advances* 2017, *7* (23), 14254–14261.
76. Garrett, T. R.; Bhakoo, M.; Zhang, Z. Bacterial adhesion and biofilms on surfaces. *Progress in Natural Science* 2008, *18* (9), 1049–1056.
77. Boks, N. P.; Kaper, H. J.; Norde, W.; Busscher, H. J.; van der Mei, H. C. Residence time dependent desorption of *Staphylococcus epidermidis* from hydrophobic and hydrophilic substrata. *Colloids and Surfaces B: Biointerfaces* 2008, *67* (2), 276–278.
78. Meinders, J. M.; van der Mei, H. C.; Busscher, H. J. Deposition efficiency and reversibility of bacterial adhesion under flow. *Journal of Colloid and Interface Science* 1995, *176* (2), 329–341.
79. Busscher, H. J.; Norde, W.; Sharma, P. K.; van der Mei, H. C. Interfacial re-arrangement in initial microbial adhesion to surfaces. *Current Opinion in Colloid & Interface Science* 2010, *15* (6), 510–517.
80. Hayashi, H.; Seiki, H.; Tsuneda, S.; Hirata, A.; Sasaki, H. Influence of growth phase on bacterial cell electrokinetic characteristics examined by soft particle electrophoresis theory. *Journal of Colloid and Interface Science* 2003, *264* (2), 565–568.
81. Eboigbodin, K. E.; Newton, J. R.; Routh, A. F.; Biggs, C. A. Bacterial quorum sensing and cell surface electrokinetic properties. *Applied Microbiology and Biotechnology* 2006, *73* (3), 669–675.
82. Renner, L. D.; Weibel, D. B. Physicochemical regulation of biofilm formation. *MRS Bulletin* 2011, *36* (5), 347–355.
83. De Weger, L. A.; van der Vlugt, C. I.; Wijfjes, A. H.; Bakker, P. A.; Schippers, B.; Lugtenberg, B. Flagella of a plant-growth-stimulating *Pseudomonas fluorescens* strain are required for colonization of potato roots. *Journal of Bacteriology* 1987, *169* (6), 2769–2773.
84. Spears, K. J.; Roe, A. J.; Gally, D. L. A Comparison of enteropathogenic and enterohaemorrhagic *Escherichia coli* pathogenesis . *FEMS Microbiology Letters* 2006, *255* (2), 187–202.
85. Van Houdt, R.; Michiels, C. W. Role of bacterial cell surface structures in *Escherichia coli* biofilm formation. *Research in Microbiology* 2005, *156* (5-6), 626–633.
86. Beech, I. B. Corrosion of technical materials in the presence of biofilms: Current understanding and state-of-the art methods of study. *International Biodeterioration & Biodegradation* 2004, *53* (3), 177–183.
87. Hall-Stoodley, L.; Costerton, J. W.; Stoodley, P. Bacterial biofilms: From the natural environment to infectious diseases. *Nature Reviews Microbiology* 2004, *2* (2), 95–108.
88. Kaplan, J. B. Biofilm dispersal: mechanisms, clinical implications, and potential therapeutic Uses. *Journal of Dental Research* 2010, *89* (3), 205–218.
89. Petrova, O. E.; Sauer, K. Escaping the biofilm in more than one way: desorption, detachment or dispersion. *Current Opinion in Microbiology* 2016, *30*, 67–78.
90. Hook, A. L.; Chang, C.-Y.; Yang, J.; Luckett, J.; Cockayne, A.; Atkinson, S.; Mei, Y.; Bayston, R.; Irvine, D. J.; Langer, R.; Anderson, D. G.; Williams, P.; Davies, M. C.; Alexander, M. R. Combinatorial discovery of polymers resistant to bacterial attachment. *Nature Biotechnology* 2012, *30* (9), 868–875.
91. Bazaka, K.; Crawford, R. J.; Ivanova, E. P. Do bacteria differentiate between degrees of nanoscale surface roughness? *Biotechnology Journal* 2011, *6* (9), 1103–1114.
92. Banerjee, I.; Pangule, R. C.; Kane, R. S. Antifouling coatings: Recent developments in the design of surfaces that prevent fouling by proteins, bacteria, and marine organisms. *Advanced Materials* 2010, *23* (6), 690–718.
93. Yang, X.; Zhang, W.; Qin, X.; Cui, M.; Guo, Y.; Wang, T.; Wang, K.; Shi, Z.; Zhang, C.; Li, W.; Wang, Z. Recent progress on bioinspired antibacterial surfaces for biomedical application. *Biomimetics* 2022, *7* (3), 88.
94. Chao, Y.; Zhang, T. Probing Roles of lipopolysaccharide, type 1 fimbria, and colanic acid in the attachment of *Escherichia coli* strains on inert surfaces. *Langmuir* 2011, *27* (18), 11545–11553.
95. Cheng, G.; Zhang, Z.; Chen, S.; Bryers, J. D.; Jiang, S. Inhibition of bacterial adhesion and biofilm formation on zwitterionic surfaces. *Biomaterials* 2007, *28* (29), 4192–4199.

96. Dexter, S. C.; Sullivan, J. D.; Williams, J.; Watson, S. W. Influence of substrate wettability on the attachment of marine bacteria to various surfaces. *Applied Microbiology* 1975, *30* (2), 298–308.
97. Goulter-Thorsen, R. M.; Taran, E.; Gentle, I. R.; Gobius, K. S.; Dykes, G. A. CsgA production by *Escherichia coli* o157:h7 alters attachment to abiotic surfaces in some growth environments. *Applied and Environmental Microbiology* 2011, *77* (20), 7339–7344.
98. Absolom, D. R.; Lamberti, F. V.; Policova, Z.; Zingg, W.; van Oss, C. J.; Neumann, A. W. Surface thermodynamics of bacterial adhesion. *Applied and Environmental Microbiology* 1983, *46* (1), 90–97.
99. Chen, C.; Petterson, T.; Illergård, J.; Ek, M.; Wågberg, L. Influence of cellulose charge on bacteria adhesion and viability to Pvam/CNF/PVAM-modified cellulose model surfaces. *Biomacromolecules* 2019, *20* (5), 2075–2083.
100. Gottenbos, B.; Van der Mei, H. C.; Busscher, H. J.; Grijpma, D. W.; Feijen, J. Initial adhesion and surface growth of *Pseudomonas aeruginosa* on negatively and positively charged Poly(methacrylates) . *Journal of Materials Science: Materials in Medicine* 1999, *10* (12), 853–855.
101. Zhu, X.; Jańczewski, D.; Guo, S.; Lee, S. S.; Parra Velandia, F. J.; Teo, S. L.-M.; He, T.; Puniredd, S. R.; Vancso, G. J. Polyion multilayers with precise surface charge control for antifouling. *ACS Applied Materials & Interfaces* 2014, *7* (1), 852–861.
102. Ueshima, M.; Tanaka, S.; Nakamura, S.; Yamashita, K. Manipulation of bacterial adhesion and proliferation by surface charges of electrically polarized hydroxyapatite. *Journal of Biomedical Materials Research* **2002**, *60* (4), 578–584.
103. Rzhepishevska, O.; Hakobyan, S.; Ruhal, R.; Gautrot, J.; Barbero, D.; Ramstedt, M. The surface charge of anti-bacterial coatings alters motility and biofilm architecture. *Biomaterials Science* 2013, *1* (6), 589–602.
104. Xing, R.; Lyngstadaas, S. P.; Ellingsen, J. E.; Taxt-Lamolle, S.; Haugen, H. J. The influence of surface nano roughness, texture and chemistry of tizr implant abutment on oral biofilm accumulation. *Clinical Oral Implants Research* 2014, *26* (6), 649–656.
105. Yu, P.; Wang, C.; Zhou, J.; Jiang, L.; Xue, J.; Li, W. Influence of surface properties on adhesion forces and attachment of *Streptococcus mutans* to zirconia in vitro. *BioMed Research International* 2016, *2016*, 1–10.
106. Yoda, I.; Koseki, H.; Tomita, M.; Shida, T.; Horiuchi, H.; Sakoda, H.; Osaki, M. Effect of surface roughness of biomaterials on staphylococcus epidermidis adhesion. *BMC Microbiology* 2014, *14* (1).
107. James, G. A.; Boegli, L.; Hancock, J.; Bowersock, L.; Parker, A.; Kinney, B. M. Bacterial adhesion and biofilm formation on textured breast implant shell materials. *Aesthetic Plastic Surgery* 2018, *43* (2), 490–497.
108. Helbig, R.; Günther, D.; Friedrichs, J.; Rößler, F.; Lasagni, A.; Werner, C. The impact of structure dimensions on initial bacterial adhesion. *Biomaterials Science* 2016, *4* (7), 1074–1078.
109. Chien, H.-W.; Chen, X.-Y.; Tsai, W.-P.; Lee, M. Inhibition of biofilm formation by rough shark skin-patterned surfaces. *Colloids and Surfaces B: Biointerfaces* 2020, *186*, 110738.
110. Watson, G. S.; Green, D. W.; Schwarzkopf, L.; Li, X.; Cribb, B. W.; Myhra, S.; Watson, J. A. A Gecko skin micro/nano structure – a Low adhesion, superhydrophobic, anti-wetting, self-cleaning, biocompatible, antibacterial surface. *Acta Biomaterialia* 2015, *21*, 109–122.
111. Ma, J.; Sun, Y.; Gleichauf, K.; Lou, J.; Li, Q. Nanostructure on taro leaves resists fouling by colloids and bacteria under submerged conditions. *Langmuir* 2011, *27* (16), 10035–10040.
112. Perni, S.; Prokopovich, P. Micropatterning with conical features can control bacterial adhesion on silicone. *Soft Matter* 2013, *9* (6), 1844–1851.
113. Linklater, D. P.; Nguyen, H. K.; Bhadra, C. M.; Juodkazis, S.; Ivanova, E. P. Influence of nanoscale topology on bactericidal efficiency of black silicon surfaces. *Nanotechnology* 2017, *28* (24), 245301.
114. Chang, Y.-R.; Weeks, E. R.; Ducker, W. A. Surface topography hinders bacterial surface motility. *ACS Applied Materials & Interfaces* 2018, *10* (11), 9225–9234.
115. Booth, I. R. Regulation of cytoplasmic pH in bacteria. *Microbiological Reviews* 1985, *49* (4), 359–378.
116. Stepanović, S.; Ćirković, I.; Mijač, V.; Švabić-Vlahović, M. Influence of the incubation temperature, atmosphere and dynamic conditions on biofilm formation by S*almonella spp.*. *Food Microbiology* 2003, *20* (3), 339–343.
117. Thomen, P.; Robert, J.; Monmeyran, A.; Bitbol, A.-F.; Douarche, C.; Henry, N. Bacterial biofilm under flow: first a physical struggle to stay, then a matter of breathing. *PLOS ONE* 2017, *12* (4).
118. Limoli, D. H.; Jones, C. J.; Wozniak, D. J. Bacterial extracellular polysaccharides in biofilm formation and function. *Microbiology Spectrum* 2015, *3* (3).
119. Hou, J.; Veeregowda, D. H.; van de Belt-Gritter, B.; Busscher, H. J.; van der Mei, H. C. Extracellular polymeric matrix production and relaxation under fluid shear and mechanical pressure in *Staphylococcus aureus* biofilms. *Applied and Environmental Microbiology* 2018, *84* (1).
120. Rodesney, C. A.; Roman, B.; Dhamani, N.; Cooley, B. J.; Katira, P.; Touhami, A.; Gordon, V. D. Mechano sensing of shear by *Pseudomonas aeruginosa* leads to increased levels of the Cyclic-Di-GMP signal initiating biofilm development. *Proceedings of the National Academy of Sciences* 2017, *114* (23), 5906–5911.
121. Kramer, A.; Assadian, O. Survival of microorganisms on inanimate surfaces. *Use of Biocidal Surfaces for Reduction of Healthcare Acquired Infections* 2014, 7–26.
122. Tuladhar, E.; Hazeleger, W. C.; Koopmans, M.; Zwietering, M. H.; Beumer, R. R.; Duizer, E. Residual viral and bacterial contamination of surfaces after cleaning and disinfection. *Applied and Environmental Microbiology* 2012, *78* (21), 7769–7775.

123. Donaghy, J..; Jagadeesan, B..; Goodburn, K.; Grunwald, L..; Jensen, O..; Jespers, A,D.; Kanagachandran, K.; Lafforgue H; Seefelder, W.; Quentin, M. Relationship of sanitizers, disinfectants, and cleaning agents with antimicrobial resistance. *Journal of Food Protection* 2019, *82* (5), 889–902.
124. Yang, X.; Zhang, W.; Qin, X.; Cui, M.; Guo, Y.; Wang, T.; Wang, K.; Shi, Z.; Zhang, C.; Li, W.; Wang, Z. Recent progress on bioinspired antibacterial surfaces for biomedical application. *Biomimetics* 2022, *7* (3), 2–25.
125. Jildeh, Z. B.; Wagner, P. H.; Schöning, M. J. Sterilization of objects, products, and packaging surfaces and their characterization in different fields of industry: The status in 2020. *physica status solidi (a)* 2021, *218* (13), 1–27.
126. Wales, A.; Davies, R. Co-selection of resistance to antibiotics, biocides and heavy metals, and its relevance to foodborne pathogens. *Antibiotics* 2015, *4* (4), 567–604.
127. Kaer, P.; vrek, J.; Syslov, K.; Vclavk, J.; Pavlk, D.; erven, J.; Kuzm, M. Vapor Phase hydrogen peroxide – method for decontamination of surfaces and working areas from organic pollutants. *Organic Pollutants Ten Years After the Stockholm Convention - Environmental and Analytical Update* 2012, 1–34.
128. Sandle, T. Sterility, sterilisation and microorganisms. *Sterility, Sterilisation and Sterility Assurance for Pharmaceuticals* 2013, 1–20.
129. Aparecida da Silva, K. A. In gamma radiation; INTECH Open Access Publisher: Rijeka, Croatia, 2012; pp 171–206.
130. Pruß, K.; Stirtzel, S.; Kulozik, U. Influence of the surface temperature of packaging specimens on the inactivation of B*acillus* spores by means of gaseous H_2O_2 . *Journal of Applied Microbiology* 2012, *112* (3), 493–501.
131. Unger-Bimczok, B.; Kottke, V.; Hertel, C.; Rauschnabel, J. The Influence of humidity, hydrogen peroxide concentration, and condensation on the inactivation of *Geobacillus stearothermophilus* spores with hydrogen peroxide vapor. *Journal of Pharmaceutical Innovation* 2008, *3* (2), 123–133.
132. Lambert, B. J.; Mendelson, T. A.; Craven, M. D. Radiation and ethylene oxide terminal sterilization experiences with drug eluting stent products. *AAPS PharmSciTech* 2011, *12* (4), 1116–1126.
133. Rogers, J. V.; Sabourin, C. L. K.; Choi, Y. W.; Richter, W. R.; Rudnicki, D. C.; Riggs, K. B.; Taylor, M. L.; Chang, J. Decontamination assessment of bacillus anthracis, *Bacillus subtilis*, and G*eobacillus stearothermophilus* spores on indoor surfaces using a hydrogen peroxide gas generator. *Journal of Applied Microbiology* 2005, *99* (4), 739–748.
134. Bounoure, F.; Fiquet, H.; Arnaud, P. Comparison of hydrogen peroxide and peracetic acid as isolator sterilization agents in a hospital pharmacy. *American Journal of Health-System Pharmacy* 2006, *63* (5), 451–455.
135. Singh, R.; Singh, D.; Singh, A. Radiation sterilization of tissue allografts: A review. *World Journal of Radiology* 2016, *8* (4), 1–16.
136. EPA. List N advanced search page: Disinfectants for coronavirus (COVID-19) . https://www.epa.gov/coronavirus/list-n-advanced-search-page-disinfectants-coronavirus-covid-19 (accessed Nov 12, 2022). 2021
137. van Dijk, H. F.; Verbrugh, H. A.; Abee, T.; Andriessen, J. W.; van Dijk, H. F.; ter Kuile, B. H.; Mevius, D. J.; Montforts, M. H.; van Schaik, W.; Schmitt, H.; Smidt, H.; Veening, J.-W.; Voss, A. Resisting disinfectants. *Communications Medicine* 2022, *2* (1), 1–5.
138. Harbarth, S.; Tuan Soh, S.; Horner, C.; Wilcox, M. H. Is reduced susceptibility to disinfectants and antiseptics a risk in healthcare settings? A point/counterpoint review. *Journal of Hospital Infection* 2014, *87* (4), 194–202.
139. Levy, S. B.; Marshall, B. Antibacterial resistance worldwide: Causes, challenges and responses. *Nature Medicine* 2004, *10* (S12), 122–129.
140. Mann, A.; Nehra, K.; Rana, J. S.; Dahiya, T. Antibiotic resistance in agriculture: perspectives on upcoming strategies to overcome upsurge in resistance. *Current Research in Microbial Sciences* 2021, *2*, 1–14.
141. Samtiya, M.; Matthews, K. R.; Dhewa, T.; Puniya, A. K. Antimicrobial resistance in the food chain: trends, mechanisms, pathways, and possible regulation strategies. *Foods* 2022, *11* (19), 1–20.
142. Jit, M.; Ng, D. H.; Luangasanatip, N.; Sandmann, F.; Atkins, K. E.; Robotham, J. V.; Pouwels, K. B. Quantifying the economic cost of antibiotic resistance and the impact of related interventions: Rapid methodological review, conceptual framework and recommendations for future studies. *BMC Medicine* 2020, *18* (1), 1–14.
143. Milani, E. S.; Hasani, A.; Varschochi, M.; Sadeghi, J.; Memar, M. Y.; Hasani, A. Biocide resistance in *acinetobacter baumannii*: Appraising the mechanisms. *Journal of Hospital Infection* 2021, *117*, 135–146.
144. Merchel Piovesan Pereira, B.; Wang, X.; Tagkopoulos, I. Biocide-Induced emergence of antibiotic resistance in *Escherichia coli*. *Frontiers in Microbiology* 2021, *12*, 1–12.
145. Mulder, I.; Siemens, J.; Sentek, V.; Amelung, W.; Smalla, K.; Jechalke, S. Quaternary ammonium compounds in soil: Implications for antibiotic resistance development. *Reviews in Environmental Science and Bio/Technology* 2017, *17* (1), 159–185.
146. Nabi, G.; Wang, Y.; Hao, Y.; Khan, S.; Wu, Y.; Li, D. Massive use of disinfectants against COVID-19 poses potential risks to urban wildlife. *Environmental Research* 2020, *188*, 1–12.
147. Banciu, A. R.; Ionescu, L.; Ionica, D. L.; Mitru, D.; Nita-Lazar, M. Efficiency of biocides on the aquatic systems through bacterial model. *Revista de Chimie* 2020, *71* (1), 57–60.
148. Murray, A. K. The novel coronavirus COVID-19 outbreak: Global implications for antimicrobial resistance. *Frontiers in Microbiology* 2020, *11*, 1–4.

149. Usman, M.; Farooq, M.; Hanna, K. Environmental side effects of the injudicious use of antimicrobials in the era of COVID-19. *Science of The Total Environment* 2020, *745*, 1–3.
150. Laustsen, S.; Lund, E.; Bibby, B. M.; Kristensen, B.; Thulstrup, A. M.; Møller, J. K. Effect of correctly using alcohol-based hand rub in a clinical setting. *Infection Control & Hospital Epidemiology* 2008, *29* (10), 954–956.
151. Loo, V. G. environmental interventions to control C*lostridium difficile*. *Infectious Disease Clinics of North America* 2015, *29* (1), 83–91.
152. Kang, C. I.; Kim, S. H.; Bang, J. W.; Kim, H. B.; Kim, N. J.; Kim, E. C.; Oh, M. D.; Choe, K. W. Community-acquired versus nosocomial *Klebsiella pneumoniae* bacteremia: Clinical features, treatment outcomes, and clinical implication of antimicrobial resistance. *Journal of Korean Medical Science* 2006, *21* (5), 816–822.
153. Peng, C.; Zong, Z.; Fan, H. A*cinetobacter baumannii* isolates associated with community-acquired pneumonia in West China. *Clinical Microbiology and Infection* 2012, *18* (12), 1–3.
154. He, G.-X.; Landry, M.; Chen, H.; Thorpe, C.; Walsh, D.; Varela, M. F.; Pan, H. Detection of benzalkonium chloride resistance in community environmental isolates of *Staphylococci*. *Journal of Medical Microbiology* 2014, *63* (5), 735–741.
155. Carson, R. T.; Larson, E.; Levy, S. B.; Marshall, B. M.; Aiello, A. E. Use of antibacterial consumer products containing quaternary ammonium compounds and drug resistance in the community. *Journal of Antimicrobial Chemotherapy* 2008, *62* (5), 1160–1162.
156. Weber, D. J.; Rutala, W. A.; Sickbert-Bennett, E. E. Use of germicides in health care settings- Is there a relationship between germicide use and antimicrobial resistance: A concise review. *American Journal of Infection Control* 2019, *47*, A106–A109.
157. Rutala, W. A.; Weber, D. J. Surface disinfection: Treatment time (wipes and sprays) versus contact time (liquids). *Infection Control & Hospital Epidemiology* 2018, *39* (3), 329–331.
158. Song, X.; Vossebein, L.; Zille, A. Efficacy of disinfectant-impregnated wipes used for surface disinfection in hospitals: A Review. *Antimicrobial Resistance & Infection Control* 2019, *8* (1), 1–14.
159. Hasan, J.; Crawford, R. J.; Ivanova, E. P. Antibacterial surfaces: The quest for a new generation of biomaterials. *Trends in Biotechnology* 2013, *31* (5), 295–304.
160. Otter, J. A.; French, G. L. Bacterial contamination on touch surfaces in the public transport system and in public areas of a hospital in London. *Letters in Applied Microbiology* 2009, *49* (6), 803–805.
161. Querido, M. M.; Aguiar, L.; Neves, P.; Pereira, C. C.; Teixeira, J. P. Self-disinfecting surfaces and infection control. *Colloids and Surfaces B: Biointerfaces* 2019, *178*, 8–21.
162. Bazaka, K.; Jacob, M. V.; Crawford, R. J.; Ivanova, E. P. Efficient surface modification of biomaterial to prevent biofilm formation and the attachment of microorganisms. *Applied Microbiology and Biotechnology* 2012, *95* (2), 299–311.
163. Variola, F.; Brunski, J. B.; Orsini, G.; Tambasco de Oliveira, P.; Wazen, R.; Nanci, A. nanoscale surface modifications of medically relevant metals: state-of-the art and perspectives. *Nanoscale* 2011, *3* (2), 335–353.
164. Campoccia, D.; Montanaro, L.; Arciola, C. R. A review of the biomaterials technologies for infection-resistant surfaces. *Biomaterials* 2013, *34* (34), 8533–8554.
165. Ivanova, E. P.; Hasan, J.; Webb, H. K.; Truong, V. K.; Watson, G. S.; Watson, J. A.; Baulin, V. A.; Pogodin, S.; Wang, J. Y.; Tobin, M. J.; Löbbe, C.; Crawford, R. J. Natural bactericidal surfaces: Mechanical rupture of *Pseudomonas aeruginosa* cells by cicada wings. *Small* 2012, *8* (16), 2489–2494.
166. Mrabet, B.; Nguyen, M. N.; Majbri, A.; Mahouche, S.; Turmine, M.; Bakhrouf, A.; Chehimi, M. M. Anti-fouling poly(2-hydoxyethyl methacrylate) surface coatings with specific bacteria recognition capabilities. *Surface Science* 2009, *603* (16), 2422–2429.
167. Erathodiyil, N.; Chan, H.-M.; Wu, H.; Ying, J. Y. Zwitterionic polymers and hydrogels for antibiofouling applications in implantable devices. *Materials Today* 2020, *38*, 84–98.
168. Lowe, S.; O'Brien-Simpson, N. M.; Connal, L. A. Antibiofouling polymer interfaces: poly(ethylene glycol) and other promising candidates. *Polymer Chemistry* 2015, *6* (2), 198–212.
169. Chen, S.; Yuan, L.; Li, Q.; Li, J.; Zhu, X.; Jiang, Y.; Sha, O.; Yang, X.; Xin, J. H.; Wang, J.; Stadler, F. J.; Huang, P. Durable antibacterial and nonfouling cotton textiles with enhanced comfort via zwitterionic sulfopropylbetaine coating. *Small* 2016, *12* (26), 3516–3521.
170. Bazaka, K.; Crawford, R. J.; Ivanova, E. P. Do Bacteria differentiate between degrees of nanoscale surface roughness? *Biotechnology Journal* 2011, *6* (9), 1103–1114.
171. Truong, V. K.; Lapovok, R.; Estrin, Y. S.; Rundell, S.; Wang, J. Y.; Fluke, C. J.; Crawford, R. J.; Ivanova, E. P. The Influence of nano-scale surface roughness on bacterial adhesion to ultrafine-grained titanium. *Biomaterials* 2010, *31* (13), 3674–3683.
172. Yang, M.; Ding, Y.; Ge, X.; Leng, Y. Control of bacterial adhesion and growth on honeycomb-like patterned surfaces. *Colloids and Surfaces B: Biointerfaces* 2015, *135*, 549–555.
173. Jenkins, J.; Mantell, J.; Neal, C.; Gholinia, A.; Verkade, P.; Nobbs, A. H.; Su, B. Antibacterial effects of nanopillar surfaces are mediated by cell impedance, penetration and induction of oxidative stress. *Nature Communications* 2020, *11* (1), 1–14.

174. Yasui, T.; Yanagida, T.; Shimada, T.; Otsuka, K.; Takeuchi, M.; Nagashima, K.; Rahong, S.; Naito, T.; Takeshita, D.; Yonese, A.; Magofuku, R.; Zhu, Z.; Kaji, N.; Kanai, M.; Kawai, T.; Baba, Y. Engineering nanowire-mediated cell lysis for microbial cell identification. *ACS Nano* 2019, 1–12.
175. Tiller, J. C.; Liao, C.-J.; Lewis, K.; Klibanov, A. M. Designing surfaces that kill bacteria on contact. *Proceedings of the National Academy of Sciences* 2001, *98* (11), 5981–5985.
176. Yang, W. J.; Cai, T.; Neoh, K.-G.; Kang, E.-T.; Dickinson, G. H.; Teo, S. L.-M.; Rittschof, D. Biomimetic anchors for antifouling and antibacterial polymer brushes on stainless steel. *Langmuir* 2011, *27* (11), 7065–7076.
177. Tripathy, A.; Sen, P.; Su, B.; Briscoe, W. H. Natural and bioinspired nanostructured bactericidal surfaces. *Advances in Colloid and Interface Science* 2017, *248*, 85–104.
178. Shao, W.; Liu, H.; Liu, X.; Wang, S.; Wu, J.; Zhang, R.; Min, H.; Huang, M. Development of silver sulfadiazine loaded bacterial cellulose/sodium alginate composite films with enhanced antibacterial property. *Carbohydrate Polymers* 2015, *132*, 351–358.
179. Deng, J.; Wu, K.; Yang, Y.; Zhang, Y.; Lin, C. Antimicrobial activity and cytocompatibility of silver nanoparticles coated catheters via a biomimetic surface functionalization strategy. *International Journal of Nanomedicine* 2015, 7241–7243.
180. Richards, T.; Harrhy, J. H.; Lewis, R. J.; Howe, A. G.; Suldecki, G. M.; Folli, A.; Morgan, D. J.; Davies, T. E.; Loveridge, E. J.; Crole, D. A.; Edwards, J. K.; Gaskin, P.; Kiely, C. J.; He, Q.; Murphy, D. M.; Maillard, J.-Y.; Freakley, S. J.; Hutchings, G. J. A residue-free approach to water disinfection using catalytic in situ generation of reactive oxygen species. *Nature Catalysis* 2021, *4* (7), 575–585.
181. Xiao, Y.; Xu, M.; Lv, N.; Cheng, C.; Huang, P.; Li, J.; Hu, Y.; Sun, M. Dual stimuli-responsive metal-organic framework-based nanosystem for synergistic photothermal/pharmacological antibacterial therapy. *Acta Biomaterialia* 2021, *122*, 291–305.
182. Li, L.; Cao, L.; Xiang, X.; Wu, X.; Ma, L.; Chen, F.; Cao, S.; Cheng, C.; Deng, D.; Qiu, L. Ros-catalytic transition-metal-based enzymatic nanoagents for tumor and bacterial eradication. *Advanced Functional Materials* 2021, *32* (1), 1–41.
183. Zuo, K.; Wang, L.; Wang, Z.; Yin, Y.; Du, C.; Liu, B.; Sun, L.; Li, X.; Xiao, G.; Lu, Y. Zinc-Doping induces evolution of biocompatible strontium–calcium-phosphate conversion coating on titanium to improve antibacterial property. *ACS Applied Materials & Interfaces* 2022, *14* (6), 7690–7705.
184. Lin, J.; Qiu, S.; Lewis, K.; Klibanov, A. M. Mechanism of bactericidal and fungicidal activities of textiles covalently modified with alkylated polyethylenimine. *Biotechnology and Bioengineering* 2003, *83* (2), 168–172.
185. Gilbert, P.; Moore, L. E. Cationic antiseptics: diversity of action under a common epithet. *Journal of Applied Microbiology* 2005, *99* (4), 703–715.
186. Thallinger, B.; Prasetyo, E. N.; Nyanhongo, G. S.; Guebitz, G. M. antimicrobial enzymes: an emerging strategy to fight microbes and microbial biofilms. *Biotechnology Journal* 2013, *8* (1), 97–109.
187. Beyth, N.; Houri-Haddad, Y.; Baraness-Hadar, L.; Yudovin-Farber, I.; Domb, A. J.; Weiss, E. I. Surface antimicrobial activity and biocompatibility of incorporated polyethylenimine nanoparticles. *Biomaterials* 2008, *29* (31), 4157–4163.
188. JENG, H. U. E. I. W. A. N. G. A. N. N. A.; SWANSON, J. A. M. E. S. Toxicity of metal oxide nanoparticles in mammalian cells. *Journal of Environmental Science and Health, Part A* 2006, *41* (12), 2699–2711.
189. Joost, U.; Juganson, K.; Visnapuu, M.; Mortimer, M.; Kahru, A.; Nõmmiste, E.; Joost, U.; Kisand, V.; Ivask, A. Photocatalytic antibacterial activity of nano-TiO_2 (anatase)-based thin films: Effects on *Escherichia coli* cells and fatty acids. *Journal of Photochemistry and Photobiology B: Biology* 2015, *142*, 178–185.
190. Sadrieh, N.; Wokovich, A. M.; Gopee, N. V.; Zheng, J.; Haines, D.; Parmiter, D.; Siitonen, P. H.; Cozart, C. R.; Patri, A. K.; McNeil, S. E.; Howard, P. C.; Doub, W. H.; Buhse, L. F. Lack of significant dermal penetration of titanium dioxide from sunscreen formulations containing nano- and submicron-size TiO_2 particles. *Toxicological Sciences* 2010, *115* (1), 156–166.
191. Foster, H. A.; Ditta, I. B.; Varghese, S.; Steele, A. Photocatalytic disinfection using titanium dioxide: Spectrum and mechanism of antimicrobial activity. *Applied Microbiology and Biotechnology* 2011, *90* (6), 1847–1868.
192. Kubacka, A.; Diez, M. S.; Rojo, D.; Bargiela, R.; Ciordia, S.; Zapico, I.; Albar, J. P.; Barbas, C.; Martins dos Santos, V. A.; Fernández-García, M.; Ferrer, M. Understanding the antimicrobial mechanism of TiO_2-based nanocomposite films in a pathogenic bacterium. *Scientific Reports* 2014, *4* (1), 1–9.
193. Fik, C. P.; Krumm, C.; Muennig, C.; Baur, T. I.; Salz, U.; Bock, T.; Tiller, J. C. Impact of functional satellite groups on the antimicrobial activity and hemocompatibility of telechelic poly(2-methyloxazoline)s. *Biomacromolecules* 2011, *13* (1), 165–172.
194. Kumar, R.; Münstedt, H. Silver ion release from antimicrobial polyamide/silver composites. *Biomaterials* 2005, *26* (14), 2081–2088.
195. Gao, G.; Lange, D.; Hilpert, K.; Kindrachuk, J.; Zou, Y.; Cheng, J. T. J.; Kazemzadeh-Narbat, M.; Yu, K.; Wang, R.; Straus, S. K.; Brooks, D. E.; Chew, B. H.; Hancock, R. E. W.; Kizhakkedathu, J. N. The biocompatibility and biofilm resistance of implant coatings based on hydrophilic polymer brushes conjugated with antimicrobial peptides. *Biomaterials* 2011, *32* (16), 3899–3909.
196. Knetsch, M. L.; Koole, L. H. New strategies in the development of antimicrobial coatings: The example of increasing usage of silver and silver nanoparticles. *Polymers* 2011, *3* (1), 340–366.

197. Cleophas, R. T.; Sjollema, J.; Busscher, H. J.; Kruijtzer, J. A.; Liskamp, R. M. Characterization and activity of an immobilized antimicrobial peptide containing bactericidal PEG-hydrogel. *Biomacromolecules* 2014, *15* (9), 3390–3395.
198. Li, H.; Williams, G. R.; Wu, J.; Lv, Y.; Sun, X.; Wu, H.; Zhu, L.-M. Thermosensitive nanofibers loaded with ciprofloxacin as antibacterial wound dressing materials. *International Journal of Pharmaceutics* 2017, *517* (1-2), 135–147.
199. Han, Y.; Xu, X.; Tang, J.; Shen, C.; Lin, Q.; Chen, H. Bottom-up fabrication of zwitterionic polymer brushes on intraocular lens for improved biocompatibility. *International Journal of Nanomedicine* 2016, *Volume 12*, 127–135.
200. Neut, D.; Dijkstra, R. J.; Thompson, J. I.; van der Mei, H. C.; Busscher, H. J. A gentamicin-releasing coating for cementless hip prostheses-longitudinal evaluation of efficacy using *in vitro* bio-optical imaging and its wide-spectrum antibacterial efficacy. *Journal of Biomedical Materials Research Part A* 2012, *100A* (12), 3220–3226.
201. Iyamba, J.-M. L.; Okombe, D. T.; Zakanda, F. N.; Malongo, T. K.; Unya, J. W.; Lukukula, C. M.; Balega, N. za. Adherence of *Staphylococcus aureus* to catheter tubing inhibition by quaternary ammonium compounds. *Pan African Medical Journal* 2016, *25*, 1–8.
202. Zanini, S.; Polissi, A.; Maccagni, E. A.; Dell'Orto, E. C.; Liberatore, C.; Riccardi, C. Development of antibacterial quaternary ammonium silane coatings on polyurethane catheters. *Journal of Colloid and Interface Science* 2015, *451*, 78–84.
203. Shi, Z.; Zhang, Y.; Dai, R.; Chen, S.; Zhang, M.; Jin, L.; Wang, J.; Zhao, W.; Zhao, C. Rationally Designed magnetic poly(catechol-hexanediamine) particles for bacteria removal and on-demand biofilm eradication. *Colloids and Surfaces B: Biointerfaces* 2020, *186*, 1–26.
204. Ma, M.; Kazemzadeh-Narbat, M.; Hui, Y.; Lu, S.; Ding, C.; Chen, D. D.; Hancock, R. E.; Wang, R. Local delivery of antimicrobial peptides using self-organized TiO_2 nanotube arrays for peri-implant infections. *Journal of Biomedical Materials Research Part A* 2011, *100A* (2), 278–285.
205. Sibel Akalın, A. Dairy-derived antimicrobial peptides: action mechanisms, pharmaceutical uses and production proposals. *Trends in Food Science & Technology* 2014, *36* (2), 79–95.
206. Cassin, M. E.; Ford, A. J.; Orbach, S. M.; Saverot, S. E.; Rajagopalan, P. The design of antimicrobial LL37-modified collagen-hyaluronic acid detachable multilayers. *Acta Biomaterialia* 2016, *40*, 119–129.
207. Mohammed, I.; Said, D. G.; Dua, H. S. Human antimicrobial peptides in ocular surface defense. *Progress in Retinal and Eye Research* 2017, *61*, 1–22.
208. Zhang, Q.-Y.; Yan, Z.-B.; Meng, Y.-M.; Hong, X.-Y.; Shao, G.; Ma, J.-J.; Cheng, X.-R.; Liu, J.; Kang, J.; Fu, C.-Y. Antimicrobial peptides: mechanism of action, activity and clinical potential. *Military Medical Research* 2021, *8* (1), 1–25.
209. Zhang, L.-juan; Gallo, R. L. Antimicrobial peptides. *Current Biology* 2016, *26* (1), 1–6.
210. Mookherjee, N.; Anderson, M. A.; Haagsman, H. P.; Davidson, D. J. Antimicrobial host defence peptides: Functions and clinical potential. *Nature Reviews Drug Discovery* 2020, *19* (5), 311–332.
211. Pfalzgraff, A.; Brandenburg, K.; Weindl, G. Antimicrobial peptides and their therapeutic potential for bacterial skin infections and wounds. *Frontiers in Pharmacology* 2018, *9*, 1–23.
212. Roudi, R.; Syn, N. L.; Roudbary, M. Antimicrobial peptides as biologic and immunotherapeutic agents against cancer: A comprehensive overview. *Frontiers in Immunology* 2017, *8*, 1–10.
213. Munita, J. M.; Arias, C. A. Mechanisms of antibiotic resistance. *Microbiology Spectrum* 2016, *4* (2), 1–24.
214. Mwangi, J.; Hao, X.; Lai, R.; Zhang, Z.-Y. Antimicrobial peptides: New hope in the war against multidrug resistance. *Zool. Res.* 2019, *40* (6), 488–505.
215. Yazici, A.; Ortucu, S.; Taskin, M.; Marinelli, L. Natural-based antibiofilm and antimicrobial peptides from microorganisms. *Current Topics in Medicinal Chemistry* 2019, *18* (24), 2102–2107.
216. van Hoek, M. L.; Prickett, M. D.; Settlage, R. E.; Kang, L.; Michalak, P.; Vliet, K. A.; Bishop, B. M. The Komodo Dragon (Varanus Komodoensis) Genome and identification of innate immunity genes and clusters. *BMC Genomics* 2019, *20* (1), 1–18.
217. Braun, M. S.; Sporer, F.; Zimmermann, S.; Wink, M. Birds, Feather-degrading bacteria and preen glands: the antimicrobial activity of preen gland secretions from turkeys (*Meleagris gallopavo*) is amplified by keratinase. *FEMS Microbiology Ecology* 2018, *94* (9), 1–29.
218. Wang, X.; Sun, Y.; Wang, F.; You, L.; Cao, Y.; Tang, R.; Wen, J.; Cui, X. A novel endogenous antimicrobial peptide Camp 211-225 derived from casein in human milk. *Food & Function* 2020, *11* (3), 2291–2298.
219. Moyer, T. B.; Heil, L. R.; Kirkpatrick, C. L.; Goldfarb, D.; Lefever, W. A.; Parsley, N. C.; Wommack, A. J.; Hicks, L. M. Pepsavi-MS reveals a proline-rich antimicrobial peptide in *Amaranthus tricolor*. *Journal of Natural Products* 2019, *82* (10), 2744–2753.
220. Gharsallaoui, A.; Oulahal, N.; Joly, C.; Degraeve, P. Nisin as a food preservative: Part 1: physicochemical properties, antimicrobial activity, and main uses. *Critical Reviews in Food Science and Nutrition* 2015, *56* (8), 1262–1274.
221. Srivastava, S.; Dashora, K.; Ameta, K. L.; Singh, N. P.; El-Enshasy, H. A.; Pagano, M. C.; Hesham, A. E. L.; Sharma, G. D.; Sharma, M.; Bhargava, A. Cysteine-rich antimicrobial peptides from plants: The future of antimicrobial therapy. *Phytotherapy Research* 2020, *35* (1), 256–277.

222. Avila, E. E. Functions of antimicrobial peptides in vertebrates. *Current Protein & Peptide Science* 2017, *18* (11), 1098–1119.
223. Chen, C.; Wang, A.; Zhang, F.; Zhang, M.; Yang, H.; Li, J.; Su, P.; Chen, Y.; Yu, H.; Wang, Y. The protective effect of fish-derived cathelicidins on bacterial infections in zebrafish, *Danio rerio*. *Fish & Shellfish Immunology* 2019, *92*, 519–527.
224. Peng, H.; Purkerson, J. M.; Schwaderer, A. L.; Schwartz, G. J. Metabolic acidosis stimulates the production of the antimicrobial peptide cathelicidin in rabbit urine. *American Journal of Physiology-Renal Physiology* 2017, *313* (5), 1–24.
225. Tedde, V.; Bronzo, V.; Puggioni, G. M.; Pollera, C.; Casula, A.; Curone, G.; Moroni, P.; Uzzau, S.; Addis, M. F. Milk cathelicidin and somatic cell counts in dairy goats along the course of lactation. *Journal of Dairy Research* 2019, *86* (2), 217–221.
226. Nagaoka, I.; Tamura, H.; Reich, J. Therapeutic potential of cathelicidin peptide LL-37, an antimicrobial agent, in a murine sepsis model. *International Journal of Molecular Sciences* 2020, *21* (17), 5973–5989.
227. Wei, L.; Yang, J.; He, X.; Mo, G.; Hong, J.; Yan, X.; Lin, D.; Lai, R. Structure and function of a potent lipopolysaccharide-binding antimicrobial and anti-inflammatory peptide. *Journal of Medicinal Chemistry* 2013, *56* (9), 3546–3556.
228. Pace, B. T.; Lackner, A. A.; Porter, E.; Pahar, B. The role of defensins in HIV pathogenesis. *Mediators of Inflammation* 2017, *2017*, 1–12.
229. Koehbach, J.; Craik, D. J. The vast structural diversity of antimicrobial peptides. *Trends in Pharmacological Sciences* 2019, *40* (7), 517–528.
230. Almarwani, B.; Phambu, N.; Hamada, Y. Z.; Sunda-Meya, A. Interactions of an anionic antimicrobial peptide with zinc(II): Application to bacterial mimetic membranes. *Langmuir* 2020, *36* (48), 14554–14562.
231. Lewies, A.; Wentzel, J.; Jacobs, G.; Du Plessis, L. The potential use of natural and structural analogues of antimicrobial peptides in the fight against neglected tropical diseases. *Molecules* 2015, *20* (8), 15392–15433.
232. Holani, R.; Shah, C.; Haji, Q.; Inglis, G. D.; Uwiera, R. R. E.; Cobo, E. R. Proline-Arginine rich (PR-39) cathelicidin: structure, expression and functional implication in intestinal health. *Comparative Immunology, Microbiology and Infectious Diseases* 2016, *49*, 95–101.
233. Ulm, H.; Wilmes, M.; Shai, Y.; Sahl, H.-G. Antimicrobial host defensins – specific antibiotic activities and innate defense modulation. *Frontiers in Immunology* 2012, *3*, 1–4.
234. Zhang, L.; Yan, J.; Yin, Z.; Tang, C.; Guo, Y.; Li, D.; Wei, B.; Xu, Y.; Gu, Q.; Wang, L. Electrospun vancomycin-loaded coating on titanium implants for the prevention of implant-associated infections. *International Journal of Nanomedicine* 2014, 3027–3036.
235. Jeong, G. M.; Seong, H.; Im, S. G.; Sung, B. H.; Kim, S. C.; Jeong, K. J. Coating of an antimicrobial peptide on solid substrate via initiated chemical vapor deposition. *Journal of Industrial and Engineering Chemistry* 2018, *58*, 51–56.
236. Mouro, C.; Gouveia, I. C. Antimicrobial functionalization of wool: assessment of the effect of cecropin-b and [Ala5]-triTrp7 antimicrobial peptides. *The Journal of The Textile Institute* 2016, *107* (12), 1575–1583.
237. Majhi, S.; Arora, A.; Mishra, A. Surface Immobilization of a short antimicrobial peptide (AMP) as an antibacterial coating. *Materialia* 2019, *6*, 1–9.
238. Paris, J.-B.; Seyer, D.; Jouenne, T.; Thébault, P. Various methods to combine hyaluronic acid and antimicrobial peptides coatings and evaluation of their antibacterial behaviour. *International Journal of Biological Macromolecules* 2019, *139*, 468–474.
239. Ye, Z.; Zhu, X.; Mutreja, I.; Boda, S. K.; Fischer, N. G.; Zhang, A.; Lui, C.; Qi, Y.; Aparicio, C. Biomimetic mineralized hybrid scaffolds with antimicrobial peptides. *Bioactive Materials* 2021, *6* (8), 2250–2260.
240. Raman, N.; Marchillo, K.; Lee, M.-R.; Rodríguez López, A. de; Andes, D. R.; Palecek, S. P.; Lynn, D. M. Intraluminal release of an antifungal β-peptide enhances the antifungal and anti-biofilm activities of multilayer-coated catheters in a rat model of venous catheter infection. *ACS Biomaterials Science & Engineering* 2015, *2* (1), 112–121.
241. Akhavan, B.; Michl, T. D.; Giles, C.; Ho, K.; Martin, L.; Sharifahmadian, O.; Wise, S. G.; Coad, B. R.; Kumar, N.; Griesser, H. J.; Bilek, M. M. Plasma activated coatings with dual action against fungi and bacteria. *Applied Materials Today* 2018, *12*, 72–84.
242. Gabriel, M.; Nazmi, K.; Veerman, E. C.; Nieuw Amerongen, A. V.; Zentner, A. Preparation of LL-37-grafted titanium surfaces with bactericidal activity. *Bioconjugate Chemistry* 2006, *17* (2), 548–550.
243. Cao, P.; Yuan, C.; Xiao, J.; He, X.; Bai, X. A biofilm resistance surface yielded by grafting of antimicrobial peptides on stainless steel surface. *Surface and Interface Analysis* 2018, *50* (4), 516–521.
244. van Rensburg, W. The tyrocidines in the creation of antimicrobial cellulose and sterilising materials. PhD thesis, Stellenbosch University, Department of Biochemistry: Stellenbosch, South Africa, 2019. https://scholar.sun.ac.za/handle/10019.1/108461
245. van Rensburg, W.; Rautenbach, M. Creating Robust antimicrobial materials with sticky tyrocidines. *Antibiotics* 2022, *11* (2), 174–193.
246. Dubos René J.; Cattaneo, C. Studies on a bactericidal agent extracted from a soil *Bacillus*. *Journal of Experimental Medicine* 1939, *70* (3), 249–256.

247. Dubos René J.; Hotchkiss, R. D. The production of bactericidal substances by aerobic sporulating *Bacilli*. *Journal of Experimental Medicine* 1941, *73* (5), 629–640.
248. Dimick, K. P. The hemolytic action of gramicidin and tyrocidin. *Experimental Biology and Medicine* 1951, *78* (3), 782–784.
249. Henderson, J. The status of tyrothricin as an antibiotic agent for topical application. *Journal of the American Pharmaceutical Association (Scientific ed.)* 1946, *35* (5), 141–147.
250. Van Epps, H. L. René Dubos: Unearthing antibiotics. *Journal of Experimental Medicine* 2006, *203* (2), 259–259.
251. Rammelkamp, C. H.; Weinstein, L. Toxic effects of tyrothricin, gramicidin and tyrocidine. *Journal of Infectious Diseases* 1942, *71* (2), 166–173.
252. Hotchkiss, R. D.; Dubos, R. J. Bactericidal fractions from an aerobic sporulating *Bacillus*. *Journal of Biological Chemistry* 1940, *136* (3), 803–804.
253. Spathelf, B. M.; Rautenbach, M. Anti-listerial activity and structure–activity relationships of the six major tyrocidines, cyclic decapeptides from *Bacillus aneurinolyticus*. *Bioorganic & Medicinal Chemistry* 2009, *17* (15), 5541–5548.
254. Rautenbach, M.; Vlok, N. M.; Stander, M.; Hoppe, H. C. Inhibition of malaria parasite blood stages by tyrocidines, membrane-active cyclic peptide antibiotics from *Bacillus brevis*. *Biochimica et Biophysica Acta (BBA) - Biomembranes* 2007, *1768* (6), 1488–1497.
255. Troskie, A. M.; Rautenbach, M.; Delattin, N.; Vosloo, J. A.; Dathe, M.; Cammue, B. P.; Thevissen, K. Synergistic activity of the tyrocidines, antimicrobial cyclodecapeptides from *Bacillus aneurinolyticus*, with amphotericin B and caspofungin against C*andida albicans* biofilms. *Antimicrobial Agents and Chemotherapy* 2014, *58* (7), 3697–3707.
256. Troskie, A. M.; de Beer, A.; Vosloo, J. A.; Jacobs, K.; Rautenbach, M. Inhibition of agronomically relevant fungal phytopathogens by tyrocidines, cyclic antimicrobial peptides isolated from *Bacillus aneurinolyticus*. *Microbiology* 2014, *160* (9), 2089–2101.
257. Rautenbach, M.; Troskie, A. M.; Vosloo, J. A.; Dathe, M. E. Antifungal membranolytic activity of the tyrocidines against filamentous plant fungi. *Biochimie* 2016, *130*, 122–131.
258. Kumar, V.; van Rensburg, W.; Snoep, J. L.; Paradies, H. H.; Borrageiro, C.; de Villiers, C.; Singh, R.; Joshi, K. B.; Rautenbach, M. Antimicrobial nano-assemblies of tryptocidine C, a tryptophan-rich cyclic decapeptide, from ethanolic solutions. *Biochimie* **2023**, 204, 22–32.
259. Tang, X.-J.; Thibault, P.; Boyd, R. K. Characterisation of the tyrocidine and gramicidin fractions of the tyrothricin complex from *Bacillus brevis* using liquid chromatography and mass spectrometry. *International Journal of Mass Spectrometry and Ion Processes* 1992, *122*, 153–179.
260. Spathelf, B. Qualitative structure-activity relationship of the major tyrocidines, cyclic decapeptides from *Bacillus aneurinolyticus*. PhD thesis, Stellenbosch University, Department of Biochemistry: Stellenbosch, South Africa, 2010. https//scholar.sun.ac.za/handle/10019.1/4001
261. Munyuki, G.; Jackson, G. E.; Venter, G. A.; Kövér, K. E.; Szilágyi, L.; Rautenbach, M.; Spathelf, B. M.; Bhattacharya, B.; van der Spoel, D. β-sheet structures and dimer models of the two major tyrocidines, antimicrobial peptides from *Bacillus aneurinolyticus*. *Biochemistry* 2013, *52* (44), 7798–7806.
262. Loll, P. J.; Upton, E. C.; Nahoum, V.; Economou, N. J.; Cocklin, S. The high-resolution structure of tyrocidine a reveals an amphipathic dimer. *Biochimica et Biophysica Acta (BBA) - Biomembranes* 2014, *1838* (5), 1199–1207.
263. Dubos, R. J.; Hotchkiss, R. D.; Coburn, A. F. The effect of gramicidin and tyrocidine on bacterial metabolism. *Journal of Biological Chemistry* 1942, *146* (2), 421–426.
264. Aranda, F. J.; de Kruijff, B. Interrelationships between Tyrocidine and Gramicidin A′ in their interaction with phospholipids in model membranes. *Biochimica et Biophysica Acta (BBA) - Biomembranes* 1988, *937*, 195–203.
265. Bohg, A.; Ristow, H. DNA-Supercoiling is affected in vitro by the peptide antibiotics tyrocidine and gramicidin. *European Journal of Biochemistry* 1986, *160* (3), 587–591.
266. Bohg, A.; Ristow, H. Tyrocidine-induced modulation of the dna conformation in *Bacillus brevis*. *European Journal of Biochemistry* 1987, *170* (1-2), 253–258.
267. Danders, W.; Marahiel, M. A.; Krause, M.; Kosui, N.; Kato, T.; Izumiya, N.; Kleinkauf, H. Antibacterial action of gramicidin s and tyrocidines in relation to active transport, in vitro transcription, and spore outgrowth. *Antimicrobial Agents and Chemotherapy* 1982, *22* (5), 785–790.
268. Leussa, N.-N.A. Characterisation of small cyclic peptides with anti listerial and antimalarial activity. PhD thesis, Stellenbosch University, Department of Biochemistry: Stellenbosch, South Africa.2014. http://scholar.sun.ac.za/handle/10019.1/86161

Chapter 2

Bacterial production, isolation, and characterisation of cyclodecapeptides from tyrothricin

2.1 Introduction

The continual rise in antimicrobial resistance towards current conventional antimicrobial compounds is becoming ever more prevalent. This is due to the extensive utilisation of antimicrobial compounds, such as antibiotics, promoting a selective pressure towards the targets leading to resistance development [1]. Furthermore, the ability of various microbial pathogens to adhere to and colonise various surface types results in both surface contamination and spread, but also poses increased difficulty in the removal of the microbial target. The downstream effect is a negative impact towards both the agricultural and medical sectors, respectively [2]. Therefore, a dire need to alleviate the arising issue is the development of novel antimicrobial compounds in formulations that can prevent the initial adhesion and surface colonisation of these pathogens to surfaces. A select group of promising compounds are antimicrobial peptides (AMPs). AMPs are positively charged, amphipathic peptides (6-50 residues) which display variation in their length, amino acid composition and exhibition of broad-spectrum activity [3]. AMPs elicit various modes of activity by either directly interacting with the membrane of the target cell, resulting in pore formation or membrane disruption, or non-membrane processes and targets such as cellular respiration and proteins [3]. Due to the multiple modes of action of AMPs, there is a very limited potential of resistance development by target cells, thus promoting AMPs as a viable candidate for surface formulation development for antimicrobial activity [4].

The group of AMPs selected for this study, the tyrocidines (Trcs) and analogues, are cyclodecapeptides (CDPs) produced by the soil bacterium *Brevibacillus parabrevis* (*Br. parabrevis*) within the tyrothricin complex [5]. This complex consists of two parts, the cationic cyclic decapeptide tyrocidines and neutral linear pentapeptides, gramicidins (Grms). The tyrocidines exhibit a highly conserved primary structure with amino acid variability at residue position three and four, residue seven and residue nine [6-7]. Variation in analogue synthesis, A, B or C occurs by substitution at residue position three and four with tryptophan (Trp) or phenylalanine (Phe). Furthermore, substitution at residue position seven with tyrosine (Tyr), or Trp or Phe results in the synthesis of the tyrocidines (Trcs), tryptocidines (Tpcs) or phenycidines (Phcs), respectively (Table 2.1) [6-7].

Table 2.1 Summary of identified Trcs and analogues within the tyrothricin extract profile from *Br. parabrevis*

Peptide Identity	Abbreviations	Sequence [#]	Theoretical monoisotopic M_r [a]	Monoisotopic *m/z* $[M+H]^+$	Monoisotopic *m/z* $[M+2H]^{2+}$
Phenycidines					
Phenycidine A	PhcA, FA	Cyclo-(fP**Ff**NQ**F**VOL)	1253.6597	1254.6675	627.8377
Phenycidine A_1	$PhcA_1$, FA_1	Cyclo-(fP**Ff**NQ**F**VKL)	1267.6753	1268.6832	634.8455
Tyrocidines					
Tyrocidine A	TrcA, YA	Cyclo-(fP**Ff**NQ**Y**VOL)	1269.6546	1270.6624	635.351
Tyrocidine A_1	$TrcA_1$, YA_1	Cyclo-(fP**Ff**NQ**Y**VKL)	1283.6703	1284.6781	642.8430
Tyrocidine B	TrcB, YB	Cyclo-(fP**Wf**NQ**Y**VOL)	1308.6655	1309.6733	655.3406
Tyrocidine B'	TrcB', YB'	Cyclo-(fP**Fw**NQ**Y**VOL)	1308.6655	1309.6733	655.3406
Tyrocidine B_1	TrcB1, YB1	Cyclo-(fP**Wf**NQ**Y**VKL)	1322.6812	1323.6890	662.3484
Tyrocidine B_1'	$TrcB_1$', YB_1'	Cyclo-(fP**Fw**NQ**Y**VKL)	1322.6812	1323.6890	662.3484
Tyrocidine C	TrcC, YC	Cyclo-(fP**Ww**NQ**Y**VOL)	1347.6764	1348.6842	674.8460
Tyrocidine C_1	$TrcC_1$, YC_1	Cyclo-(fP**Ww**NQ**Y**VKL)	1361.6921	1362.6999	681.8539
Tryptocidines					
Tryptocidine A	TpcA, WA	Cyclo-(fP**Ff**NQ**W**VOL)	1292.6706	1293.6784	647.3431
Tryptocidine A_1	$TpcA_1$, WA_1	Cyclo-(fP**Ff**NQ**W**VKL)	1306.6862	1307.6941	654.3509
Tryptocidine B	TpcB, WB	Cyclo-(fP**Wf**NQ**W**VOL)	1331.6815	1332.6893	666.8486
Tryptocidine B_1	$TpcB_1$, WB_1	Cyclo-(fP**Wf**NQ**W**VKL)	1345.6971	1346.7050	673.8564
Tryptocidine C	TpcC, WC	Cyclo-(fP**Ww**NQ**W**VOL)	1370.6924	1371.7002	686.3540
Tryptocidine C_1	$TpcC_1$, WC_1	Cyclo-(fP**Ww**NQ**W**VKL)	1384.7080	1385.7159	696.3618
Gramicidines					
Val-Gramicidin A*	VGA	Formyl-(V)GAlAvVvW-lWlWlW	1881.0783	1882.0862	941.5470
Ile-Gramicidin A*	IGA	Formyl-(I)GAlAvVvW-lWlWlW	1895.094	1896.1018	948.5548
Val-Gramicidin B*	VGB	Formyl-(V)GAlAvVvW-lFlWlW	1842.0674	1843.0753	922.0415
Ile-Gramicidin B	IGB	Formyl-(I)GAlAvVvW-lFlWlW	1856.0831	1857.0909	929.0494
Val-Gramicidin C	VGC	Formyl-(V)GAlAvVvW-lYlWlW	1858.0624	1859.0702	930.0390
Ile-Gramicidin C	IGC	Formyl-(I)GAlAvVvW-lYlWlW	1872.078	1873.0858	937.0468

[#] Standard conventional one letter amino acid abbreviations used in peptide sequence except O representing Ornithine as described by *Tang et. al. [6].* Lower case letter represents D-amino acids and upper-case representing L-amino acids.

[a] Theoretical monoisotopic molar mass determined using the sum of monoisotopic Mr values of amino acid residues in the peptide sequence

[*] Low detected levels in tyrocidine mixture

The purification, isolation, and identification of single tyrocidines and analogues is a difficult and tedious task [6]. Additionally, variation between different *Br. parabrevis* producer strains cause differences in the produced analogue profiles, thus adding an additional layer of difficulty when seeking the production of specific analogues. Following a developed and optimised large scale-production methodology developed by our group (BIOPEP™ Peptide Group) [8], prior screening of the producer colonies using high-resolution electrospray mass spectrometry (HR-ESMS) ensures the producer selected can produce the analogues of interest. This ensures the quality control of the producer strain and identification of any potential producer mutation which may shift the desired profile for the targeted tyrocidines and analogues of that production.

The use of mass spectrometry is a powerful analytical analysis tool that allows for the identification, elemental composition and the overall purity and abundance of the sample via the molecular mass. Two techniques which are used in conjunction with this study are HR-ESMS and ultra-performance liquid chromatography (UPLC). The use of HR-ESMS allows for the identification of molecular mass via the generation of multiple charged species from the sample due to the high sensitivity and accuracy [9]. However, the limitations of HR-ESMS are the inability to distinguish between charged species with the same mass and charge, as these species will not be able to be distinguished from one another. Linking UPLC with HR-ESMS (UPLC-MS) resolves this analysis problem. UPLC-MS is a powerful technique that allows for the separation of all species at a high resolution within a complex sample and the subsequent identification of the species and species abundance present within the sample with high accuracy.

The focus of this study is to characterise the variability in selected tyrocidine *Br. parabrevis* producer strains followed by the production and purification of crude peptide extracts from the selected producer strains namely: *Br. parabrevis* DSMZ 5618, ATCC 8185 and ATCC 10068. Profile variability and analogue identification analysis were performed using HR-ESMS followed by isolation and characterisation of tyrocidine analogues of crude and commercial extracts. Successful peptide extraction was performed and analysed via UPLC linked to HR-ESMS, to determine the identity and abundance of the Trc and Trc analogues compared to the total amount of cyclic peptide present within the crude and commercial extracts.

2.2 Materials

Br. parabrevis producer strains DSMZ 5618, ATCC 8185 and ATCC 10068 were obtained from BIOPEP™ culture collection at Stellenbosch University (Cape Town, South Africa). Tyrothricin extract (extract from *Br. Parabrevis* formerly known as *Bacillus aneurinolyticus* and *B. brevis*) was

obtained from Sigma-Aldrich (St. Louis, MA, USA). Agar, D-glucose, sodium chloride (NaCl), tryptone, calcium chloride ($CaCl_2$), sodium chloride (NaCl), monopotassium phosphate (KH_2PO_4), ferric sulphate ($FeSO_4$), manganese sulphate ($MnSO_4$), magnesium sulphate ($MgSO_4$), diethyl-ether, acetone, and ethanol (EtOH, > 99.8%) were supplied by Merck (Darmstadt, Germany). Acetonitrile (ACN, HPLC-grade, far UV cut-off) was purchased from Romil Ltd (Cambridge, United Kingdom). Analytical grade water (MQH_2O) was obtained using a reverse osmosis purification plant, through a Millipore-Q® water purification system (Milford, USA). The 96-well cell culture plates were supplied by Thermo-Fisher Scientific (Waltham, MA, USA). Petri dishes were supplied by Lasec (Cape Town, South Africa) and sterile Falcon® tubes by Becton Dickson Labware (Lincoln Park, USA).

2.3 Methods

2.3.1 Tyrocidine and analogues production

Producer strains (*Br. parabrevis* DSMZ 5618, ATCC 8185 and ATCC 10068), selected strains from BIOPEP culture collection, were streaked out onto tryptone-soy agar (TSA) plates (30 g/L TS broth (TSB) and 1.5% agar) using standard sterile techniques and incubated for 7 days at 37 °C. Selected colonies were picked up and extracted directly with 50% ACN overnight. ACN extracts were collected via centrifugation and analysed via HR-ESMS, as described in 2.3.3.

The producer strain with low gramicidin A production (*Br. parabrevis* ATCC 10068_lowVGA), selected following strain production characterization, was streaked out on TSA plates (30 g/L and 1.5% agar) using standard sterile techniques and incubated for 24 hours at 37 °C. Subsequently, overnight cultures were prepared by inoculating 20 mL TSB media with fast-growing colonies from pre-culture agar plates and incubated for 24 hours at 37 °C on a shaker set at 150 rpm. Peptide production by *Br. parabrevis* proceeded for 10 days with incubation at 37 °C as described by Vosloo *et al*. [1].

2.3.2 Extraction of tyrocidines and analogues

The extraction methodology was developed by the BIOPEP™ Peptide Group (Stellenbosch University, South Africa) [8] and is currently protected under a non-disclosure agreement. In brief, the *Br. parabrevis* production culture was exposed to acidification followed by centrifugation at 10 621 ×*g* for 10 minutes to obtain the wet biomass. The wet biomass was exposed to various extraction and precipitation steps allowing for crude peptide extracts to be obtained. The linear gramicidins were removed following 12 washes with diethyl ether: acetone (1:1; *v/v*) with centrifugation between each wash (3030 ×*g* for 5 minutes). Crude peptide extracts were dried under

nitrogen (N_2) gas flow followed by resuspension in 50% ACN in water (*v/v*). Commercial peptide was treated with diethyl-ether: acetone (1:1; *v/v*) and centrifuged between each wash (3030 ×*g* for 5 minutes) to remove linear gramicidins resulting in a purified tyrocidine mixture (Trc mix). Resuspended crude peptide and Trc mix were transferred to clean, pyrolyzed analytically weighed vials and subjected to lyophilization before weighing on a six-digit analytical scale (Mettler Toledo, Columbus, USA).

2.3.3 HR-ESMS and UPLC-MS characterisation of CDP extracts from tyrothricin

All peptide samples were resuspended in 50 % ACN in water (*v/v*) to a final concentration of 0.100 mg/mL and centrifuged in a 200 µL glass insert (contained in an Eppendorf tube) at 3030 ×*g* for 10 minutes allowing for the removal of any particulates. Peptide identity was confirmed using HR-ESMS while peptide extract contributions were calculated using UPLC-MS obtained data. Injection volumes of 2 µL for HR-ESMS analysis while 3 µL for UPLC-MS were injected into the UPLC-MS system. The system consisted of a Water Acquity UPLC® and a Waters Synapt G2 quadrupole time-of-flight (TOF) mass spectrometer and an acuity UPLC LG 500 nm photo-diode array detector. Samples for UPLC-MS analysis were injected into a Waters Acquity UPLC® HSS T3 column (2.1 x 150 mm, 1.8 µm particle size), set at a minimum column temperature of 50 °C and maximum temperature of 60.7 °C at a flow rate of 0.3 mL/min. Elution of the peptide was achieved using a linear solvent gradient program (Table 2.2) with solvent A and B consisting of 1% formic acid (1% *v/v*) in water and 100% acetonitrile.

Table 2.2 The linear gradient program used during UPLC-MS analysis of the crude peptide extracts and the respective purified tyrocidines and analogues.

Minutes	% Eluant A	% Eluant B	Curve*
0.00	0	0	6
0.50	100	0	6
1.00	70	30	6
10.0	40	60	6
15.0	20	80	6
15.1	0	0	6
18.0	100	0	6

*Curve 6 depicts linear gradient (Waters™)

Instrument parameters were set at: cone and capillary voltage set at 15 V and 2.5 kV respectively, and ionization source temperature set at 120 ° C. Nitrogen was used as the desolvation gas set at a flow of 650 L/hour at 275°C. Data was collected via continuum scanning in positive mode over an *m/z* range of 300-2000. Analysis of all sample characterisation was done using Waters MassLynx™ software V4.1.

To determine peptide identity and integrity, the determined *m/z* values and monoisotopic *Mr* of each peptide was assessed using part per million (ppm) mass error. The following equation for ppm calculation was utilised:

$$\text{ppm} = \frac{M_\text{r}\ (\text{theoretical}) - M_\text{r}\ (\text{experimental})}{M_\text{r}\ (\text{theoretical})} \times 10^6$$

2.4 Results and discussion

2.4.1 Analysis of tyrothricin CDP profiles from selected Br. parabrevis producers

Variability of the tyrothricin profiles between and within different producer strains and colonies of the same strain have been reported throughout literature [8,10]. Factors such as supplementation, culture conditions and culture media are known to have an influence on the overall tyrothricin profile [6]. The tyrothricin complex, by the soil bacterium *Br. parabrevis,* consists of cationic CDPs (Trcs), and neutral linear peptides, Grms [6-7] (Table 2.1).

Successful culture extraction and direct injection HR-ESMS analysis allowed the fast assessment of various cultures and strains. This eased the selection of high CDPs producing cultures with low Grms. Example ion and mass spectra of such an extract is given in Figure 2.1. The tendency of Trcs to display variation in their oligomerisation profile with the production of monomers, dimers, and trimers (Figure 2.1A), results in purification and identification becoming more tedious and time-consuming. Furthermore, certain Trcs have identical molecular masses, making it difficult to distinguish between the different analogues when using UPLC-MS and HR-ESMS, such as YB/B', YB_1/YB_1' which will be identified together for the remainder of the chapter. Furthermore, the ability of the Trcs to form homo- and hetero-dimers results in identical molecular masses thereby making the presence of these analogues, TrcA-TrcC, TrcB-TrcB indistinguishable from one another without the use of more advanced mass spectroscopic methods and analysis. Figure 2.1A and B indicate the presence of the expected monomeric Trcs and linear Grm analogues (described in Table 2.1).

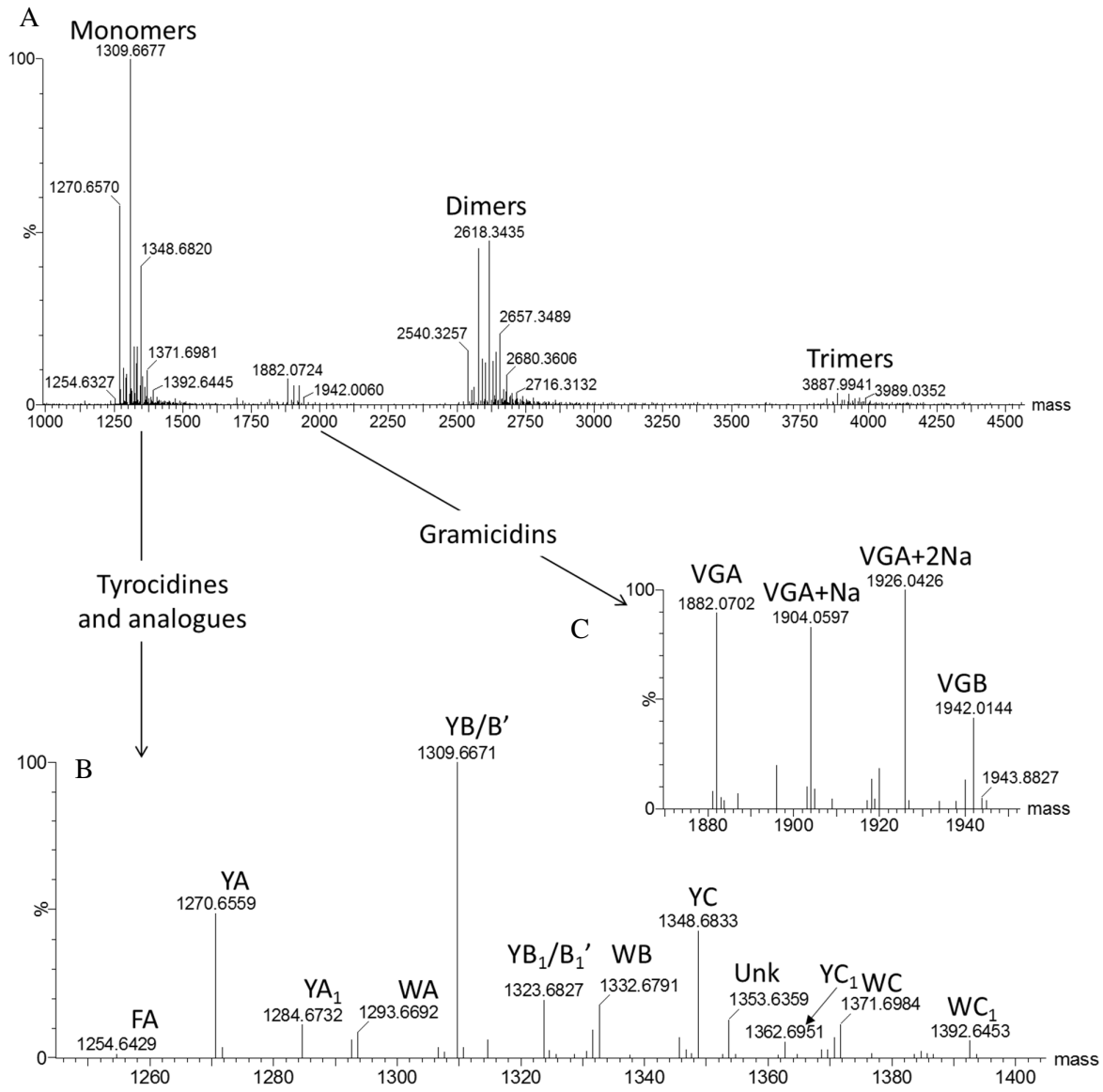

Figure 2.1 HR-ESMS analysis of the crude unsupplemented production extract by *Br. parabrevis* species. A. The extracted producer spectrum showing the HR-ESMS MaxEnt 3® analysis over a mass range of 1000 – 4500 showing the monomers, dimers, and trimers species. B. Deconvoluted enlarged HR-ESMS of tyrocidines monomeric analogues within the unsupplemented extract. C. Transformed enlarged HR-ESMS of linear gramicidins present within production extract.

The peptide extracts from the different strains were extracted and analysed to determine and compare variability in the synthesis of major CDPs, namely tyrocidine A (TrcA), tyrocidine B (TrcB) and tyrocidine C (TrcC), as well as linear Grms (VGA) production. These differences were observed using HR-ESMS and the production profile variation was compared between the three selected producer strains, ATCC 10068 (Figure 2.2), DSMZ 5618 (Figure 2.3) and ATCC 8185 (Figure 2.4), as well as minor variability in most cultures from the selected strain.

From the mass spectra of strain ATCC 10068 culture extracts (Figure 2.2) there is some variability in the peptide analogue ion signal and therefore amount produced, as well as variability in the production of specific analogues. The spectra in Figure 2.2 A and C both show the presence of the TrcC analogue, even though it is at low amounts, while those in Figure 2.2 B, D and E do not show TrcC or it is in present in undetectable amounts. Furthermore, a high Grm content, specifically VGA, is observed in some of the spectra (Figures 2.2 D and E) and could potentially contribute >50% of the peptide material. This is due to the Grms having a much lower ionization response compared to that of the Trcs, with this previously being elucidated by the BIOPEP™ Peptide Group. Interestingly, the culture extract in Figure 2.2 F exhibited a dominant Grm production of about 100% and very low levels of Trcs.

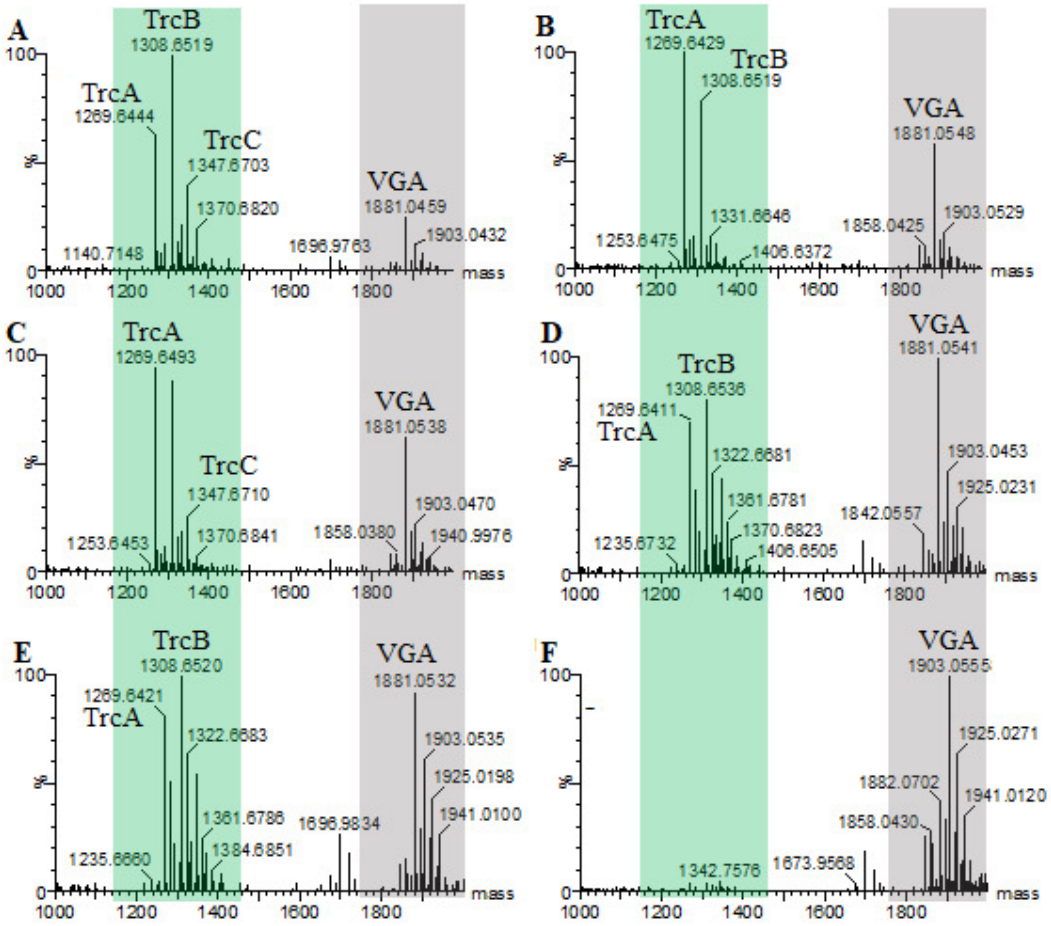

Figure 2.2 Examples of the deconvoluted mass spectra extracts from colonies of *Br. parabrevis* ATCC 10068 cultures analysed using HR-ESMS, with A-F representing the culture extract from the same subculture and freezer stock. Cyclodecapeptides signals are highlighted in green and linear gramicidins signals are highlighted in grey.

Observations of Grms: The TrcC signal ratio between the different culture extracts of strain ATCC 10068 indicated that extracts without the Trp-rich TrcC or with very low amounts of TrcC have a lower amount of Grm production when compared to extracts with a low amount of TrcC. This could correlate to a decreased availability of Trp from Trp anabolism for the tyrocidine synthetase complex to incorporate in this Trp-rich peptide, as well for the biosynthesis of Grms that also are Trp-rich. The highest cyclodecapeptide signals for extracts from *Br. parabrevis* ATCC 10068 fluctuate between TrcA and TrcB, indicating the ability of this specific strain being able to produce higher amounts of these two specific analogues, containing only Phe or Phe and one Trp in the aromatic dimer moiety. The malleability of CDP production over time and with aromatic amino acid supplementation was reported in detail by Vosloo *et al.* [12].

Br. parabrevis DSMZ 5618, which is supposedly analogous to strain ATCC 10068 [13], shows a distinct difference in appreciable amounts of the Trp-rich TrcC analogue produced in comparison to the other two producer strains, ATCC 10068 and ATCC 8185 (Figure 2.3). In the spectra in Figure 2.3 A, B and C there are approximately equal signals observed for TrcA and TrcC, with the dominant analogue being TrcB. This observation correlates with findings by Bas Vogt. *et al.* [13] in which the major *m/z* values of Trcs obtained from DSM-5618 were 1309 (TrcB). However, the production of equal amounts of TrcA and TrcC was not observed by this group. This can be indicative of mutation shifting in the production for equal amounts of TrcA and TrcC [13]. Furthermore, the amount of linear Grms in these extracts is much greater than the cyclodecapeptides when the weaker ionization signal is considered. Similarly, to the trend observed for peptide extracts from cultures of strain ATCC 10068, a higher amount of TrcC is produced (Figure 2.3 D) correlating with a higher production of linear Grms. This could indicate that this strain has an alternative source of Trp, other than the media Trp, eliminating the competition between the tyrocidine synthetase complex and the gramicidin synthetase complex. Although this strain shows consistent high tyrothricin production, the amount of Grms produced would compromise the extraction yield and purification of the CDPs. Previous studies by the Rautenbach group at Stellenbosch University showed large CDP loss with repeated extractions to remove Grms, as well as reverse phase columns containing matrices such as C_{18} being coated with Grms [personal communication, C. de Villiers and M. Rautenbach].

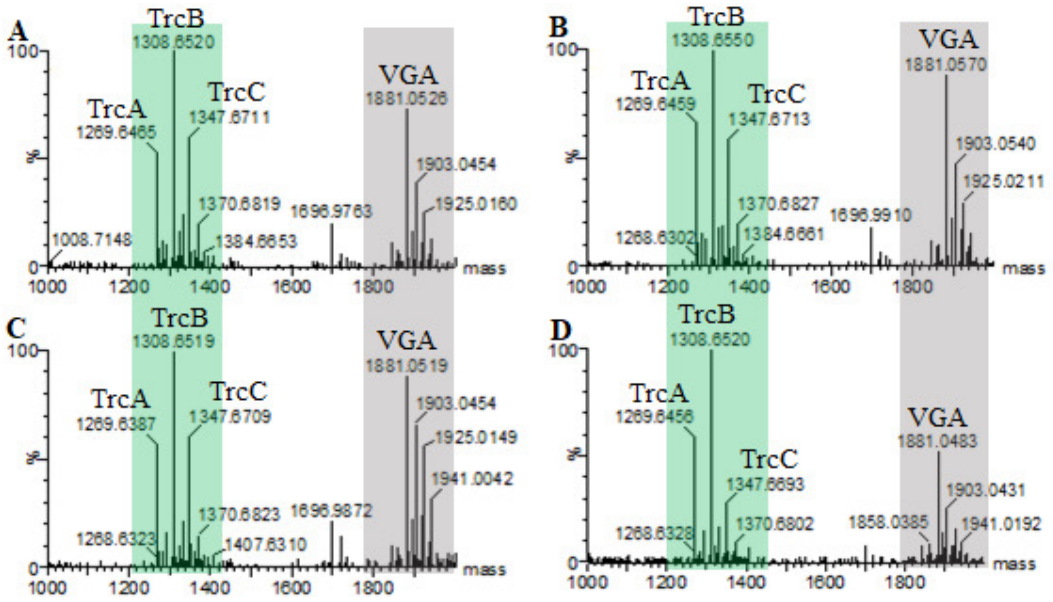

Figure 2.3 Examples of the deconvoluted mass spectra extracts from colonies of *Br. parabrevis* DSMZ 5618 cultures analysed using HR-ESMS, with A-D representing the culture extract from the same subculture and freezer stock. Cyclodecapeptides signals are highlighted in green and linear gramicidins signals are highlighted in grey.

The tyrothricin extract of strain ATCC 8185 of the CDPs, specifically, TrcA and TrcB shown in Figure 2.4 exhibits a similar trend as strain ATCC 10068 (refer to Figure 2.2). However, the amount of linear Grms observed are considerately lower than those observed in the ATCC 10068 and DSMZ 5618 culture extracts (compare Figure 2.4 with 2.2 and 2.3). Furthermore, the TrcA (1269.6) analogue appears to be produced at a higher amount when comparing strain production to ATCC 10068 and DSMZ 5618. TrcA contains two Phe residues at variable position 3 and 4 whereas TrcB has a Trp at position 3 and Phe at position 4 and TrcC has Trp at position 3 and 4 (Table 2.1). Due to the low amount of linear Grms seen in Figure 2.4 and the requirement of Trp for the synthesis, it possibly indicates that this producer favours a higher amount of Phe to be taken up by the cell, increasing the competition by the tyrocidine synthetase complex and the gramicidin synthetase complex for Trp. In this competition, Trc synthesis is favoured by decreasing linear Grms production (as seen in Figure 2.4) and although the amount of TrcB fluctuates, it is more abundant. Furthermore, as the amount of TrcC is considerably less compared to ATCC 10068 and DSMZ 5618 (Figure 2.2 and 2.3), it confirms the potential favoured uptake of Phe in the peptide structure thus ensuring there is limited availability of Trp in the cell to feed both TrcB, TrcC and linear Grms production. This may be attributed to an increased demand by the producer that will result in triggering the *de novo* synthesis, via the shikimate pathway for either Phe or Trp, at the start of fermentation based on the amino acid availability presented in the media, or if limited, synthesis of the required amino acid will occur [12]. As observed for ATCC 10068 and ATCC 8185, the CDP contribution is shifted to more Phe-containing analogues

thereby also decreasing linear Grms synthesis due to the demand for Phe being higher, initiating *de novo* synthesis via the shikimate pathway of Trp to Phe conversion. Furthermore, the reverse is observed for DSMZ 5618, whereby the Trcs analogue contribution is shifted to having more TrcB and TrcC analogues, furthermore, increasing linear Grm production as the overall cellular availability of Trp has increased.

The profile differences between the different producer strains and within the strains are evident and have an overall role on the selection of the producer to be used for crude peptide production due to analogue variability along with differences in linear Grm production, in particular Val-gramicidin A (VGA) (Table 2.3). Obtained results for the calculated linear Grm amounts of ATCC 10068 are similar to findings by Vosloo *et al.* [8, 12] and Spathelf [14] who determined an amount of 30-40% Grms in tyrothricin extracts.

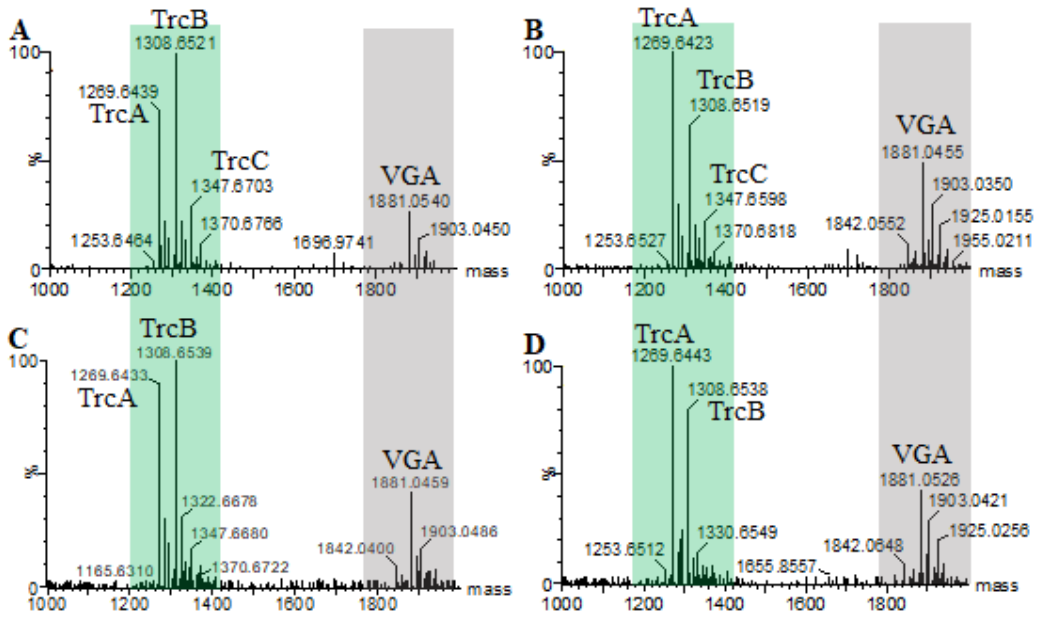

Figure 2.4 Examples of the deconvoluted mass spectra extracts from colonies of *Br. parabrevis* ATCC 8185 cultures analysed using HR-ESMS, with A-D representing the culture extract from the same subculture and freezer stock. Cyclodecapeptides signals are highlighted in green and linear gramicidins signals are highlighted in grey.

When there is a lower amount of TrcC produced, a decrease in the linear Grm signal is observed, whereas a high amount of TrcC production results in a higher linear Grm signal. This can potentially be attributed to the role of the *de novo* synthesis via the shikimate pathway, resulting in the modulation for more Phe residues to be taken up and introduced into the cell resulting in a decreased availability of Trp residues. The effect is less TrcC production observed in the ATCC 10068 strain which correlates with the obtained peptide signals by Vosloo *et al.* [12] in which the contribution of L-Trp[3] D-Trp[4], resulting in the production of TrcC, remains between the range of 10%-20% and only shows

a large contribution after 192 hours. This can potentially be attributed to variance in the secondary metabolite synthesis and/or a bacterial-controlled modulation of the non-ribosomal peptide synthetases (NRPS) system, the control of the transportation of Trp from the culture environment or lastly, control of the Trp synthesis via the shikimate pathway [15]. Therefore, the variances observed between producer strains for the CDP analogues as well as the synthesis of the Grms are related to the control of Phe/Trp availability which potentially impacts which analogue is being produced.

Table 2.3 Production profile summary of selected *Br. parabrevis* tyrocidine producer strains selected from BIOPEP culture library. Values for each peptide are their approximate % mole contribution and indicated as red/blue heatmap to highlight differences.

Strain ID	FS Label	TrcA	TrcB	TrcC	$TrcA_1$	$TrcB_1$	$TrcC_1$	VGA
ATCC 8185	FS WR	22.1	25.6	7.4	5.5	5.7	2.1	14.8
ATCC 8185	FS WR	20.	15.9	5.1	7.0	5.5	2.4	23.1
ATCC 8185	FS AV	16.9	14.1	8.9	7.0	6.2	1.5	27.9
ATCC 8185	FS AV	24.1	14.8	3.7	3.9	3.6	1.2	26.0
ATCC# 10068	FS AV	17.1	29.6	10.3	2.9	2.8	3.1	14.7
ATCC 10068	FS AV	20.2	18.9	2.4	3.4	2.9	1	34.8
ATCC 10068	FS SB	15.9	25.8	4.8	3.3	3.7	0.9	26.0
ATCC 10068	FS AV	13.0	15.4	9.7	5.9	6.8	4.4	29.8
ATCC 10068	FS AV	14.4	18.6	7.5	7.5	8.8	3.1	26.5
ATCC 10068*	FS SB	0.9	1.4	0.5	0.8	1.2	0.7	89.5
DSMZ 5618	FS AV	13.1	22.3	12.2	3.6	4.1	1.8	28.2
DSMZ 5618	FS SB	16.3	18.4	12.0	2.2	3.9	2.1	30.0
DSMZ 5618	FS SB	11.9	25.2	10.3	1.7	2.1	1.5	33.5
DSMZ 5618	FS AV	11.4	21.3	6.3	1.7	2.1	1.4	36.7

FS – freezer stock, #low VGA producers used for production, *unusual tyrothricin profile, percent abundance was determined by calculating extracted peak intensity of each peptide as a percentage of the sum of the peak intensity of all peptides observed in extract, with each response factor of all peptides assumed to have similar response factors due to similarities in analogue structure. Analysis was performed utilising Waters MassLynx® 4.1 Software (Waters Corporation, Massachusetts, USA)

Due to linear Grm requiring a Trp residue at variable position 11, as seen in Table 2.1, when TrcC is being produced it is observed that a higher amount of linear Grms is biosynthesised, which may be attributed to the excess availability of Trp within the cell. Conversely, when there is a low amount of

Trp is present due to one of the three above-mentioned reasons by bacterial control, a lower amount of TrcC and linear Grms are produced, as observed by the low signals seen in the ATCC 8185 spectra (refer to Figure 2.3). Therefore, the synthesis of specific Trcs and Grms is influenced by the availability of the Trp amino acid for the cell and the specific producer being used. Trp limitation in the media may result in the producer being required to initiate *de novo* synthesis allowing for more Trp to be present, however, this may result in Grm synthesis by the gramicidin synthetase enzyme complex due to the increase in Trp availability [12]. If no Trp limitation is present, but the demand for Phe is increased, the bacterial producer may utilise *de novo* synthesis for Phe production, thereby limiting the amount of Trp available to be utilised by the gramicidin enzyme synthetase, resulting in a decreased amount of linear Grms synthesised [12, 16].

2.4.2 Characterisation of CDP extract from commercial tyrothricin

To determine Trc analogue abundance within the commercial Trc mixture, crude fractionation was performed with modifications, as described by Hotchkiss and Dubos [5], in which the commercial mixture was exposed to a 1:1 (*v/v*) of DEE:acetone resulting in the formation of an insoluble fraction that contained the Trcs, and a soluble fraction containing Grms. Continual wash exposure ensures the linear Grms go into solution leaving behind only the desired Trcs. This method manipulates the Trcs and Grms hydrophobicity properties thereby allowing for separation of the more hydrophobic Grms. It is assumed, however, that both the linear Grms and some of the more hydrophobic Trcs may be removed in the DEE:acetone wash step. The extracted Trc complex was subjected to UPLC-MS analysis revealing relatively pure Trcs and analogue extract. Furthermore, separation of the CDP analogues revealed different analogues from which their abundance contribution was determined (Figure 2.5).

Successful purification of the commercial tyrothricin extract resulted in the separation of the linear Grms and the Trcs. Analysis of the pure Trc extract using UPLC-MS (Figure 2.5) confirmed that all six major tyrocidine analogues were in the extract, namely, TrcC, $TrcC_1$, TrcB, $TrcB_1$, TrcA and $TrcA_1$. Obtained peptide abundance calculations for each Trc and Trc analogue correlate with those previously indicated in literature [2]. The most abundant peptides obtained in the extract were TrcB $\geq$ TrcA $\geq$ TrcC > $TrcB_1$ > $TrcA_1$ > $TrcC_1$ with TpcC, and TpcA only present in trace amounts (Table 2.4). Furthermore, the elution profile of Trc analogues correlates with previously obtained results with A analogues (TrcA/A_1 and TpcA) eluting last, followed by B analogues (TrcB/B_1 and TpcB) and lastly C analogues (TrcC/$TrcC_1$ and TpcC) due to the hydrophobic nature of the analogues being exploited. The obtained percentage abundance results following extraction and identification yielded similar results to those previously obtained by Troskie *et al.* [17] indicating both consistency in the commercial production and the method used for purification.

Table 2.4 Summary of the detected tyrocidine peaks extracted from tyrocidine commercial peptide extract, indicating peptide identity, monoisotopic M_r, UPLC-MS retention time and percentage abundance of Trc peaks obtained in the total Trc extracted.

				% Abundance	
Peptide	**Observed M_r (Theoretical M_r)**	**ppm error**	**R_t (min)**	**Trc in commercial extract**	**Troskie *et al.* [16]**
TpcA	1292.6440 (1292.6706)	20.56	11.72	Trace	Trace
TrcA	1269.6324 (1269.6538)	17.50	11.32	18.2	17.6
$TrcA_1$	1283.6450 (1283.6706)	20.56	11.20	11.1	13.2
TpcB	1331.6632 (1331.6815)	13.74	10.89	2.4	3.1
TrcB	1308.6516 (1308.6655)	10.63	10.44	24.6	21.3
$TrcB_1$	1322.6591 (1322.6812)	16.67	10.35	15.0	15.7
TrcC	1347.6548 (1347.6764)	16.04	9.84	18.0	14.3
$TrcC_1$	1361.6775 (1361.6921)	10.69	9.79	9.27	10.3
TpcC	1370.6781 (1370.6924)	10.43	10.29	1.4	3.5

[a] % Abundance determined by calculating extracted peak area of each peptide as a percentage of the sum of the peak areas of all peptides observed in extract, with each response factor of all peptides assumed to have similar response factors due to similarities in analogue structure.
[b] Theoretical monoisotopic M_r calculated from the molecular mass of all the constituent amino acids determined from purified peptide.
[c] Retention time determined from UPLC-MS analysis

2.4.3 Characterisation of CDP extract from Br. parabrevis ATCC 10068 cultures

To assess the similarities between the crude commercial purified extract and the Trcs following a production, *Br. parabrevis* ATCC 10068 (Figure 2.1 A) was selected and used as the target producer organism. This is due to the low presence of linear Grms, which would make purification easier, and similarities in production profile to that of the commercial tyrocidine. This ensures surface antimicrobial activity and biophysical changes can be correlated between both extracts. The culture extract of *Br. parabrevis* ATCC 10068 resulted a crude mixture containing Trcs, tryptocidines, phenycidine and linear Grms within the tyrothricin complex, correlating with obtained results from Figure 2.1 A. This successfully indicates that the production profile of the producer has remained consistent and that no mutations or shifts in production had occurred. To further compare the extracted peptide profile to that of the commercial peptide profile, UPLC-MS (Figure 2.6) analysis was performed to determine retention times and peak identity for the peptide extract.

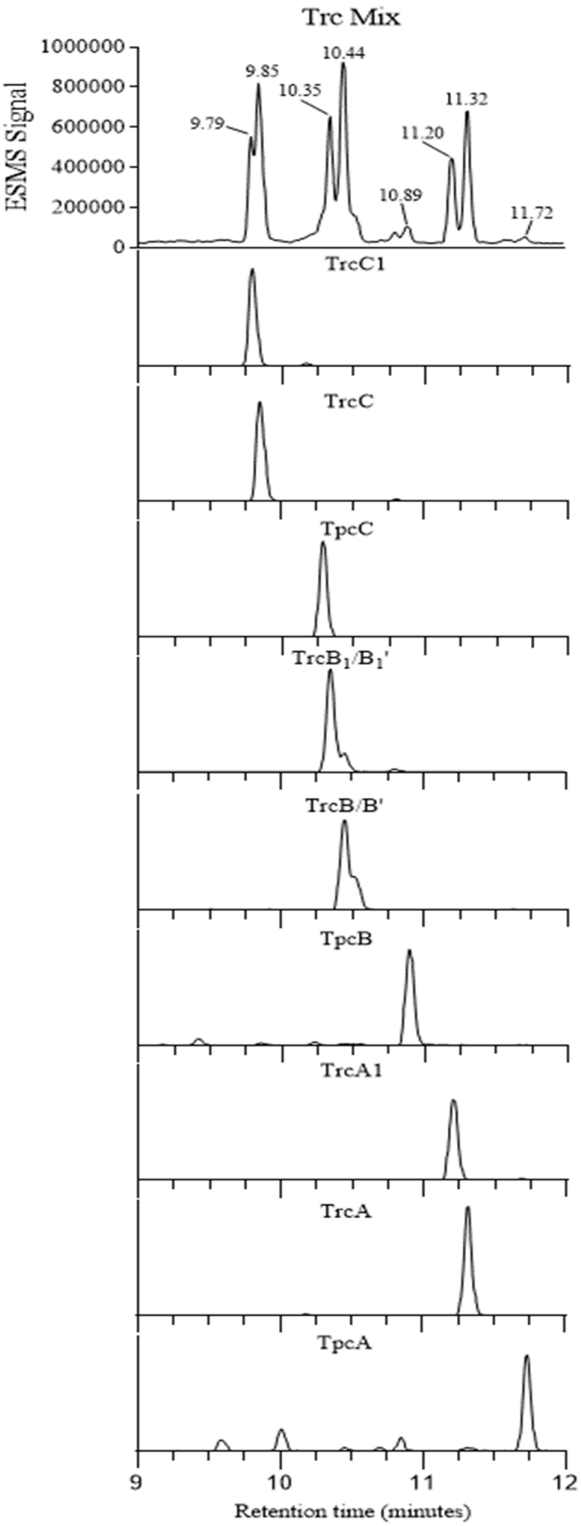

Figure 2.5 Representative UPLC-MS chromatographic profile of the purified commercial mixture of different Trcs and their analogues. The identifier profiles were generated using the doubly charged ion of the specific peptide as identifier. The retention time for each extracted ion peak is provided in the top total ion chromatogram and the y-axis representing the ES-MS signal. Profiles were used to calculate the % abundance in Table 2.3. Asymmetric peak shapes are related to the inclination of the CDPs to form higher order oligomers at higher concentrations and over time. Each indicated peptide peak was confirmed using HR-ESMS spectra associated with each of the peaks in the chromatogram profile (2.7.1 Supplementary information). Observed tailing peaks/shoulders for TrcB and $TrcB_1$ are related to the minor TrcB' and $TrcB_1$'.

Furthermore, a detailed HR-ESMS analysis of each peak within the CDP extract confirmed monomeric analogues but also revealed stable higher-order oligomers (refer to 2.7 supplementary information). To determine and compare the contribution of the various analogues present between that of the production and commercial extracts, the signal contribution of each analogue peak was determined and used to calculate the peak area, which provided an indication as to the abundance of that specific analogue within the sample. It was assumed that the ion response of all the CDPs is similar in the HR-ESMS due to their conserved structure.

Percentage abundance comparison between the commercial crude extract and our in-house production extract (Table 2.5) revealed TrcA and TrcB to be the most abundant analogues in comparison to the commercial extract having TrcB/B_1 followed by TrcA/A_1 then finally TrcC/C_1. Furthermore, the production of the rare PhcA is observed at 2% abundance in our production extract, whereas the commercial extract has it at very low trace amounts. The production of PhcA is induced by the supplementation of the media with the Phe amino acid, as the NRPS are being modulated by concentration dependent incorporation of Phe into position 7 [12]. Furthermore, TGS media was shown to contain 1.2 mM Trp [8, 12], however, the amount of Trp-containing analogues (TrcC) that were produced were considerably less than those of the Phe-containing analogues (TrcA and TrcB). This observed analogue difference of TrcA synthesis between the commercial Trc mix and Trc crude of 28.7% indicates the favoured uptake and utilisation of Phe that is present within the TGS media. Furthermore, the potential higher demand for Phe may result in the use of *de novo* synthesis via the shikimate pathway by this specific producer due to a higher affinity by the peptide synthetases [12] shifting the uptake for more Phe, resulting in overall lower production of TrcC in the crude extract compared to the commercial extract.

The in-house crude extract analogue abundances correlate with those previously found by Vosloo e*t al.* [8]. It was shown that in unsupplemented media, the producer strain *Br. parabrevis* ATCC 10068, predominantly produced the TrcA and TrcB analogues with low levels of VGA (linear Grms) [8], correlating with our observed CDP abundances for the same producer strain. Further correlation concerning the *Br. parabrevis* producer profile are by Masoudi [18] who showed the same order of production with TrcA (45.4%), TrcB (21.6%) and TrcC (7.2%) compared to those obtained in Table 2.5 with TrcA (46.9%), TrcB (29.9%) and TrcC (6.6%). Higher amounts of TrcA and TrcB can be related to the low amount of TrcC produced, indicating that less Trp is available for TrcC production.

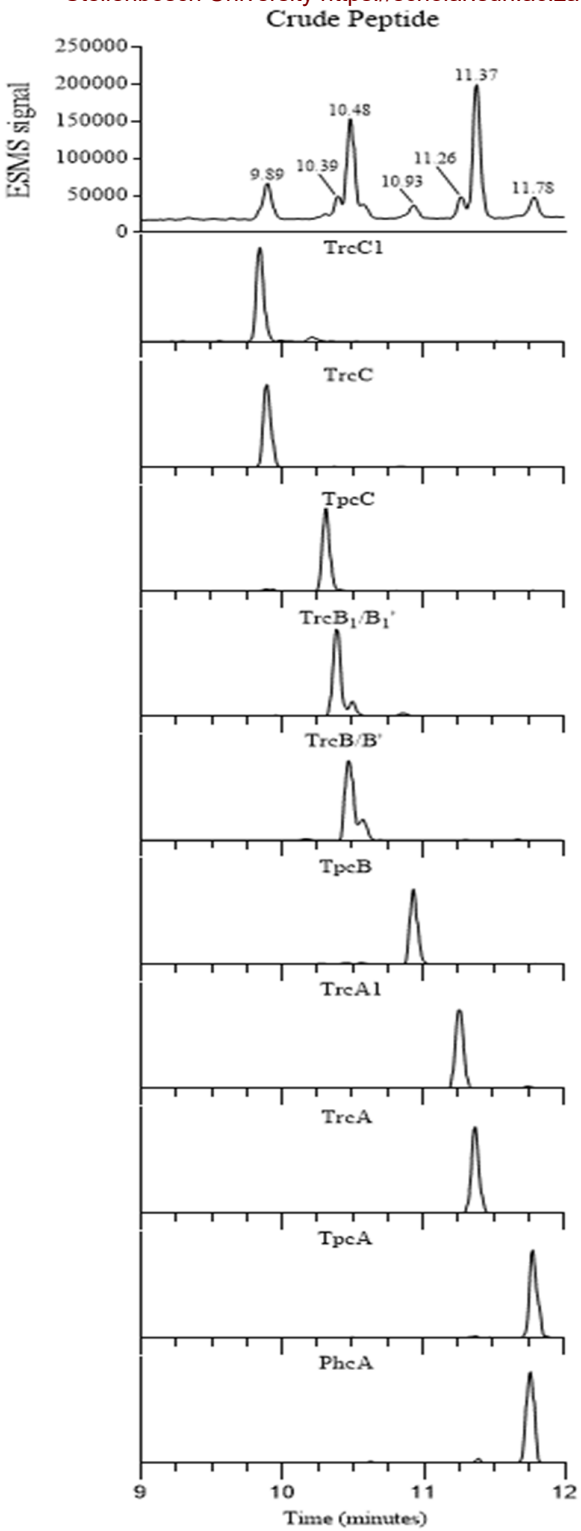

Figure 2.6 Representative UPLC-MS chromatographic profile of the purified in-house crude extract mixture of different Trcs and their analogues. The identifier profiles were generated using the doubly charged ion of the specific peptide as identifier. The retention time for each extracted ion peak is provided in the top total ion chromatogram and the y-axis representing the ES-MS signal. Profiles were used to calculate the % abundance in Table 2.4. Asymmetric peak shapes are related to the inclination of the CDPs to form higher order oligomers at higher concentrations and over time. Each indicated peptide peak was confirmed using HR-ESMS spectra associated with each of the peaks in the chromatogram profile (2.7.2 Supplementary information). Observed frontal peaks for TrcB and $TrcB_1$ are related to the minor TrcB' and $TrcB_1$'.

Interestingly, Masoudi [18] did not observe the minor analogues, namely $TrcA_1$ and $TrcB_1$, indicating the loss of these analogues in extraction or that they were not produced. These analogues were found in our extract at 3.6% and 4.8%, respectively. This may indicate that the producer strain used in this study produced higher amounts of these hydrophobic analogues prior to extraction and the resulting amount post extraction was high enough for reliable detection.

Table 2.5 Summary of the detected tyrocidine peaks extracted from crude peptide extract, indicating peptide identity, monoisotopic M_r, UPLC-MS retention time and percentage abundance of Trc peaks obtained in the total Trc extracted.

				% Abundance [c]	
Peptide	**Observed Mr (Theoretical Mr)[a]**	**ppm error**	**Rt (min)[b]**	**Trc in commercial extract**	**Trc in crude extract**
PhcA	1253,6472 (1253.6597)	9.98	11.75	-	2.0
TpcA	1292,6503 (1292.6706)	15.70	11.79	Trace	2.1
TrcA	1269,6343 (1269.6538)	16.00	11.37	18.2	46.9
$TrcA_1$	1283.6498 (1283.6703)	15.94	11.26	11.1	3.6
TpcB	1331,6632 (1331.6815)	13.74	10.93	2.4	3.5
TrcB	1308.6517 (1308.6655)	10.56	10.48	24.6	29.9
$TrcB_1$	1322.6588 (1322.6812)	16.91	10.39	15.0	4.8
TrcC	1347.6527 (1347.6764)	17.60	9.89	18.0	6.6
$TrcC_1$	1361.6781 (1361.6921)	10.25	9.84	9.27	Trace
TpcC	1370.6803 (1370.6924)	8.83	10.31	Trace	Trace

[a] % Abundance determined by calculating expressed peak area of each peptide as a percentage of the sum of the peak areas of all peptides observed in extract, with each response factor of all peptides assumed to have similar response factors due to similarities in analogue structure.
[b] Theoretical monoisotopic M_r calculated from the molecular mass of all the constituent amino acids determined from purified peptide.
[c] Retention time determined from UPLC-MS analysis

2.5 Conclusion

Due to the production of the Trcs being non-ribosomal and secondary metabolites, the influence of various cellular factors such as metabolic pathways, membrane amino acids transporters and overall amino acid availability have a crucial role in peptide synthesis. Tyrocidine production was observed to show variation between producer strains ATCC 10068, ATCC 8185 and DSMZ 5618, specifically when comparing TrcA, TrcB and TrcC production. ATCC 10068 and ATCC 8185 shared considerable similarity towards TrcA and TrcB production with limited TrcC and linear Grms while

DSMZ 5618, however, revealed increased levels of TrcC and linear Grm production. This difference in production profile may be attributed to the demand of the producer towards a specific amino acid, Phe or Trp, with variation in analogue production being influenced by the incorporation at position three and four of the dipeptide unit. Cellular demand of a specific amino acid may result in *de novo* synthesis via the shikimate pathway, in which the synthesis of Phe from Trp or Trp from Phe can occur, altering the overall amino acid availability and thus directly impacting which analogues are to be synthesised. Furthermore, due to linear Grms requiring Trp, a decrease in this amino acid will result in a decreased synthesis as seen in ATCC 10068 and ATCC 8185 but not in DSMZ 5618 due to the demanded amino acid shift facilitated by *de novo* synthesis via the shikimate pathway.

Successful purification of commercial tyrocidine and crude production extract revealed that the commercial analogue abundance was TrcB/B1, TrcA/A_1 and TrcC/C_1 with a very low amount of TpcC analogues and PhcA whereas the crude peptide extraction resulted in an abundance of TrcA (46.6%) and TrcB (29.9%) and low amount of the Lys^9- containing analogues (TrcA_1/B_1/C_1). The obtained peptide abundances from the peptide extractions in this study correlated to those previously obtained in literature [8, 12]. Interestingly, the crude peptide extract resulted in a 2% abundance of PhcA which was not observed to be in the commercial extract.

The pure commercial peptide (98.6%) extracts were obtained and will be utilised in the rest of the study in the antimicrobial (Chapter 3) and biophysical analyses (Chapter 4), for the identification of the most optimal formulation.

2.6 References

1. Davies, J.; Davies, D. Origins and evolution of antibiotic resistance. *Microbiology and Molecular Biology Reviews* 2010, *74* (3), 417-433.
2. Manyi-Loh, C.; Mamphweli, S.; Meyer, E.; Okoh, A. Antibiotic use in agriculture and its consequential resistance in environmental sources: potential public health implications. *Molecules* 2018, *23* (4), 795.
3. Peters, B.; Shirtliff, M.; Jabra-Rizk, M. Antimicrobial peptides: primeval molecules or future drugs?. *PLoS Pathogens* 2010, *6* (10), e1001067.
4. Kim, S.; Kim, S.; Bang, Y.; Kim, S.; Lee, B. In vitro activities of native and designed peptide antibiotics against drug sensitive and resistant tumor cell lines. *Peptides* 2003, *24* (7), 945-953.
5. Hotchkiss, R.; Dubos, R. The isolation of bactericidal substances from cultures of *Bacillus brevis*. *Journal of Biological Chemistry* 1941, *141* (1), 155-162.
6. Tang, X.; Thibault, P.; Boyd, R. Characterisation of the tyrocidine and gramicidin fractions of the tyrothricin complex from *Bacillus brevis* using liquid chromatography and Mass Spectrometry. *International Journal of Mass Spectrometry and Ion Processes* 1992, *122*, 153-179.
7. Ruttenberg, M.; Mach, B. Studies on amino acid substitution in the biosynthesis of the antibiotic polypeptide tyrocidine*. *Biochemistry* 1966, *5* (9), 2864-2869.
8. Vosloo, J.; Stander, M.; Leussa, A.; Spathelf, B.; Rautenbach, M. Manipulation of the tyrothricin production profile of *Bacillus aneurinolyticus*. *Microbiology* 2013, *159* (Pt_10), 2200-2211.
9. Kind, T.; Fiehn, O. Advances in structure elucidation of small molecules using mass spectrometry. *Bioanalytical Reviews* 2010, *2* (1-4), 23–60.
10. Dubos, R.; Hotchkiss, R. The production of bactericidal substances by aerobic sporulating Bacilli. *Journal of Experimental Medicine* 1941, *73* (5), 629-640.
11. Dubos, R.; Cattaneo, C. Studies on a bactericidal agent extracted from a soil Bacillus. *Journal of Experimental Medicine* 1939, *70* (3), 249-256.
12. Vosloo, J.; Rautenbach, M. Following tyrothricin peptide production by *Brevibacillus parabrevis* with electrospray mass spectrometry. *Biochimie* 2020, *179*, 101-112.
13. Vogt, T.; Schinzel, S.; Bechinger, B. Biosynthesis of isotopically labeled gramicidins and tyrocidins by *Bacillus brevis*. *Journal of Biomolecular NMR* 2003, *26* (1), 1-11.
14. Spathelf, B. Qualitative structure-activity relationship of the major tyrocidines, cyclic decapeptides from *Bacillus aneurinolyticus*. PhD thesis, Stellenbosch University, Department of Biochemistry: Stellenbosch, South Africa, 2010. http://scholar.sun.ac.za/handle/10019.1/4001
15. Herrmann, K.; Weaver, L. The shikimate pathway. *Annual Review of Plant Physiology and Plant Molecular Biology* 1999, *50* (1), 473-503.
16. Sarges, R.; Witkop, B. Gramicidin A. IV. Primary sequence of valine and isoleucine gramicidin A. *Journal of the American Chemical Society* 1964, *86* (9), 1862-1863.
17. Troskie, A.; de Beer, A.; Vosloo, J.; Jacobs, K.; Rautenbach, M. Inhibition of agronomically relevant fungal phytopathogens by tyrocidines, cyclic antimicrobial peptides isolated from *Bacillus aneurinolyticus*. *Microbiology* 2014, *160* (9), 2089-2101.
18. Masoudi, Y. Characterisation and formulation of natural cyclodecapeptides with anti-candida activity. MSc Thesis, Stellenbosch University, Department of Biochemistry: Stellenbosch, South Africa, 2021. https://scholar.sun.ac.za/handle/10019.1/109933
19. Spathelf, B.; Rautenbach, M. anti-listerial activity and structure–activity relationships of the six major tyrocidines, cyclic decapeptides from *Bacillus aneurinolyticus*. *Bioorganic & Medicinal Chemistry* 2009, *17* (15), 5541-5548.

2.7 Supplementary information

2.7.1 Peptide peak identity conformation of CDP extract from commercial tyrothricin

Commercial and crude Trc mix was obtained and purified as described in 2.3.2 following a method previously described by Spathelf and Rautenbach [19]. Characterisation of peptide extracts was performed using UPLC-MS and analogue identity was confirmed using HR-ESMS as described in 2.3.3 [1]. The retention time (R_t) of each peptide analogue is summarised in Table 2.4 correlating to the respective peaks shown in Figure 2.5.

HR-ESMS coupled with UPLC revealed the ability and nature of each of the CDPs in the extracts to oligomerise (aggregate) into higher-order structures such as dimers and trimers which are stable under HR-ESMS conditions. Briefly, Figure 2.7 AI, BI and CI show the spectra of Trc analogues, $TrcC_1$ (1361.6775), TrcC (1347.6548) and TpcC (1370.6781) revealing monomers, dimers, and trimers, respectively and Figure 2.7 AII, BII, CII shows the monomer spectrum of $TrcC_1$ (1361.6775), TrcC (1347.6548) and TpcC (1370.6781) present within the respective sample peak confirming analogue identity and presence. The presence of TrcC in AII, $TrcC_1$ in BII and $TrcB_1$ in CII is attributed to the peak overlaps and the purification via a C_{18} – high performance liquid chromatography (HPLC) method is required to remove these analogues when a pure sample is desired.

Spectra in Figure 2.8 AI, BI and CI reveal the presence of $TrcB_1$ (1322.6591), TrcB (1308.6516) and TpcB (1331.6632) monomers, dimers, and trimer oligomers (aggregates). Figure 2.8 AII, BII and CII show the enlarged spectrum confirming the major monomeric analogue within the peak. Peak overlap is observed again with the presence of TrcB in AII and $TrcB_1$ in BII.

Lastly, spectra in Figure 2.9 AI, BI and CI indicate $TrcA_1$ (1283.6450), TrcA (1269.6324) and TpcA (1292.6440) oligomers (aggregates) namely monomers, dimer, and trimers for each analogue, respectively. Enlarged HR-ESMS spectrum in Figure 2.9 AII, BII and CII confirm the major analogue present correlating to the selected and shown peaks in Figure 2.5. Furthermore, peak overlap is observed due to the presence of TrcA in Figure 2.9 AII and CII and $TrcA_1$ in Figure 2.9 BII.

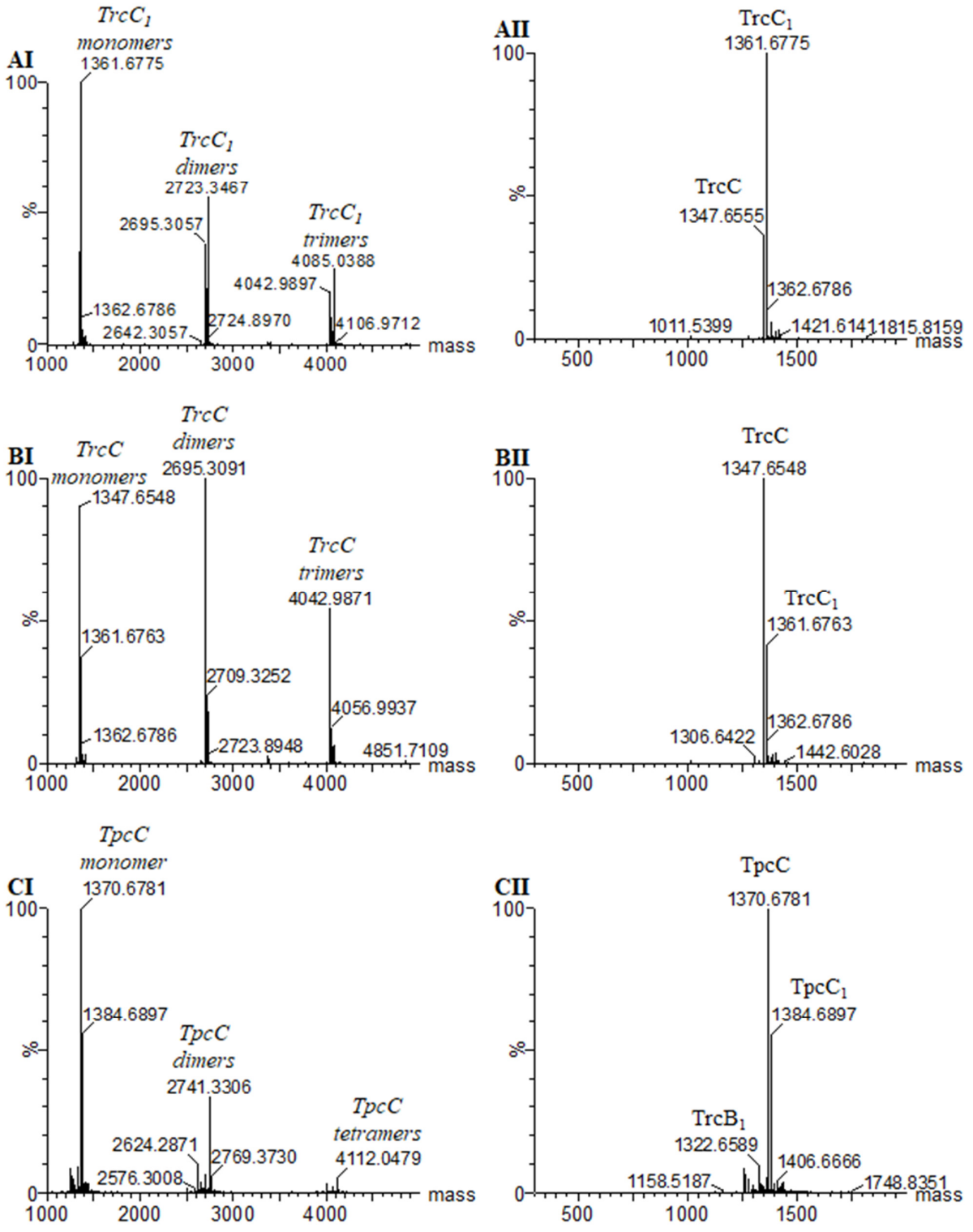

Figure 2.7 HR-ESMS analysis of CDP extract from commercial tyrothricin. AI – CI: HR-ESMS spectrum of $TrcA_1$, TrcA and TpcA monomers, dimers, and trimers, respectively. AII – CII: The enlarged spectrum of $TrcA_1$, TrcA and TpcA from 300 – 2000 Da showing the monomeric analogue present within the sample and peak. Peptide abundance and retention time are provided in Table 2.3.

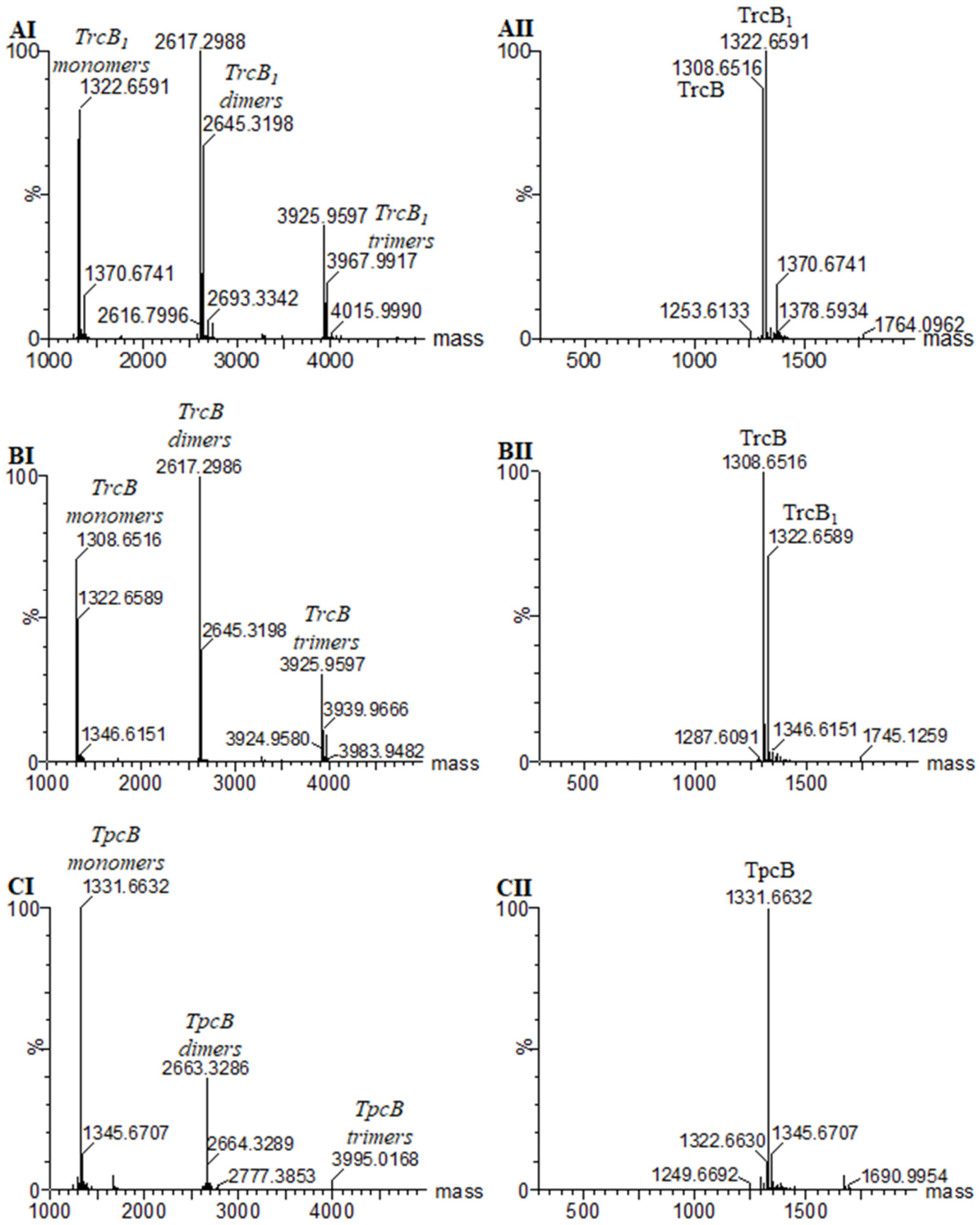

Figure 2.8 HR-ESMS analysis of CDP extract from commercial tyrothricin. AI – CI: HR-ESMS spectrum of $TrcB_1$, TrcB and TpcB monomers, dimers, and trimers, respectively. AII – CII: The enlarged spectrum of $TrcB_1$, TrcB and TpcB from 300 – 2000 Da showing the monomeric analogue present within the sample and peak. Peptide abundance and retention time are provided in Table 2.3.

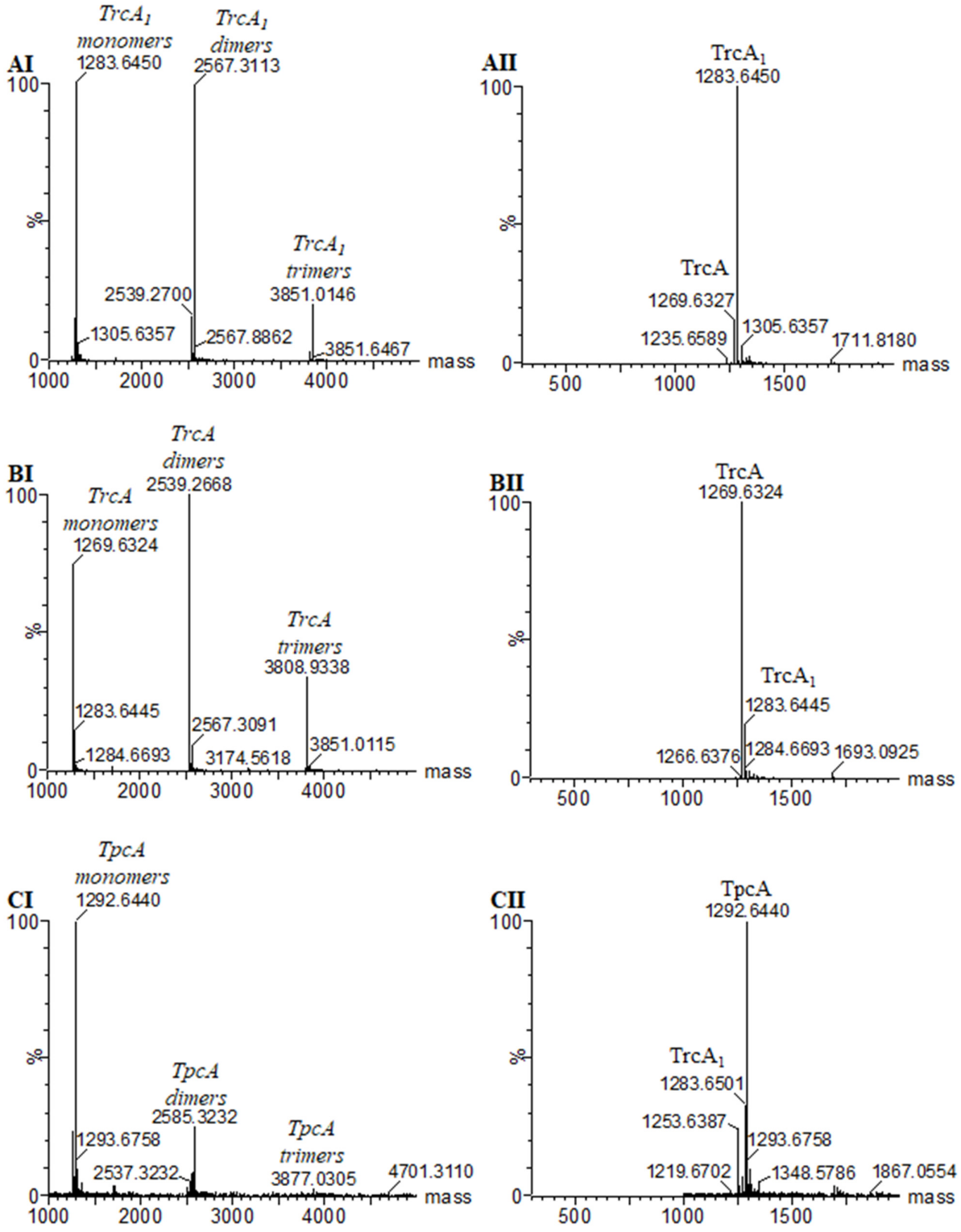

Figure 2.9 HR-ESMS analysis of CDP extract from commercial tyrothricin. AI – CI: HR-ESMS spectrum of $TrcC_1$, TrcC and TpcC monomers, dimers, and trimers, respectively. AII – CII: The enlarged spectrum of $TrcC_1$, TrcC and TpcC from 300 – 2000 Da showing the monomeric analogue present within the sample and peak. Peptide abundance and retention time are provided in Table 2.3.

2.7.2 Peptide peak identity conformation of crude CDP extract from Br. parabrevis ATCC 10068

As observed for the commercial Trc mix, a similar nature for the crude extract is seen of the Trc analogues in their nature to produce monomers, dimers, and trimer oligomers (aggregates) as revealed using Direct HR-ESMS, shown in Figure 2.10 AI-CI, 2.11 AI-CI and 2.12 AI – CI, respectively. Analogue retention time along with percentage abundance within the sample is provided in Table 2.4 which correlate to selected analogue peaks in Figure 2.6

Figure 2.10 AI, BI and CI reveal the presence of $TrcC_1$ (1361.6781), TrcC (1347.6527) and TpcC (1370.6803) monomers, dimers, and trimer oligomeric (aggregate) structures indicating that these structures are highly stable due to them not being removed or disrupted when exposed to the conditions of HR-ESMS. Monomeric molecules of $TrcC_1$ (1361.6781), TrcC (1347.6527) and TpcC (1370.6803) are indicated in the enlarged HR-ESMS spectra in Figure 2.10 AII, BII and CII, confirming major analogue identity within the selected peak. Peak overlap is observed due to the presence of TrcC in Figure 2.10 AI and $TrcC_1$ in Figure 2.10 BI.

Similarly, to obtain results for the commercial Trc mix, Figure 2.11 AI, BI and CI revealed $TrcB_1$ (1322.6588), TrcB (1308.6517) and TpcB (1331.6632) monomeric, dimeric, and trimeric oligomers (aggregates) present within the extract. Figure 2.11 AII, BII and CII confirm the monomeric molecule of $TrcB_1$ (1322.6588), TrcB (1308.6517) and TpcB (1331.6632), respectively, that are found as the major analogue within each of the selected peaks.

Lastly, Figure 2.12 presents the presence of $TrcA_1$ (1283.6498), TrcA (1269.6343), TpcA (1292.6503) and PhcA (1253.6472) monomers, dimers, and trimers in AI, BI, CI and DI, respectively. Furthermore, Figure 2.12 AII, BII, CII and DII provide the enlarged HR-ESMS spectra confirming the major analogue present within the peaks shown in Figure 2.6. Interestingly, PhcA, Figure 2.12 DI and DII, is only identified and present within the crude peptide extract compared to the commercial extract, as elaborated on in section 2.4.3.

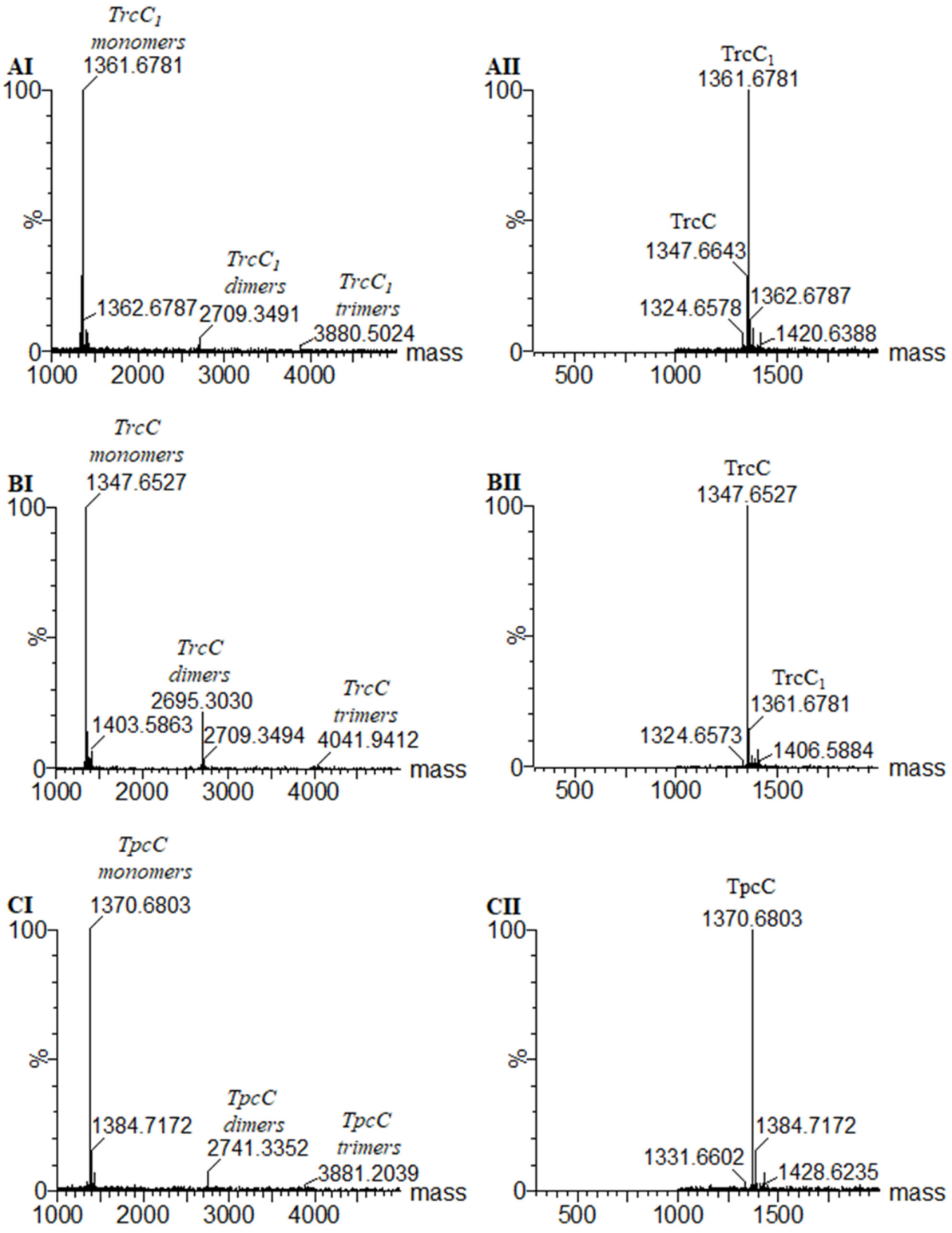

Figure 2.10 HR-ESMS analysis of CDP extract from *Br. parabrevis* ATCC 10068. AI – CI: HR-ESMS spectrum of $TrcC_1$, TrcC and TpcC monomers, dimers, and trimers, respectively. AII – CII: The enlarged spectrum of $TrcC_1$, TrcC and TpcC from 300 – 2000 Da showing the monomeric analogue present within the sample and peak. Peptide abundance and retention time are provided in Table 2.3.

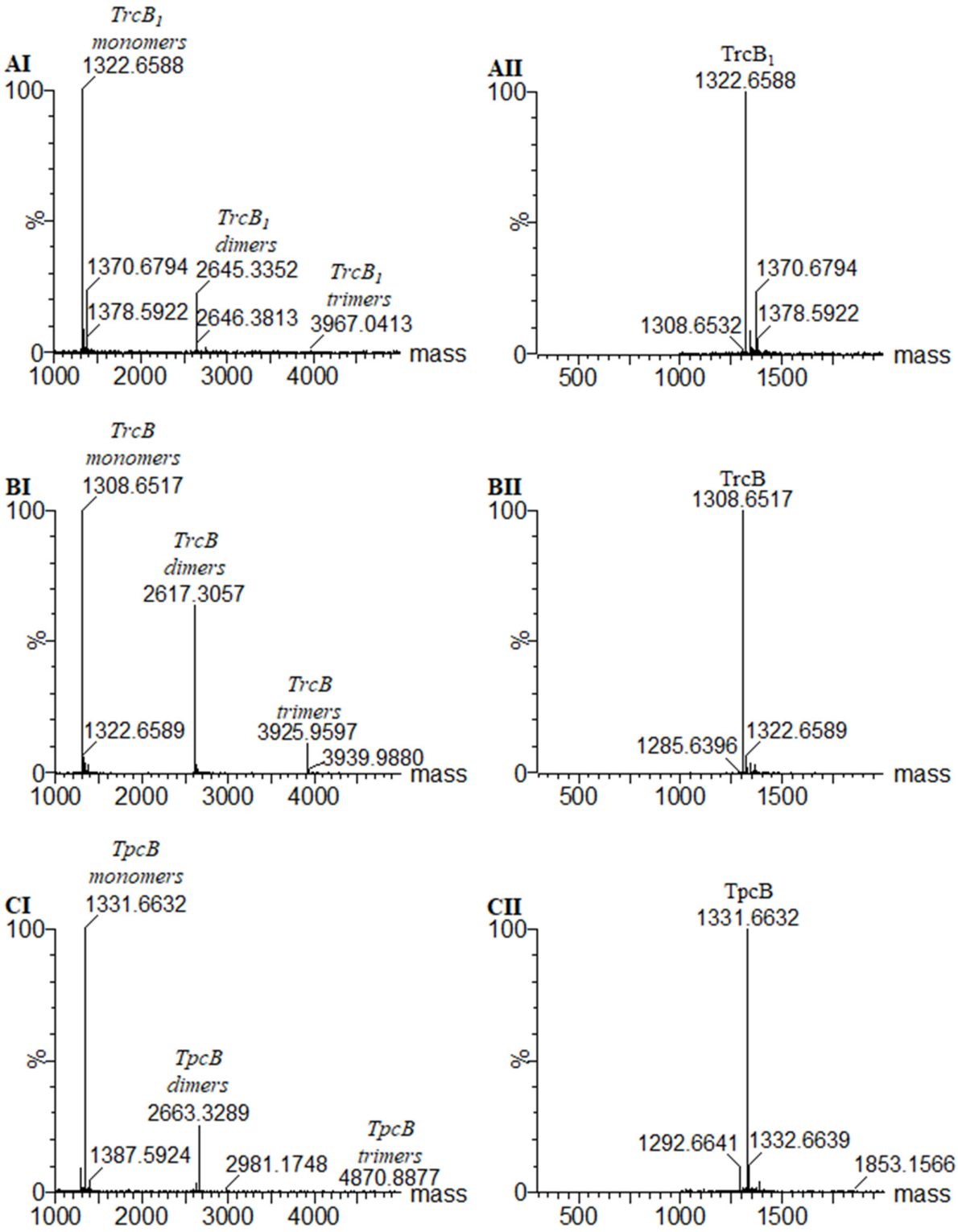

Figure 2.11 HR-ESMS analysis of CDP extract from *Br. parabrevis* ATCC 10068. AI – CI: HR-ESMS spectrum of $TrcC_1$, TrcC and TpcC monomers, dimers, and trimers, respectively. AII – CII: The enlarged spectrum of $TrcC_1$, TrcC and TpcC from 300 – 2000 Da showing the monomeric analogue present within the sample and peak. Peptide abundance and retention time are provided in Table 2.3.

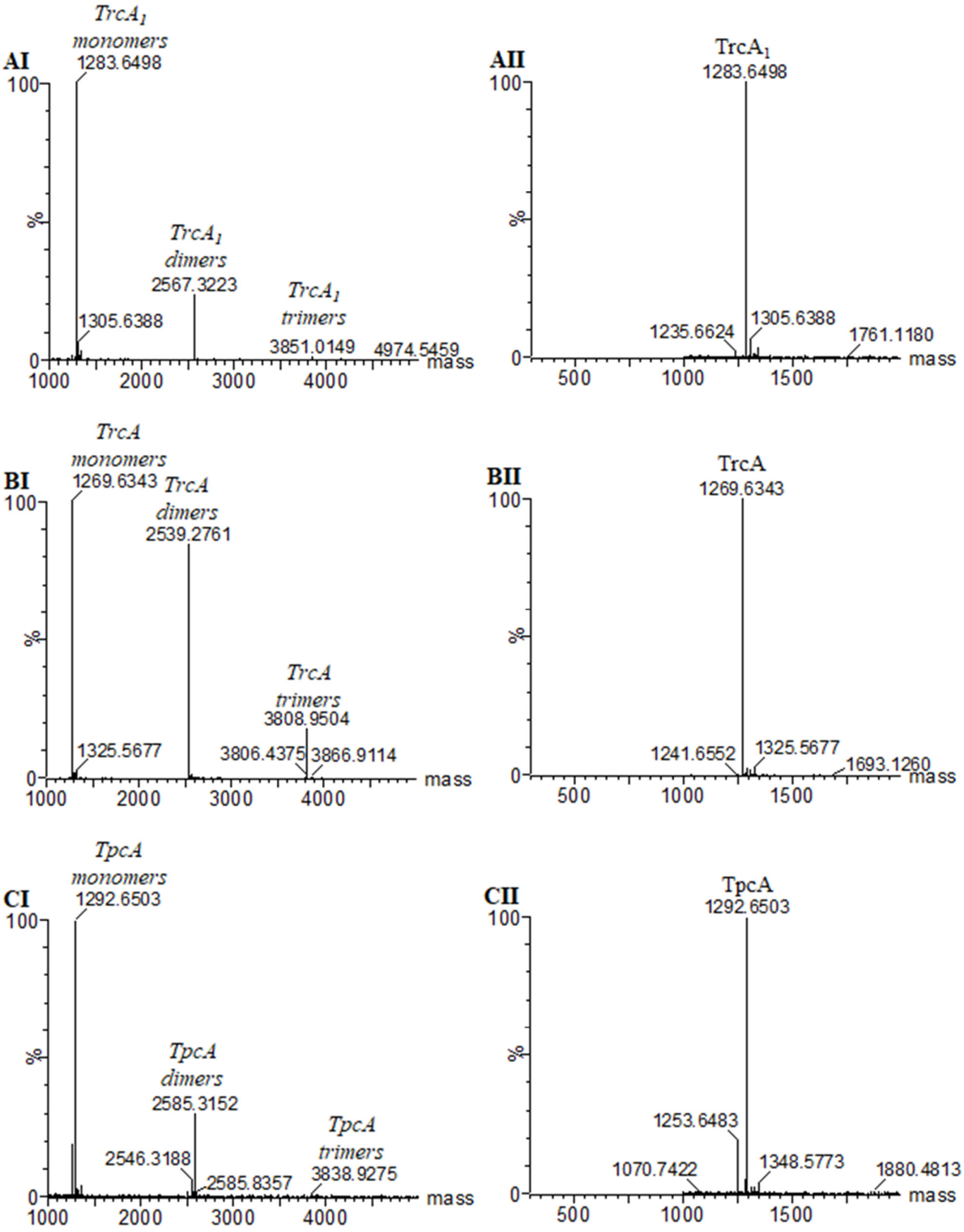

PTO for complete figure

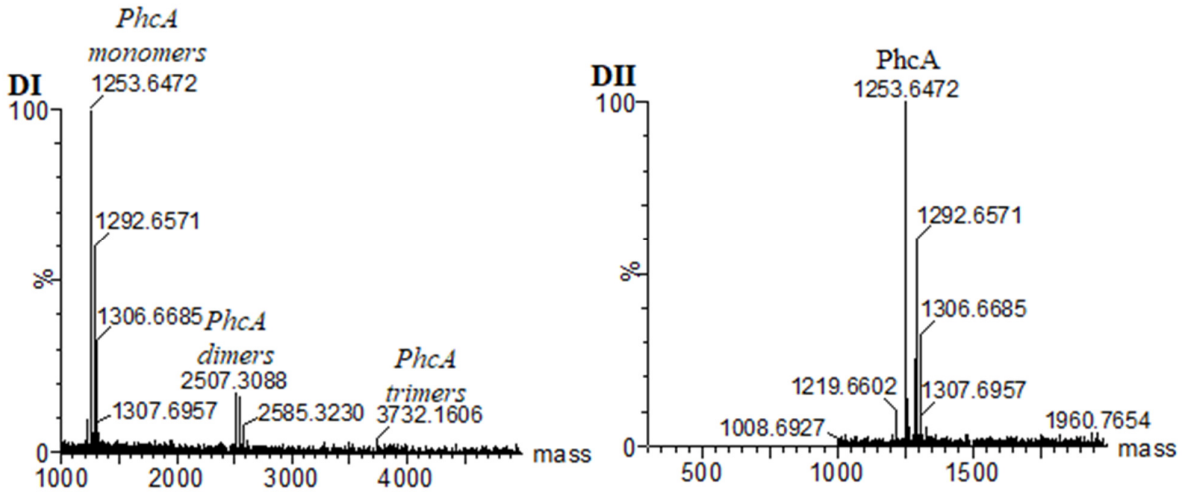

Figure 2.12 HR-ESMS analysis of CDP extract from *Br. parabrevis* ATCC 10068. AI – CI: HR-ESMS spectrum of $TrcC_1$, TrcC and TpcC monomers, dimers, and trimers, respectively. AII – CII: The enlarged spectrum of $TrcC_1$, TrcC and TpcC from 300 – 2000 Da showing the monomeric analogue present within the sample and peak. Peptide abundance and retention time are provided in Table 2.3.

Chapter 3

The influence of solvent focused formulations on bioactivity of tyrocidines towards *Listeria monocytogenes* and *Staphylococcus aureus*

3.1 Introduction

Surface colonisation and adhesion by harmful microorganisms in both the medical and industrial sectors are becoming a great threat. Coupled with the ever-increasing rise in antibiotic-resistant pathogens [1], alternative and more effective ways are needed to address this rising problem. The ability of pathogenic organisms to colonise, adhere and form biofilms on various surfaces leads to prolonged exposure and increased susceptibility to these pathogens, promoting a reservoir for these pathogens to persist, transmit and infect [2,3] homes, hospitals and industrial workplaces [4]. To address this, various cleaning and disinfecting methods have been developed and agreed upon so long they are applied and used inappropriately [5]. However, there are areas of disagreement as to the most efficient and effective methods of environmental cleaning and disinfection of surfaces [6]. The role of disinfectants is the eradication and removal of pathogens post surface contamination, but this is not an effective approach as this does not prevent further surface contamination due to the disinfectants having a short duration of action/activity [7].

An example is the food spoilage organism, *Listeria monocytogenes,* of which many strains have been isolated from various food processing environments and products due to the control of the food pathogen within these facilities being a continual challenge [8,9]. Its prevalence within these environments can be attributed to its ability to survive at low temperatures, aerobic and facultative anaerobic respiration, and the ability to form biofilms on different surfaces [8-10]. Studies conducted in Italy at a pork slaughtering plant found that *L. monocytogenes* contamination was detected in the utilised knives, carcass surfaces (23% of samples) and the floor and drains of wash areas (25% of samples) [11]. Further studies were conducted within the poultry [12,13], cheese [14], beef [15,16], and ready-to-eat [17] industries with similar results being obtained. Although standard cleaning and disinfecting practises were strictly applied and followed, *L. monocytogenes* was and is still prevalent and cannot effectively be eradicated. This persistence is due to the ability of *L. monocytogenes* to form biofilms allowing additional protection against disinfection and cleaning efforts [18]. Another problematic pathogen in the healthcare industry is *Staphylococcus aureus*, a Gram-positive bacterium that causes a wide range of clinical diseases, with infection being common within the hospital and community settings [19]. Studies have shown that within hospital environments, the surfaces such as bed rails, patient chairs, sinks and bedside tables are severely contaminated [4,20-22]. A surface study

conducted by Laila *et al.* [23] within the Provincial Hospital Centre in Morocco detected 88% bacterial growth from the 200 swabs taken. From these samples, 31.7% of the bacterial growth was Gram-negative multidrug resistance (MDR) bacteria and of the Gram-positive bacteria, 44.7% was identified as MDR *S. aureus* [23]. Another study by Huang *et al.* [24] found that surfaces such as laminated tabletops, cloth curtains and plastic chairs were able to sustain *S. aureus* survival for up to 12 days. As a major focus is being placed on circumventing antibiotic resistance, the rise in potential resistance development towards current cleaning and disinfecting agents is not receiving the attention it deserves to combat this problem [25]. Therefore, it is vital that an alternative approach is developed with a focus on surface treatment that prevents initial contamination, maintains surface sterility, and prolonged compound activity and is capable of a wide range of applications which are generally regarded as safe (GRAS) status.

A possible solution to the above-mentioned problem is the development of antimicrobial formulations or materials incorporating antimicrobial peptides (AMPs). Although the potential antimicrobial materials can kill and inhibit bacterial spread and contamination on surfaces [25], their shortfalls are that active ingredients have poor antimicrobial activity, only short-term stability, and are prone to induce microbial resistance [25]. AMPs serve as the most likely candidates for the active ingredient in antimicrobial formulations or self-sterilising materials that can be utilised for surface sterilisation and protection. Nisin, a successfully utilised AMPs with generally regarded as safe (GRAS) status, has a wide array of applications ranging from biomedical applications [27] to food preservation [28]. Because of nisin's success, further development and incorporation of alternative AMPs are being explored with the following characteristics being desired: long-term high stability, inexpensive and easily synthesised, does not decompose or emit toxic products, water-insoluble, broad-spectrum antimicrobial activity and non-toxic and non-irritating [29].

The tyrocidines (Trcs) are a group of non-ribosomal antimicrobial cyclodecapeptides synthesised by the soil bacterium, *Brevibacillus parabrevis*, as part of a complex with linear gramicidins (Grms) known as the tyrothricin complex [30] (refer to Chapter 2 for more details). Due to the nature of the Trcs, selectivity is not limited, as the Trcs have broad-spectrum activity towards various Gram-positive bacteria such as *L. monocytogenes* [31], *S. aureus* [32], *Micrococcus luteus* [31] and certain environmental Gram-negative bacteria [33]. Additional targets include a broad range of filamentous fungi, including *Botrytis cinerea* and *Aspergillus fumigatus* [34,35], but also the human fungal pathogen *Candida albicans* [36]. The rapid membranolytic activity of the Trcs and multiple modes of action makes resistance development not likely to occur, as reported in a recent study [37]. Being toxic to eukaryotic cells, the Trcs have been limited to topical creams and throat lozenges in their medical applications [38]. However, for topical applications and surface sterilisation, the potential of

low resistance development, selectivity towards multiple targets, the capability of sticking to various materials [39], low environmental, oral and topical toxicity, heat and pH stability, low water solubility and degradation resistant character, while remaining biodegradable [40,41] the Trcs are perfectly suited active ingredients for antimicrobial formulations or self-sterilising materials. However, to develop active formulations and functional materials one must consider that the Trcs readily form higher order oligomers/aggregates (refer to Chapter 2, Figure 2.1) resulting in a decrease in selectivity and activity.

The focus of this chapter is to assess the influence of six different solvents and additives (Table 3.1), in varying combinations (Table 3.2), on the overall antimicrobial activity of tyrocidine mixture (Trc mix) towards *L. monocytogenes* and *S. aureus*. The effect of solvents and varying additives have been shown to influence the different structural interactions and conformations of peptides [42,43]. The relationship between the relative M_r and dielectric constant was determined to provide insight into the influence the different formulations had on the activity and mode of action. It is expected that the different conditions will influence the aggregation and activity of the peptide.

Table 3.1 Summary of solvent system and additive utilised for tyrocidine (Trc) formulations development and used in this study.

Solvent (Abbreviation)	Elementary composition	M_r *	Character	ε *	Dipole moment
Acetonitrile (ACN)	C_2H_3N	41.03	Polar aprotic	37.5	3.92 D
Isopropanol (IPA)	C_3H_8O	60.06	Polar protic	19.92	1.66 D
Propylene-glycol (PG)	$C_3H_8O_2$	76.05	Polar protic	36.95	2.27 D
Tertiary-butanol (TBA)	$C_4H_{10}O$	74.07	Polar protic	10.9	1.70 D
Methanol (MeOH)	CH_4O	32.03	Polar protic	32.7	1.69 D
Ethanol (EtOH)	C_2H_6O	46.04	Polar protic	24.55	1.68 D
Additive	**Elementary composition**	**M_r ***	**Character**	**ε ***	**Dipole moment**
Glycerol (Glr)	$C_3H_8O_3$	92.04	Polar protic	41.01	2.62 D
Zinc Chloride ($ZnCl_2$)	$ZnCl_2$	136.29	Polar, ionic	NA	NA
Calcium Chloride ($CaCl_2$)	$CaCl_2$	110.98	Polar ionic	NA	NA

***- Data used for dielectric constant (ε) and relative molecular weight (M_r) calculations – refer to section 3.4.5**

3.2 Materials

Tyrothricin extract (extract from *Brevibacillus parabrevis*), gramicidin S (extract from *Aneurinibacillus migulanus)*, tert-butyl alcohol (TBA) and iso-propyl alcohol (IPA), resazurin

sodium salt were supplied by Sigma-Aldrich (St. Louis, MA, USA). Absolute ethanol (EtOH, >99.8%), yeast extract, tryptone and chloroform were supplied by Merck (Darmstadt, Germany). Methanol (MeOH) and acetonitrile (ACN, HPLC-grade, far UV cut off) were provided by Romil Ltd. (Microsep, Johannesburg, South Africa). Analytical grade water (MQH_2O) used for all peptide formulations was obtained using a reverse osmosis purification plant, through a Millipore-Q® water purification system (Milford, USA). Cell culture plates (96-well plates) were supplied by Thermo-Fisher Scientific (Waltham, MA, USA). Petri dishes were supplied by Lasec (Cape Town, South Africa) and sterile Falcon® tubes were supplied by Becton Dickson Labware (Lincoln Park, USA). Polycarbonate syringe filters (0.22 µM and 0.45 µM) were from Merck-Millipore (MA, USA). Glucose, agar, sodium chloride (NaCl), calcium chloride ($CaCl_2$), hydrochloric acid and brain heart infusion growth medium (BHI) were supplied by Merck (Wadeville, Gauteng). Propylene-glycol (PG) was gifted by Plascon® (Plascon, South Africa). *L. monocytogenes* B73 was obtained from the BIOPEP™ bacterial library (Stellenbosch University, South Africa) and *S. aureus* RN4220 was gifted by Prof. E Strauss of the Biochemistry department (Stellenbosch University, South Africa).

3.3 Methods

3.3.1 Culturing of target organisms

Freezer stocks of *Listeria monocytogenes* B73 were streaked out onto BHI agar plates (brain heart infusion medium and 1.5% (*m/v*) agar) and grown at 37°C for 46 hours until visible colonies were present. *S. aureus* RN4220 freezer stocks were streaked out onto LB agar media plates (Luria Betrani medium containing 1% *m/v* tryptone, 0.5% *m/v* yeast extract, 1% *m/v* NaCl and 1.5% *m/v* agar made up in water) and grown at 37°C for 24 hours until visible colonies were present. All procedures followed standard sterile biosafety level 2 culturing techniques. For overnight starter cultures, three to five colonies were selected and inoculated into 20 mL of respective optimal growth media and grown overnight for 16 hours. Subcultures were prepared using 1% of overnight culture into 10 mL of fresh media and incubated until the mid-log growth phase was reached. All grown cultures were incubated at 37°C and slanted at 150 RPM. The mid-log growth phase and cell concentrations were determined from previously obtained plate count data in our laboratory: *L. monocytogenes* (OD_{600} = 0.4, ± 1.3 x 10^8 cells/mL) and *S. aureus* (OD_{600} = 0.3, ± 1.4 x 10^8 cells/mL) with optical density measured at 600 nm at a light path length of 1 cm.

3.3.2 Development of Trc-formulations for antimicrobial activity

The Trc mix was made up to two final analytical concentrations of 0.500 mg/mL and 0.100 mM (calculated using average peptide M_r =1308) at a final solvent concentration of 10% (*v/v*) for each of the six solvent systems: ACN, TBA, IPA, EtOH, MeOH and PG. The 0.500 mg/mL Trc mix was then

formulated separately with 1% glycerol (Glr), 5 µM $ZnCl_2$ and 1% Glr in combination with 5.00 µM $ZnCl_2$. The 0.100 mM Trc mix was formulated separately with 100 µM $ZnCl_2$, 100 µM $CaCl_2$ and 1% Glr in combination with 100 µM $CaCl_2$. The details of the formulations used in this study are summarized in Table 3.2. Each formulation was made up to a final 10% (*v/v*) solvent concentration and allowed to incubate for 1 hour. Following incubation, 200 µL of the formulations were added to a 96-well microtiter plate (dilution plate) and serially diluted. A sample volume range of 10.0 – 100.0 µL was transferred into the corresponding well in a new 96-well microtiter plate (activity plate) resulting in either a final dried peptide range of 5 µg – 0.0534 µg or 13.8 µg – 0.107 µg in the wells at a final solvent concentration of 1% (*v/v*), following overnight drying. A control peptide solution of GS was made up to 0.500 mg/mL followed by 10.0 µL transferred to a 96-well microtiter plate (activity plate) and allowed to dry overnight. Treated plates were sterilized for one hour under chloroform following drying prior to testing. The Trc mix formulation inhibition concentrations (µg/mL) were determined and correlated to a fixed amount of Trc mix (µg/cm^2) dried to the surface of the well following exposure. The determined IC_{50} concentrations correlate to the initial concentration of peptide in the 10 µL that the target cells experience.

Table 3.2 A summary of the different additives and ratios for the Trc-peptide formulations made up in each of the six solvent systems assessed towards the bacterial targets.

Formulant	Trc mix: formulant (*m/m*)	Final concentration of formulant (µM)
Solvent	-	-
$ZnCl_2$	1:20	5 µM
$ZnCl_2$	1:1	100 µM
1% Glr + $ZnCl_2$	1:20	1% (*v/v*) + 5 µM
1% Glr	1:20	1% (*v/v*)
$CaCl_2$	1:1	100 µM
1% Glr + $CaCl_2$	1:1	1% (*v/v*) + 100 µM

3.3.3 Antimicrobial activity assays of Trc-formulations towards selected targets

L. monocytogenes B73 and *S. aureus* RN4220 were cultured and grown as described in 3.3.1 to the correct OD_{600}. A volume of 10 µL of the grown selected target was pipetted into the sterilized 96-well microtiter plate (activity plate) and incubated for 1 hour at 37 °C. Following incubation, 90 µL PBS (phosphate buffered saline: 0.8% *m/v* NaCl, 0.02% *m/v* KCl, 0.144% Na_2HPO_4, 0.024% *m/v* KH_2PO_4; pH = 7.4) and 10 µL resazurin dye (0.3 mg/mL in PBS) was added to the plates and incubated at 37 °C. Resazurin conversion was measured at Ex_{530} and Em_{590} after 30 minutes incubation and measured every hour for two hours using the Tecan Spark 10M Multimode Microplate Reader, controlled by the Spark Control® Software provided by the Tecan Group Ltd (Mennehof,

Switzerland).The measured fluorescence was converted to % inhibition of metabolism described by the following equation:

$$\%\ \textbf{metabolic inhibition} = 100 - \frac{100\ \times (\textbf{Em}_{590\ \textbf{of well}} - \textbf{Average of Em}_{590}\ \textbf{of blank})}{\textbf{Mean Em}_{590}\textbf{of growth control} - \textbf{Mean Em}_{590}\ \textbf{blank}}$$

Growth control (0% metabolic inhibition) constituted of wells containing growth media with cells, resazurin dye and PBS and the blank (background) was no cells, resazurin dye and PBS.

3.3.4 Data analysis

Data analysis was performed using GraphPad Prism® V 6.0 and V 5.0 (San Diego, CA, USA). Calculation of microbial inhibition was determined using non-linear regression calculations by fitting the experimental data to a sigmoidal curve using a defined variable slope (Hill slope constrained to less than 7) and an upper and lower constraint set to less than 110 and 0, respectively fitted using the following equation from Rautenbach *et. al.* [44]:

$$\mathbf{y} = \frac{\textbf{bottom} + (\textbf{top} - \textbf{bottom})}{\mathbf{1} + \mathbf{10}^{\textbf{log}\mathbf{IC}_{50}\ \textbf{x activity slope}}}$$

The bottom and top parameters represent the highest and lowest metabolic inhibition percentages for the different tested formulations of Trc mix. Determined parameters used in this study as described by Rautenbach *et. al.* [44] and Du Toit and Rautenbach [45] are: MIC or IC_{max} (minimum inhibitory concentration), IC_{50} (inhibitory concentration required for 50% microbial inhibition) toward the target bacteria when exposed to the Trc formulations.

3.4 Results

Surface adherence and consequently surface contamination by both *L. monocytogenes* and *S. aureus* RN4220 is a developing problem within the food and health industry [1-6,8]. Furthermore, the lack of effective, GRAS and non-antibiotic-containing surface protection agents against these organisms and others serves as a niche target area for antimicrobial surface formulation development. The aim of this study is to assess the influence of six different solvents (refer to Table 3.1) in combination with varying ratios of different formulants (refer to Table 3.2) on the antimicrobial activity of the Trc peptide mix towards *L. monocytogenes* B73 and *S. aureus* RN4220. This was achieved by using a modified high-performance solid surface assay developed by Van Rensburg *et al*. [58] following the assay protocols developed by Du Toit and Rautenbach [45].

3.4.1 Trc formulation (1:20 ratio) activity towards L. monocytogenes

The tested antimicrobial activity of the Trc formulations ACN, EtOH, IPA, MeOH and TBA in both the solvent and 5 µM $ZnCl_2$ showed a higher degree of sensitivity toward the microbial target

(Figure 3.1). Furthermore, it can be observed that the MIC concentrations for these two formulations in these solvents were similar, except for ACN formulation where there is an apparent two-fold dilution difference between 5 µM $ZnCl_2$ (25 µg/mL Trc mix) and the solvent formulation alone containing 12.5 ug/mL Trc mix. However, upon further analyses, we found no significant difference for this difference (refer to Figure 3.2: ACN, Table 3.2), as this result could be due to the inherent error of the assay.

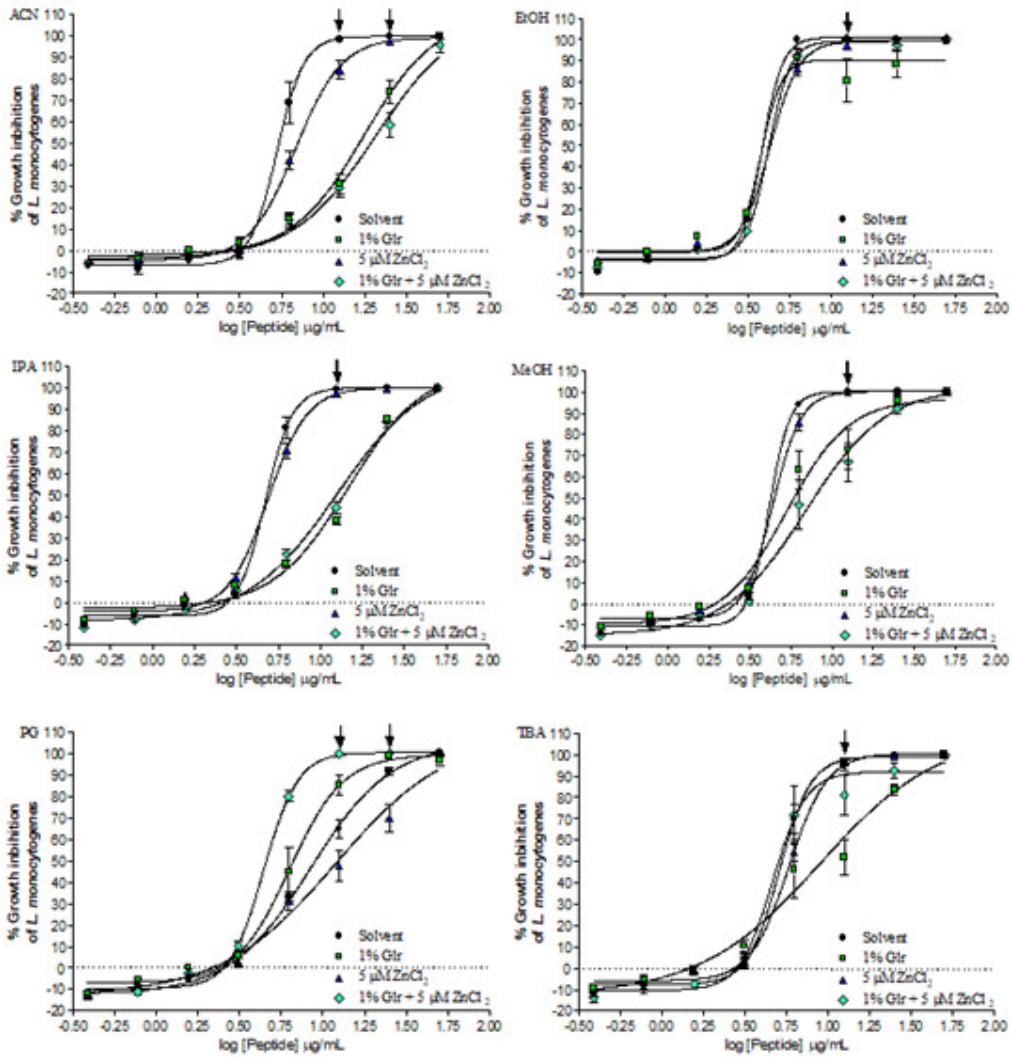

Figure 3.1 Antibacterial activity of surface dried Trc mix that was prepared in six different solvents systems (ACN, EtOH, IPA, MeOH, PG and TBA) in a final 10% (*v/v*) and in combination with one or two additives (1% Glr and 5 µM $ZnCl_2$). The top concentration represents 50 µg/mL (correlating to 500 µg/mL in one hour formulation incubation solution) with doubling dilutions down to 0.39 µg/mL (correlating to 3.91 µg/mL in one hour incubation solution). The MIC is represented with the black arrows, correlating to the concertation required to inhibit >95% of the bacterial target (Refer to Table 3.3B). Each data point represents the average of three biological repeats, with three technical repeats per assay (n = 9) with the standard error of the mean (SEM). The sigmoidal dose-response curves fitted the experimental data with R^2-values of > 0.99.

The antimicrobial activity of the formulations that contain 1% Glr for ACN, IPA ($P < 0.0001$) and TBA ($P < 0.05$) showed a significant decrease in selectivity towards *L. monocytogenes* and thus a much higher observed IC_{50} value. For ACN and IPA Trc mix formulations, there is a significant difference ($P < 0.0001$) in the observed effect of both 1% Glr and 1% Glr + 5 µM $ZnCl_2$ additives for the Trc mix formulation (Figure 3.2, refer to supplementary data, Table S3.1) with both ACN and IPA as Trc mix solvents exhibited similar dose-response to the microbial target. Furthermore, the influence of EtOH on Trc mix remained consistent in combination with 1% Glr and 1% Glr + 5 µM $ZnCl_2$. This may be attributed to the overall solvent character (refer to Table 3.1) and interaction with Glr thereby mitigating its negative effect on the peptide equilibria and activity. This is because the Trcs are known to readily form dimers and higher order structures (refer to Chapter 2, Figure 2.1) and these dimers/higher order oligomers have previously been shown in a few studies [33,35,48,49] to either form dimers via hydrogen bonding or by the hydrophobic effect required by the peptide to form dimers. Interestingly, obtained antimicrobial results for PG showed the opposite effects as compared to the other five tested solvent systems and formulations. This may be due to the similar nature and structure between PG and Glr. When PG is not in the presence of Glr, it may disrupt or compete with the peptide for hydrogen bonding like Glr. Alternatively, it may bind with water, thereby competing for H-bonds or removing the hydrophobic effect on the peptide. Overall, this will hinder the peptides' ability to form higher order structures depending on extended H-bond networks and/or hydrophobic clustering, respectively. Furthermore, it can be seen in Figure 3.1 that when in the presence of 1% Glr and/or 1% Glr + 5uM $ZnCl_2$, antimicrobial activity of the Trc formulation is returned to similar levels as those seen for the other solvent systems, and although there is no significant difference between the added 1% Glr and 1% Glr + 5 µM $ZnCl_2$ to the solvent alone, there is indeed a significant difference when compared to without any 1% Glr. Lastly, EtOH formulations (Figures 3.1 and 3.2) show no significant difference in microbial sensitivity and activity for the four tested formulations. This may be attributed to the hydroxyl groups found in EtOH and as described above for Glr, when EtOH is used, there are competing hydroxyl groups in the aqueous environment thereby allowing Glr to interact with either the free water or EtOH that could influence the peptide monomer, dimer, and higher oligomer equilibria.

Comparing peptide formulations at a specific condition between the different solvents allows for the identification of which solvent was the most sensitive at that state but also allows for the significant determination of the most optimal solvent and condition. As seen in Figure 3.3, all the solvents alone and not in combination with any formulants showed a significant difference of $P < 0.001$ when comparing to PG. However, there was no observed significant difference between any of the other

solvent formulations indicating that none improved the activity towards *L. monocytogenes* when there are no other additives.

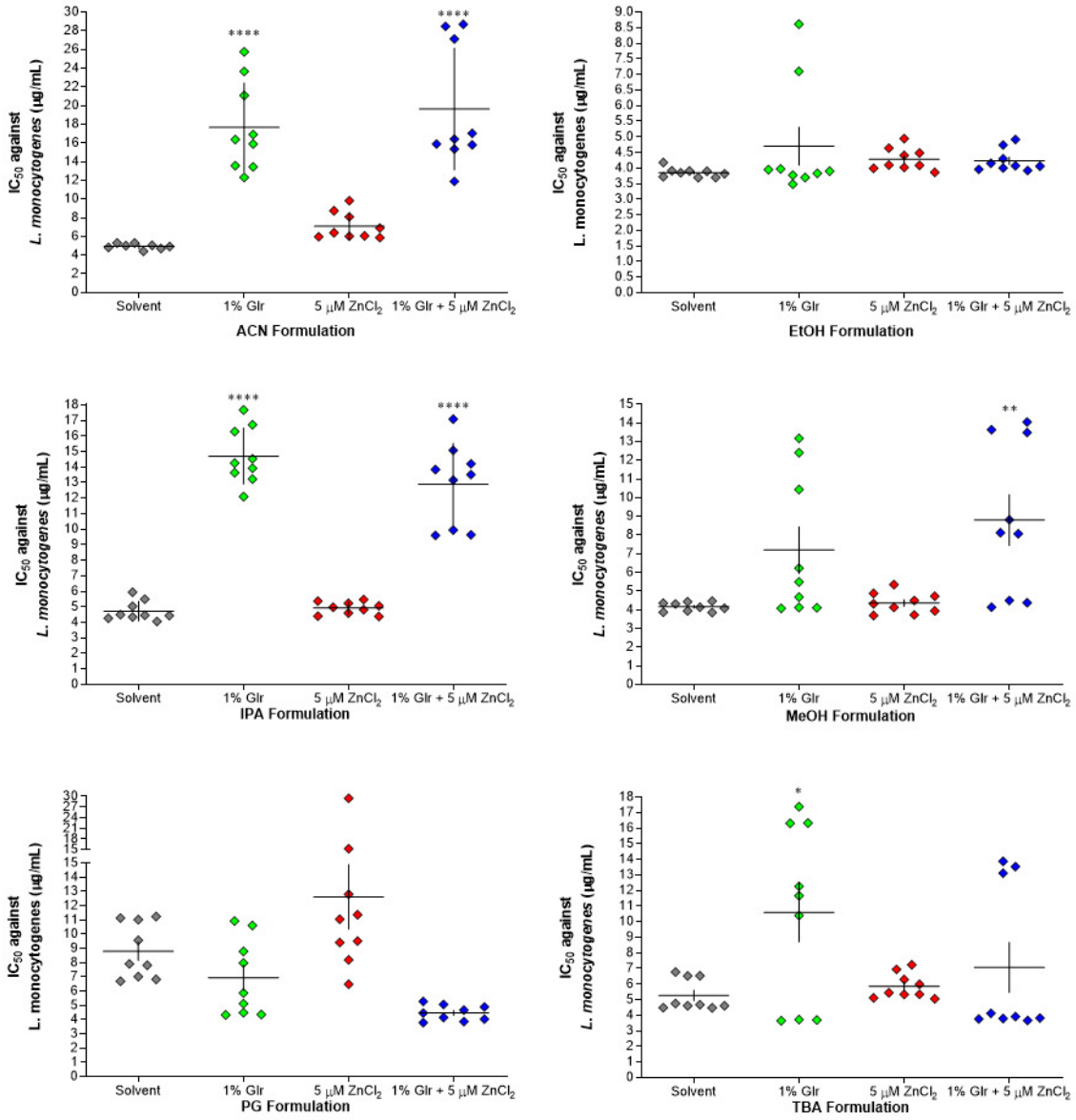

Figure 3.2 Scatter plot comparisons representing the IC_{50} values (µg/mL) (refer to Table 3.3A) obtained within each solvent formulation system tested 10% (*v/v*) ACN, EtOH, IPA, MeOH, PG and TBA in water) with $ZnCl_2$ and Glr additives. Error bars represent the mean SD for three biological repeats with three technical repeats per assay (n = 9). Statistical analysis between solvent as the control and the other conditions was performed using One-way ANOVA with Bonferroni's multiple comparison test with *P < 0.05, **P < 0.01, ***P < 0.001 and ****P < 0.0001.

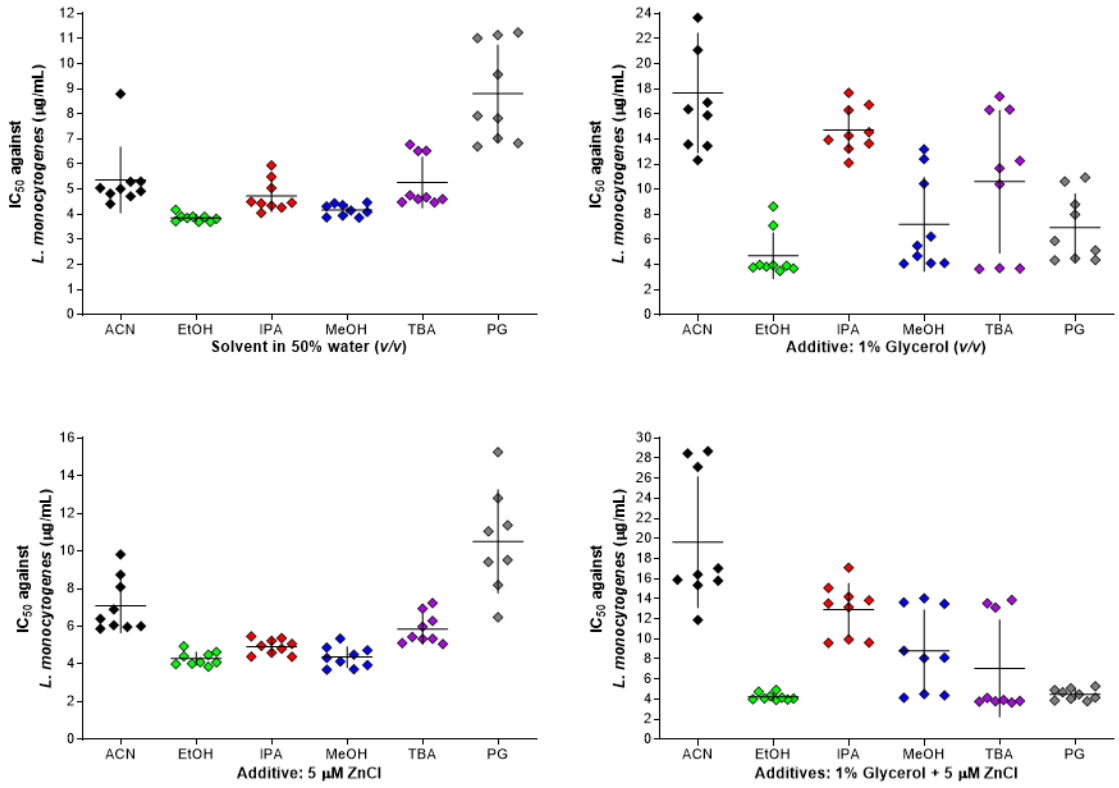

Figure 3.3 The scatter plot represents the IC_{50} values (µg/mL) (refer to Table 3.3A) obtained when comparing the effect, the different solvents (ACN, EtOH, IPA, MeOH, PG and TBA) have towards Trc mix antimicrobial activity within the specific tested peptide formulation conditions (solvent, 1% Glr, 5 µM $ZnCl_2$ and 1% Glr + 5 µM $ZnCl_2$). Error bars represent the SD for three biological repeats with three technical repeats per assay (n = 9). Full statistical analysis comparison can be found in the supplementary data, Table S3.1

It is evident that when comparing the influence of 1% Glr on each of the solvent system's activity, Glr results in a large scatter and has a significant influence on the activity performance of the Trc formulations (refer to Table S3.2). Trc mix in ACN has the highest IC_{50} value for both 1% Glr alone and in combination with 5 µM $ZnCl_2$ (1% Glr + 5 µM $ZnCl_2$) being significantly different ($P < 0.0001$) from EtOH, MeOH and PG in both formulation conditions, followed by a significant difference of $P < 0.001$ for IPA with only 1% Glr and TBA with 1% Glr + 5 µM $ZnCl_2$. Furthermore, EtOH in combination with 1% Glr and 1% Glr + 5 µM $ZnCl_2$ resulted in the lowest IC_{50} value in both conditions which were significantly different from the five other tested solvents ($P < 0.0001$ in 1% Glr and $P < 0.001$ in 1% Glr + 5 µM $ZnCl_2$). This large variability induced by Glr may not only be attributed to its role in disrupting optimal peptide conformation but may be due to Glr metabolism by *L. monocytogenes* [46]. The scatter and spread of IC_{50} values observed in Figure 3.2 – 3.3 for 1% Glr and 1% Glr + 5 µM $ZnCl_2$, may be due to Glr uptake. Previous studies conducted by Joseph *et. al.* [46] have shown that when under stress, *L. monocytogenes* can take up Glr as it is a carbon

source, increasing cellular metabolism. This uptake can be driven due to the stress placed by the Trcs [47], and as there is now an abundance of Glr available to the stressed cell, metabolism upregulation will result in the poor performance of the formulations, correlating to the results observed above. Interestingly, EtOH, as an organic solvent for Trc mix, when in combination with 1% Glr and/or 1% Glr + 5 µM $ZnCl_2$ did not result in similar scatter or increased IC_{50} towards *L. monocytogenes* B73. This could be due to the EtOH having a role in removing Glr from the cell environment by allowing Glr interaction with the peptide aggregates/nanostructures preventing its accessibility for metabolic uptake. However, without the addition of 1% Glr in any of the formulations, there is no significant difference between each of the solvent groups, except for the PG formulations ($P < 0.001$). This may be due to the nature of the Trc mix containing a combination of multiple Trc analogues and thus promoting the formation of multiple homo- and heterodimers which can occur in a variety of solvents. Proposed by Loll *et al.* [48] and Munyuki *et al.* [49], dimeric Trc may be the active moieties responsible for eliciting activity due to the amphipathic character of β-sheet type Trc unidirectional dimers that allows membrane interaction. Therefore, using optimal solvent and formulation conditions could stabilise the dimers and larger oligomers from which active dimers can be released.

3.4.2 Trc formulation (1:1 ratio) activity towards L. monocytogenes

The antimicrobial activity of ACN, EtOH, IPA, MeOH and TBA towards *L. monocytogenes* resulted in similar obtained MIC values of 6.25 µg/mL when comparing the solvent, 100 µM $ZnCl_2$ and 100 µM $CaCl_2$ formulation conditions (Figure 3.4 A-D) with there being no significant difference within the solvent groups when comparing the tested conditions (Figure 3.5 A-D). However, TBA showed a significant difference in the obtained MIC value of 1.56 µg/mL when in combination with 1% Glr + 100 µM $CaCl_2$ (refer to Figure 3.4E and 3.5E) towards *L. monocytogenes* B73. Furthermore, when comparing the obtained IC_{50} values of 1% Glr + 100 µM $CaCl_2$ in TBA to the other three tested formulation conditions, there was a significant difference of $P < 0.0001$ and $P < 0.001$ to the solvent, and 100 µM $CaCl_2$ and 100 µM $ZnCl_2$ respectively.

To understand the role that formulants have and if they have a significant effect on the peptide's ability to elicit an antimicrobial response, IC_{50} comparisons were deduced between all tested solvents within the same formulation groups. No significant differences were observed when comparing the solvent alone formulation, the 1:1 formulation containing 100 µM $ZnCl_2$ and 100 µM $CaCl_2$, and the 1:20 ratio formulation. This may be attributed to the major influence of the self-assembling nature of the tyrocidines [48,49] driven by the aqueous environment, regardless of the organic solvent modifiers and additives. Furthermore, increasing the concentration of additives seems to retain the activity regardless of the solvent or formulation ratios. However, the introduction of 1% Glr with 100 µM $CaCl_2$ showed a significant decrease in the IC_{50} values when comparing TBA to the other

four solvents ($P < 0.05$ for IPA, $P < 0.01$ for MeOH and $P < 0.001$ for ACN and EtOH). Furthermore, the addition of 1% Glr did not result in a similar decrease in activity versus those obtained for the 1:20 ratio formulations. This indicates the significance of the 100 µM $CaCl_2$ in the peptide formulation and may be indicative of a structural or mode of action role Ca^{2+} has on the Trcs. Previous studies conducted by Spathelf [54] and Leussa [55] showed that when the Trcs were formulated in combination with $CaCl_2$, there was an increase in non-lytic anti-listerial activity postulating a more specific cell activity. Therefore, in the presence of Ca^{2+}, the tyrocidines can negate the possible negative structural effects of Glr, as observed in Figure 3.6 with the low antimicrobial IC_{50} values, by potentially changing the mode of action which can be further improved with the use of specific solvents such as TBA.

Table 3.3 Summary of the A: IC_{50} and B: MIC values obtained for different Trc formulations assessed against *L. monocytogenes* with (n) representing the total number of technical repeats per condition and SD representing the standard deviation within the assessed condition.

A.	IC_{50} ± SD µg/mL (n)						
	Solvent (9)	1% Glr (9)	5 µM $ZnCl_2$ (9)	1% Glr + 5 µM $ZnCl_2$ (9)	100 µM $ZnCl_2$ (4)	100 µM $CaCl_2$ (4)	1% Glr + 100µM $CaCl_2$ (4)
ACN	5.4 ± 1.2	17.6 ± 4.5	6.8 ± 1.4	20.4 ± 6.2	2.4 ± 0.3	2.4 ± 0.3	3.0 ± 0.6
EtOH	3.8 ± 0.1	3.8 ± 1.7	4.3 ± 0.3	4.2 ±0.3	3.1±1.3	3.1±1.2	3.1±1.4
IPA	4.7 ± 0.6	14.7 ± 1.7	4.9 ± 0.4	12.6 ± 2.5	2.7±0.4	2.7±0.4	2.1±0.1
MeOH	4.2 ± 0.2	5.3 ± 3.5	4.3 ± 0.5	6.9 ± 3.9	2.9±0.7	3.3±0.6	2.4±0.5
PG	8.8 ± 1.8	6.3 ± 2.5	11.9 ±6.4	4.4 ± 0.5	1.0±0.9	1.0±1.5	0.1±0.3
TBA	5.3 ± 1.0	8.9 ± 5.4	5.8 ±0.8	4.6 ± 4.6	2.5±0.3	2.9±0.5	0.7±0.3

B.	MIC µg/mL (n)						
	Solvent (9)	1% Glr (9)	5 µM $ZnCl_2$ (9)	1% Glr + 5 µM $ZnCl_2$ (9)	100 µM $ZnCl_2$ (4)	100 µM $CaCl_2$ (4)	1% Glr + 100µM $CaCl_2$ (4)
ACN	12.5	50.0	25.0	50.0	6.3	6.3	6.3
EtOH	6.2	6.2	12.5	6.2	12.5	12.5	6.3
IPA	12.5	50.0	12.5	50.0	12.5	12.5	6.3
MeOH	12.5	25.0	12.5	50.0	6.3	6.3	6.3
PG	50.0	25.0	50.0	12.5	12.5	25.0	1.6
TBA	12.5	50.0	12.5	25.0	6.3	12.5	1.6

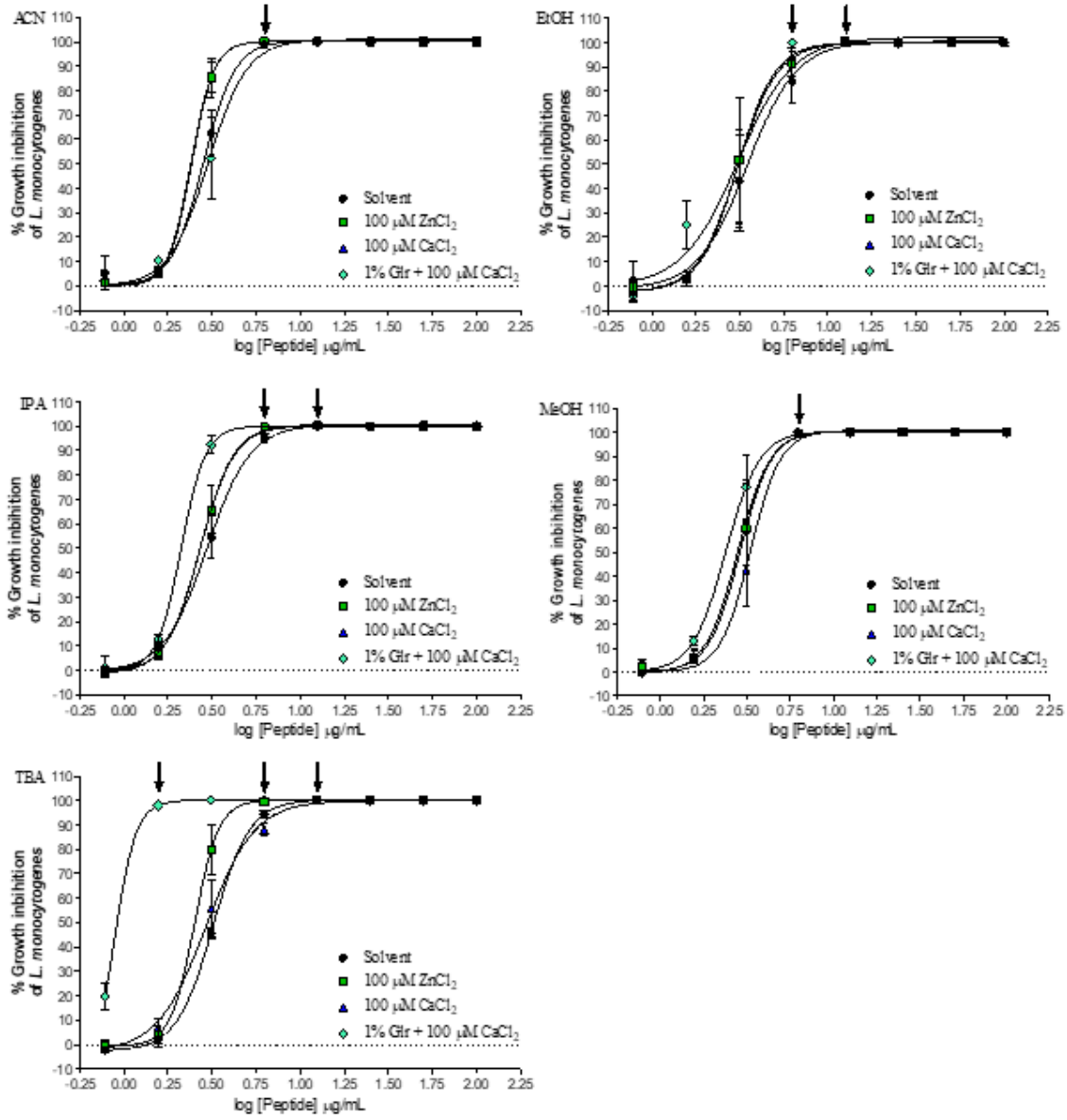

Figure 3.4 Antibacterial activity of surface dried Trc mix that was prepared in five different solvents systems (ACN, EtOH, IPA, MeOH and TBA) in combination with one or two additives (100 µM $ZnCl_2$, 100 µM $CaCl_2$ and 1% Glr + 100 µM $CaCl_2$). The top concentration represents 100 µg/mL (correlating to 1000 µg/mL in 1-hour formulation incubation solution) with doubling dilutions down to 0.781 µg/mL (correlating to 7.81 µg/mL in 1-hour incubation solution). The MIC is represented with the black arrows, correlating to the concertation required to inhibit >95% of the bacterial target (Refer to Table 3.3B). The sigmoidal dose-response curves fitted the experimental data with a R^2-vaules of >0.98. Each data point represents the average of two biological repeats, with two technical repeats per assay (n = 4) with the standard error of the mean (SEM).

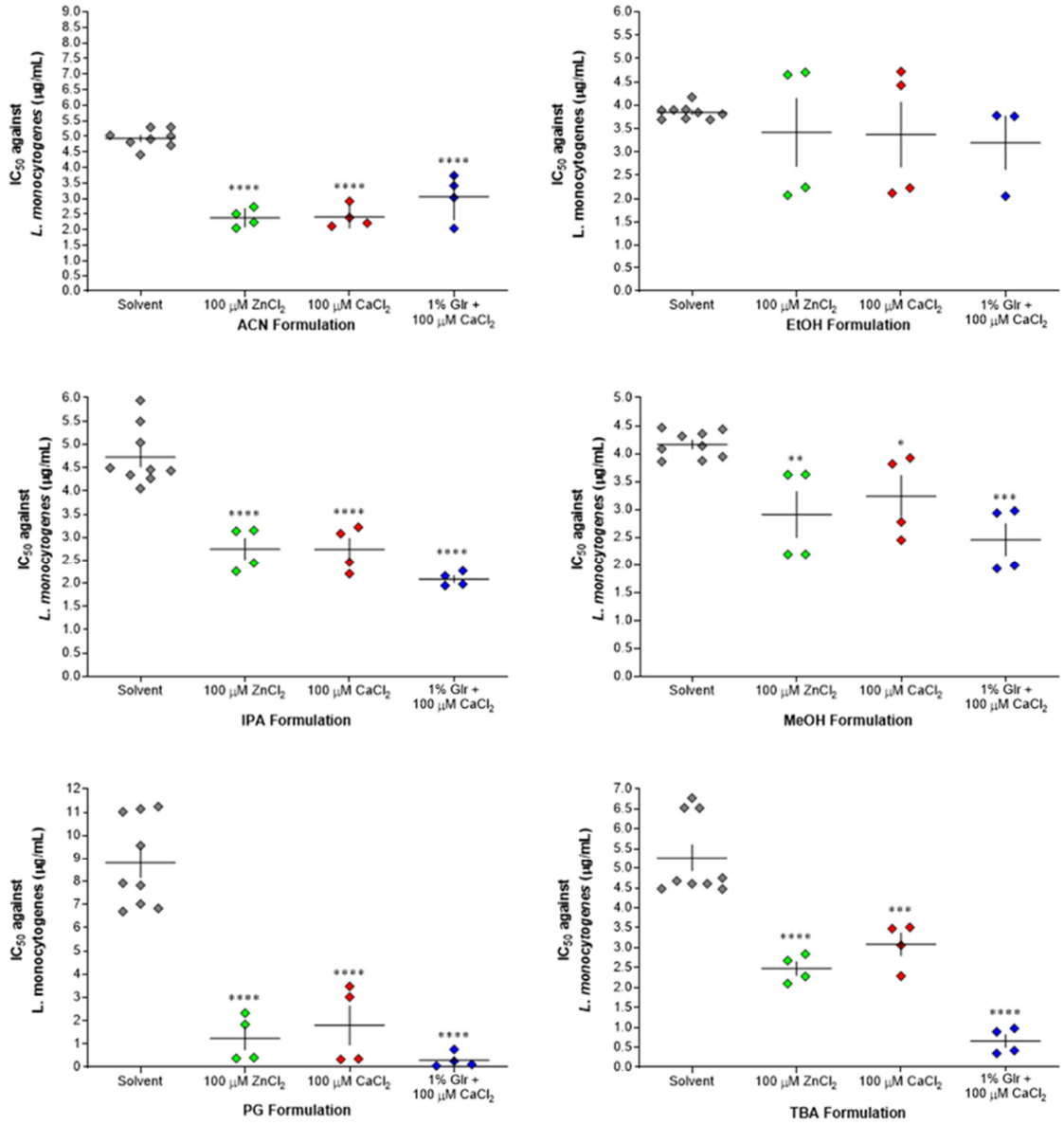

Figure 3.5 Scatter plot comparisons representing the IC_{50} values (µg/mL) (Refer to Table 3.3A) obtained within each solvent formulation system tested (ACN, EtOH, IPA, MeOH, PG and TBA). Error bars represent the SD for two biological repeats with two technical repeats per assay (n = 4). Statistical analysis between solvent as the control and the other conditions was performed using One-way ANOVA with Bonferroni's multiple comparison test with *P < 0.05, **P < 0.01, ***P < 0.001 and ****P < 0.0001.

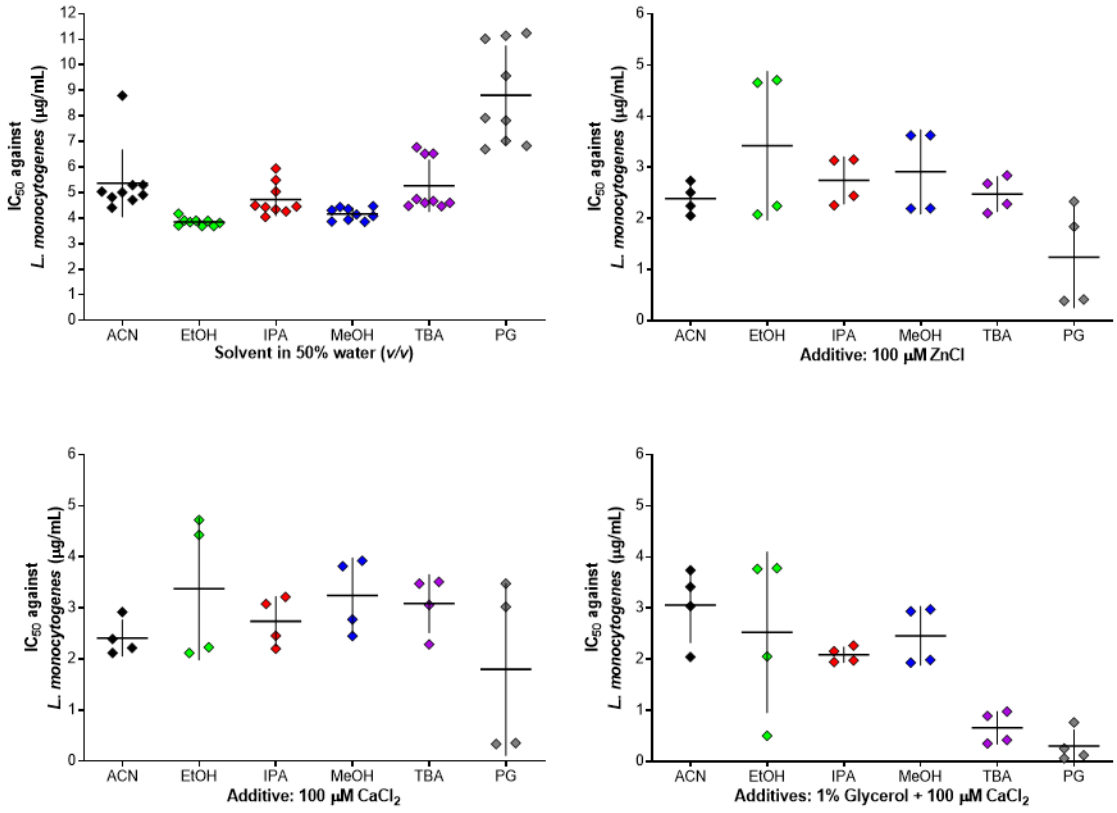

Figure 3.6 The scatter plot represents the IC_{50} values (µg/mL) (Refer to Table 3.3A) obtained when comparing the effect, the different solvents (ACN, EtOH, IPA, MeOH and TBA) towards Trc mix antimicrobial activity within the specific tested peptide formulation conditions (solvent, 100 µM $ZnCl_2$, 100 µM $CaCl_2$ and 1% Glr + 100 µM $CaCl_2$). Error bars represent the SD for two biological repeats with two technical repeats per assay (n = 4). Full statistical analysis comparison can be found in the supplementary data, Table S3.1.

3.4.3 Antimicrobial activity of various Trc formulation conditions towards S. aureus

As described earlier, the ability of microbial targets to adhere to and colonise various surfaces is not only an attributed feature of *L. monocytogenes* [2,3] but also the ability of various other microbial targets to adhere to surfaces that allows for a reservoir for pathogens to cause infection and spread [2]. One such persisting and problematic pathogen within the health system is *S. aureus*, which has been shown to adhere and survive on surfaces for periods of weeks to months [2,50]. With both *L. monocytogenes* and *S. aureus* capable of surface adhesion and contamination, they differ from one another in their cellular makeup and metabolism. To effectively combat both targets, the Trc formulations tested against *L. monocytogenes* were also tested against *S. aureus* with the focus on selecting the most effective broad-spectrum formulation based on antimicrobial activity.

3.4.3.1 Influence of additives (1:20) within solvent groups towards overall Trc formulations activity towards S. aureus

The antimicrobial activity of the different Trc formulation additives (solvent, 1% Glr, 5 µM $ZnCl_2$ and 1% Glr + 5 µM $ZnCl_2$) within each of the solvent groups was tested against *S. aureus* (IC_{50} values were determined from respective dose-response curves, with dose-response curves data not shown). Comparing the effect the additives had within each solvent group, ACN, EtOH, IPA, MeOH and TBA (Figure 3.7), did not seem to show a large range of variability for the obtained IC_{50} values, with only the formulations containing 1% Glr having significantly higher IC_{50} values when compared to those without ($P < 0.05$ – $P < 0.0001$). This result is in stark contrast to those observed for *L. monocytogenes*, as the formulations that contained Glr showed the greatest degree of "scatter", which may be attributed to cellular stress or the ability of *L. monocytogenes* to metabolise Glr as a secondary carbon source, as described in 3.4.1. This observed increase in the IC_{50} value for additives containing 1% Glr may be due to the polar nature of Glr, and the ability of Glr to interact with the polar region of the peptide resulting in steric hindrance or reducing the hydrophobic effect required by the peptide [48,49]. When assessing the role the additives have towards PG (Figure 3.7), the inverse effect is observed as compared to the other five solvents. Due to the similarity in structure between PG and Glr, when PG and 1% Glr are in combination, they may work in a synergistic manner thus stabilizing the peptide and resulting in significantly improved IC_{50} values ($P<0.0001$) when compared to the solvent and 5 µM $ZnCl_2$.

Tighter data points can be observed for ACN, EtOH, IPA and MeOH compared to those of PG and TBA. This may be attributed to either the organism and how it responds and reacts when exposed to the formulation or an equilibrium of the peptide conformation/oligomerisation before and during drying. The latter can result in a more favourable and stable conformation by the peptide on the surface promoting better selectivity towards the target. However, when formulated in PG and TBA, the peptide may be more sensitive to small changes in the environment. When comparing PG and TBA, it is evident that PG promotes a more unstable formulation compared to TBA, which can be attributed to either the similar nature of PG and Glr or the low volatility of PG leading to a change in surface chemistry. As described earlier, when not in the presence of Glr, PG may compete for H-bonding resulting in disruption for higher order oligomerisation, but when in combination of Glr, PG and Glr interact thus allowing oligomerisation and significantly improved IC_{50} ($P<0.0001$). However, as PG is the least volatile (boiling point 188 °C [51]) of all the organic solvents in this study and being used as an excipient within aqueous medical products [52], there may be an alternative effect occurring. As the boiling point required to evaporate PG is high, water is expected to first be removed in the drying process, thus, leaving a high concentration of PG to interact with the peptides in the Trc mix.

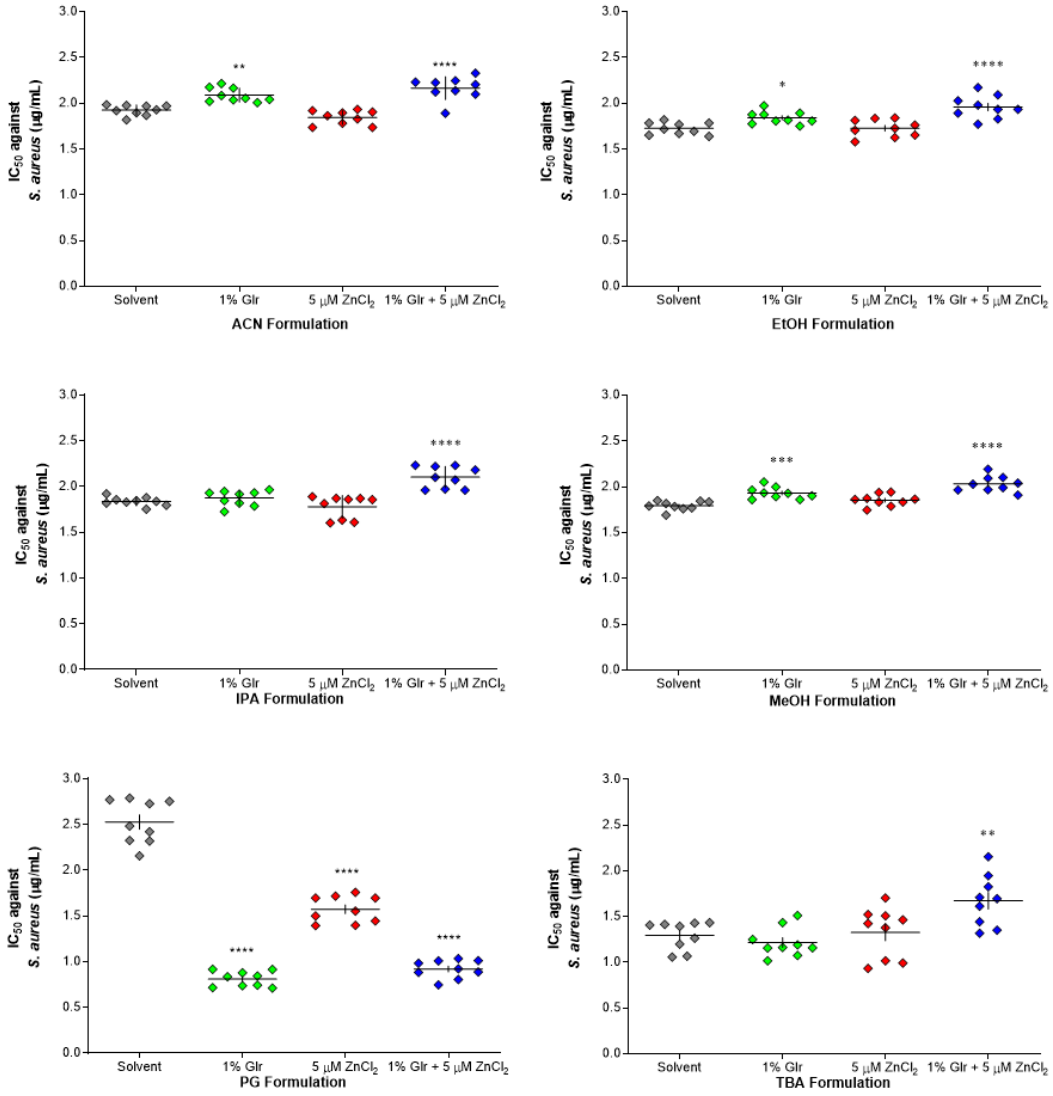

Figure 3.7 Scatter plot comparisons representing the IC_{50} values (µg/m) (Refer to Table 3.4A) obtained assessing the additive (solvent, 1% Glr, 5 µM $ZnCl_2$, and 1% Glr + 5 µM $ZnCl_2$) effect within each solvent system (ACN, EtOH, IPA, MeOH, PG and TBA). Error bars represent the mean SD for three biological repeats with three technical repeats per assay (n = 9). Statistical analysis between solvent as the control and the other conditions was performed using One-way ANOVA with Bonferroni's multiple comparison test with *P<0.05, **P<0.01, ***P<0.001 and ****P<0.0001.

This high concentration of viscous PG may lead to binding and possibly clumping the peptide and the oligomers together on the surface, due to it being used as a binding agent [52]. When re-exposed to the target aqueous environment, as PG may trap the oligomeric structures, active peptide moieties such as amphipathic dimers cannot effectively be released to illicit their activity, resulting in poor activity when only in combination with PG. However, when in the presence of Glr, PG and Glr may act as a chaotropic agent resulting in a better release of dimers and when exposed to the microbial target. Therefore, assessing formulations antimicrobial activity against *S. aureus*, none of the Trc formulations decreased or improved the overall IC_{50} value when compared to the solvent control, but

rather slightly increased or maintained the IC_{50} value, except for that of PG having the inverse effect compared to the other five solvents.

3.4.3.2 Influence of additives (1:1) within solvent groups towards overall Trc formulations activity towards S. aureus

The influence of metal ions has been studied and assessed against AMPs with various valence metal ions having varied effects on the AMPs [53]. This is no different for the Trcs and thus to further evaluate and compare the validity of the formulations towards *S. aureus*, the influence of 1:1 additive (100 µM $ZnCl_2$, 100 µM $CaCl_2$ and 1% Glr + 100 µM $CaCl_2$) formulations were assessed within each of the solvent groups (IC_{50} values were determined from respective dose-response curves, with dose-response curves data not shown) (Figure 3.8). Increasing the $ZnCl_2$ concentration from 5 µM to 100 µM had no significant influence on the antimicrobial activity against *S. aureus* for ACN, IPA, MeOH and TBA peptide formulations. However, the increase in concentration of $ZnCl_2$ significantly increased ($P < 0.001$) the IC_{50} value of the EtOH formulation. These observations show that the Trcs antimicrobial activity is not enhanced by the addition of Zn^{2+}, but that Zn^{2+} may potentially have an alternative role in peptide oligomerisation and stabilisation for activity. Furthermore, 100 µM $ZnCl_2$ with PG caused a significant increase ($P < 0.0001$) of the IC_{50}. This can be attributed to a similar effect as observed with the earlier 1:20 ratio formulations for PG whereby PG has an antagonistic effect on the peptide. This will either result in the peptide folding into an unfavourable conformation for optimal selectivity and activity or PG binds and sticks peptide units together, preventing the dimers from disassociating when in contact with the organism [48].

Due to $CaCl_2$ previously being shown by Spathelf [54] and Leussa [55] to improve the activity of the Trcs against listeria and potentially altering the mode of action from lytic to non-lytic [55], the influence towards a different target and cellular makeup was determined. Interestingly, ACN and MeOH did not show any significant changes to the IC_{50} when compared to the solvent control, however, EtOH, IPA, TBA and PG resulted in a significant increase ($P < 0.001$ and $P < 0.0001$) in IC_{50} values. This increase in IC_{50} (decrease in activity) may be due to the Ca^{2+} competing with the Trcs for the binding site on the negatively charged phospholipid headgroups of *S. aureus* cell membrane, thus potentially preventing full anchoring of the peptide. This slight decrease in activity correlates with obtained results obtained by Marques *et al.* [56] in which Trc A and analogues did not show an increase in antibacterial activity towards MRSA when exposing the peptide to increasing Ca^{2+} concentration.

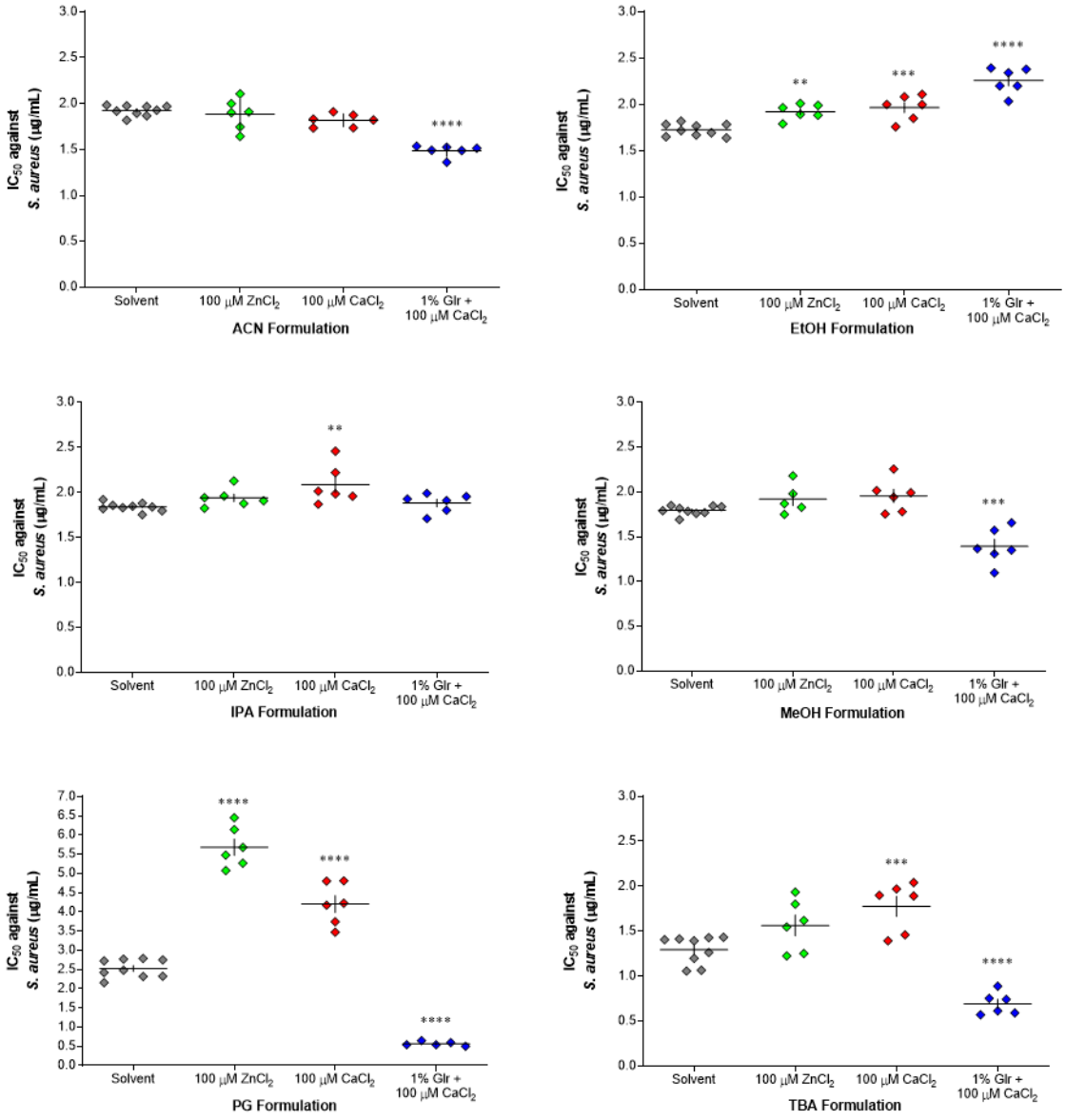

Figure 3.8 Comparative scatter plot comparisons representing the IC50 values (µg/mL) (refer to Table 3.4A) obtained assessing the additive (solvent, 100 µM $ZnCl_2$, 100 µM $CaCl_2$ and 1% Glr + 100 µM $CaCl_2$) effect within each solvent system (ACN, EtOH, IPA, MeOH, PG and TBA). Error bars represent the mean SD for three biological repeats with two technical repeats per assay (n = 6). Statistical analysis between solvent as the control and the other conditions was performed using One-way ANOVA with Bonferroni's multiple comparison test with *P < 0.05, **P < 0.01, ***P < 0.001 and ****P < 0.0001.

The combination of 1% Glr and 100 µM $CaCl_2$ rendered interesting results when compared to the solvent control and the $CaCl_2$ formulation. ACN, MeOH, PG and TBA all resulted in a significant decrease ($P < 0.0001$) in IC_{50} (improved activity) against *S. aureus*, however, EtOH resulted in a significant increase ($P < 0.0001$) in IC_{50} (decrease in activity) followed by IPA, showing no significant change in activity ($P > 0.05$). The improved activity observed for ACN, MeOH and TBA

may be the result of a complex association effect which is driven by Glr and Ca^{2+}. This interaction can potentially result in an interaction between Glr and the peptide, whereby Glr does not compete for the target binding but rather binds to the peptide, as it has previously been shown that the Trcs bind to sugar moieties – carbohydrates [39] (see section 3.4.5). This forces the peptide into an alternative conformation state that may be stabilised by the high concentration of Ca^{2+}, and due to a high concentration of Ca^{2+} within the target membrane, this peptide- Ca^{2+} stabilised conformation may result in an alternative mode of action on the target membrane and cell. PG is observed to have significantly improved activity for the 1% Glr + 100 µM $CaCl_2$ formulation. This may be due to the structural nature of PG and Glr, in their similarities and competition with binding to the peptide. However, without 1% Glr, PG in combination with 100 µM $CaCl_2$ does not improve activity but rather decreases the formulation activity (increases IC_{50}). This may be related to the structure of PG in which it may cause competition by either binding to the target or binding to the peptide. If binding to the peptide, PG has an extra OH group present which may force the peptide into a very unstable or unfavourable conformation for activity. Alternatively, as described earlier, as water is removed first from the formulation, the high concentration of PG may act as a glue thereby "clumping/trapping" the peptide oligomers, hindering the release of dimeric units when re-exposed to the microbial target. However, when in combination with Glr, that effect may be counteracted or negated by the binding of Glr to PG, potentially allowing for a more optimal peptide conformation state or more "free" oligomers scaffolds which potentially allow the release of peptide dimeric units.

3.4.3.3 Influence of specific Trc formulation additives between solvents groups on activity against S. aureus

Understanding the role and impact the solvent has on the peptide formulation is vital, due to the nature of the solvent contributing to the stability and folding of the peptide which will dictate the structure [57]. All six solvents were assessed within each formulation condition and compared based on improving activity below the threshold selected to determine the most optimal solvent (Figure 3.9) Comparing all six solvents (Figure 3.9), TBA and PG show the most significant influence towards antimicrobial activity when compared against the other four solvents, with TBA improving activity while PG decreased activity (Table S3.2: Solvent). When combined with 1% Glr with PG, TBA and PG both showed a significant difference in antimicrobial activity when compared to the other four solvents by improving the antimicrobial activity of the formulation showing the most IC_{50} improvement (Figure 3.9 B). For 5 µM $ZnCl_2$ and 1% Glr + 5 µM $ZnCl_2$, the addition of 5 µM $ZnCl_2$ results in a higher degree of "scatter" and may be attributed to the interaction of zinc with the peptide resulting in a non-optimal yet still active conformation of the peptide (Figure 3.9 C and D).

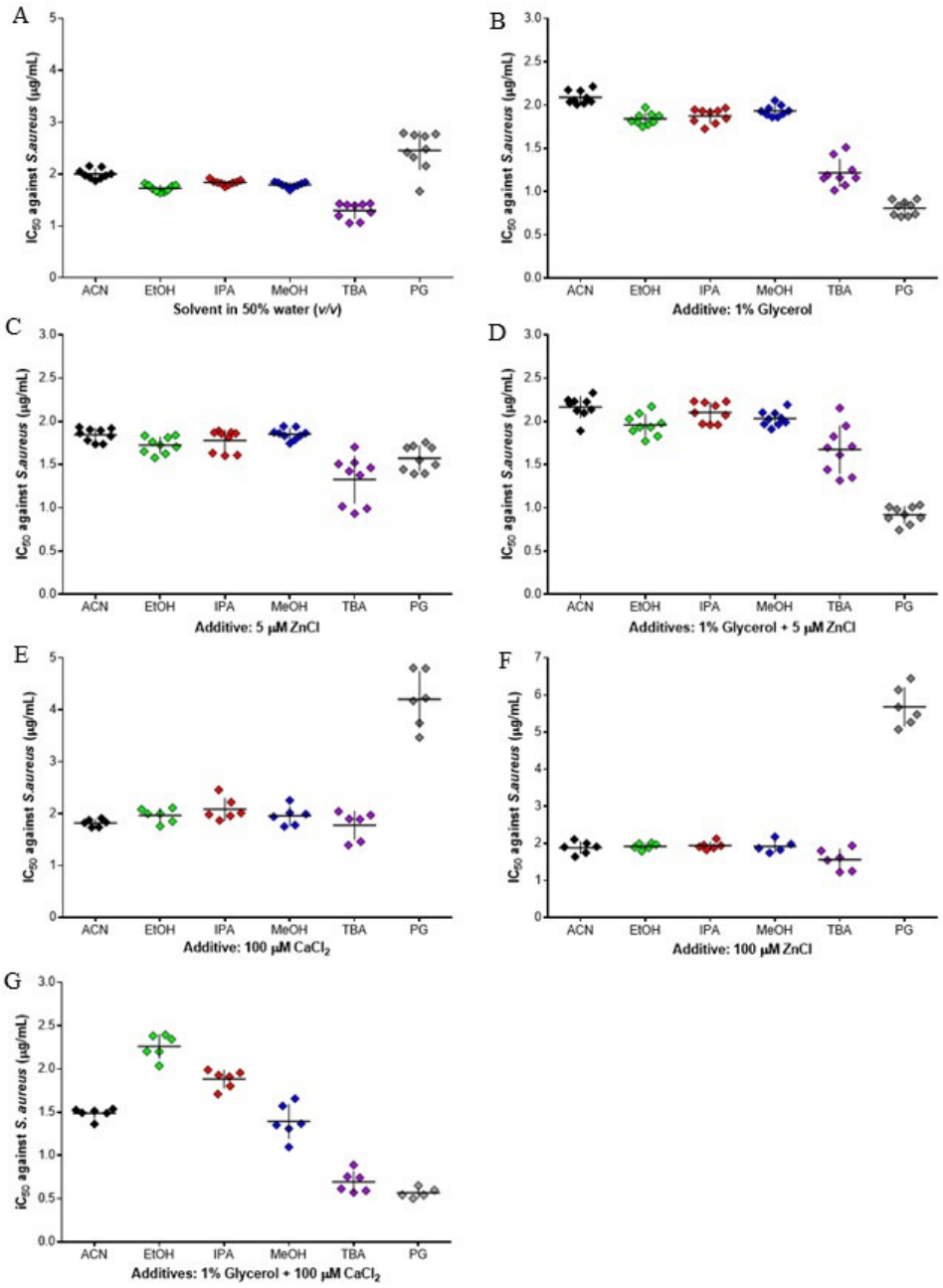

Figure 3.9 The scatter plot represents the IC_{50} values (µg/mL) (refer to Table 3.4A) obtained when comparing the effect, the different solvents (ACN, EtOH, IPA, MeOH and TBA) towards the specific Trc mix antimicrobial activity within the specific tested peptide formulation conditions. Error bars represent the SD for two biological repeats with two technical repeats per assay (n = 4). Statistical analysis was performed using One-way ANOVA with Bonferroni's multiple comparison test. Full statistical analysis comparison can be found in the supplementary data, Table S3.2.

Furthermore, only the TBA and PG formulations with Glr and/or the chloride salts show a significant improvement in activity compared to the other four solvents. PG significantly decreased the antimicrobial activity when in combination with 100 µM $ZnCl_2$ and $CaCl_2$ with the other five solvents having no significant difference between them (Figure 3.9 E and F). As elaborated in section 3.4.3.1

and section 3.4.3.2, when PG is not in combination with Glr, there may be an antagonistic effect towards the peptide which drives the peptide into undesirable conformations/structures for eliciting activity, but when Glr is present the effect could be negated.

Assessing the solvent influence towards 1% Glr + 100 µM $CaCl_2$ formulation, the differences in solvent influence can clearly be observed towards antimicrobial activity (Figure 3.9 G). The observed differences in activity when comparing each solvent reveals PG>TBA>MeOH≥ACN>IPA>EtOH, with EtOH and IPA significantly decreasing activity (increased IC_{50}), ACN and MeOH sharing a similar IC_{50} followed by TBA and PG significantly improving activity (decreased IC_{50}) when being compared (refer to Table S3.2 for statistical analysis). These observed differences may potentially be attributed to the binding, association or competition between the peptide and the solvent, Glr or Ca^{2+} which may influence the final peptide conformation/oligomerisation in being unfavourable, in the case of EtOH and IPA, or very stable and favourable, TBA and PG, to illicit activity.

Table 3.4 Summary of the A: IC_{50} and B: MIC values obtained for different Trc formulations assessed against *S. aureus* with (n) representing the total number of technical repeats per condition and SD representing the standard deviation within the assessed condition.

A:	IC_{50} ± SD µg/mL (n)						
	Solvent (9)	1% Glr (9)	5µM $ZnCl_2$ (9)	1% Glr + 5µM $ZnCl_2$ (9)	100µM $ZnCl_2$ (6)	100µM $CaCl_2$ (6)	1% Glr + 100 µM $CaCl_2$ (6)
ACN	1.9 ± 0.05	2.0 ± 0.07	1.8 ± 0.07	2.0 ± 0.12	1.8 ± 0.15	1.8 ± 0.07	1.5 ± 0.06
EtOH	1.7±0.06	1.8±0.07	1.7±0.09	1.8±0.12	1.9±0.08	1.9±0.12	2.6±0.13
IPA	1.8±0.05	1.8±0.08	1.8±0.12	2.0±0.11	1.9±0.09	2.1±0.20	1.9±0.10
MeOH	1.8±0.05	1.8±0.06	1.8±0.06	2.0±0.08	1.9±0.15	1.9±0.17	1.4±0.18
PG	2.5±0.22	0.8±0.08	1.6±0.14	0.9±0.09	5.6±0.48	4.0±0.49	0.8±0.05
TBA	1.3±0.15	1.1±0.15	1.3±0.26	1.6±0.26	1.5±0.26	1.7±0.25	0.7±0.11

B:	MIC µg/mL (n)						
	Solvent (9)	1% Glr (9)	5 µM $ZnCl_2$ (9)	1% Glr + 5 µM $ZnCl_2$ (9)	100 µM $ZnCl_2$ (6)	100 µM $CaCl_2$ (6)	1% Glr + 100 µM $CaCl_2$ (6)
ACN	3.1	3.1	3.1	3.1	3.1	3.1	3.1
EtOH	3.1	3.1	3.1	3.1	3.1	3.1	3.1
IPA	6.3	3.1	3.1	3.1	6.2	6.2	3.1
MeOH	3.1	3.1	3.1	3.1	3.1	3.1	3.1
PG	6.2	3.1	6.2	3.1	25.0	12.5	1.6
TBA	6.2	3.1	3.1	3.1	3.1	3.1	1.6

3.4.4 Relationship of formulation IC_{50} with solvent dielectric constant and relative formulation M_r

The Trc formulations assessed towards *L. monocytogenes* and *S. aureus* revealed that the presence or absence of Glr played a significant role towards the overall antimicrobial ability of the formulation. To develop a functional and usable antimicrobial formulation, the solvent and Glr influence was assessed via calculating the relative dielectric constant (ε) and relative molar mass (M_r) for all formulations and comparing it to the antimicrobial IC_{50} values (Figure 3.10).

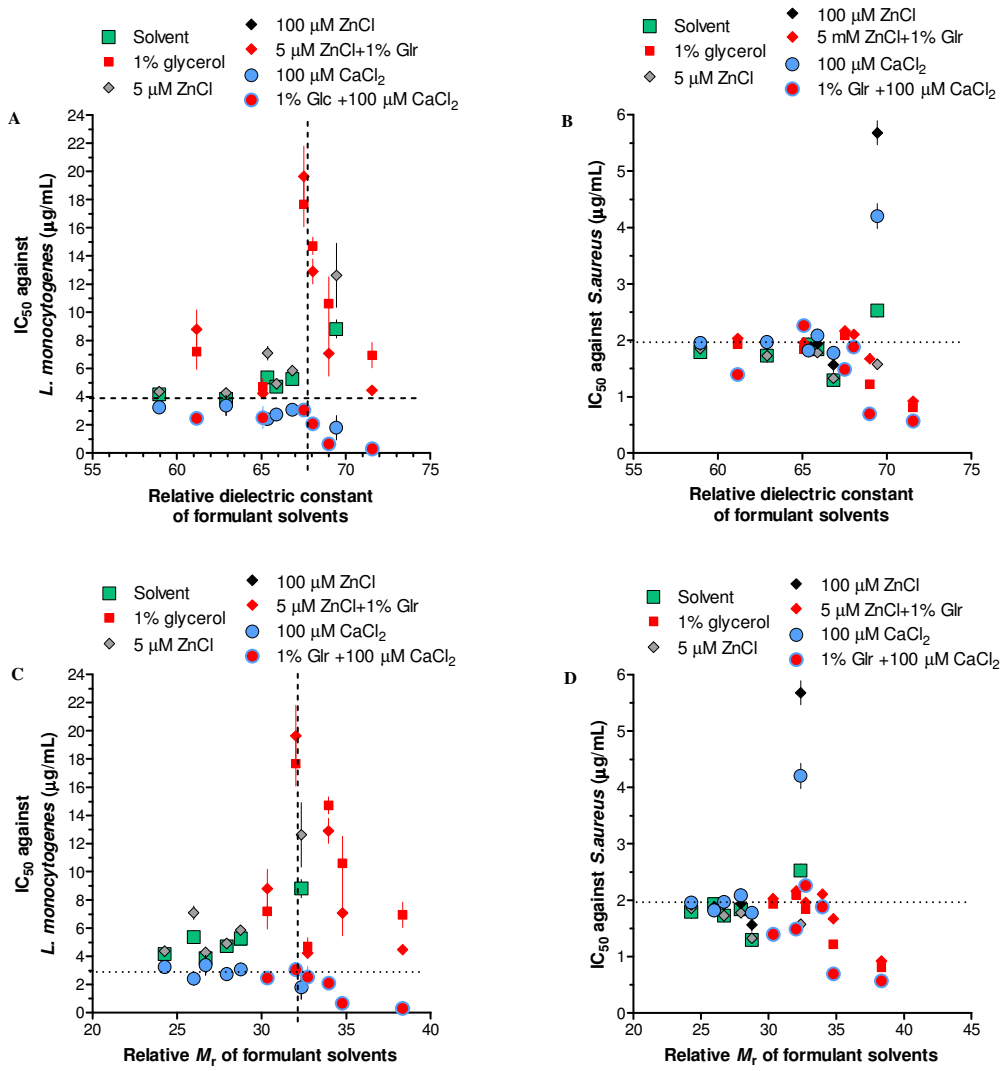

Figure 3.10 Comparative scatter plot of the influence of 1% Glr towards all the different Trc mix formulation solvents (ACN, EtOH, MeOH, IPA, TBA and PG) and conditions (1% Glr, 5 µM $ZnCl_2$, 1% Glr + 5 µM $ZnCl_2$, 100 µM $ZnCl_2$, 100 µM $CaCl_2$ and 1% Glr + 100 µM $CaCl_2$) on Trc mix antimicrobial IC_{50} values towards *L. monocytogenes* (A and C) and *S. aureus* (B and D), versus the dielectric constant and relative molecular weight of the formulations, respectively. Error bars represent the SD (n = 4-6). Refer to Table 3.1 for dielectric and relative M_r values used in calculations. Dotted line indicates arbitrary cut-off value from IC_{50} (horizontal) and relative M_r (vertical) by inspection of all solvent formulations.

The influence of the ε and relative M_r towards *L. monocytogenes* (Figure 3.10 A and C) shows that formulations which contain 1% Glr, excluding 1% Glr + 100 µM $CaCl_2$, result in an increase in IC_{50} as the ε and M_r increases until a breakpoint of around ε = 68 and relative M_r = 32 – 33 whereby the IC_{50} then sharply decreases until ε = 72 and relative M_r = 37. First, the high IC_{50} values towards *L. monocytogenes* may be due to these cells utilising Glr as a carbon source [46], as it has been shown that when under stress *L. monocytogenes* will increase Glr uptake metabolism [46]. Second, Glr may compete with the peptide for binding to the target or compete with the peptide in preventing dimer formation, thus hindering, and influencing the peptide from going into the optimal conformation to illicit activity or bind to the target cell. Furthermore, at ε = 65 and relative M_r = 32 -33, there is a breakpoint in which the formulation can be improved or become more unstable resulting in either improvement or loss of activity. As seen for the solvent and 5 µM $ZnCl_2$, as the ε and M_r increase, there is a concomitant increase in the IC_{50}, whereas when in combination with Glr, increasing the ε and relative M_r, the overall formulation is improved with the decreasing IC_{50}. The relative M_r findings show that a balance is required between the peptide and additives that act as either crowding agents or as conformation/oligomer stabilising factors. This would influence the ability of monomeric peptide units to form active dimers, influencing activity, or preventing/stabilising the formation of larger oligomeric structures. Previous research has shown that the addition of $CaCl_2$ results in the Trcs exhibiting an increased activity towards *L. monocytogenes* [54,55] and correlates with obtained formulation results for 100 µM $CaCl_2$ and 1% Glr + 100 µM $CaCl_2$ formulations seen in Figure 3.10 A and C resulting in lower IC_{50} values below the selected threshold. Therefore, it may be postulated that the presence of Ca^{2+} may stabilise the Trcs and overall promote an alternative mode of action correlating to previously seen results [55].

Assessing the influence of ε and relative formulation M_r towards the activity of the Trc formulations against *S. aureus* (Figure 3.10 B and D), it is evident that 1% Glr does not increase the IC_{50} value compared to those observed for Figure 3.10 A and C. This may be due to *S. aureus* not readily metabolising Glr as a carbon source when under metabolic stress, that Glr does not influence or compete with the peptide for the bacterial target or cause the peptide to go into a non-active conformation. The 1% Glr formulations resulted in having ε ≥ 65 and the relative formulation $M_r \geq 33$ resulted in improved activity (lower IC_{50}). Furthermore, formulations containing 1% Glr + 100 µM $CaCl_2$, had the most improved activity with the IC_{50} values being slightly lower than 1% Glr formulations and again having the ε > 65. Interestingly, two active groupings can be observed when assessing the relative M_r of the formulation, with the majority of the formulations of M_r 25 - 30 and 35 – 35 having similar IC_{50} values, while formulations from M_r 35 - 40 had a greater spread but better IC_{50} values and therefore activity.

The above findings would suggest that the solvents and additives act as chaotropic agents towards the peptide oligomeric units. The nature of the Trcs to form different dimeric units via hydrogen bonding or the hydrophobic effect [48,49], would further suggest they can form larger oligomers. These oligomers would have a hydrophobic core and a polar outer surface as the Trcs are amphipathic in structure [48,49]. The defined relative M_r range would suggest that the solvents and additives are small enough to integrate and disrupt the hydrophobic core, destabilizing large oligomer formation, but are not small enough to compete and disrupt the hydrogen bonds required for the active state of the amphipathic peptide dimers. If the formulations' relative M_r is less than 33 there would be potential competition and disruption of dimer hydrogen bonds. If greater than 44, there may be no integration into the hydrophobic core resulting in higher oligomer units' formation.

3.5 Conclusions

The influence of solvents and additives on the antimicrobial activity of the Trcs was determined against *L. monocytogenes* and *S. aureus.* Peptide formulations containing 1% Glr significantly increased the IC_{50} value for all solvents except for PG towards *L. monocytogenes*. This could be due to Glr being taken up and metabolised by *L. monocytogenes* cells when under stress, which occurred when exposed to the Trcs. PG, regardless of its chemical similarity to Glr, showed the inverse influence on peptide activity, but surprisingly showed that it improved Trc mix activity when in combination with Glr. This can be due to the interaction between PG and Glr, freeing the peptide to orientate and form dimers needed for activity. The addition of 5 µM $ZnCl_2$ did not enhance the activity against *L. monocytogenes*, however, when the concentration was increased to 100 µM the activity was enhanced. This may indicate that the higher Zn^{2+} concentration stabilises the peptides' higher order structures or assist in binding to the target cell. The addition of 100 µM $CaCl_2$ correlated with previously observed findings by Leussa [54] and Spathelf [55], with significantly improved activity of the Trc formulations. Furthermore, the addition of 1% Glr with $CaCl_2$ did not have the loss of activity as those with the addition of 1% Glr alone. This may indicate that although Glr can be metabolised by *L. monocytogenes*, there may be a very potent non-lytic mode of action induced by the presence of Ca^{2+}, as proposed by Leussa [55].

Trc formulations tested against *S. aureus* did yield similar results to that of *L. monocytogenes.* The addition of 1% Glr led to a maintained activity for ACN, EtOH, MeOH and IPA as organic modifiers. Furthermore, the addition of 5 µM and 100 µM $ZnCl_2$ maintained the antimicrobial activity of the Trcs compared to the solvent control. This maintained activity indicates the *S. aureus* active moieties of the peptides in these formulations are highly stable. The formulations with 100 µM $CaCl_2$ did not enhance the antimicrobial activity of the Trc mix in any of the solvents. This indicates that Ca^{2+} may have a selective influence mode of action against *L. monocytogenes* but may rather act as a stabiliser

for the peptide in solution with *S. aureus* as target. As observed with *L. monocytogenes*, PG formulations significantly improved or enhanced activity in combination with 1% Glr but increased the IC_{50} with the other additives. TBA showed the most promise as a solvent, with maintained activity in all conditions.

The 1% Glr + $CaCl_2$ TBA formulation of Trc mix had the highest activity against both *S. aureus* and *L. monocytogenes* compared to the other formulations. This may be related to the chaotropic ability of the solvent and additives being within the optimal relative formulation M_r range of 33 - 44. The 1% Glr + $CaCl_2$ TBA formulations are small enough to integrate within the hydrophobic core, destabilising and disrupting oligomeric formation, but not small enough to compete for hydrogen bonds required by dimers for activity. Therefore, from this study, it is concluded that Trc mix in 1% Glr + 100 µM $CaCl_2$ in TBA is the best formulation of the formulations tested and worthy of further development.

3.6 References

1. Lode, H. Clinical impact of antibiotic-resistant gram-positive pathogens. *Clinical Microbiology and Infection* 2009, *15* (3), 212-217.
2. Boyce, J. environmental contamination makes an important contribution to hospital infection. *Journal of Hospital Infection* 2007, *65*, 50-54.
3. Boyce, J.; Potter-Bynoe, G.; Chenevert, C.; King, T. Environmental contamination due to methicillin-resistant S*taphylococcus aureus*: Possible infection control implications. *Infection Control and Hospital Epidemiology* 1997, *18* (9), 622-627.
4. Boyce, J.; Havill, N.; Otter, J.; Adams, N. Widespread environmental contamination associated with patients with diarrhea and methicillin-resistant S*taphylococcus aureus* colonization of the gastrointestinal tract. *Infection Control & Hospital Epidemiology* 2007, *28* (10), 1142-1147.
5. Boyce, J. Modern technologies for improving cleaning and disinfection of environmental surfaces in hospitals. *Antimicrobial Resistance & Infection Control* 2016, *5* (1).
6. Dancer, S. Controlling hospital-acquired infection: focus on the role of the environment and new technologies for decontamination. *Clinical Microbiology Reviews* 2014, *27* (4), 665-690.
7. Siedenbiedel, F.; Tiller, J. Antimicrobial polymers in solution and on surfaces: overview and functional principles. *Polymers* 2012, *4* (1), 46-71.
8. Swaminathan, B.; Gerner-Smidt, P. The epidemiology of human listeriosis. *Microbes and Infection* 2007, *9* (10), 1236-1243.
9. Carpentier, B.; Cerf, O. Review — Persistence of *Listeria monocytogenes* in food industry equipment and premises. *International Journal of Food Microbiology* 2011, *145* (1), 1-8.
10. Gandhi, M.; Chikindas, M. *Listeria*: A foodborne pathogen that knows how to survive. *International Journal of Food Microbiology* 2007, *113* (1), 1-15.
11. Lariviére-Gauthier, G.; Letellier, A.; Kérouanton, A.; Bekal, S.; Quessy, S.; Fournaise, S.; Fravalo, P. Analysis of *Listeria monocytogenes* strain distribution in a pork slaughter and cutting plant in the province of Quebec. *Journal of Food Protection* 2014, *77* (12), 2121-2128.
12. Barbalho, T.; Almeida, P.; Almeida, R.; Hofer, E. Prevalence of Listeria Spp. At a poultry processing plant in brazil and a phage test for rapid confirmation of suspect colonies. *Food Control* 2005, *16* (3), 211-216.
13. Chiarini, E.; Tyler, K.; Farber, J.; Pagotto, F.; Destro, M. *Listeria monocytogenes* in two different poultry facilities: Manual and automatic evisceration. *Poultry Science* 2009, *88* (4), 791-797.
14. Barancelli, G.; Camargo, T.; Gagliardi, N.; Porto, E.; Souza, R.; Campioni, F.; Falcão, J.; Hofer, E.; Cruz, A.; Oliveira, C. Pulsed-Field gel electrophoresis characterization of *Listeria monocytogenes* isolates from cheese manufacturing plants in São Paulo, Brazil. *International Journal of Food Microbiology* 2014, *173*, 21-29.
15. Barros, M.; Nero, L.; Silva, L.; d'Ovidio, L.; Monteiro, F.; Tamanini, R.; Fagnani, R.; Hofer, E.; Beloti, V. *Listeria monocytogenes*: Occurrence in beef and identification of the main contamination points in processing plants. *Meat Science* 2007, *76* (4), 591-596.
16. Camargo, A.; Dias, M.; Cossi, M.; Lanna, F.; Cavicchioli, V.; Vallim, D.; Pinto, P.; Hofer, E.; Nero, L. Serotypes and pulsotypes diversity of *Listeria monocytogenes* an a beef-processing environment. *Foodborne Pathogens and Disease* 2015, *12* (4), 323-326.
17. Ricci, A.; Allende, A.; Bolton, D.; Chemaly, M.; Davies, R.; Fernández Escámez, P.; Girones, R.; Herman, L.; Koutsoumanis, K.; Nørrung, B.; Robertson, L.; Ru, G.; Sanaa, M.; Simmons, M.; Skandamis, P.; Snary, E.; Speybroeck, N.; Ter Kuile, B.; Threlfall, J.; Wahlström, H.; Takkinen, J.; Wagner, M.; Arcella, D.; Da Silva Felicio, M.; Georgiadis, M.; Messens, W.; Lindqvist, R. *Listeria monocytogenes* contamination of ready-to-eat foods and the risk for human health in the EU. *EFSA Journal* 2018, *16* (1).
18. Møretrø, T.; Langsrud, S. Listeria Monocytogenes: Biofilm formation and persistence in food-processing environments. *Biofilms* 2004, *1* (2), 107-121.
19. Tong, S.; Davis, J.; Eichenberger, E.; Holland, T.; Fowler, V. Staphylococcus Aureus Infections: Epidemiology, pathophysiology, clinical manifestations, and management. *Clinical Microbiology Reviews* 2015, *28* (3), 603-661.
20. Carling, P.; Briggs, J.; Hylander, D.; Perkins, J. An evaluation of patient area cleaning in 3 hospitals using a novel targeting methodology. *American Journal of Infection Control* 2006, *34* (8), 513-519.
21. Carling, P.; Bartley, J. Evaluating hygienic cleaning in health care settings: What you do not know can harm your patients. *American Journal of Infection Control* 2010, *38* (5), S41-S50.
22. White, L.; Dancer, S.; Robertson, C.; McDonald, J. Are hygiene standards useful in assessing infection risk?. *American Journal of Infection Control* 2008, *36* (5), 381-384.
23. Chaoui, L.; Mhand, R.; Mellouki, F.; Rhallabi, N. Contamination of the surfaces of a health care environment by Multidrug-Resistant (MDR) Bacteria. *International Journal of Microbiology* 2019, *2019*, 1-7.

24. Huang, R.; Mehta, S.; Weed, D.; Price, C. Methicillin-Resistant *Staphylococcus aureus* survival on hospital fomites. *Infection Control & Hospital Epidemiology* 2006, *27* (11), 1267-1269.
25. van Dijk, H.; Verbrugh, H.; Abee, T.; Andriessen, J.; van Dijk, H.; ter Kuile, B.; Mevius, D.; Montforts, M.; van Schaik, W.; Schmitt, H.; Smidt, H.; Veening, J.; Voss, A. Resisting disinfectants. *Communications Medicine* 2022, *2* (1).
26. Jain, A.; Duvvuri, L.; Farah, S.; Beyth, N.; Domb, A.; Khan, W. Antimicrobial polymers. *Advanced Healthcare Materials* 2014, *3* (12), 1969-1985.
27. Shin, J.; Gwak, J.; Kamarajan, P.; Fenno, J.; Rickard, A.; Kapila, Y. Biomedical applications of nisin. *Journal of Applied Microbiology* 2016, *120* (6), 1449-1465.
28. Reichenberg, G.; Ophir, A.; Nir, Y. Nisin as an antibacterial substance in active packaging: Use of ethylene methyl acrylate and co-polyamide to enhance its effectiveness. *International Journal of Material Science* 2015, *5* (2), 45-53.
29. Kenawy, E.; Worley, S.; Broughton, R. The chemistry and applications of antimicrobial polymers: A State-of-the-art review. *Biomacromolecules* 2007, *8* (5), 1359-1384.
30. Hotchkiss, R.; Dubos, R. The isolation of bactericidal substances from cultures of *Bacillus brevis*. *Journal of Biological Chemistry* 1941, *141* (1), 155-162.
31. Spathelf, B.; Rautenbach, M. anti-listerial activity and structure–activity relationships of the six major tyrocidines, cyclic decapeptides from *Bacillus aneurinolyticus*. *Bioorganic & Medicinal Chemistry* 2009, *17* (15), 5541-5548.
32. Dubos, R.; Hotchkiss, R.; Coburn, A. The effect of gramicidin and tyrocidine on bacterial metabolism. *Journal of Biological Chemistry* 1942, *146* (2), 421-426.
33. Rautenbach, M.; Vosloo, J.; van Rensberg, W.; Engelbrecht, Y. Natural antimicrobial peptides as green microbicides in agriculture: A proof of concept study on the tyrocidines from soil bacteria; *Green Economy Research Report*, Green Fund, Development Bank of Southern Africa; Midrand, 2015.
34. Troskie, A.; de Beer, A.; Vosloo, J.; Jacobs, K.; Rautenbach, M. Inhibition of agronomically relevant fungal phytopathogens by tyrocidines, cyclic antimicrobial peptides isolated from *Bacillus aneurinolyticus*. *Microbiology* 2014, *160* (9), 2089-2101.
35. Rautenbach, M.; Troskie, A.; Vosloo, J.; Dathe, M. Antifungal Membranolytic Activity of the tyrocidines against filamentous plant fungi. *Biochimie* 2016, *130*, 122-131.
36. Troskie, A.; Rautenbach, M.; Delattin, N.; Vosloo, J.; Dathe, M.; Cammue, B.; Thevissen, K. Synergistic activity of the tyrocidines, antimicrobial cyclodecapeptides from *Bacillus aneurinolyticus*, with amphotericin b and caspofungin against *Candida albicans* biofilms. *Antimicrobial Agents and Chemotherapy* 2014, *58* (7), 3697-3707.
37. Wenzel, M.; Rautenbach, M.; Vosloo, J.; Siersma, T.; Aisenbrey, C.; Zaitseva, E.; Laubscher, W.; van Rensburg, W.; Behrends, J.; Bechinger, B.; Hamoen, L. The multifaceted antibacterial mechanisms of the pioneering peptide antibiotics tyrocidine and gramicidin S. *mBio* 2018, *9* (5).
38. Rammelkamp, C.; Weinstein, L. Toxic effects of tyrothricin, gramicidin and tyrocidine. *Journal of Infectious Diseases* 1942, *71* (2), 166-173.
39. van Rensburg, W. The tyrocidines in the creation of antimicrobial cellulose and sterilising materials. PhD thesis, Stellenbosch University, Department of Biochemistry: Stellenbosch, South Africa, 2019. https://scholar.sun.ac.za/handle/10019.1/108461
40. Dubos, R.; Cattaneo, C. Studies on a bactericidal agent extracted from a soil *Bacillus*. *Journal of Experimental Medicine* 1939, *70* (3), 249-256.
41. Hotchkiss, R.; Dubos, R. The isolation of bactericidal substances from cultures of *Bacillus brevis*. *Journal of Biological Chemistry* 1941, *141* (1), 155-162.
42. Wałęsa, R.; Broda, M. The influence of solvent on conformational properties of peptides with aib residue—A DFT Study. *Journal of Molecular Modeling* 2017, *23* (12).
43. Nandakumar, A.; Ito, Y.; Ueda, M. Solvent effects on the self-assembly of an amphiphilic polypeptide incorporating α-helical hydrophobic blocks. *Journal of the American Chemical Society* 2020, *142* (50), 20994-21003.
44. Rautenbach, M.; Gerstner, G.; Vlok, N.; Kulenkampff, J.; Westerhoff, H. Analyses of dose–response curves to compare the antimicrobial activity of model cationic α-helical peptides highlights the necessity for a minimum of two activity parameters. *Analytical Biochemistry* 2006, *350* (1), 81-90.
45. du Toit, E.; Rautenbach, M. A sensitive standardised micro-gel well diffusion assay for the determination of antimicrobial activity. *Journal of Microbiological Methods* 2000, *42* (2), 159-165.
46. Joseph, B.; Mertins, S.; Stoll, R.; Schär, J.; Umesha, K.; Luo, Q.; Müller-Altrock, S.; Goebel, W. Glycerol metabolism and Prfa activity in *Listeria monocytogenes*. *Journal of Bacteriology* 2008, *190* (15), 5412-5430.
47. Csonka, L. Physiological and genetic responses of bacteria to osmotic stress. *Microbiological Reviews* 1989, *53* (1), 121-147.
48. Loll, P.; Upton, E.; Nahoum, V.; Economou, N.; Cocklin, S. The high resolution structure of tyrocidine a reveals an amphipathic dimer. *Biochimica et Biophysica Acta (BBA) - Biomembranes* 2014, *1838* (5), 1199-1207.

49. Munyuki, G.; Jackson, G.; Venter, G.; Kövér, K.; Szilágyi, L.; Rautenbach, M.; Spathelf, B.; Bhattacharya, B.; van der Spoel, D. B-sheet structures and dimer models of the two major tyrocidines, antimicrobial peptides from *Bacillus aneurinolyticus*. *Biochemistry* 2013, *52* (44), 7798-7806.
50. Huang, R.; Mehta, S.; Weed, D.; Price, C. Methicillin-Resistant *Staphylococcus aureus* survival on hospital fomites. *Infection Control & Hospital Epidemiology* 2006, *27* (11), 1267-1269.
51. Duell, A.; Pankow, J.; Gillette, S.; Peyton, D. Boiling points of the propylene glycol + glycerol system at 1 atmosphere pressure: 188.6–292 °C without and with added water or nicotine. *Chemical Engineering Communications* 2018, *205* (12), 1691-1700.
52. van der Vossen, A.; van der Velde, I.; Smeets, O.; Postma, D.; Eckhardt, M.; Vermes, A.; Koch, B.; Vulto, A.; Hanff, L. Formulating a poorly water soluble drug into an oral solution suitable for paediatric patients; Lorazepam as a model drug. *European Journal of Pharmaceutical Sciences* 2017, *100*, 205-210.
53. Huan, Y.; Kong, Q.; Mou, H.; Yi, H. Antimicrobial peptides: Classification, design, application and research progress in multiple fields. *Frontiers in Microbiology* 2020, *11*.
54. Spathelf, B. Qualitative structure-activity relationship of the major tyrocidines, cyclic decapeptides from *Bacillus aneurinolyticus*. PhD thesis, Stellenbosch University, Department of Biochemistry: Stellenbosch, South Africa, 2010. http://scholar.sun.ac.za/handle/10019.1/4001
55. Leussa, N.-N.A. Characterisation of small cyclic peptides with anti listerial and antimalarial activity. PhD thesis, Stellenbosch University, Department of Biochemistry: Stellenbosch, South Africa.2014. http://scholar.sun.ac.za/handle/10019.1/86161.
56. Marques, M.; Citron, D.; Wang, C. Development of tyrocidine a analogues with improved antibacterial activity. *Bioorganic & Medicinal Chemistry* 2007, *15* (21), 6667-6677.
57. Prabhu, N.; Sharp, K. Protein−Solvent interactions. *Chemical Reviews* 2006, *106* (5), 1616-1623.
58. van Rensburg, W.; Laubscher, W.; Rautenbach, M. High throughput method to determine the surface activity of antimicrobial polymeric materials. *MethodsX* 2021, *8*, 101593.

3.7 Supplementary Information

3.7.1 Summary of full statistical analysis against L. monocytogenes

Table S3.1 Summary of the statistical analysis between different Trc formulation solvent conditions and the specific assessed additive towards *L. monocytogenes*. Statistical analysis was performed using One-Way ANOVA (Bonferroni's multiple comparison test). *P < 0.05, **P < 0.01, *** P < 0.001, **** P < 0.0001 and ns – not significant.

Solvent					
	EtOH	IPA	MeOH	TBA	PG
ACN	ns	ns	ns	ns	****
EtOH		ns	ns	ns	****
IPA			ns	ns	****
MeOH				ns	****
TBA					****
1% Glr					
	EtOH	IPA	MeOH	TBA	PG
ACN	****	ns	****	**	****
EtOH		****	ns	*	ns
IPA			**	ns	***
MeOH				ns	ns
TBA					ns
5 µM $ZnCl_2$					
	EtOH	IPA	MeOH	TBA	PG
ACN	***	*	***	ns	****
EtOH		ns	ns	ns	****
IPA			ns	ns	****
MeOH				ns	****
TBA					****
1% Glr + 5 µM $ZnCl_2$					
	EtOH	IPA	MeOH	TBA	PG
ACN	****	**	****	****	****
EtOH		***	ns	ns	ns
IPA			ns	***	*
MeOH				ns	ns
TBA					ns

100 µM $ZnCl_2$					
	EtOH	IPA	MeOH	TBA	PG
ACN	ns	ns	ns	ns	ns
EtOH		ns	ns	ns	*
IPA			ns	ns	ns
MeOH				ns	ns
TBA					ns

100 µM $CaCl_2$					
	EtOH	IPA	MeOH	TBA	PG
ACN	ns	ns	ns	ns	ns
EtOH		ns	ns	ns	ns
IPA			ns	ns	ns
MeOH				ns	ns
TBA					ns

1% Glr + 100 µM $CaCl_2$					
	EtOH	IPA	MeOH	TBA	PG
ACN	ns	ns	ns	**	**
EtOH		ns	ns	*	*
IPA			ns	ns	ns
MeOH				ns	*
TBA					ns

3.7.2 Summary of full statistical analysis against S. aureus

Table S3.2 Summary of the statistical analysis between different Trc formulation solvent conditions and the specific assessed additive towards *S. aureus*. Statistical analysis was performed using One-Way ANOVA (Bonferroni's multiple comparison test) .*P < 0.05, **P <0.01, *** P < 0.001, **** P < 0.0001 and ns – not significant.

Solvent					
	EtOH	IPA	MeOH	TBA	PG
ACN	*	ns	ns	****	****
EtOH		ns	ns	****	****
IPA			ns	****	****
MeOH				****	****
TBA					****

1% Glr

	EtOH	IPA	MeOH	TBA	PG
ACN	****	***	*	****	****
EtOH		ns	ns	****	****
IPA			ns	****	****
MeOH				****	****
TBA					****

5 µM $ZnCl_2$

	EtOH	IPA	MeOH	TBA	PG
ACN	ns	ns	ns	**	****
EtOH		ns	ns	****	ns
IPA			ns	****	ns
MeOH				****	**
TBA					*

1% Glr + 5 µM $ZnCl_2$

	EtOH	IPA	MeOH	TBA	PG
ACN	ns	ns	ns	****	****
EtOH		ns	ns	**	****
IPA			ns	****	****
MeOH				***	****
TBA					****

100 µM $ZnCl_2$

	EtOH	IPA	MeOH	TBA	PG
ACN	ns	ns	ns	ns	****
EtOH		ns	ns	ns	****
IPA			ns	ns	****
MeOH				ns	****
TBA					****

100 µM $CaCl_2$

	EtOH	IPA	MeOH	TBA	PG
ACN	ns	ns	ns	ns	****
EtOH		ns	ns	ns	****
IPA			ns	ns	****
MeOH				ns	****
TBA					****

1% Glr + 100 µM $CaCl_2$

	EtOH	IPA	MeOH	TBA	PG
ACN	****	***	ns	****	****
EtOH		***	****	****	****
IPA			****	****	****
MeOH				****	****
TBA					ns

Chapter 4

Influence of formulations on fluorescence of the tyrocidines

4.1 Introduction

Previous studies conducted on the Trcs revealed that they are not only able to dimerize but also able to further undergo extended oligomerisation via non-covalent polar and hydrophobic interactions [1-5]. Unwanted oligomerisation, masking important groups that are needed for interaction with cellular targets, would lead to steric hindrance and/or influences on peptide activity. Polar interactions would entail hydrogen bonds in which the peptide backbone amides would participate, as well as the side chains of Asn, Gln, Lys and Tyr. Other polar interactions would be dipolar and other electrostatic interactions by the polar amino acid side chain groups, as well as dipolar and induced dipolar interactions with aromatic side chains. The ability to participate in hydrophobic interactions can be driven by the presence of three aromatic amino acids in the Trcs structure, namely Tyr, Trp and Phe, as well as hydrophobic residues Val, Leu and Pro. Furthermore, the three aromatic amino acids are intrinsic fluorophores [5-7], which can be used to track changes in aromatic interactions and the overall influence on peptide oligomerisation. As a peptide mixture was used, it contains all six analogues, meaning that Trp, Tyr and Phe residues are present. However, Trp was selected as the major fluorophore to be followed in this study for the assessment of oligomerisation and self-assembly states of the Trc mix peptide alone and in formulation. This is attributed to the high sensitivity of Trp to its local environment and its solvatochromic character [7,8]. The fluorescence of Trp exposed to a polar environment will be prone to quenching, as well as a red-shifted emission maximum [7-9]. Alternatively, in a hydrophobic environment, the Trp fluorescence will typically be enhanced with a blue-shifted emission maximum [7-9]. Additionally, if there is aromatic stacking this would lead to a FRET (fluorescence resonance energy transfer) type response with fluorescence quenching leading to an overall decrease in Trp intensity, while maintaining a blue-shifted emission maximum. Furthermore, Trp can be quenched when externally adding quenchers or by nearby polar groups within the protein [8]. Additionally, solvent polarity may have a significant effect on fluorescence emission in which increased polarity will lead to an increase in expected quenching [8]. These observed changes to the Trp emission spectra often occur due to a response in conformational changes, subunit association or denaturation in aqueous solutions [8,10].

For this study, the Trcs were formulated with either six solvent systems (ACN, TBA, EtOH, MeOH, IPA and PG) alone or in combination with various additives (Glr, $ZnCl_2$ and $CaCl_2$) with the aim of improving bioactivity by influencing peptide stability. The Trc mix consists of six analogues that

share a highly conserved sequence, with variation at position three and four (dipeptide unit) giving rise to the different Trc analogues namely TrcA (L-Phe^3-D-Phe^4), TrcB (L-Phe^3-D-Trp^4) and TrcC (L-Trp^3-D-Trp^4) [11]. Additionally, changes at position 9 from L-Orn^9 to D-Lys^9 give rise to the three other analogues: TrcA_1, TrcB_1 and TrcC_1. As it has previously been shown that the amino acids at position three and four facilitate a large role in peptide oligomerisation, the focus and interest in the Trcs biophysical properties are reported in this chapter by investigating changes to the higher order oligomerisation and self-assembly via fluorometric analysis of the Trp residues.

4.2 Materials

Tyrocidine mixture (Trc mix) was extracted from commercial tyrothricin and described in full detail in Chapter 2. Tertiary butyl alcohol (TBA) and iso-propyl alcohol (IPA) were supplied by Sigma-Aldrich (St. Louis, MA, USA). Analytical grade ethanol (EtOH, >99.8%) was supplied by Merck (Darmstadt, Germany). Methanol (MeOH) and acetonitrile (ACN, HPLC-grade, far UV cut-off) were provided by Romil Ltd. (Microsep, Johannesburg, South Africa). Analytical grade water (MQH_2O) used for all peptide formulations was obtained by filtering water from a reverse osmosis purification plant, through a Millipore-Q® water purification system (Milford, USA). The 96-well black flat bottom plates were supplied by Thermo Fisher Scientific (Denmark). Calcium chloride ($CaCl_2$) and zinc chloride ($ZnCl_2$) were supplied by Merck (Wadeville, Gauteng). Propylene-glycol (PG) was gifted by Plascon® (Plascon, South Africa).

4.3 Methods

4.3.1 Fluorescence spectroscopy

Peptide formulations were prepared as previously described in Chapter 3 (refer to Table 3.2) to a final solvent concentration of 10% (*v/v*) at two final analytical stock concentrations of 0.500 mg/mL and 0.100 mM for each of the six solvent systems: ACN, TBA, IPA, EtOH, MeOH and PG. The freshly prepared 0.500 mg/mL Trc mix was then formulated separately with 1% glycerol (Glr), 5 µM $ZnCl_2$ and 1% Glr in combination with 5.00 µM $ZnCl_2$. The 0.100 mM Trc mix was formulated separately with 100 µM $ZnCl_2$, 100 µM $CaCl_2$ and 1% Glr in combination with 100 µM $CaCl_2$ (refer to Chapter 3: Table 3.2 for all formulation conditions). Doubling dilutions were prepared for all peptide formulations with 0.500 mg/mL in triplicate and 0.100 mM in duplicate in black 96-well microtiter plates using filter sterilized MQH_2O. Fluorescence spectroscopy was performed using two different instruments: Readings for 0.500 mg/mL formulations were performed on the Tecan Spark 10M Multimode Microplate Reader and controlled by the Spark Control™ software provided by the Tecan Group Ltd (Mennedorf, Switzerland), while 0.100 mM readings were obtained on the Varioskan 3.01.15 instrument and data was collected with the SkanIT software 2.4.3. For fluorescence studies

on all formulations, excitation was at 280 nm and emission was recorded from 300 nm to 400 nm with Varioskan (emission bandwidth set at 2 nm and gain machine set) and 320 nm to 400 nm for Tecan Spark 10M Multimode Microplate Reader (with the emission bandwidth set at 10 nm with 10 flashes, gain 60). Results were analysed and represented using GraphPad Prism® V 5.0.

4.4 Results and Discussion

4.4.1 Fluorescence spectroscopy analysis of the Trc mix and peptide formulations

Before determining if formulating the Trcs with specific additives directly influence the peptides' oligomerisation, the influence of the solvents alone on the Trc mix fluorescence was determined. It is expected that increasing the peptide concentration from 3.125 µM Trc mix to 100 µM Trc mix, would result in a linear increase in the peptides' fluorescence quantum yield. However, only MeOH and PG as peptide solvents led to a true linear trend when the linear fit to the data was compared with a quadratic fit model (Figure 4.1 A) with this further elaborated on in Figure 4.3 and 4.4 later in the chapter.

Although it is known that ACN is the most polar solvent that was tested, as expected the lower alcohols would also result in Trp quenching due to their polar nature. Of the alcohols tested, MeOH led to the highest quenching, followed by EtOH, IPA and then TBA (Figure 4.1 B). ACN and EtOH showed a statistically similar response over the whole concentration range of Trc mix, while all the solvents showed a statistically similar response at 3.125 µg/mL and 6.25 µg/mL Trc mix (refer to supplementary data for statistical analyses). The Trc mix fluorescence differed for each of the solvent groups at 12.5 µg/mL or 25 µg/mL and above, which correlates with the estimated critical micellular concentration (CMC) of 15 µM and 24 µM for TrcA and TrcC, respectively [unpublished data from BIOPEP Group], 23 µM for TrcB [12] and 18 µM for TpcC [13,14]. These results suggest that the observed quenching can be attributed to the peptide conformation and oligomerisation in solution (concentration dependent) above the specific CMC in the solvent. This oligomerisation would cause the environment of Trp residue to be influenced by either aromatic stacking or the Trp being moved into a hydrophobic pocket, resulting in less Trp-aromatic stacking induced FRET [8]. As previously shown by Loll *et al.* [15] and Munyuki *et al.* [16], the Trcs form higher order structures via hydrogen bonding, aromatic stacking, or the hydrophobic effect [15,16]. Rautenbach *et al.* [13] showed the oligomerisation of TpcC, a minor peptide in the Trc mix, is dependent on both hydrogen bonding and aromatic stacking. Recently Kumar *et al.* [17] showed that the nanostructures formed by TpcC are dependent on the ethanol concentration, correlating with Trp fluorescence in an atypical non-linear trend. Due to this, the observed quenching can be attributed to the solvent system influencing the formation of larger oligomers. The more polar solvents would support oligomerisation while the less

polar solvents could be more effective in lowering the hydrophobic effect on the peptide that is leading to larger structure formation at higher concentrations. Oligomerisation, supported by the hydrophobic effect, could lead to the Trp residues undergoing aromatic stacking and subsequent quenching [13,16]. If the Trp residues are placed in a hydrophobic solvent environment, for example TBA, this would typically lead to an increase in fluorescence and quantum yield.

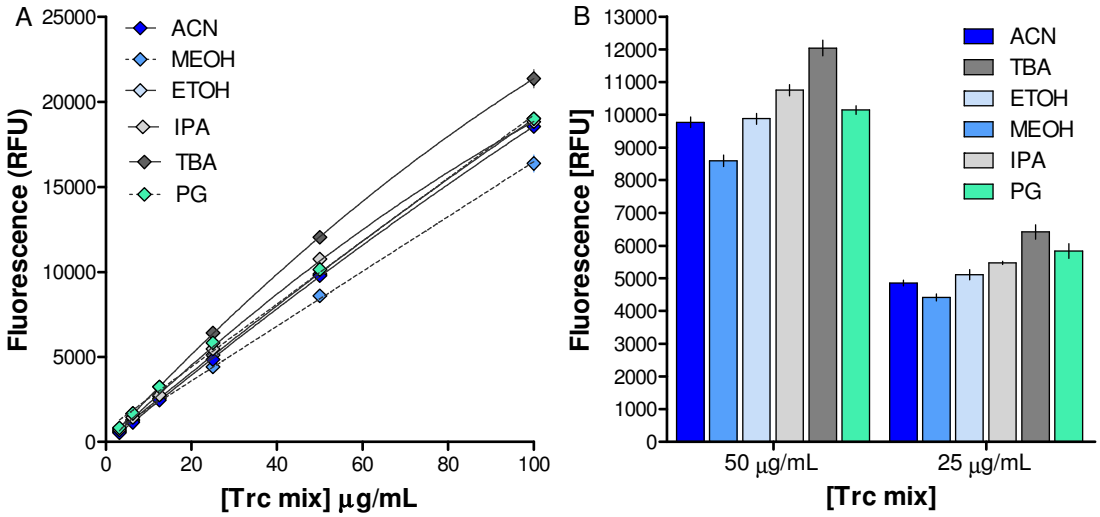

Figure 4.1 Solvent-peptide comparison representing the total quantum yield as relative fluorescence units (RFU) determined from the fluorescence spectra (refer to Supplementary data Figure S4.1). In graph A, the peptide concentration trend for each solvent is shown with the best linear fits shown as a dotted line and the best quadratic fit as a solid line. All model fits were compared and only those statistically better are shown, with R^2>0.995. Each data point is the average of six determinations. In graph B, Trc mix alone at 25 µM and 50 µM in the final solvent concentration of 10% (*v/v*) are compared. Error bars represent the mean SD for three biological repeats with duplicate technical repeats (n = 6).

The observed results may be more complex and can possibly be linked to the role of alcohol (OH) groups and hydrophobic groups present in the solvent environment. The OH groups could form hydrogen bonds with the peptide amide backbone and/or the polar amino acid side chains of Asn, Gln, Lys and Tyr, thereby preventing inter-peptide hydrogen bonding. Furthermore, as the OH groups would be able to form hydrogen bonds with the water molecules, this may result in a decrease in the hydrophobic effect preventing the Trp residue from being placed in a hydrophobic peptide pocket, which is possibly the case with the smallest alcohol, MeOH. On the other hand, the hydrophobic groups in the higher alcohols could interact with Val, Leu, Pro and the aromatic amino acids. These solvent interactions could lead to peptide units not associating into larger oligomeric structures and prevent aromatic stacking leading to FRET by Trp, due to the long-range dipolar interaction [8,13].

To further evaluate the influence of the formulations at 50 µM Trc mix, where overt oligomerisation is expected, the total quantum yield for each formulation condition was determined and set relative to the solvent (Figure 4.2). This allowed for the effect of the additive to be understood and possibly determine the additive's larger role on the Trc peptides.

The 50 µM peptide formulations in ACN revealed that additives such as 5 µM $ZnCl_2$, 1% Glr, 100 µM $CaCl_2$ and 1% Glr + 5 µM $ZnCl_2$ result in dequenching (Figure 4.2 A). Alternatively, at a higher $ZnCl_2$ concentration, slight quenching can be observed for the Trcs. For 100 µM $CaCl_2$ and 1% Glr + 100 µM $CaCl_2$, the inverse is observed with the former dequenching the peptide while the latter results in quenching. The quenching is a possible effect of 1% Glr interacting with both peptide and water, as well as the availability of the hydroxyl groups for interaction. As discussed above, the availability of hydroxyl groups within the solvent environment may contribute to preventing large structure oligomerisation via hydrogen bonding or the lowering water activity and resulting hydrophobic effect [13,14]. Therefore, if in ACN alone, the Trcs Trp underwent quenching, the introduction of the OH groups by Glr would result in the inverse effect in which the peptide would be prevented to undergo large structure formation or prevent aromatic stacking, thereby allowing the Trp to be in a more "open" or favourable environment which does not influence the energy transfer from the ground to excited state when Trp is excited.

Interestingly, 5 µM $ZnCl_2$ and 100 µM $CaCl_2$ result in dequenching of the Trp residue. This may be attributed to the energy states within the Trp when it undergoes excitation. It is known that electron-deficient groups may cause Trp quenching or influence the balance between the ground and excited quantum yield energy states of the Trp fluorophore [8]. It can be observed that when 1% Glr is in combination with either 5 µM or 100 µM $ZnCl_2$, and $CaCl_2$ respectively, the overall relative RFU quantum yield is lower/less than when not formulated together. This may be due to the combined effect of each additive on the peptide. No change in relative RFU was observed for 100 µM $ZnCl_2$ which may suggest that there may be a breakpoint in the additive concentration and the influence on the peptide.

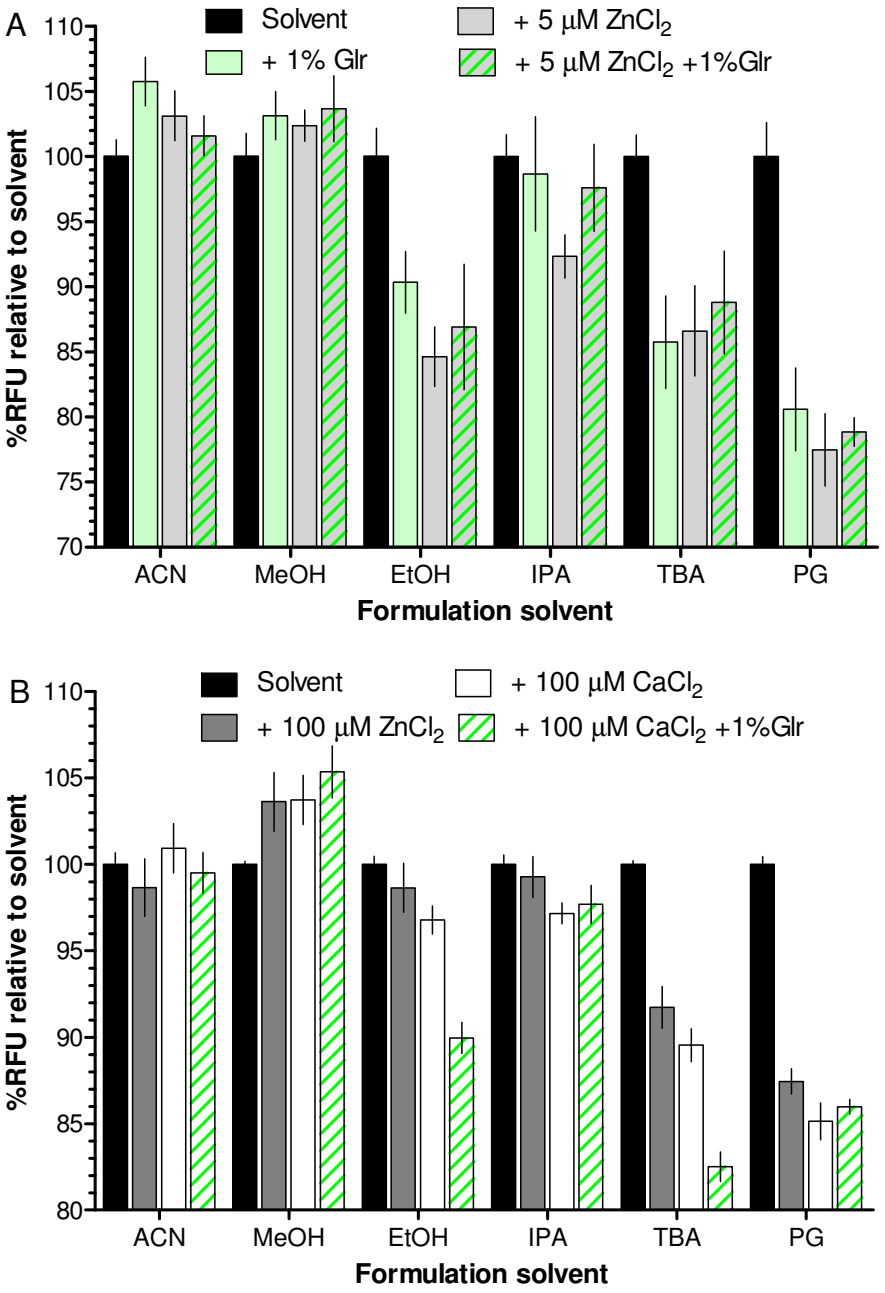

Figure 4.2 Comparison of fluorescence in different formulations of 50 µg/mL Trc mix. The bar-plot represents each Trc mix formulation (A: 1% Glr, 5 µM $ZnCl_2$, 1% Glr + 5 µM $ZnCl_2$. B: 100 µM $ZnCl_2$, 100 µM $CaCl_2$ and 1% Glr + 100 µM $CaCl_2$) compared against the of solvent controls (ACN, MeOH, EtOH, IPA, TBA, PG) to determine the influence the formulations have towards the peptides expected fluorescence yield (provided as relative fluorescence shifts - % RFU), at a final Trc mix concentration of 50 µM. Error bars represent the SD for six repeats (n = 6). Refer to Table S4.1 for full statistical analysis.

Differentiating results are observed for TBA and EtOH (Figure 4.2) with regards to the quantum yield of the Trc formulations within each Trc mix formulation at 50 µM compared to ACN findings. Quenching is observed in both solvent conditions for all peptide formulations while 100 µM $ZnCl_2$

and 100 µM $CaCl_2$ showed no quenching and slight quenching respectively. The observed quenching when 1% Glr is present may be attributed to the addition of more OH groups within the formulation leading to more hydrogen bonding within the solution. This means hydrogen bonding could occur between the solvent and Glr, competing with and removing hydrogen bonds that were possibly present between the peptide and the solvent. This potentially could lead to more interactions between peptide oligomers leading to large oligomeric structures being formed. The formation of these structures may lead to aromatic stacking of the Trp residue leading to a loss in quantum yield of the fluorophore. Additionally, collisional quenching may be due to interactions between the fluorophore Trp and the additive/quencher leading to deactivation of the fluorophore when in contact with the ionic molecule in solution. Furthermore, static quenching by complex formation leading to changes in ground and excited state energy levels by potential ion-induced dipole interactions, dipole-dipole interactions, or conformational changes in the fluorophore structure within the peptide or interactions between the electron-deficient groups/ions may result in quenching of the Trp [8].

PG results shown in Figure 4.2 A (Trc mix at 50 µM) suggest that formulations result in peptide fluorescence quenching for the tested conditions. Due to the similarities in structure and polarity between PG and Glr, and the presence of the OH groups, there would now be a much larger concentration of OH groups available to participate in hydrogen bonding with the solvent and/or peptide, thereby increasing the amount of free water molecules in the solution. This will be more pronounced in the solvent PG with 1% Glr than in ACN, EtOH, TBA, IPA and MeOH due to both having similar properties which make them ideal as binding agents. This suggests that the solvent and additive would interact more readily with each other, increasing the degree of hydrogen bonding which would not limit the degree of oligomerisation. As there is now more water available, it would drive the hydrophobic effect on the peptide, pushing aromatic stacking that will increase the quenching.

Additionally, the fluorophore may not experience major hydrogen bonding with Glr, unlike in the other formulations, due to a proposed preferential interaction with PG. As there was no shift in maxima between the solvent and additive state (refer to supplementary data for shift maxima Table S4.3), there is possibly no overt interaction between the additive or solvent with the fluorophore itself and thus no stabilisation of the ground or excited state occurred [8]. The observed quenching for the other four additives may be attributed to the role of the electron-deficient ions when they are disassociated into their ionic species and may interact with the fluorophore, resulting in quenching [8]. Additionally, the 1% Glr + 100 µM $CaCl_2$ did not show a similar result to that of 1% Glr + 5µM $ZnCl_2$ which may suggest that the number of ionic species within the solution contributes to a larger

degree to quenching via interaction with the fluorophore and that there is no one isolated factor which can directly be labelled as responsible for quenching or no quenching of a fluorophore.

To determine whether polarity or peptide concentration were responsible for major changes to the peptide's total quantum yield over a concertation range, the quadratic or linear regression fits were done over the peptide's concentration range against the total peptide quantum yield for all the peptide formulations. Findings which resulted in a quadratic fit ($P<0.05$) over the concentration range would indicate that the observed quenching or dequenching is due to the peptide concentration. However, a linear regression fit ($P>0.05$) would suggest that there is a solvent or polarity effect on the peptides' polar groups leading to the observed quenching or dequenching of the peptide's quantum yield. Furthermore, the role of the additivities in influencing the polarity or concentration effect would be better understood to confirm the findings presented in Figure 4.2. Results presented in Figure 4.3 and Figure 4.4 reveal that for the solvents ACN, EtOH and TBA there was a peptide concentration influence (quadratic fit) whereas MeOH, IPA and PG had a polarity effect on the peptide fluorescence character. Assessing the role of the additives within a specific solvent system, the effects differ between the solvents and formulations. All three additive conditions shifted the fit from quadratic to linear for ACN (Figure 4.3), indicating that the additives promote the peptide Trp to being exposed to more of the polar environment by potentially decreasing the oligomerisation or aromatic stacking. Furthermore, the combination of 1% Glr + 5 µM $ZnCl_2$ seems to result in all conditions having a linear fit which may indicate that under these additive conditions, the peptide fluorescence becomes more concentration sensitive. This is observed for all the solvent conditions except for EtOH, which may be due to the combination of the 1% Glr interacting with more water molecules decreasing the hydrophobic effect, the salts being trapped by 1% Glr or the solvent preventing it from acting in a chaotropic manner. When in combination with 1% Glr or 5 µM $ZnCl_2$ in MeOH, EtOH and TBA (Figure 4.3), the peptide is influenced in a concentration-based manner rather than by polarity which is most interesting for MeOH as it revealed dequenching when compared to the solvent control (Figure 4.2) at a fixed concentration. However, over a concentration range, the peptide concentration has a greater overall influence.

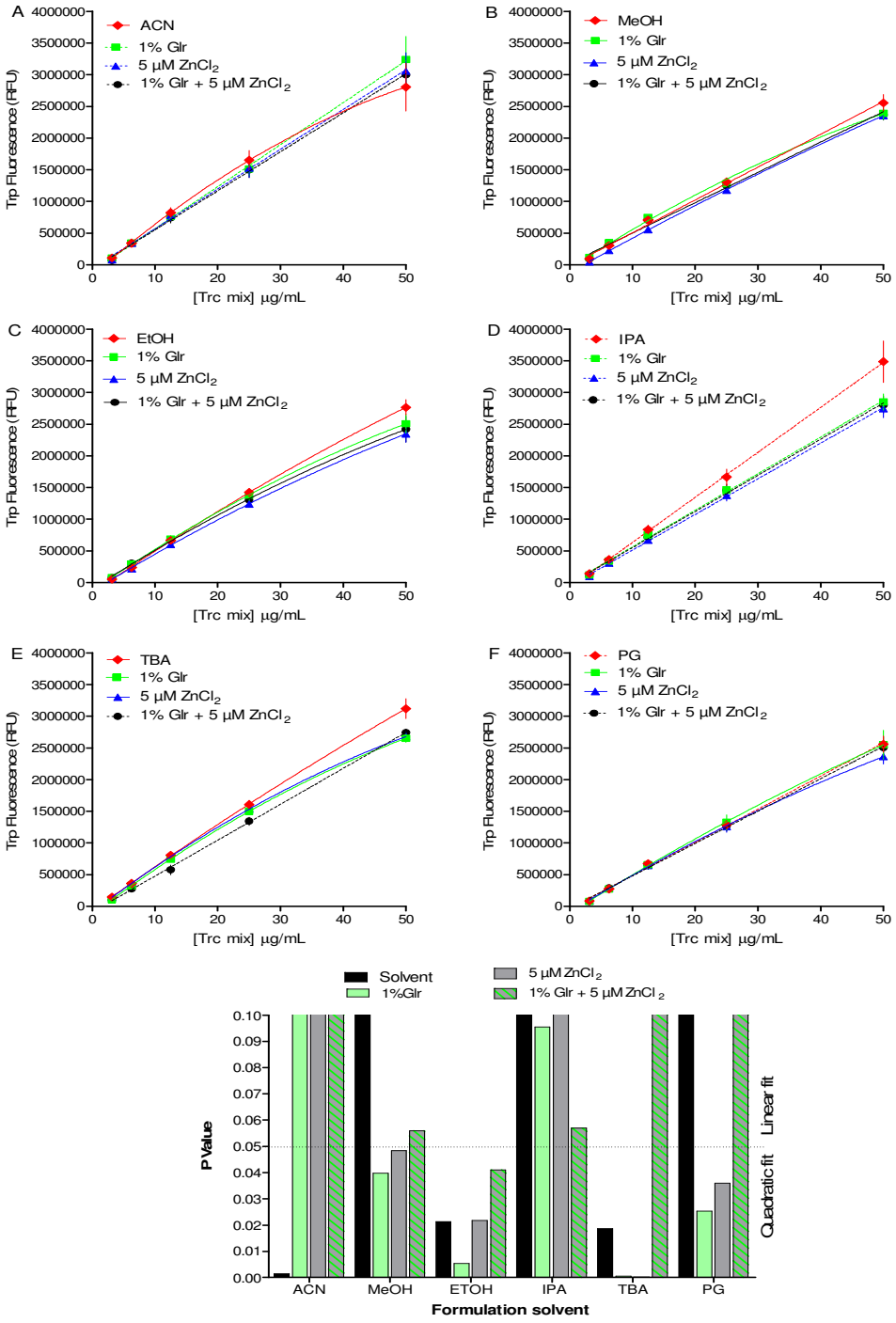

Figure 4.3 Fluorescence trends of different formulations of Trc mix. The line plots of total Trp fluorescence (300-400 nm emission) comparing the effect of the specifically tested peptide formulation conditions (solvent, 1% Glr, 5 µM $ZnCl_2$, 1% Glr + 5 µM $ZnCl_2$) have towards the Trc mix peptides over a concentration range from 3.125 µg/mL to 50 µg/mL within each solvent group. Solvent systems assessed were A. ACN, B. MeOH, C. IPA, D. MeOH, E. TBA and F. PG with each data point representing the average of six repeats with the standard error of the mean (SEM). The best line fit was statistically selected via a comparative best fit model, and all shown fits have $R^2 \geq 0.998$, with solid lines showing a quadratic fit and dotted lines a linear fit as shown in the bar graph.

Investigating the influence when increasing the salt concentration from 5 µM to 100 µM is revealed in Figure 4.4 for each of the solvents and formulations of the Trc peptides.

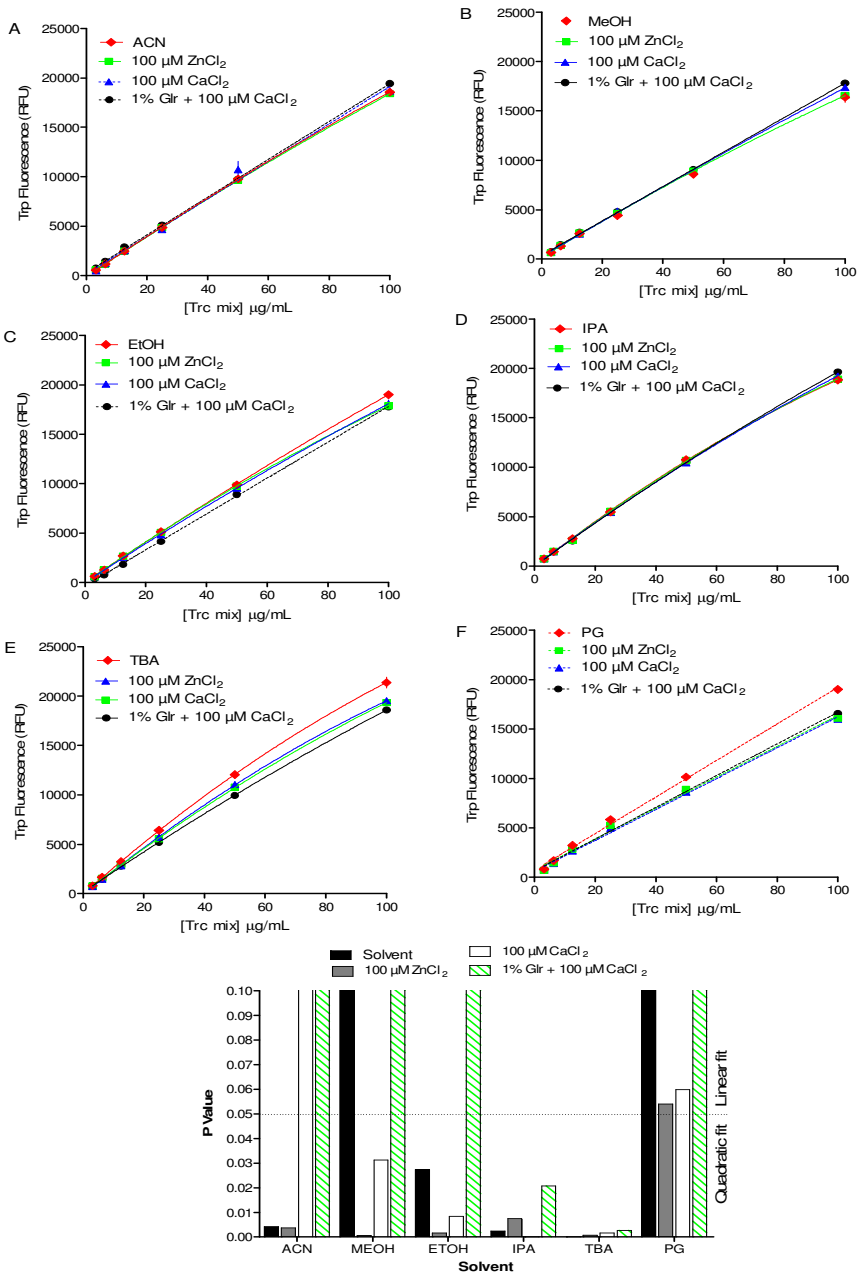

Figure 4.4 Fluorescence trends of different formulations of Trc mix. The line plots of total Trp fluorescence (300-400 nm emission) comparing the effect the specific tested peptide formulation conditions (solvent, 100 µM $ZnCl_2$, 100 µM $CaCl_2$ and 1% Glr + 100 µM $CaCl_2$) have towards the Trc mix peptides over a concentration range from 3.125 µg/mL to 50 µg/mL within each solvent group. Solvent systems assessed were A. ACN, B. MeOH, C. EtOH, D. IPA, E. TBA and F. PG with each data point representing the average of six repeats with the standard error of the mean (SEM). The best line fit was selected statistically via a comparative best fit model and all shown fits have $R^2 \geq 0.998$, with solid lines showing a quadratic fit and dotted lines a linear fit, as shown in the bar graph.

It should firstly be noted that the concentration range for the Trc peptide is up to 100 µM which results in IPA changing from a linear fit to a quadratic fit when comparing the results of Figure 4.3 to Figure 4.4. This suggests that when the peptide is made up in IPA, polarity has an important oligomerisation role breakpoint of 50 µM but at higher concentrations, the solvent polarity cannot influence or prevent the peptide oligomerisation. All solvent systems, with the addition of 100 µM $ZnCl_2$ or 100 µM $CaCl_2$ result in a quadratic fit, except for PG which results in a linear fit for both salts and ACN with $CaCl_2$. For peptide in PG, it may be due to the extra OH groups which act like that of Glr thereby decreasing the hydrophobic effect on the peptide preventing aromatic stacking or higher order oligomerisation. For peptide in ACN, the 100 µM $CaCl_2$ may act as a chaotropic agent thereby disrupting oligomerisation which results in more peptide Trp units being exposed to the polar environment as ACN is the most polar solvent of those assessed. ACN, MeOH, EtOH and PG with 1% Glr + 100 µM $CaCl_2$ all result in a linear fit whereas IPA and TBA result in quadratic fits for this formulation. This may be due to the presence of the 1% Glr and the OH groups which decrease the hydrophobic effect, as mentioned earlier, whereas for IPA and TBA there may be a potential interaction between the 1% Glr and the 100 µM $CaCl_2$. This could decrease the amount of the chaotropic effect on the peptide meaning more peptide units can oligomerise due to increasing the peptide concentration.

4.5 Conclusion

The Trcs nature to form higher structures and the effect of local solvent and formulation environment surrounding the peptide investigated in this chapter revealed a highly sensitive relationship that is influenced by more than a single factor. The Trc solvent studies revealed a CMC of 12.5 µg/mL or 25 µg/mL and above for all solvent groups. These findings correlated to previously found results by the BIOPEP group, thereby attributing the observed quenching to potentially be reliant on the peptide conformation or oligomerisation in the solution above a certain CMC within the specific solvent system. This suggests that oligomerisation may be influenced either by having more polar solvents supporting higher order oligomerisation while less polar solvents may influence the hydrophobic effect on the Trcs, driving Trp aromatic stacking and leading to quenching.

Investigation into the effect of the additives when in formulation with the Trcs revealed that 1% Glr alone or in formulation with the four other additives had a lower relative RFU quantum yield. This would suggest that 1% Glr introduces more OH groups which will lead to a higher amount of hydrogen bonds within the solution. This may allow for more hydrogen bonding between the solvent and Glr and less between the peptide and solvent, therefore driving more peptide interactions leading to more oligomeric structure formation. Additionally, when not in formulation with 1% Glr, the

observed quenching for the four additives may be linked to either the interaction between the fluorophore and the electron-deficient ions, collisional quenching leading to deactivation of the fluorophore or static quenching leading to changes in the fluorophore ground and excited states via complex formation (dipole-dipole interactions, ion-induced dipole interaction or fluorophore conformational changes within the peptide).

Linear and quadratic fits were performed to determine whether observed quenching occurred due as a result of peptide concentration or the influence of solvent polarity in the peptide environment. With ACN, EtOH and TBA quenching was due to a peptide concentration influence (quadratic fit) whereas IPA, PG and MeOH had a polarity effect on the peptide (linear fit). Interestingly, 1% Glr + 5 µM $ZnCl_2$ had a linear fit for all solvent conditions except that of EtOH suggesting that in EtOH the 1% Glr is more prone to interacting with water molecules thereby decreasing the hydrophobic effect or trapping the salts preventing them from acting in a chaotropic manner. Most notably, peptide quantum yields showed a concentration influence (quadratic) for four of the six solvent systems and formulations of 100 µM $ZnCl_2$, $CaCl_2$ and 1% Glr + salts while PG and ACN resulted in linear fits for both salts and only 100 µM $CaCl_2$, respectively. The additional OH groups introduced by PG may decrease the hydrophobic effect preventing aromatic stacking whereas for 100 µM $CaCl_2$ in ACN, the salt may act in a chaotropic manner disrupting oligomerisation and exposing more Trp residues to the polar environment.

The ability to follow biophysical changes of the Trcs by following Trp fluorescence revealed how sensitive the Trcs are to their local aqueous environment. Moreover, the Trcs ability to be manipulated by changing the solvent polarity or introducing additives resulted in observable changes to the fluorescence profile of Trp that can be translated to changes in the peptide conformation and higher order oligomers. These findings suggest that there is no single factor that may be solely responsible for the final state of oligomerisation. However, these results promote the idea that the Trcs can be manipulated to find the most optimal operational concentrations and conditions which limit peptide aggregation but promote the formation of more favourable oligomers, which will be investigated in Chapter 5, for optimal bioactivity.

4.6 References

1. Ruttenberg, M.; King, T.; Craig, L. The chemistry of tyrocidine. VII. studies on association behavior and implications regarding conformation*. *Biochemistry* 1966, *5* (9), 2857-2864.
2. Ruttenberg, M.; King, T.; Craig, L. The use of the tyrocidines for the study of conformation and aggregation behavior. *Journal of the American Chemical Society* 1965, *87* (18), 4196-4198.
3. Laiken, S.; Printz, M.; Craig, L. Circular dichroism of the tyrocidines and gramicidin S-A. *Journal of Biological Chemistry* 1969, *244* (16), 4454-4457.
4. Kuo, M.; Gibbons, W. Determination of individual side-chain conformations, tertiary conformations, and molecular topography of tyrocidine A from scalar coupling constants and chemical shifts. *Biochemistry* 1979, *18* (26), 5855-5867.
5. Paradies, H. Aggregation Of tyrocidine in aqueous solutions. *Biochemical and Biophysical Research Communications* 1979, *88* (3), 810-817.
6. Jelokhani-Niaraki, M.; Prenner, E.; Kay, C.; McElhaney, R.; Hodges, R.; Kondejewski, L. Conformation and other biophysical properties of cyclic antimicrobial peptides in aqueous solutions. *The Journal of Peptide Research* 2001, *58* (4), 293-306.
7. Beyer, C.; Gibbons, W.; Craig, L.; Longworth, J. Heterogeneous tryptophan environments in the cyclic peptides tyrocidines B and C. *Journal of Biological Chemistry* 1974, *249* (10), 3204-3211.
8. Lakowicz J. Principles of fluorescence spectroscopy. *Springer Science & Business Media*. 2013
9. Lakowicz, J.; Weber, G. Quenching of protein fluorescence by oxygen. detection of structural fluctuations in proteins on the nanosecond time scale. *Biochemistry* 1973, *12* (21), 4171-4179.
10. Sethuraman, S.; Rajendran, K. Multicharacteristic behavior of tyrosine present in the microdomains of the macromolecule gum arabic at various pH conditions. *ACS Omega* 2018, *3* (12), 17602-17609.
11. Tang, X.; Thibault, P.; Boyd, R. Characterisation of the tyrocidine and gramicidin fractions of the tyrothricin complex from bacillus brevis using liquid chromatography and mass spectrometry. *International Journal of Mass Spectrometry and Ion Processes* 1992, *122*, 153-179.
12. Williams, R.; Yphantis, D.; Craig, L. Noncovalent association of tyrocidine B. *Biochemistry* 1972, *11* (1), 70-77.
13. Rautenbach, M.; Kumar, V.; Vosloo, J.; Masoudi, Y.; van Wyk, R.; Stander, M. Oligomerisation of tryptocidine C, a trp-rich cyclodecapeptide from the antimicrobial tyrothricin complex. *Biochimie* 2021, *181*, 123-133.
14. Masoudi Y. Characterisation and formulation of natural cyclodecapeptides with anti-candida activity. MSc thesis, Stellenbosch University, Department of Biochemistry: Stellenbosch, South Africa.2011. https://scholar.sun.ac.za/handle/10019.1/109933
15. Loll, P.; Upton, E.; Nahoum, V.; Economou, N.; Cocklin, S. The high resolution structure of tyrocidine A reveals an amphipathic dimer. *Biochimica et Biophysica Acta (BBA) - Biomembranes* 2014, *1838* (5), 1199-1207.
16. Munyuki, G.; Jackson, G.; Venter, G.; Kövér, K.; Szilágyi, L.; Rautenbach, M.; Spathelf, B.; Bhattacharya, B.; van der Spoel, D. B-Sheet structures and dimer models of the two major tyrocidines, antimicrobial peptides from bacillus Aneurinolyticus. *Biochemistry* 2013, *52* (44), 7798-7806.
17. Kumar, V.; van Rensburg, W.; Snoep, J.; Paradies, H.; Borrageiro, C.; de Villiers, C.; Singh, R.; Joshi, K.; Rautenbach, M. Antimicrobial nano-assemblies of tryptocidine C, a tryptophan-rich cyclic decapeptide, from ethanolic solutions. *Biochimie* 2022.

4.7 Supplementary Data

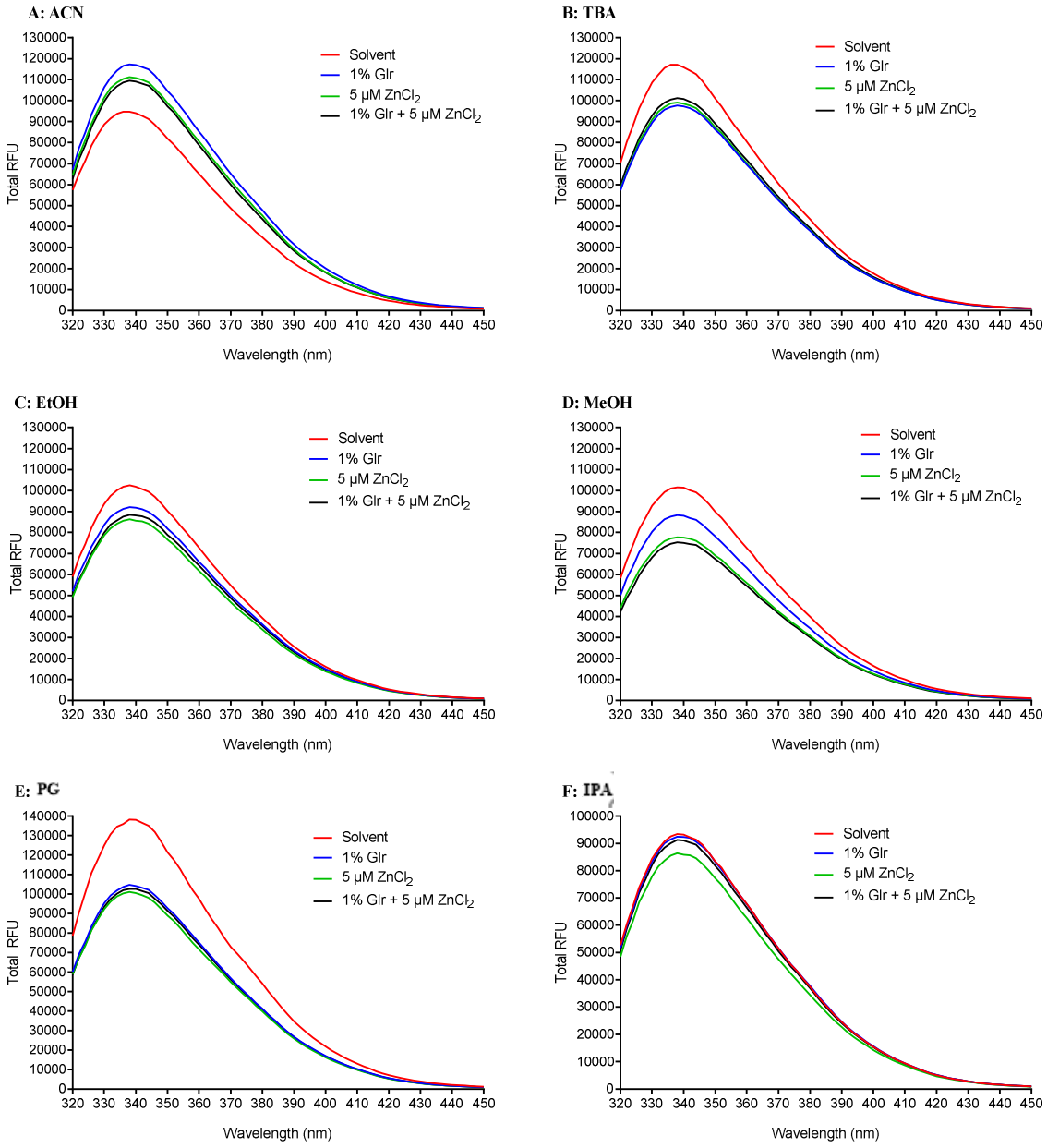

Figure S4.1 Fluorescence emission spectra for the Trcs alone and in formulation with additives (1% Glr, 5 uM $ZnCl_2$, and 1% Glr + 5 uM $ZnCl_2$) in the solvent environment: A: ACN, B: TBA, C: EtOH, D: MeOH, E:PG and F: IPA. Solutions excitation was at 280 nm and scanned over an emission range of 300nm – 450nm. The total fluorescence yield is provided as relative fluorescent units (RFU)

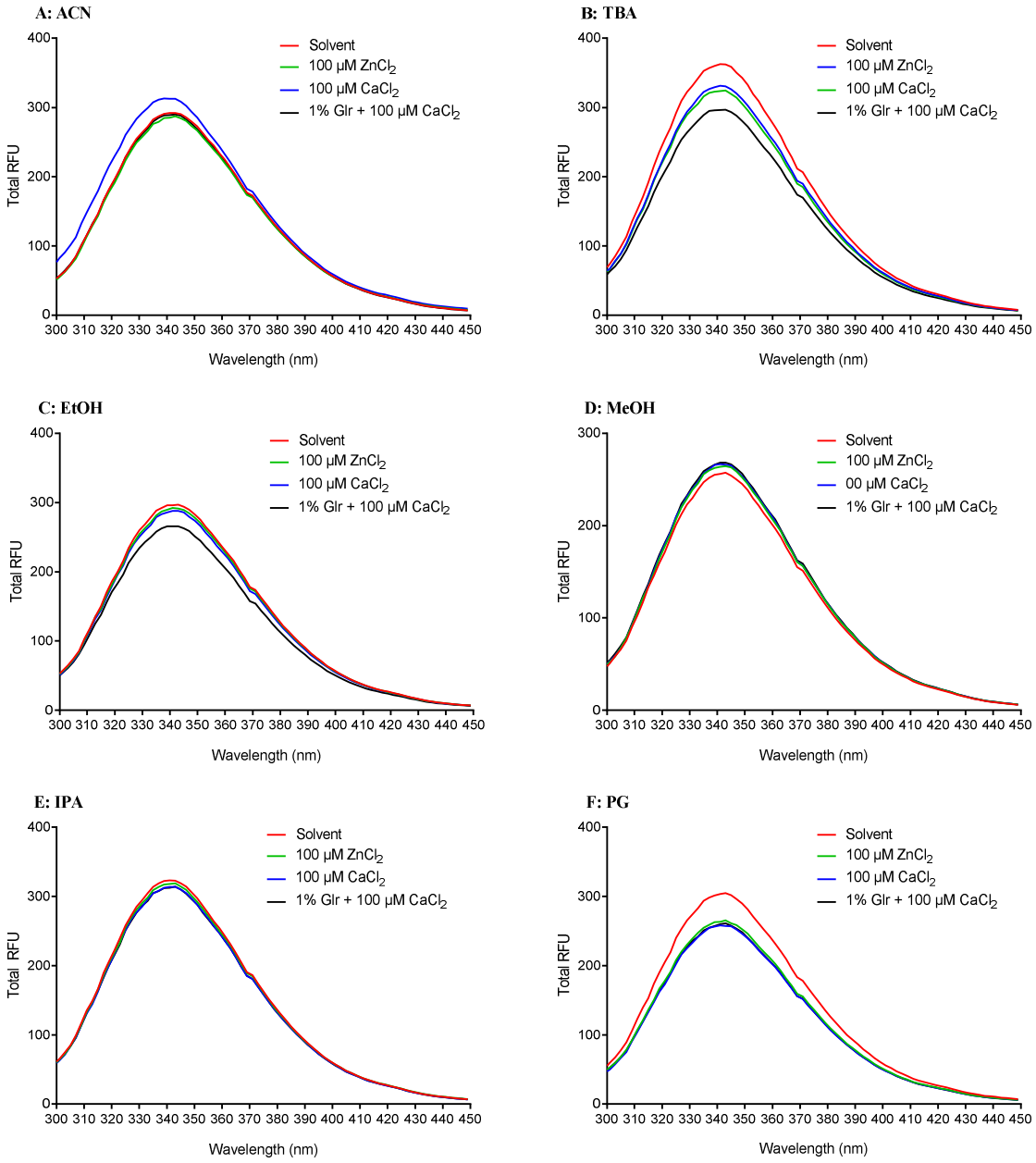

Figure S4.2 Fluorescence emission spectra for the Trcs alone and in formulation with additives (100 µM $ZnCl_2$, 100 µM $CaCl_2$ and 1% Glr + $CaCl_2$) in the solvent environment: A: ACN, B: TBA, C: EtOH, D: MeOH, E: IPA and F: PG. Excitation was at 280 nm and emission scanned over a range of 300 nm – 450 nm. The total fluorescence yield is provided as relative fluorescent units (RFU).

Table S4.1 Summary of the statistical analysis performed for Trc mix alone in each solvent system (ACN, MeOH, EtOH, IPA, TBA and PG) and in different formulations (1% Glr, 5 µM $ZnCl_2$ and 1% Glr +5 µM $ZnCl_2$) at a fixed peptide concentration of 50 µM. Two-Way ANOVA statistical analysis was performed (Bonferroni's multiple comparison test). *P < 0.05, **P < 0.01, ***P < 0.001 and ****P < 0.0001

	ACN		
	1% Glr	5 µM $ZnCl_2$	1% Glr +5 µM $ZnCl_2$
Solvent	Ns	ns	ns
1% Glr		ns	ns
5 µM $ZnCl_2$			ns
	MeOH		
	1% Glr	5 µM ZnCl2	1% Glr +5 µM $ZnCl_2$
Solvent	ns	ns	ns
1% Glr		ns	ns
5 µM $ZnCl_2$			ns
	EtOH		
	1% Glr	5 µM ZnCl2	1% Glr +5 µM $ZnCl_2$
Solvent	ns	**	*
1% Glr		ns	ns
5 µM $ZnCl_2$			ns
	IPA		
	1% Glr	5 µM ZnCl2	1% Glr +5 µM $ZnCl_2$
Solvent	ns	ns	ns
1% Glr		ns	ns
5 µM $ZnCl_2$			ns
	TBA		
	1% Glr	5 µM ZnCl2	1% Glr +5 µM $ZnCl_2$
Solvent	*	*	ns
1% Glr		ns	ns
5 µM $ZnCl_2$			ns
	PG		
	1% Glr	5 µM ZnCl2	1% Glr +5 µM $ZnCl_2$
Solvent	*	**	**
1% Glr		ns	ns
5 µM $ZnCl_2$			ns

Table S4.2 Summary of the statistical analysis performed for Trc mix alone in each solvent system (ACN, MeOH, EtOH, IPA, TBA and PG) and in different formulations (100 µM $ZnCl_2$, 100 µM $CaCl_2$ and 1% Glr + 100 µM $CaCl_2$) at a fixed peptide concentration of 100 µM. Two-Way ANOVA statistical analysis was performed (Bonferroni's multiple comparison test). *P < 0.05, **P < 0.01, ***P < 0.001 and ****P < 0.0001

	ACN		
	100 µM $ZnCl_2$	100 µM $CaCl_2$	1% Glr +100 µM $CaCl_2$
Solvent	ns	ns	ns
100 µM $ZnCl_2$		ns	ns
100 µM $CaCl_2$			ns
	MeOH		
	100 µM $ZnCl_2$	100 µM $CaCl_2$	1% Glr +100 µM $CaCl_2$
Solvent	ns	ns	*
100 µM $ZnCl_2$		ns	ns
100 µM $CaCl_2$			ns
	EtOH		
	100 µM $ZnCl_2$	100 µM $CaCl_2$	1% Glr +100 µM $CaCl_2$
Solvent	ns	ns	****
100 µM $ZnCl_2$		ns	****
100 µM $CaCl_2$			**
	IPA		
	100 µM $ZnCl_2$	100 µM $CaCl_2$	1% Glr +100 µM $CaCl_2$
Solvent	ns	ns	ns
100 µM $ZnCl_2$		ns	ns
100 µM $CaCl_2$			ns
	TBA		
	100 µM $ZnCl_2$	100 µM $CaCl_2$	1% Glr +100 µM $CaCl_2$
Solvent	****	****	****
100 µM $ZnCl_2$		ns	****
100 µM $CaCl_2$			***
	PG		
	100 µM $ZnCl_2$	100 µM $CaCl_2$	1% Glr +100 µM $CaCl_2$
Solvent	****	****	****
100 µM $ZnCl_2$		ns	ns
100 µM $CaCl_2$			ns

Table S4.3 Summary of the emission maxima of the Trc peptide alone or in formulations at 50 µM and 100 µM with the specific formulation additives (1% Glr, 5 µM $ZnCl_2$, 1% Glr + 5 µM $ZnCl_2$, 100 µM $ZnCl_2$, 100 µM $CaCl_2$ and 1% Glr + 100 µM $CaCl_2$).

	Maximum wavelength ± SD							
	Solvent (50µg/mL)	1% Glr (50µg/mL)	5 µM $ZnCl_2$ (50µg/mL)	1% Glr + 5 µM $ZnCl_2$ (50 µg/mL)	Solvent 100 µM	100 µM $ZnCl_2$	100 µM $CaCl_2$	1% Glr + 100 µM $CaCl_2$
ACN	336 ± 2	338 ± 1	338 ± 1	338 ± 1	343 ± 2	341 ± 1	341 ± 1	343 ± 1
TBA	338 ± 1	338 ± 0	338 ± 1	338 ± 1	339 ± 2	339 ± 2	341 ± 2	341 ± 1
EtOH	338 ± 1	338 ± 1	338 ± 0	338 ± 1	343 ± 1	341 ± 1	343 ± 1	343 ± 1
MeOH	338 ± 2	338 ± 1	338 ± 1	338 ± 1	343 ± 1	343 ± 1	343 ± 1	343 ± 1
IPA	338 ± 2	338 ± 0	338 ± 1	338 ± 1	341 ± 1	341 ± 2	341 ± 2	343 ± 1
PG	338 ± 1	338 ± 1	338 ± 2	338 ± 1	341 ± 1	341 ± 1	343 ± 1	341 ± 2

Chapter 5

Ion mobility mass spectrometry to assess to oligomerisation of the tyrocidines in formulations

5.1 Introduction

Uncontrolled microbial surface contamination and spread of resistant pathogens have forced a directional shift in importance to limit the use of antibiotics to the need for alternative, green and effective surface antimicrobial control methods within the medical, industrial and food sectors [1-3]. Limitations of standard cleaning and disinfection methods have prompted interest in the incorporation of antimicrobial peptides (AMPs) due to limited observed resistance, multiple modes of action and the need for low effective concentrations [4-7]. A viable AMPs for surface formulations are the tyrocidines (Trcs) [8-11], however, understanding the influence various solvents and formulations have on the peptides' higher order oligomerisation is critical for optimal incorporation and application development. Previously conducted studies on the Trcs revealed that the peptide shows a strong degree of aggregation within an aqueous solution with peptide association being larger in water and lower in low dielectric constant solvent systems [12-16]. Furthermore, peptide aggregation is influenced by both hydrophobic interactions within the aqueous environment and the amino acid spatial alignment specifically the amino acid variations at position three and four [12-17,22-24]. These parameters directly influence the overall peptide secondary structure and the self-assembly of the peptide units into various oligomeric structures [18-20,22]. Structural studies performed on TrcA revealed that the peptide forms four β-sheet strands as an amphipathic dimer stabilised by four intramolecular hydrogen bonds [19]. Furthermore, oligomer formation of TrcA [18], TrcB [17] and TrcC [19,20] indicated that the β-sheet structures form dimeric units via hydrogen bonding and hydrophobic interactions, further allowing for a scaffold effect that is capable of forming larger peptide oligomeric aggregates. Studies conducted by the Masoudi *et al.* [21] have shown that peptide aggregation can be influenced by various carbohydrate formulations which directly change the manner of elicited activity by the Trcs towards their targets.

This chapter focuses on investigating the influence of various solvent systems and peptide formulations on the Trcs and the impact on higher order oligomerisation. The three main Trc analogues TrcA, TrcB/B' and TrcC were assessed in six different solvent conditions (ACN, TBA, EtOH, MeOH, IPA and PG) to determine the influence that solvent polarity has on the peptide conformation by using the cross collational section (CCS) values obtained via ion mobility mass spectrometry (IM-MS). Differences between the three assessed analogues, TrcA, TrcB and TrcC, lie

within the aromatic amino acids at position three and four (TrcA: L-Phe^3-D-Phe^4; TrcB/B': L-Trp^3-D-Phe^4 and TrcC: L-Trp^3-D-Trp^4) which have been shown to be important in influencing peptide oligomerisation and activity [22-24]. Furthermore, the ionic species of monomeric and dimeric peptide units were assessed in various peptide formulations (refer to Chapter 3, Table 3.1 for formulation compositions) to determine the impact of the formulations on stabilising or preventing higher order oligomerisation. Therefore, the peptide oligomerisation profiles are of interest as their understating will allow for more optimal development for peptide surface formulations.

One technique to study oligomerisation is ion mobility (IM) linked to mass spectrometry (MS), both of which are well-established analytical techniques. IM separates gas-phase ions based on the compound's mobility to move within a medium and is highly dependent on the shape and charge of the ion [25-28]. MS is used to analyse gas-phase ions determining their mass-to-charge (*m/z*) ratio [27,28], with both techniques being important for structural and biophysical studies [28]. Two types of technologies can be used in IM-MS namely travelling wave ion mobility (TWIM-MS) and drift-time ion mobility (DTIM-MS) (Figure 5.1). Briefly, DTIM-MS has the ions exposed to a drift gas that migrate through the tube due to a static uniform electric field being applied to the ions (Figure 5.1A) whereas TWIM-MS is comprised of rings of stacked electrodes which has a travelling voltage wave of positive and negative radio frequency applied to adjacent electrodes which result in the attraction of the ions [26,27]. Therefore, the application of a pulsing direct current on each electrode allows for the propulsion of the ions along the electrode [26,27]. Ion separation is achieved by altering the pulse speed and charge extent to which more mobile ions move with the wave whereas lower mobile ions roll through the wave increasing the time taken to move through the gas phase (Figure 5.1B) [27]. Both analytical techniques allow for the determination of the collisional cross-section (CCS), however, ion drift times for DTIM-MS are dependent on the CCS [26,27]. CCS allows for the determination of the compound structural information by giving an indication of the ion's shape and size which are specific to each ion [26,27]. DTIM-MS is able to determine CCS via direct calculation from drift time, whereas TWIM-MS requires drift time calibration with compounds of similar CCS values for CCS calculation [27]. Furthermore, if IM is linked to ESMS (IM-MS), this allows for structural analysis to be performed specifically studies on the polar interactions (such as hydrogen bonds and ionic interactions) due to ESMS removing the aqueous environment around the analyte [29,30]. As IM-MS reveals stable non-covalent oligomers, it can be used to determine the ionic/electrostatic contribution to the stability of various oligomers within each peptide formulation and the influence of each formulation on peptide oligomerisation. This can be studied as previous

studies conducted by Rautenbach *et al*. [15], and Van Wyk [31] revealed highly stable oligomeric structures are formed by the Trcs under IM-MS conditions.

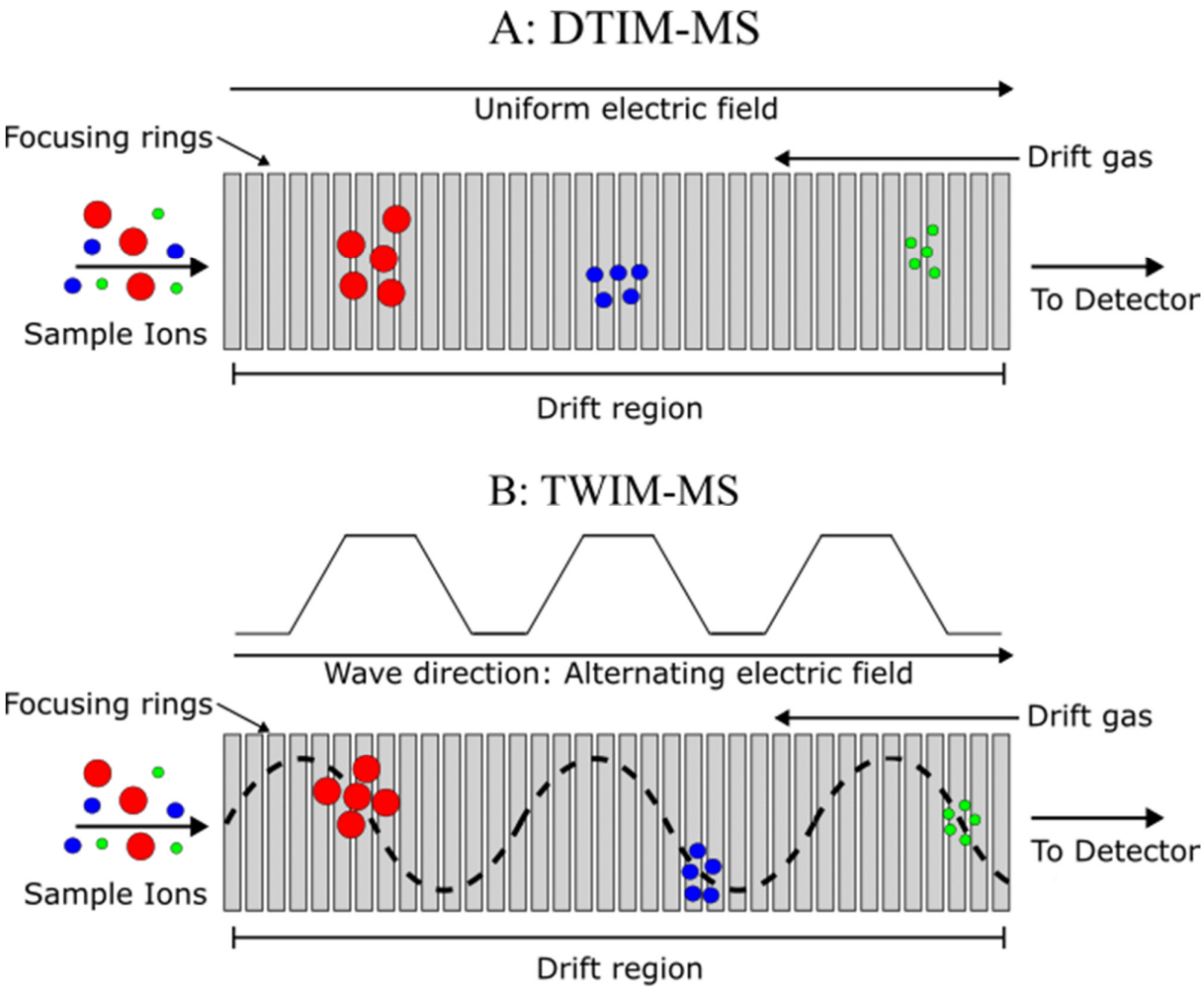

Figure 5.1 Schematic representing the difference between DTIM-MS and TWIM-MS ion mobility. Larger ions are represented in orange/red, medium ions in blue and small ions in green. A) DTIM-MS, separation achieved by ions passing through the applied drift gas. Small ions are less hindered whereas larger ions interact more with the gas thereby hindered more. B) TWIM-MS separation is achieved via electrically charged rings applied with direct current (DC) allowing for ion movement. Smaller ions have higher mobility due to rolling whereas larger ions have lower mobility thereby taking longer. [Adapted from Lanucara *et. al* [27]]

5.2 Materials

Tyrocidine mixture (Trc mix) was extracted from commercial tyrothricin and described in full detail in Chapter 2. Tertiary butyl alcohol (TBA) and iso-propyl alcohol (IPA) were supplied by Sigma-Aldrich (St. Louis, MA, USA). Analytical grade ethanol (EtOH, >99.8%) was supplied by Merck (Darmstadt, Germany). Methanol (MeOH) and acetonitrile (ACN, HPLC-grade, far UV cut-off) were provided by Romil Ltd. (Microsep, Johannesburg, South Africa). Analytical grade water (MQH_2O) used for all peptide formulations was obtained by filtering water from a reverse osmosis purification

plant, through a Millipore-Q® water purification system (Milford, USA). The 96-well black flat bottom plates were supplied by Thermo Fisher Scientific (Denmark). Calcium chloride ($CaCl_2$) and zinc chloride ($ZnCl_2$) were supplied by Merck (Wadeville, Gauteng). Propylene-glycol (PG) was gifted by Plascon® (Plascon, South Africa).

5.3 Methods

5.3.1 Ion mobility mass spectrometric analysis

The peptide and peptide formulations were prepared to a final concentration of 0.100 mM and solvent concentration of 10% water *(v/v)* and MQH_2O as described earlier. Samples were centrifuged at 3030×*g* for 10 minutes allowing for the removal of any insoluble particulate material. Sample quality control and peptide analogue confirmation was done using high-resolution electrospray ionisation mass spectrometry (HR-ESMS). HR-ESMS analysis was conducted using a Waters Synapt G2 quadrupole time of flight mass spectrometer (TOF-MS) with an electrospray ionisation source (Milford, MA, USA). Samples were injected at 5 µL into the HR-ESMS system at a flow rate of 0.3 mL/minute, with the solvent system being 0.1% formic acid in 60% ACN in water *(v/v)*. Set parameters for the source temperature and cone voltage were 120 °C and 15V, respectively, with nitrogen being the desolvation gas set at 650 L/hour with a desolvation temperature set to 275 °C. Instrument mass calibration was set to 50 Da to 2000 Da using leucine-enkephalin single point-lock spray (*m/z* = 556.2771).

To study peptide aggregation and higher order oligomeric structures, ion mobility mass spectrometry linked to HR-ESMS (IM-MS) was used based on studies previously conducted by Rautenbach *et. al.* [15,41]. IM-MS analysis was done by enabling the travelling wave ion mobility cell within the HR-ESMS system. Parameters used for IM-MS detection were set to the following: Helium cell gas flow set at 180 mL/min, extraction cone at 4V, cone gas flow 50 L/hr, trap collision energy at 15V, trap gas flow to 0.40 mL/min, IM gas flow (N_2) set to 90 mL/min, mobility trap and mobility extract height set at 15V and 0V respectively with the trapping release time at 200 µs. Wave height ramp time was set to linear, starting at 8 V to 20 V, and wave velocity ramp was set to linear starting at 100 m/s to 650 m/s at a 20% wave velocity ramp. Data was collected in positive mode and scanned over an *m/z* range of 200-2100 at 0.200 scans per second. Poly-Alanine (Poly-A) was used as a calibration standard to calibrate the IM-MS travelling wave mobility cell's drift times. Data analysis was performed using the Waters MassLynx V6.0 software (Milford, MA, USA) and Driftscope V2.9 software (Milford, MA, USA). Monomeric and dimeric percentage contribution in the peptide formulations was determined by using the total signal for each molecular ion obtained from the IM-MS profiles.

5.3.2 Data analysis

All data analysis was performed using GraphPad Prism® V 6.0 and V 5.0 (San Diego, CA, USA). Analysis of all mass spectrometric data was performed using Mass Lynx v4.1 and Driftscope 2.1 software (Waters, Milford, MA, USA). Calibration of the IM-MS travelling wave drift time, a standard curve of poly-Alanine charge corrected CCS (ln Ω') verse corrected drift times (ln t' $_D$) on the x-axis and plotted according to Ruotolo *et al.* [32] using the following equations 5.1 and 5.2:

Equation 5.1:

$$t'_D = t_D - \left[\frac{c\sqrt{m/z}}{1000}\right]$$

with c = 1.4 (enhanced duty cycle (EDC) delay coefficient) which is the instrument dependent parameter [32,33], t $_D$ is the observed drift-time for poly-alanine.

Equation 5.2:

$$\Omega' = \frac{\Omega}{\left[z \times \sqrt{\frac{1}{M} + \frac{1}{m}}\right]}$$

where z is the ion charge, Ω is the CCS value of poly-alanine ion obtained from literature [34], M is the observed ion mass of the poly-alanine and m is the atomic mass of the N_2 gas (ion mobility drift gas) [33].

A standard curve was plotted of ln Ω' against ln t'$_D$ (Figure S5.1) and a linear equation, lnΩ' = Aln t'$_D$ + lnB, was extracted where the slope A represents the exponential proportion factor and B is the fit-determined parameter.

The double correction for the poly-alanine ions drift time (t"$_D$) using the exponential proportion factor (A) was determined using the following equation [32]:

Equation 5.3:

$$t"_D = t'^{A}_D \times z \times \sqrt{\frac{1}{M} + \frac{1}{m}}$$

The CCS values of the Trc mix peptide complexes were calculated as described by Ruotolo *et al.* [32] using the plotted poly-Alanine calibration curve (Figure S5.2) of t"$_D$ against the poly-alanine literature CCS values [34].

5.4 Results and Discussion

5.4.1 IM-MS monitoring of peptide oligomers in Trc mix formulations

The use of ion mobility coupled to high resolution (HR) ESMS allows for both the identification of peptides and compounds and the identification of higher order structure formation (refer to Chapter 2, Figure 2.1). It has been observed by Munyuki *et. al* [19], the Rautenbach group [15,20,21,31,35] and various other investigators [14,17] that the Trcs readily form higher order oligomers. Combining HR-ESMS with ion mobility mass spectrometry (IM-MS), allow for the separation of peptide oligomers with the same *m/z* values. However, the mixture of peptides in the Trc mix and the propensity of these cyclodecapeptides to form dimers and oligomers lead to a complex *m/z* profile. A selection of theoretical *m/z* values for the peptide homo- and heterodimers in the Trc mix are shown in Table 5.1.

Table 5.1 Summary of the potential doubly charged dimers $[2M+2H]^{2+}$ in Trc mix containing the six major Trc analogues. Bold *m/z* values indicate overlap between doubly charged dimers $[2M+2H]^{2+}$ of the Trc analogues.

	TrcA	$TrcA_1$	TrcB	$TrcB_1$	TrcC	$TrcC_1$
TrcA	1270.62					
$TrcA_1$	1277.67	1284.68				
TrcB	1290.17	**1297.18**	**1309.67**			
$TrcB_1$	**1297.18**	1304.18	**1316.68**	**1323.69**		
TrcC	**1309.67**	**1316.68**	1329.18	**1336.19**	1348.68	
$TrcC_1$	**1316.68**	**1323.69**	**1336.19**	1343.19	1355.69	1362.70

The singly charged monomers $[M+H]^+$ can share the same *m/z* values as the doubly charged dimers $[2M+2H]^{2+}$, but can be resolved using IM-MS. However, due to the overlap between certain *m/z* doubly charged dimers, 11 heterodimers of the 22 possible homo- and heterodimers cannot be differentiated from each other due to identical *m/z* values and conformational sizes which results in a problematic identification of the Trc and their analogue within the dimer. Although IM-MS theoretically could separate these dimers due to different conformations, the resolution of the travelling wave IM-MS system used for these analyses was not adequate to allow full separation. Therefore, all detected species of specific oligomers were grouped in the data analysis without considering each analogue's contribution. Plasticiser contamination from the micropipette tips was observed in all tested samples, bis(2-ethylhexyl) phthalate, (observed *m/z* = 413.2647, theoretical *m/z* = 413.2662). However, as it was present in all samples virtually at the same intensity, it was therefore assumed that did not have an influence or had a similar effect on the obtained results.

IM-MS profiles in Figure 5.2 represent an example of oligomerisation analysis of Trc mix in 10% ACN as the simplest type of formulation. Figure 5.2 A shows a 3D representation of the cation intensity versus *m/z* and drift time of the different peptide oligomer and charged states in the sample. The signal contribution of specific oligomers in the Trc mix sample in 10% ACN were obtained from the peak area of each specified *m/z* range in the ion drift profile (Figure 5.2 B). The doubly charged monomeric ions with *m/z* = 634.80-695.20 $[M+2H]^{2+}$ (Figure 5.2 C) resulted in a drift peak = 3.66 and collisional cross section (CCS) of 388-400 Å (refer to methods for calculation and Table S5.1 for CCS Å summary) correlating to the 399.1 Å observed for TpcC [20]. The mass spectrum of the drift peak at 3.66 (CCS at 388-400 Å) revealed the doubly charged monomeric species of the six major Trcs were present in the Trc mix (observed/expected): TrcA (634.8290/634.8273), $TrcA_1$ (641.8298/641.8351), TrcB/B' (654.3243/654.3328), $TrcB_1/B_1$' (661.3414/661.3406), TrcC (673.8303/673.8382) and $TrcC_1$ (680.8368/680.8460).

The singly charged monomers $[M+H]^+$ and doubly charged dimers $[2M+2H]^{2+}$ (Figure 5.2 D) were obtained by selecting for ions with *m/z* = 1270.50-1367.85, with ion peaks at 11.87 and 7.45 drift time, respectively. The dimers had a collisional cross section (CCS) of 548-577 Å and the monomers 356-381 $Å^2$, correlating to 522-571 $Å^2$ and 366-379 $Å^2$ observed for Trc dimers and monomers respectively [31,35] (Tables S5.1 and S5.2). As the size of the dimers does not correlate to an expected two-fold size increase of the monomeric species, it suggests that the observed dimeric species have compact structures. These IM-MS stable dimer structures are probably maintained by electrostatic interactions and/or hydrogen bonding, as hydrophobic interaction and weak Van der Walls forces are limited in the high energy in vacuo IM-MS environment [29,30].

The MS spectra extracted from the drift peak at 11.87 of the singly charged monomers again revealed six major analogues present within the Trc mix (observed/expected): TrcA (1269.6436/1269.6546), $TrcA_1$ (1283.6613/1283.6703), TrcB/B' (1308.6696/1308.6655), $TrcB_1/B_1$' (1322.6779/1322.6812), TrcC (1347.6764) and $TrcC_1$ (1361.6815/1361.6921). The spectra obtained for the doubly charged homo- and heterodimers indicated the presence of the six major tyrocidine homodimers and additionally, species of heterodimers. Identification of higher order oligomer ions such as tetramer ions were identified at *m/z* = 1693.50-1802.00 with peaks identified at 7.66 drift time (Figure 5.2 E) and hexamers were identified with *m/z* = 1905.30-2026.70 with a peak at 11.45 drift time (Figure 5.2 F). CCS values for the higher order oligomers were not determined due to low abundance and the scope of this study primarily focussing on the formulations' influence towards monomeric and dimeric species as they have been shown to contribute the most towards the peptide's active states.

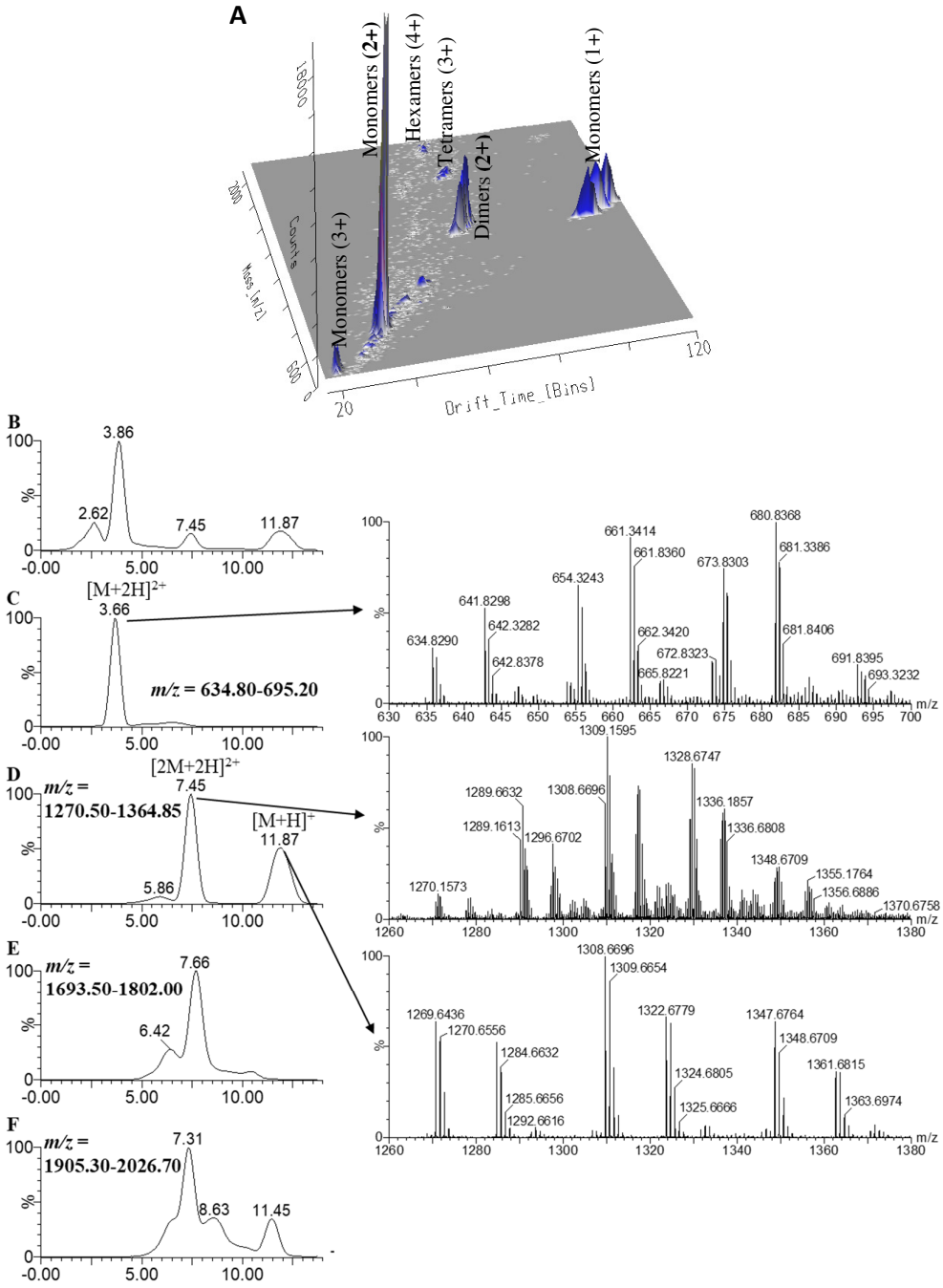

Figure 5.2 TWIM-MS positive ion drift profiles generated for the Trc mix with **A**: Drift scope 3D chromatogram with the x-axis showing the drift times (Bins), y-axis showing the total ion signal count and the z-axis showing the *m/z* ratio. **B**: TWIM-MS separation 2D chromatogram of all ionic species present within Trc mix (100 µM in 10% ACN) with **C**: doubly charged monomeric Trc mix species $[M+2H]^{2+}$, **D**: doubly charged dimeric Trc mix ionic species $[2M+2H]^{2+}$, **E**: singly charged monomeric ionic species $[M+H]^{+}$ and in **E**: and **F**: the higher order oligomeric ionic species $[nH+nM]^{+n}$ is shown. Each drift time chromatogram shows the searched ionic species *m/z* range used for a specific monomeric/oligomeric specie. The ESMS spectra are those of the dimeric and monomeric species shown with the correlating drift peaks in **C** and **D.**

The role of solvent polarity alone towards the peptide was determined by assessing the influence of the solvent towards the CCS values of the peptide in $Å^2$ (Table 5.2). Following the CCS values allow for further understanding of the complex formation and peptide conformation and if solvent polarity has a major effect on structure stabilization. It has previously been shown that the role of solvents as a co-solvent directly influences the self-assembly of an amphiphilic peptide [36], by either enhancing the hydrophobic interactions between assemblies or causing the hydrophobic cores to stabilize the polar edges, improving the assembly kinetics [36]. As shown in Table 5.2, it is observed that changes in peptide conformation can be seen between a relaxed (red) or compact (blue) state depending on the peptide analogue and the solvent system the peptide is exposed to. Comparing the singly charged monomeric species of TrcA, TrcB and TrcC, TrcA results in a more compact peptide structure (blue) in IPA and TBA. However, the monomeric peptide conformation moves to a relaxed state in PG. For all the solvents the doubly charged monomer is a more relaxed or extended conformation for TrcB (except in ACN) and TrcC. In general, TrcB and TrcA as monomers, dimers and doubly charged dimers showed the largest CCS values. Additionally, the doubly charged dimers show the largest CCS($Å^2$) error suggesting that peptide conformation is is depended on the peptide and solvent system. If the peptide is more hydrophobic like TrcA the dimer state cannot reach a stable compact or relaxed state in the more polar solvents such as ACN, MeOH, EtOH and TBA. TrcB is also more unstable in ACN, TBA and EtOH. Conversely, if the peptide is more polar such as TrcC, the peptide is not well stabilised in IPA and PG. This may be due to the availability of hydrogens to partake in hydrogen bonding or the solvents influencing the behaviour and hydrophobic effect on the peptide towards its optimal conformation.

Interestingly, a clear trend of conformational change is observed from TrcA to TrcC in which the peptide moves from a compact conformation for the hydrophobic TrcA analogues whereas the peptide is found to be in a more relaxed conformation for the polar TrcC analogues, with TrcB/B' portraying the average conformation behaviour of these two peptide analogues. The influence of the specific solvents TBA, EtOH and MeOH seems to be more dominant in driving a more compact peptide conformation of TrcA. Whereas, in TrcC, all solvents but ACN and TBA result in a more relaxed structure. These differences in peptide conformation may be attributed to the amino acids present at position three and four in the specific peptide analogues namely: TrcA having Phe^3-Phe^4, TrcB with Trp^3-Phe^4 and TrcC having Trp^3-Trp^4. Although the influence of the amino acid does not seem to have as much of a major role on the monomeric peptide conformation, the amino acid role is substantially more crucial in driving the peptide into a more relaxed or compact conformation in the dimer conformations. This can potentially be explained by the finding of Loll *et al*. [18] in which it was found that D-Phe^4 stabilises the strand-strand association within the monomer via hydrophobic

interactions. As the aqueous environment contains a higher concentration of polar molecules, the drive by the hydrophobic effect on the peptide will push the peptide into a more compact state which would be further stabilized by the Phe^4. However, in the presence of the Trp^4, this effect is less, which may be attributed to the ability of Trp to form a hydrogen bond thereby allowing the side chain to form a hydrogen bond with the solvent group or aqueous environment. This would "open" the peptide and drive it into a different, more relaxed conformation as seen for TrcC. For TrcB, as it still contains Phe^4, the effect as described above would be expected, however, the higher polarity of the solvent (ACN, TBA and EtOH) would influence the peptide in a much larger manner thereby negating the stabilisation effect through the hydrophobic interactions of Phe^4.

Table 5.2 Summary of determined CCS Ω ($Å^2$) values for Trc ionic species TrcA, TrcB/B' and TrcC in 10% (*v/v*) of the respective solvents (ACN, TBA, EtOH, MeOH, IPA and PG) from their respective drift times and the control Poly-Alanine calibration linear curve (Figure S5.2) with [n] representing the total number of technical repeats per sample and SE representing the standard error within the assessed condition. In the heatmap, red indicates a more relaxed conformation and blue, a more compact conformation of the peptide or its dimer (assessed per column).

Solvent	TrcA CCS Ω ($Å^2$) [3]			TrcB/B' CCS Ω ($Å^2$) [3]			TrcC CCS Ω ($Å^2$) [3]		
	$[M+H]^+$	$[M+2H]^{2+}$	$[2M+2H]^{2+}$	$[M+H]^+$	$[M+2H]^{2+}$	$[2M+2H]^{2+}$	$[M+H]^+$	$[M+2H]^{2+}$	$[2M+2H]^{2+}$
ACN	356±0.3	389±1.0	548±0.7	363±1.1	392±2.6	558±2.2	368±0.3	394±0.3	566±2.4
TBA	356±0	388±0	551±2.5	362±1.0	394±0	559±2.5	366±0	394±0	569±0
EtOH	357±1.0	388±0	549±2.5	361±0	394±0	558±2.5	368±1.9	394±0	569±0
MeOH	356±0	388±0	549±2.5	363±0	394±0	556±0	368±1.6	394±0	569±0
IPA	356±1.0	388±0	548±0	361±0	394±0	556±0	367±1.0	394±0	568±2.4
PG	357±1.2	388±0	548±0	363±0	394±0	556±0	368±0	394±0	568±2.4

* Also includes the CCS values TrcA-TrcC dimers

Comparing each solvent's total IM-MS signal for all formulations (Figure 5.3), formulations containing 1% Glr resulted in significantly ($P < 0.01$, $P < 0.001$) higher total signal compared to formulations without Glr, at the specific conditions (refer to Tables S5.3, S5.4 and S5.5 for full statistical analysis) when compared to the solvent control. This is probably not a mass spectrometric phenomenon but suggests that 1% Glr prevents the formation of higher oligomers and promotes and/or stabilises monomeric and dimeric species, allowing the detection of these species. The lower ion signal for formulations without Glr suggests a lower potential of additives to disrupt oligomerisation by acting as chaotropic agents. In the case of the chloride salts as additives, one would expect a decrease in the total signal because of the counter ion effect of the chloride ions [37,38]. However, this counter ion effect was minimal and probably neutralised by Glr in the formulation for all the solvent systems except PG.

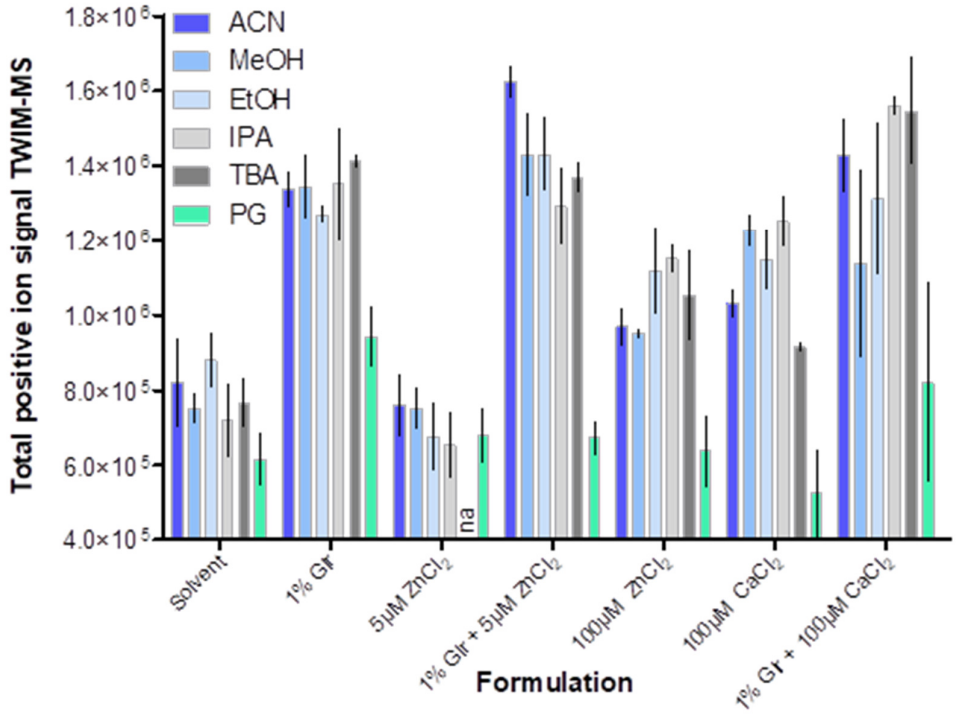

Figure 5.3 Total TWIM-MS ionic signal for the monomeric and dimeric of the Trc mix in the respective formulation conditions (1% Glr, 5 µM $ZnCl_2$, 1% Glr + 5 µM $ZnCl_2$, 100 µM $ZnCl_2$, 100 µM $CaCl_2$ and 1% Glr + 100 µM $CaCl_2$) at a fixed peptide concentration of 100 µM. Error bars represent the standard error of mean (SEM) for three technical repeats (n = 3). Full statistical analysis was performed compared against the solvent alone and reported in Table S5.3 and Table S5.4. na - No TWIM-MS data was obtained for the peptide formulation condition.

No overt counter ion effect was observed at a low $ZnCl_2$ concentration. Interestingly, the signal intensity of the Trc mix in 100 µM $ZnCl_2$ and 100 µM $CaCl_2$ was significantly higher than with the solvent alone (except for PG). This is also a good indication that the metal salts promoted and supported monomers and dimers in solution, leading to their higher concentration and detection. This may be due to binding of metal salts to the peptides and/or a chaotropic effect, both of which would limit oligomerisation and subsequent loss of signal.

To investigate the role and effect of oligomerisation, the percentage contribution of each monomeric and dimeric peptide specie in the 100 µM Trc mix peptide formulation were determined from the extracted ions peak and compared (Figure 5.4) in solvent alone and in formulation with glycerol (Glr) and selected chloride salts (5 µM $ZnCl_2$, 1 % Glr + 5 µM $ZnCl_2$, 100 µM $ZnCl_2$, 100 µM $CaCl_2$ and 1% Glr + 100 µM $CaCl_2$). It should be noted that the IM-MS profiles for the monomeric and dimeric species are expressed as a percentage contribution to the total profile signal. From these analyses, we confirmed that in all formulations containing 1% Glr, there is an increase in the percentage contribution of doubly charged dimers with a loss in singly charged dimers when compared to the

respective formulations without 1% Glr. This may indicate that the presence of Glr within the formulation may stabilise hydrogen bonding/electrostatic and ionic interactions thereby decreasing the release of monomeric species from the formulation.

Alternatively, Glr may compete for hydrogen bonds and water and limit the formation of larger oligomers, allowing the formation of stable dimers. Furthermore, for all the 100 µM salt formulations there was a significant increase ($P < 0.05$, $P < 0.0001$) in doubly charged monomers when compared to the solvent control (refer to addendum Table S5.5 for detailed statistical analysis). This may indicate the ability of the high salt concentration to disrupt hydrogen bonding and thereby oligomer formation by acting as chaotropic agents or cause an induced conformational change of the peptide, limiting the formation of dimers. The contribution of singly charged monomers remains relatively constant for all the peptide formulations except for those with the 100 µM salt in the formulation, namely: ACN, TBA, EtOH and IPA. For these formulations, there were a significant decrease (ACN $P < 0.001$, TBA $P < 0.01$, EtOH $P < 0.01$ and IPA $P < 0.0001$) in singly charged monomers leading to the increase in doubly charged monomers. This suggests that the peptide seed structures may readily interact with these singly charged monomers and incorporate them into larger oligomeric structures. If these singly charged monomeric species are released from larger oligomers, they would be released as singly charged monomers, increasing their presence in solution. Furthermore, the formulation with 1% Glr and 100 µM $CaCl_2$ with all solvents, except PG, again resulted in the increased contribution of doubly charged dimers and singly charged monomers, while doubly charged monomers decreased, (Figure 5.4 A-E). This further illustrated the nature of Glr to promote dimer formation by modulating the contribution of the hydrogen bonds and electrostatic interactions in the formulation.

Interestingly, when investigating all the formulations, it was observed that all formulations containing 100 µM $CaCl_2$ resulted in a large, detected ion peak at a drift time of 2.09. However, for Trc formulations in solvent alone, 1% Glr or 100 µM $ZnCl_2$, a small peak was observed at a similar drift time of 2.09 (refer to Figure 5.5 and Figure 5.6). However, the observed peak in Figure 5.5 differs from the observed peak at 2.09 in Figure 5.6. The observed peak in Figure 5.5 may potentially be either contaminants, fragmented peptide moieties or peptide-iron complexes due to residual iron possibly being present within the salt stock used. Whereas the peak in Figure 5.6 suggests the potential formation of triply charged peptide- Ca^{2+} complexes $[M+Ca+H]^{3+}$.

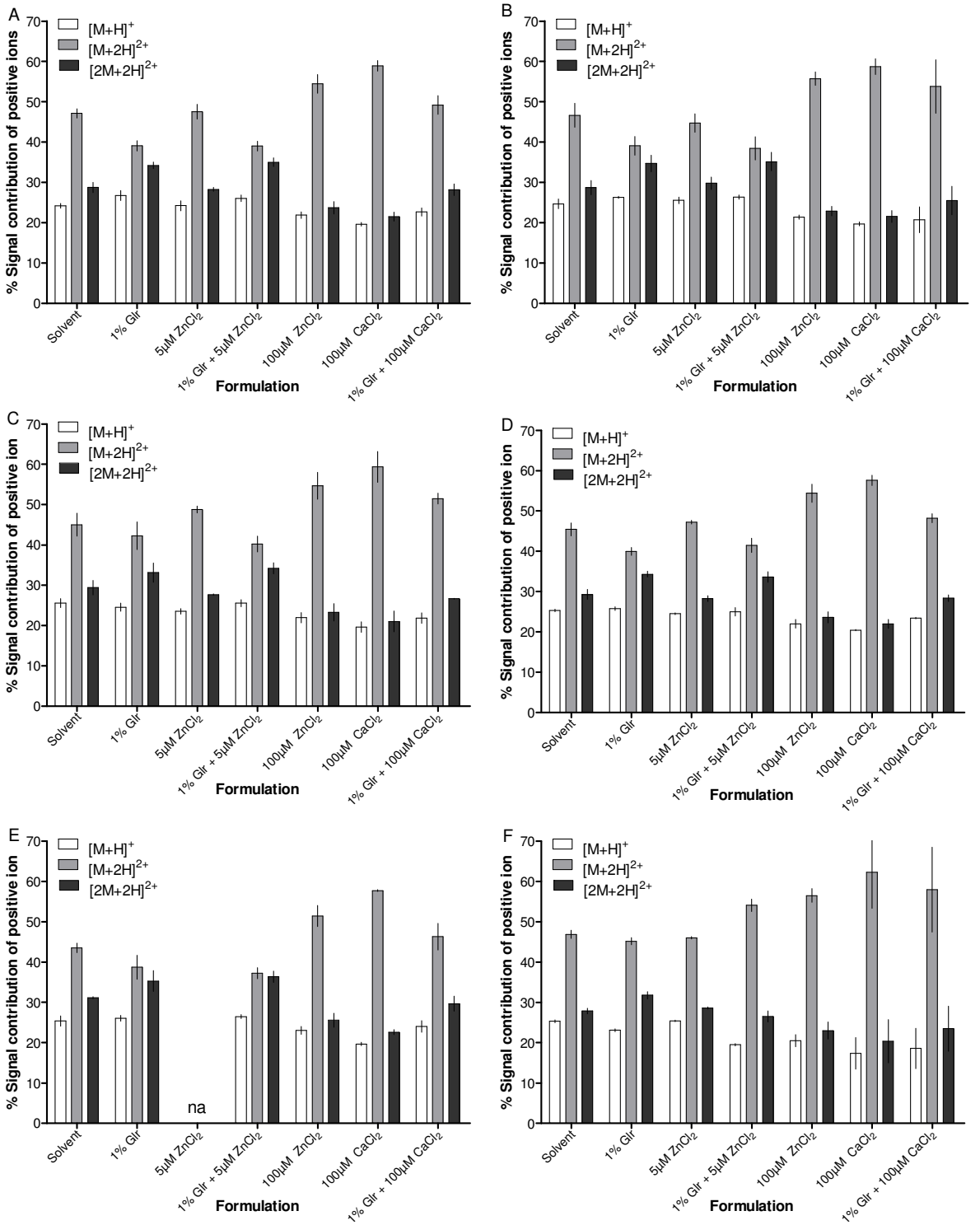

Figure 5.4 Bar plot representing the percentage contribution of the positive Trc peptide ions alone and in formulation with 1% Glr, 5 µM $ZnCl_2$, 1% Glr + 5 µM $ZnCl_2$, 100 µM $ZnCl_2$, 100 µM $CaCl_2$ and 1% Glr + 100 µM $CaCl_2$ in the respective solvent systems (A: ACN, B: TBA, C: EtOH, D: MeOH, E: IPA and F: PG) at a fixed peptide concentration of 100 µM Trc mix. Error bars represent the standard error of the mean for three technical repeats per sample (n = 3). Statistical analysis comparison can be found in Table S5.5 in the supplementary data.

As described by Loll *et.al.* [18] and Munyuki *et.al.* [19], the Trcs form amphipathic β-sheets dimers with four intramolecular hydrogen bonds that are used in stabilising the peptide structure. Additionally, the β-turns that are formed at the tight turns within the peptide due to the antiparallel β-sheet may provide anchoring for the metal ion, as was found for iturin A_2 [39]. However, as Ca^{2+} only observed to form the triply charged peptide-Ca^{2+} complex and not Zn^{2+}, this would suggest that the atomic radius of the metal has an important role. As the nature of IM-MS is harsh, any observed conformation or complex would be highly stable to survive the conditions. Ca^{2+} has an atomic radius of 1.80 Å whereas Zn^{2+} has a smaller more compact atomic radius of 1.42 Å [40]. Previous work conducted by the BIOPEP group has shown that other metals such as Mg^{2+} (1.45 Å), Ca^{2+} (1.80 Å) and Fe^{2+} (1.56 Å) form metal complexes with the peptides in the Trc mix [unpublished results, C de Villiers]. This would suggest that the pocket within the peptide requires an optimal specific size (1.45 Å – 1.80 Å) to form a highly stable complex, with Zn^{2+} being just too small and would therefore not allow for a stable interaction or passing through the pocket. Conversely, Ca^{2+} and larger atomic radius metal ions, such as Fe^{2+} can sit in the pocket and form a stable triply charged complex that can survive the harsh IM-MS conditions, and these may be stabilised by electrostatic interactions (coordination bonds) with the carbonyl groups present in the β-turn and the nearby carbonyl groups of the Asn and Gln side chains [18,19].

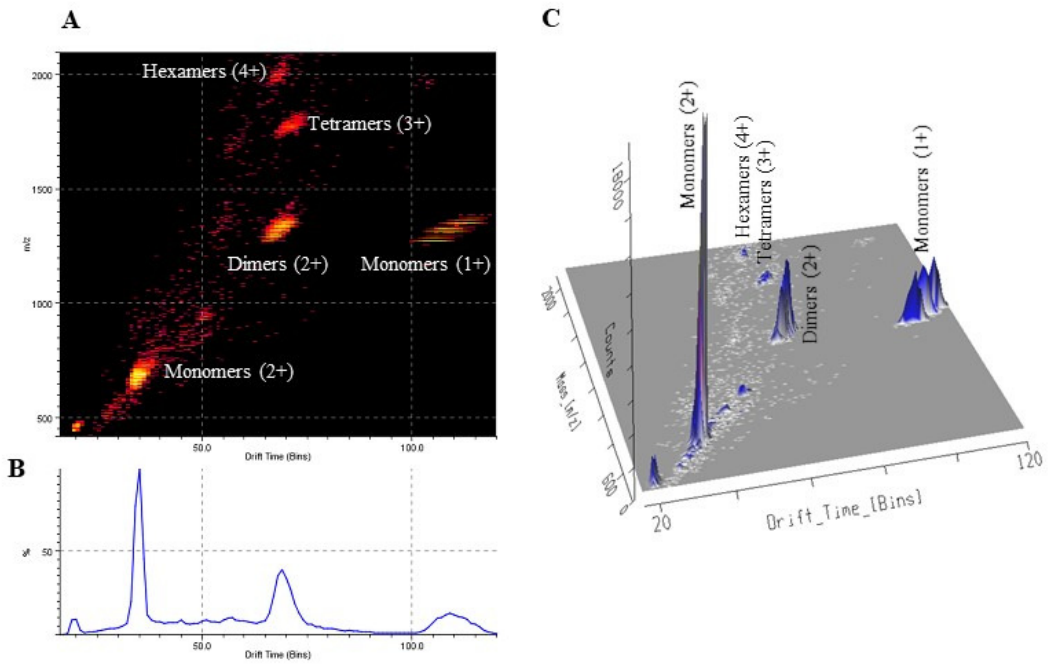

Figure 5.5 IM-MS of 100 µM Trc mix in 10% acetonitrile. Drift scope 3D chromatogram with the x-axis showing drift times (Bins), y-axis showing the total signal count and the z-axis showing the *m/z* ratio. A. 10 % ACN solvent only formulation; B. Ion profile for Trc mix formulation; C. 3D Profile of 100 µM Trc mix formulation with retention time on the x-axis, *m/z* on the y-axis and signal intensity (counts) on the z-axis.

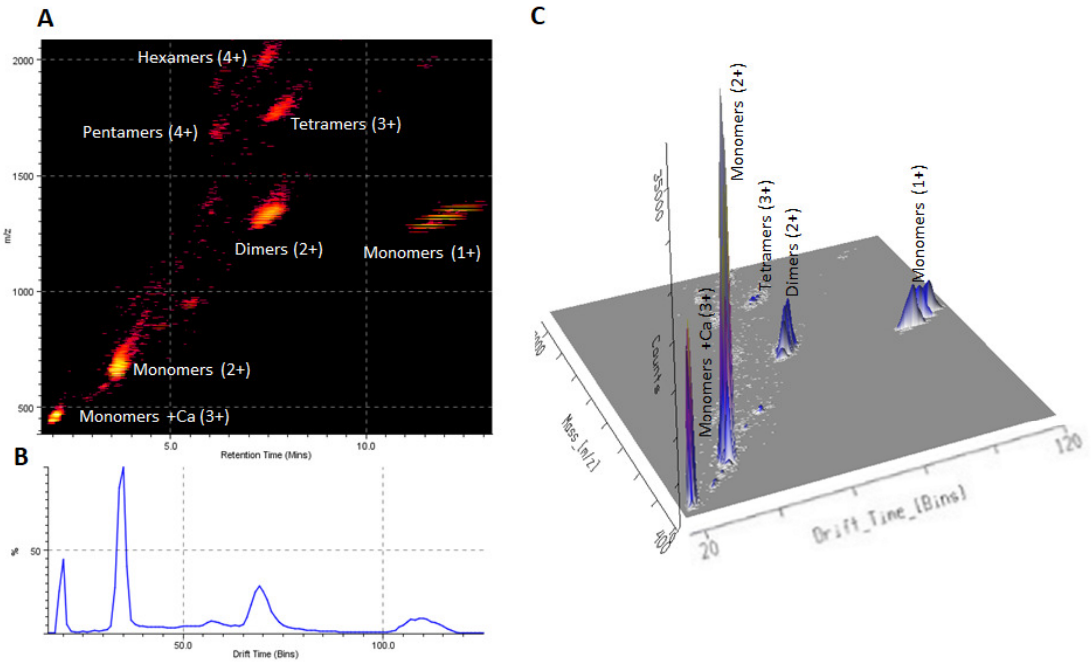

Figure 5.6 IM-MS of 100 µM Trc mix in 10% acetonitrile. Drift scope 3D chromatogram with the x-axis showing drift times (Bins), y-axis showing the total signal count and the z-axis showing the *m/z* ratio. A, 100 µM $CaCl_2$ formulation; B. Ion profile for Trc mix formulation; C. 3D Profile of 100 µM Trc mix formulation with retention time on the x-axis, *m/z* on the y-axis and signal intensity (counts) on the z-axis.

It can be hypothesised that a finite size of the metal ion is required to form a specific complex with the Trcs. This could explain the decrease of singly charged monomers as observed in Figure 5.4 as these peptide species would be taken up in complex formation. Furthermore, the presence of the peptide-Ca^{2+} complexes may contribute to preventing the formation of higher order oligomers and result in the improved antimicrobial activity that was observed for this formulation in Chapter 3, when tested against *L. monocytogenes* and *S. aureus.* Improved activity may be attributed to the incorporation of Ca^{2+} potentially masking the peptide or allowing the peptide to be placed in a more optimal conformation which would allow for the uptake of the Trcs-Ca^{2+} complex by the target, allowing the peptide to illicit its activity from within the target cell.

5.5 Conclusion

The determination of CCS values and peptide oligomer contribution showed a clear difference in the effect of the solvent system tested and the overall effect towards higher order structure formation when in combination with the additive. Polarity results for the solvent alone revealed that the peptide analogues shift from a compact conformation to a more relaxed conformation with an increase in the CCS values from the more hydrophobic TrcA analogue to the polar TrcC analogue, with TrcB having the average behaviour of both. This difference in peptide analogue polarity can be attributed to the

amino acids present at position three and four with TrcA having Phe at both positions whereas TrcC has Trp.

The 1% Glr resulted in a significant influence of the total ion signal, specifically an increase in doubly charged dimers for all formulations suggesting that formulations that contain 1% Glr prevent the formation of higher order oligomers thereby allowing for less release of monomeric species and the stabilization of dimeric species via hydrogen bonds/electrostatic interactions. Furthermore, high metal salt concentrations of 100 µM $ZnCl_2$ and 100 µM $CaCl_2$ may support the formation of monomers and dimers in solution due to the binding of metal salts or the ability of the meal salts to act as chaotropic agents thereby disrupting higher order oligomerisation. However, results showed that only Ca^{2+} resulted in a metal-peptide complex confirming the ability of the metals to prevent higher order oligomerisation by preventing the stacking of the peptide oligomers onto each other. This would facilitate a higher availability of the more active peptide moieties to associate on the surface for activity.

These findings show that the Trcs peptide is highly influenced by the peptide's aromatic characteristic, solvent polarity, and formulation additives, all possibly impacting the ability of the peptide to form various higher order oligomeric structures. Additionally, as peptide oligomerisation influences the antimicrobial ability of the Trcs (Chapter 3), these results further illustrate how these higher orders structures can be manipulated to result in the formation of more desirable peptide structures for better antimicrobial activity.

5.6 References

1. Fair, R.; Tor, Y. Antibiotics and bacterial resistance in the 21st century. *Perspectives in Medicinal Chemistry* 2014, *6*, PMC.S14459.
2. C Reygaert, W. An overview of the antimicrobial resistance mechanisms of bacteria. *AIMS Microbiology* 2018, *4* (3), 482-501.
3. Michael, C.; Dominey-Howes, D.; Labbate, M. The antimicrobial resistance crisis: causes, consequences, and management. *Frontiers in Public Health* 2014, *2*.
4. Boyce, J. Modern technologies for improving cleaning and disinfection of environmental surfaces in hospitals. *Antimicrobial Resistance & Infection Control* 2016, *5* (1).
5. Swartjes, J.; Sharma, P.; Kooten, T.; Mei, H.; Mahmoudi, M.; Busscher, H.; Rochford, E. Current developments in antimicrobial surface coatings for biomedical applications. *Current Medicinal Chemistry* 2015, *22* (18), 2116-2129.
6. Riool, M.; de Breij, A.; Drijfhout, J.; Nibbering, P.; Zaat, S. Antimicrobial peptides in biomedical device manufacturing. *Frontiers in Chemistry* 2017, *5*.
7. Bechinger, B.; Gorr, S. Antimicrobial peptides: mechanisms of action and resistance. *Journal of Dental Research* 2016, *96* (3), 254-260.
8. van Rensburg, W.; Rautenbach, M. Creating robust antimicrobial materials with sticky tyrocidines. *Antibiotics* 2022, *11* (2), 174.
9. Spathelf, B.; Rautenbach, M. Anti-listerial activity and structure–activity relationships of the six major tyrocidines, cyclic decapeptides from *Bacillus aneurinolyticus*. *Bioorganic & Medicinal Chemistry* 2009, *17* (15), 5541-5548.
10. Wigger-Alberti, W.; Stauss-Grabo, M.; Grigo, K.; Atiye, S.; Williams, R.; Korting, H. Efficacy of a tyrothricin-containing wound gel in an abrasive wound model for superficial wounds. *Skin Pharmacology and Physiology* 2012, *26* (1), 52-56.
11. Wenzel, M.; Rautenbach, M.; Vosloo, J.; Siersma, T.; Aisenbrey, C.; Zaitseva, E.; Laubscher, W.; van Rensburg, W.; Behrends, J.; Bechinger, B.; Hamoen, L. The multifaceted antibacterial mechanisms of the pioneering peptide antibiotics tyrocidine and gramicidin S. *mBio* 2018, *9* (5).
12. Ruttenberg, M.; King, T.; Craig, L. The chemistry of tyrocidine. VII. studies on association behavior and implications regarding conformation*. *Biochemistry* 1966, *5* (9), 2857-2864.
13. Ruttenberg, M.; King, T.; Craig, L. The use of the tyrocidines for the study of conformation and aggregation behavior. *Journal of the American Chemical Society* 1965, *87* (18), 4196-4198.
14. Paradies, H. Aggregation of tyrocidine in aqueous solutions. *Biochemical and Biophysical Research Communications* 1979, *88* (3), 810-817.
15. Rautenbach, M.; Kumar, V.; Vosloo, J.; Masoudi, Y.; van Wyk, R.; Stander, M. Oligomerisation of tryptocidine C, a trp-rich cyclodecapeptide from the antimicrobial tyrothricin complex. *Biochimie* 2021, *181*, 123-133.
16. Beyer, C.; Gibbons, W.; Craig, L.; Longworth, J. Heterogeneous tryptophan environments in the cyclic peptides tyrocidines B and C. *Journal of Biological Chemistry* 1974, *249* (10), 3204-3211.
17. Paradies, H.; Reichelt, H. Formation and structures of tyrocidine B oligomers in solution in the presence of water. *AIP Advances* 2020, *10* (7), 075007.
18. Loll, P.; Upton, E.; Nahoum, V.; Economou, N.; Cocklin, S. The high resolution structure of tyrocidine A reveals an amphipathic dimer. *Biochimica et Biophysica Acta (BBA) - Biomembranes* 2014, *1838* (5), 1199-1207.
19. Munyuki, G.; Jackson, G.; Venter, G.; Kövér, K.; Szilágyi, L.; Rautenbach, M.; Spathelf, B.; Bhattacharya, B.; van der Spoel, D. B-Sheet structures and dimer models of the two major tyrocidines, antimicrobial peptides from *Bacillus aneurinolyticus*. *Biochemistry* 2013, *52* (44), 7798-7806.
20. Kumar, V.; van Rensburg, W.; Snoep, J.; Paradies, H.; Borrageiro, C.; de Villiers, C.; Singh, R.; Joshi, K.; Rautenbach, M. Antimicrobial nano-assemblies of tryptocidine C, a tryptophan-rich cyclic decapeptide, from ethanolic solutions. *Biochimie* 2023, *204*, 22-32.
21. Masoudi, Y.; van Rensburg, W.; Barnard-Jenkins, B.; Rautenbach, M. The influence of cellulose-type formulants on anti-candida activity of the tyrocidines. *Antibiotics* 2021, *10* (5), 597.
22. Tang, X.; Thibault, P.; Boyd, R. Characterisation of the tyrocidine and gramicidin fractions of the tyrothricin complex from B*acillus brevis* using liquid chromatography and mass spectrometry. *International Journal of Mass Spectrometry and Ion Processes* 1992, *122*, 153-179.
23. Vosloo, J.; Stander, M.; Leussa, A.; Spathelf, B.; Rautenbach, M. Manipulation of the tyrothricin production profile of *Bacillus aneurinolyticus*. *Microbiology* 2013, *159* (Pt_10), 2200-2211.
24. Spathelf, B. Qualitative structure-activity relationship of the major tyrocidines, cyclic decapeptides from *Bacillus aneurinolyticus*. PhD thesis, Stellenbosch University, Department of Biochemistry: Stellenbosch, South Africa, 2010. http://scholar.sun.ac.za/handle/10019.1/4001
25. McDaniel, E.; Martin, D.; Barnes, W. Drift tube-mass spectrometer for studies of low-energy ion-molecule reactions. *Review of Scientific Instruments* 1962, *33* (1), 2-7.
26. Uetrecht, C.; Rose, R.; van Duijn, E.; Lorenzen, K.; Heck, A. Ion mobility mass spectrometry of proteins and protein assemblies. *Chem. Soc. Rev.* 2010, *39* (5), 1633-1655.

27. Lanucara, F.; Holman, S.; Gray, C.; Eyers, C. The power of ion mobility-mass spectrometry for structural characterization and the study of conformational dynamics. *Nature Chemistry* 2014, *6* (4), 281-294.
28. Ben-Nissan, G.; Sharon, M. The application of ion-mobility mass spectrometry for structure/function investigation of protein complexes. *Current Opinion in Chemical Biology* 2018, *42*, 25-33.
29. Bich, C.; Baer, S.; Jecklin, M.; Zenobi, R. Probing the hydrophobic effect of noncovalent complexes by mass spectrometry. *Journal of the American Society for Mass Spectrometry* 2010, *21* (2), 286-289.
30. Hilton, G.; Benesch, J. Two decades of studying non-covalent biomolecular assemblies by means of electrospray ionization mass spectrometry. *Journal of The Royal Society Interface* 2012, *9* (70), 801-816.
31. Van Wyk, R. Development of cyclodecapeptides from the tyrothricin complex as anticancer peptides. MSc thesis, Stellenbosch University, Department of Biochemistry: Stellenbosch, South Africa, 2019. https://scholar.sun.ac.za/handle/10019.1/105712
32. Ruotolo, B.; Benesch, J.; Sandercock, A.; Hyung, S.; Robinson, C. Ion mobility–mass spectrometry analysis of large protein complexes. *Nature Protocols* 2008, *3* (7), 1139-1152.
33. Michaelevski, I.; Kirshenbaum, N.; Sharon, M. T-Wave ion mobility-mass spectrometry: basic experimental procedures for protein complex analysis. *Journal of Visualized Experiments* 2010, No. 41.
34. Bush, M.; Campuzano, I.; Robinson, C. Ion mobility mass spectrometry of peptide ions: effects of drift gas and calibration strategies. *Analytical Chemistry* 2012, *84* (16), 7124-7130.
35. van Rensburg, W. The tyrocidines in the creation of antimicrobial cellulose and sterilising materials. PhD thesis, Stellenbosch University, Department of Biochemistry: Stellenbosch, South Africa, 2019. https://scholar.sun.ac.za/handle/10019.1/108461
36. Nandakumar, A.; Ito, Y.; Ueda, M. solvent effects on the self-assembly of an amphiphilic polypeptide incorporating α-helical hydrophobic blocks. *Journal of the American Chemical Society* 2020, *142* (50), 20994-21003.
37. Sikora, K.; Jaśkiewicz, M.; Neubauer, D.; Bauer, M.; Bartoszewska, S.; Barańska-Rybak, W.; Kamysz, W. Counter-ion effect on anti-staphylococcal activity and cytotoxicity of selected antimicrobial peptides. *Amino Acids* 2018, *50* (5), 609-619.
38. Sikora, K.; Jaśkiewicz, M.; Neubauer, D.; Migoń, D.; Kamysz, W. The role of counter-ions in peptides—An Overview. *Pharmaceuticals* 2020, *13* (12), 442.
39. Rautenbach, M.; Swart, P.; van der Merwe, M. The interaction of analogues of the antimicrobial lipopeptide, Iturin A2, with alkali metal ions. *Bioorganic & Medicinal Chemistry* 2000, *8* (11), 2539-2548.
40. Mark Winter, U. WebElements Periodic Table » Zinc » radii of atoms and ions. https://www.webelements.com/zinc/atom_sizes.html (accessed Sep 22, 2022).
41. Rautenbach, M.; Vlok, N.; Eyéghé-Bickong, H.; van der Merwe, M.; Stander, M. An Electrospray ionization mass spectrometry study on the “in vacuo” hetero-oligomers formed by the antimicrobial peptides, surfactin and gramicidin S. *Journal of the American Society for Mass Spectrometry* 2017, *28* (8), 1623-1637.

5.7 Supplementary Data

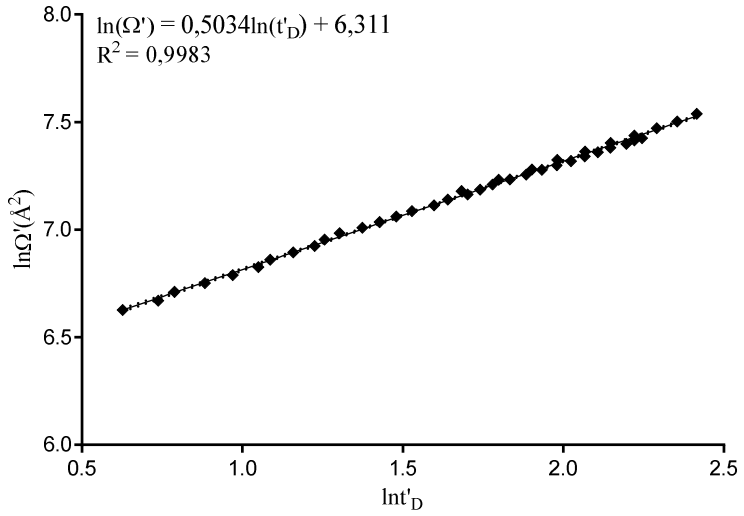

Figure S5.1 A standard linear curve of the corrected ln CCS Ω area against the corrected drift time (lnt'_D) values for Poly-Alanine, from which the gradient (exponential proportion factor) and fit-determined constant were elucidated. The linear equation along with the correlation coefficient (R^2) are displayed. The dotted lines seen represent the 95% confidence of the linear plot.

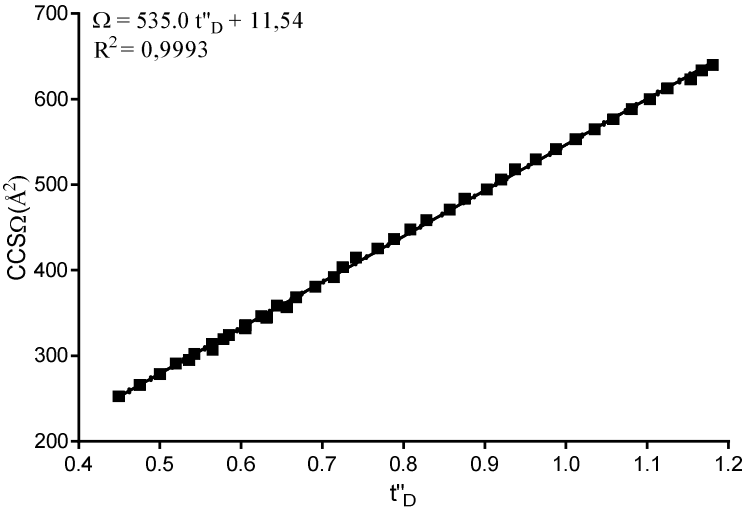

Figure S5.2 Constructed linear calibration plot using known Poly-Alanine CCS Ω values from literature plotted against the doubly corrected drift time (t''_D) of Poly-Alanine molecular ions obtained from TWIM-MS analysis. The determined linear equation and the correlation coefficient (R^2) are shown in the top left of the plot along with the dotted lines indicating the 95% confidence interval.

Table S5.1 Summary of determined average CCS Ω (Å^2) values for Trc ionic species in 10% ACN from their respective drift times and the control Poly-Alanine calibration linear curve (Figure S5.2).

Trc analogue	Amino acid sequence [a]	CCS Ω (Å^2)		
		$[M+H]^+$	$[M+2H]^{2+}$	$[2M+2H]^{2+}$
TrcA	Cyclo-(fP**Ff**NQ**Y**VOL)	356	390	549
TrcB/B'	Cyclo-(fP**Wf**NQ**Y**VOL)	363	389	557
TrcC	Cyclo-(fP**Ww**NQ**Y**VOL)	367	393	565
TpcC	Cyclo-(fP**Ww**NQ**Y**VKL)	372	394	569
$TrcA_1$	Cyclo-(fP**Ff**NQ**Y**VKL)	356	388	548
$TrcB_1/B_1'$	Cyclo-(fP**Wf**NQ**Y**VKL)	363	394	561
$TrcC_1$	Cyclo-(fP**Ww**NQ**W**VOL)	369	400	577
$TpcC_1$	Cyclo-(fP**Ww**NQ**W**VKL)	381	394	552

Table S5.2 Summary of determined average CCS Ω (Å^2) values for Trc ionic species TrcA, Trc/B'B and TrcC in 10% of the respective solvent (ACN, TBA, EtOH, MeOH, IPA and PG) from their respective drift times and the control Poly-Alanine calibration linear curve (Figure S5.2).

Solvent	Trc Mix Average CCS Ω (Å^2)		
	$[M+H]^+$	$[M+2H]^{2+}$	$[2M+2H]^{2+}$
ACN	363	392	559
TBA	362	392	561
EtOH	362	392	558
MeOH	363	392	558
IPA	362	392	558
PG	363	392	558

Table S5.3 Summary of the statistical analysis comparing the total ion signal for the respective tested additives (1% Glr, 5 µM $ZnCl_2$, 1% Glr + 5 µM $ZnCl_2$, 100 µM $ZnCl_2$, 100 µM $CaCl_2$ and 1% Glr + 100 µM $CaCl_2$) compared against each other within the specific solvent system (ACN, TBA, EtOH, PG, MeOH and IPA) at a fixed Trc Mix concentration of 100 µM (Figure 5.3). Statistical analysis as performed using Ordinary One-Way ANOVA (Bonferroni's multiple comparison test). *P < 0.05, **P < 0.01, ***P < 0.001, ****P < 0.0001.[a] correlates to solvent compared,[b] ns – not significant and nd – not determined.

A **ACN Trc Mix**	Additive				
	5 µM $ZnCl_2$	1% Glr + 5 µM $ZnCl_2$	100 µM $ZnCl_2$	100 µM $CaCl_2$	1% Glr + 100 µM $CaCl_2$
1% Glr	**	ns	ns	ns	ns
5 µM $ZnCl_2$		****	ns	ns	***
1% Glr + 5 µM $ZnCl_2$			***	**	ns
100 µM $ZnCl_2$				ns	*
100 µM $CaCl_2$					ns

B **TBA Trc Mix**	Additive				
	5 µM $ZnCl_2$	1% Glr + 5 µM $ZnCl_2$	100 µM $ZnCl_2$	100 µM $CaCl_2$	1% Glr + 100 µM $CaCl_2$
1% Glr	ND	ns	ns	*	ns
5 µM $ZnCl_2$		ND	ND	ND	ND
1% Glr + 5 µM $ZnCl_2$			ns	*	ns
100 µM $ZnCl_2$				ns	*
100 µM $CaCl_2$					***

C **EtOH Trc Mix**	Additive				
	5 µM $ZnCl_2$	1% Glr + 5 µM $ZnCl_2$	100 µM $ZnCl_2$	100 µM $CaCl_2$	1% Glr + 100 µM $CaCl_2$
1% Glr	**	ns	ns	ns	ns
5 µM $ZnCl_2$		****	ns	*	***
1% Glr + 5 µM $ZnCl_2$			ns	ns	ns
100 µM $ZnCl_2$				ns	ns
100 µM $CaCl_2$					ns

D **PG Trc Mix**	Additive				
	5 µM $ZnCl_2$	1% Glr + 5 µM $ZnCl_2$	100 µM $ZnCl_2$	100 µM $CaCl_2$	1% Glr + 100 µM $CaCl_2$
1% Glr	ns	ns	ns	ns	ns
5 µM $ZnCl_2$		ns	ns	ns	ns
1% Glr + 5 µM $ZnCl_2$			ns	ns	ns
100 µM $ZnCl_2$				ns	ns
100 µM $CaCl_2$					ns

E	MeOH Trc Mix	Additive				
		5 µM $ZnCl_2$	1% Glr + 5 µM $ZnCl_2$	100 µM $ZnCl_2$	100 µM $CaCl_2$	1% Glr + 100 µM $CaCl_2$
1% Glr		**	ns	ns	ns	ns
5 µM $ZnCl_2$			***	ns	*	ns
1% Glr + 5 µM $ZnCl_2$				*	ns	ns
100 µM $ZnCl_2$					ns	ns
100 µM $CaCl_2$						ns

F	IPA Trc Mix	Additive				
		5 µM $ZnCl_2$	1% Glr + 5 µM $ZnCl_2$	100 µM $ZnCl_2$	100 µM $CaCl_2$	1% Glr + 100 µM $CaCl_2$
1% Glr		****	ns	ns	ns	ns
5 µM $ZnCl_2$			***	*	**	****
1% Glr + 5 µM $ZnCl_2$				ns	ns	ns
100 µM $ZnCl_2$					ns	ns
100 µM $CaCl_2$						ns

Table S5.4 Summary of the statistical analysis comparing the total ion signal for the respective tested solvent system alone (ACN, TBA, EtOH, PG, MeOH and IPA) against each tested peptide formulation (1% Glr, 5 µM $ZnCl_2$, 1% Glr + 5 µM $ZnCl_2$, 100 µM $ZnCl_2$, 100 µM $CaCl_2$ and 1% Glr + 100 µM $CaCl_2$) at a fixed Trc Mix concentration of 100 µM (Figure 5.3). Statistical analysis as performed using Ordinary One-Way ANOVA (Bonferroni's multiple comparison test). *P < 0.05, **P < 0.01, ***P < 0.001, ****P < 0.0001.[a] correlates to solvent compared,[b] ns – not significant and nd – not determined.

Solvent control	Solvent [a] versus specific additive					
	1% Glr	5 µM $ZnCl_2$	1% Glr + 5 µM $ZnCl_2$	100 µM $ZnCl_2$	100 µM $CaCl_2$	1% Glr + 100 µM $CaCl_2$
ACN [a]	**	ns	****	ns	ns	***
TBA [a]	***	nd	**	ns	ns	****
EtOH [a]	ns	ns	**	ns	ns	ns
PG [a]	ns	ns	ns	ns	ns	ns
MeOH [a,b]	**	ns	***	ns	*	ns
IPA [a,b]	***	ns	**	ns	**	****

Table S5.5 Summary of the statistical analysis performed for each percentage contribution of the positive Trc peptide ions alone in each solvent systems (A: ACN, B: TBA, C: EtOH, D: PG, E: IPA and F: MeOH) against each Trc formulation at a fixed peptide concentration of 100 µM found in Figure 5.4. Ordinary One-Way ANOVA statistical analysis was performed (Bonferroni's multiple comparison test). *P < 0.05, **P < 0.01, ***P < 0.001, ****P < 0.0001, ns – not significant and ND – not determined.

A: ACN	Formulations					
Ionic Species	1% Glr	5 µM $ZnCl_2$	1 % Glr + 5 µM $ZnCl_2$	100 µM $ZnCl_2$	100 µM $CaCl_2$	1% Glr + 100 µM $CaCl_2$
$[M+2H]^{2+}$	****	ns	****	****	****	ns
$[2M+2H]^{2+}$	****	ns	****	***	****	ns
$[M+H]^{+}$	ns	ns	ns	ns	***	ns
B: TBA	Formulations					
Ionic Species	1% Glr	5 µM $ZnCl_2$	1 % Glr + 5 µM $ZnCl_2$	100 µM $ZnCl_2$	100 µM $CaCl_2$	1% Glr + 100 µM $CaCl_2$
$[M+2H]^{2+}$	**	ND	***	****	****	ns
$[2M+2H]^{2+}$	*	ND	**	**	****	ns
$[M+H]^{+}$	ns	ND	ns	ns	**	ns
C: EtOH	Formulations					
Ionic Species	1% Glr	5 µM $ZnCl_2$	1 % Glr + 5 µM $ZnCl_2$	100 µM $ZnCl_2$	100 µM $CaCl_2$	1% Glr + 100 µM $CaCl_2$
$[M+2H]^{2+}$	ns	ns	*	****	****	**
$[2M+2H]^{2+}$	ns	ns	*	**	****	ns
$[M+H]^{+}$	ns	ns	ns	ns	**	ns
D: PG	Formulations					
Ionic Species	1% Glr	5 µM $ZnCl_2$	1 % Glr + 5 µM $ZnCl_2$	100 µM $ZnCl_2$	100 µM $CaCl_2$	1% Glr + 100 µM $CaCl_2$
$[M+2H]^{2+}$	ns	ns	ns	*	****	**
$[2M+2H]^{2+}$	ns	ns	ns	ns	ns	ns
$[M+H]^{+}$	ns	ns	ns	ns	ns	ns
E: IPA	Formulations					
Ionic Species	1% Glr	5 µM $ZnCl_2$	1 % Glr + 5 µM $ZnCl_2$	100 µM $ZnCl_2$	100 µM $CaCl_2$	1% Glr + 100 µM $CaCl_2$
$[M+2H]^{2+}$	****	ns	***	****	****	*
$[2M+2H]^{2+}$	****	ns	***	****	****	ns
$[M+H]^{+}$	ns	ns	ns	**	****	ns
F: MeOH	Formulations					
Ionic Species	1% Glr	5 µM $ZnCl_2$	1 % Glr + 5 µM $ZnCl_2$	100 µM $ZnCl_2$	100 µM $CaCl_2$	1% Glr + 100 µM $CaCl_2$
$[M+2H]^{2+}$	**	ns	**	****	****	**
$[2M+2H]^{2+}$	*	ns	*	*	**	ns
$[M+H]^{+}$	ns	ns	ns	ns	ns	ns

Chapter 6

Summative conclusions and future studies

6.1 Introduction

The main aim of this study was to develop and assess various solvents and additives in formulation with the tyrocidines (Trcs), in developing an optimal antimicrobial solid surface Trc formulation(s). To achieve this aim, Trcs were purified from a commercial Trc mix and compared against a Trcs producer profile from *Brevibacillus parabrevis* ATCC 10068. Thereafter, the antimicrobial activity of the Trc mix formulations, using six solvents and six different additive combinations, were evaluated against the Gram-positive pathogens, *Listeria monocytogenes* and *Staphylococcus aureus,* to find the optimal formulation(s) that can be used on surfaces. Subsequently, the influence of the various formulations on the biophysical properties of the Trcs was investigated to elucidate if there are structural (conformational) changes of the peptides in the Trc mix and if this can be linked to the anti-bacterial activity.

6.2 Conclusion of experimental results

6.2.1 Bacterial production, isolation, and characterisation of cyclodecapetides from tyrothricin

The aim of Chapter 2 was to identify the variability between the various peptide analogues produced by three different *Brevibacillus parabrevis* producer strains using HR-ESMS, after which the purified commercial Trc analogue profile would be compared to the selected producer strains. Three producer strains: ATCC 10068, DSMZ 5618 and ATCC 8185 were analysed and the variability in TrcA, TrcB TrcC and VGA production were compared. ATCC 10068 resulted in fluctuations between TrcA and TrcB but was limited to low amounts of TrcC, correlating to findings by Vosloo *et. al* [1,2]. Interestingly, extracts containing low to a limited amount of TrcC resulted in low amounts of VGA, therefore, suggesting that for ATCC 10068 there is a decreased availability of Trp for the tyrocidine synthetase complex for these two Trp-rich peptides. DSMZ 5618 resulted in equal amounts of the TrcA and TrcC analogues with the dominant analogue being TrcB, correlating to findings by Bas Vogt. *et al.* [3]. Furthermore, as with ATCC 10068, a correlation between amounts of TrcC production and VGA production was observed in DSMZ 5618. This suggests that although DSMZ 5618 is an analogous strain of ATCC 10068, the producer has eliminated the competition between the tyrocidine synthetase and the gramicidin synthetase complex by having an alternative Trp source other than the media Trp. Lastly, ATCC 8185 resulted in TrcA being produced at higher amounts followed by TrcB when compared to ATCC 10068, however, the amount of TrcC and VGA is

considerably lower than those in ATCC 10068 and DSMZ 5618. As suggested with ATCC 10068, the producer favours the uptake of Phe but due to the limited uptake of Trp, competition between the more favoured tyrocidine synthetase and gramicidin synthetase occurs leading to lower amounts of VGA. Therefore, the specific Trcs and Grms synthetases are both influenced by the availability of specific aromatic amino acid, Phe or Trp, with variation in analogue production being influenced by the incorporation at position three and four of the dipeptide unit for the Trcs. Cellular demand of a specific amino acid may result in *de novo* synthesis via the shikimate pathway, in which the synthesis of Phe from Trp or Trp from Phe can occur [20]. If Trp is limited within the media, the producer may initiate *de novo* synthesis via the shikimate pathway increasing Trp availability leading to a higher amount of TrcC and linear Grms production [2,4]. However, if Trp is not limited but the demand for Phe is increased, the producer can utilise the same *de novo* synthesis for Phe production, limiting the Trp required by the gramicidin synthetase pathway leading to decreased amount of TrcC and linear Grms but an increased amount of TrcA and TrcB.

Development of Trc formulations for bioactivity and biophysical analysis requires a pure extract (<95%) of the commercial Trc mix. The pure commercial peptide resulted in a purity of 98.6% with UPLC-MS analysis of the pure tyrocidine extract revealing all six major analogues with the percentage abundance order being TrcB ≥ TrcA ≥ TrcC > $TrcB_1$ > $TrcA_1$ > $TrcC_1$ correlating with previously obtained results [5]. The in-house production using ATCC 10068 yielded a production profile correlating to previous findings with TrcA > TrcB> TrcC > $TrcB_1$ > $TrcA_1$ > $TrcC_1$ [1,2].

6.2.2 Biological activity of tyrocidines and formulations

The aim of Chapter 3 was to assess the influence of six solvents in combination with varying ratios of different formulants on the antimicrobial activity of the Trc mix towards *L. monocytogenes* and *S. aureus* utilising a modified high throughput method [6]. Additionally, as the Trcs have been shown to readily form dimers and higher order structures [7,8], assessing how different solvents and varying additives affect this, is required for optimal formulation development, specifically for surface treatments.

6.2.2.1 Bioactivity towards L. monocytogenes and S. aureus

The tested antimicrobial activity against *L. monocytogenes* and *S. aureus* of the Trc mix 1:20 ratio formulations (solvent, 1% Glr, 5 µM $ZnCl_2$ and 1% Glr + 5 µM $ZnCl_2$) within each solvent group revealed that the formulation conditions containing 1% Glr resulted in significantly higher IC_{50} values when compared to formulations without 1% Glr. This observed increase in the presence of 1% Glr may be due to the polar nature of Glr, and the ability of it to interact with the polar region of the peptide. This may result in steric hindrance or the reduction of the hydrophobic effect required by the

peptide for higher order structure formation. Additionally, in the case of *L. monocytogenes,* the 1% Glr formulations had the most influence on the overall activity of each of the tested solvents resulting in the largest scatter and significant influence on the peptides' activity. The large variability caused by 1% Glr may not only be attributed to disrupting the optimal peptide conformation but also may be due to the uptake and metabolism of Glr by *L. monocytogenes* when under stress [21].

Assessing the bioactivity of the 1:1 peptide formulation (solvent, 100 µM $ZnCl_2$, 100 µM $CaCl_2$ and 1% Glr + 100 µM $CaCl_2$) against *L. monocytogenes* and *S. aureus* revealed that higher $ZnCl_2$ salt concentrations had no significant increase in the antimicrobial activity for ACN, IPA, MeOH and TBA in both targets. However, for EtOH as the solvent, $ZnCl_2$ resulted in a significant increase in IC_{50} against *S. aureus,* but not towards *L. monocytogenes*. This suggests that Zn^{2+} modulates the antimicrobial activity in that it may have a role in peptide structure and oligomerisation that is solvent dependent. Bioactivity comparison of 100 µM $CaCl_2$ in the Trc formulations resulted in EtOH, IPA, TBA and PG formulations exhibiting a significant increase in IC_{50} towards *S. aureus* but maintenance of activity against *L. monocytogenes.* This increased IC_{50} suggests that Ca^{2+} may be competing with the Trcs for the binding site on the negatively charged phospholipid headgroups of *S. aureus* preventing full peptide anchoring. Conversely, Ca^{2+} does not influence the activity against *L. monocytogenes* implying possibly a different target or mode of action.

Interestingly, TBA peptide formulations of 1% Glr + 100 µM $CaCl_2$ showed a significant decrease in IC_{50} towards both *L. monocytogenes* and *S. aureus* when compared against the other solvent groups. Furthermore, the addition of 1% Glr in formulations did not result in a similar decrease in activity as observed for the *L. monocytogenes* 1:20 ratio formulations, indicating the importance of $CaCl_2$ in the formulation. It can be proposed that against *L. monocytogenes,* in the presence of Ca^{2+}, the Trcs can negate the negative effect of Glr by changing the mode of action which can be further improved by using TBA. Thereby, correlating to previous studies by Spathelf [9] and Luessa [10] where they revealed a non-lytic mode of action when the Trcs were formulated with $CaCl_2$ when tested against *L. monocytogenes*. Conversely, when working against an alternative target cell such as *S. aureus*, the improved activity may be attributed to a complex association effect driven by Glr and calcium, in which Glr binds to the peptide, forcing the peptide into an active conformation that may be stabilised by the high calcium concentration.

Significantly improved IC_{50} values were observed for PG formulations containing 1% Glr whereas PG formulations not containing 1% Glr resulted in significantly higher IC_{50} values towards both *L. monocytogenes* and *S. aureus*. This may be attributed to the similarities in structure and nature between PG and Glr in which the solvent alone would promote more unstable peptide structures by possibly clumping the peptide and the oligomers together on the surface due to it being used as a

binding agent [11]. When the PG formulation is exposed to the bacterial target, PG may trap the oligomeric structures and active peptide moieties, preventing the effective release of amphipathic dimers [7]. Improved activity for PG containing 1% Glr formulations suggests that when PG and 1% Glr are in combination, they may either work in a synergistic manner in stabilising the peptide resulting in improved activity or may interact with each other preventing the negative effect elicited on the peptide. For both targets, PG caused a significant increase in activity for 1% Glr + 100 µM $CaCl_2$, however, without 1% Glr caused PG to significantly decrease in activity only for *S. aureus.* These findings correlate to the earlier results suggesting that PG has an antagonistic effect on the peptide which is negated in the presence of Glr.

In order to select for the best formulation, it should firstly be defined that an optimal formulation is able to illicit a high degree of activity (having a low IC_{50}) not only towards one target but towards both tested targets in this study. This is because of the wide range of applications that surface formulations will be used in. Therefore, to determine the most optimal formulation condition, all the solvents and formulation parameters were assessed by comparing the IC_{50} of both targets against each other as shown in Figure 6.1. It can be observed that for the solvents alone, only EtOH results in the best, most consistent activity towards both *L. monocytogenes* and *S. aureus* whereas the five other solvents result in low activity towards *L. monocytogenes* but high activity towards *S. aureus* and a higher degree of spread (Figure 6.1). This may be attributed to the polar nature of EtOH, as being the second most polar alcohol tested, in which the polarity in solution needs to be balanced to allow for the peptide to reach a more optimal active conformation. Additionally, the presence of the hydroxyl group and their orientation in EtOH results in improve the association and interaction for hydrogen bonding with either water or the peptide when in solution. Therefore, EtOH serves as the best solvent to be used with the Trcs especially in preliminary studies where no additives are being used. The addition of additives resulted in improved, less scatter and much more stable formulations as observed in the dotted black box in Figure 6.1. Furthermore, the addition of Glr seemed to have a much larger influence on the more polar solvents by increasing the activity of the formulation towards both targets (lowered IC_{50}) when compared to the solvents only. The formulations within the black dotted box (Figure 6.1) serve as a good starting point in formulation development, especially when assessing various additive influences. Finally, of all the formulations assessed, PG and TBA when in formulation with 1% Glr + 100 µM $CaCl_2$ serves as the best formulations towards both targets (red dotted box in Figure 6.1). Additionally, of the two solvents, TBA serves as the better formulation base as it has a slightly lower overall IC_{50} compared to PG. Therefore, based on the summary provided above and the results in Figure 6.1, TBA in combination with 1% Glr + 100 µM is the best overall formulation developed in this study against both *L. monocytogenes* and *S. aureus*.

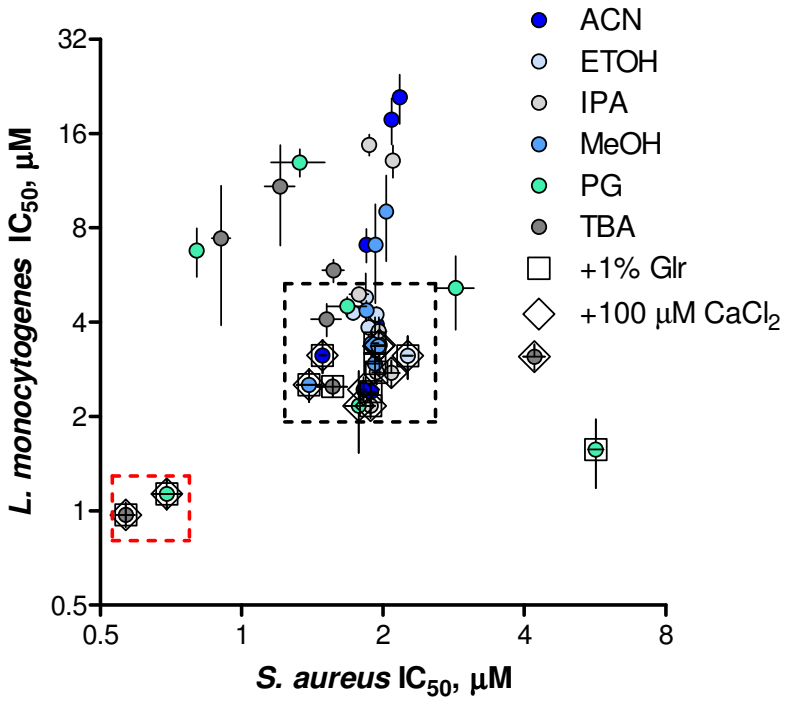

Figure 6.1 Comparative IC_{50} scatter plot assessing the different solvent-peptide formulations values obtained for both *L. monocytogenes* and *S. aureus* against each other in determining the best formulation. Error bars represent the SD (n =3-7) with each data point representing a collection of 3 – 7 technical repeats per condition assessed. The black dotted box represents the clustering of peptide formulations which indicate formulations that are good for development whereas the red dotted box represents the best identified formulations of those developed.

6.2.3 Biophysical, chemical and activity relationships of Trc formulations

6.2.3.1 Relationships between Trc mix activity and formulant chemistry

The presence or absence of Glr has a major influence towards the overall antimicrobial ability of the Trc formulations. Therefore, to develop a functional and usable antimicrobial formulation, the solvent and Glr influence was assessed by calculating the relative dielectric constant (ε) and relative molar mass (M_r) for all formulations and comparing it to the antimicrobial IC_{50} values (Figure 6.2).

Focusing on the influence of the ε and relative M_r for formulations which contain 1% Glr, excluding 1% Glr + 100 µM $CaCl_2$, resulted in an increase in IC_{50} against *L. monocytogenes* until a breakpoint at ε = 68 and the relative formulation M_r = 32-33, whereas there was no increase in IC_{50} when assessed against *S. aureus* over the same ε and relative M_r range. This difference may be due to *L. monocytogenes* cells utilising Glr as a carbon source when under stress [46] whereas *S. aureus* does not. Additionally, Glr may compete with the peptide for binding to *L. monocytogenes* or may hinder the peptide optimal conformation by competing with the peptide, thereby, preventing binding to the target cell. Inversely, for *S. aureus*, Glr may not influence or compete with the peptide for the

bacterial target or cause the peptide to go into a non-active conformation. The 1% Glr + 100 µM $CaCl_2$ formulations resulted in improved activity with lower IC_{50} values against both microbial targets, suggesting that the presence of calcium may stabilise the Trcs and overall promote an alternative mode of action, correlating to previously seen results [55]. A clear breakpoint of $\varepsilon = 65$ and relative M_r = 32-33 towards both targets is observed (Figure 6.2). This suggests that the formulations can be improved or become more unstable resulting in either improvement or loss of activity. They can act as either crowding agents by influencing the ability of monomeric peptide units to form active dimers influencing activity or by preventing/stabilising the formation of larger oligomeric structures.

As the Trcs form various dimeric units via hydrogen bonds or the hydrophobic effect [7,8] it would result in these peptide units having a hydrophobic core and a polar outer surface. Therefore, the defined M_r range of 33-40 suggests the following:

- If the solvents and additives are within the defined relative M_r range, they are small enough to disrupt the hydrophobic core, destabilising larger oligomers, but not small enough to compete for hydrogen bonds required by the active moiety.
- If the formulation relative M_r is less than 33, there would be hydrogen bond competition whereas a relative M_r greater than 44 would result in no core disruption but in larger oligomer formation.

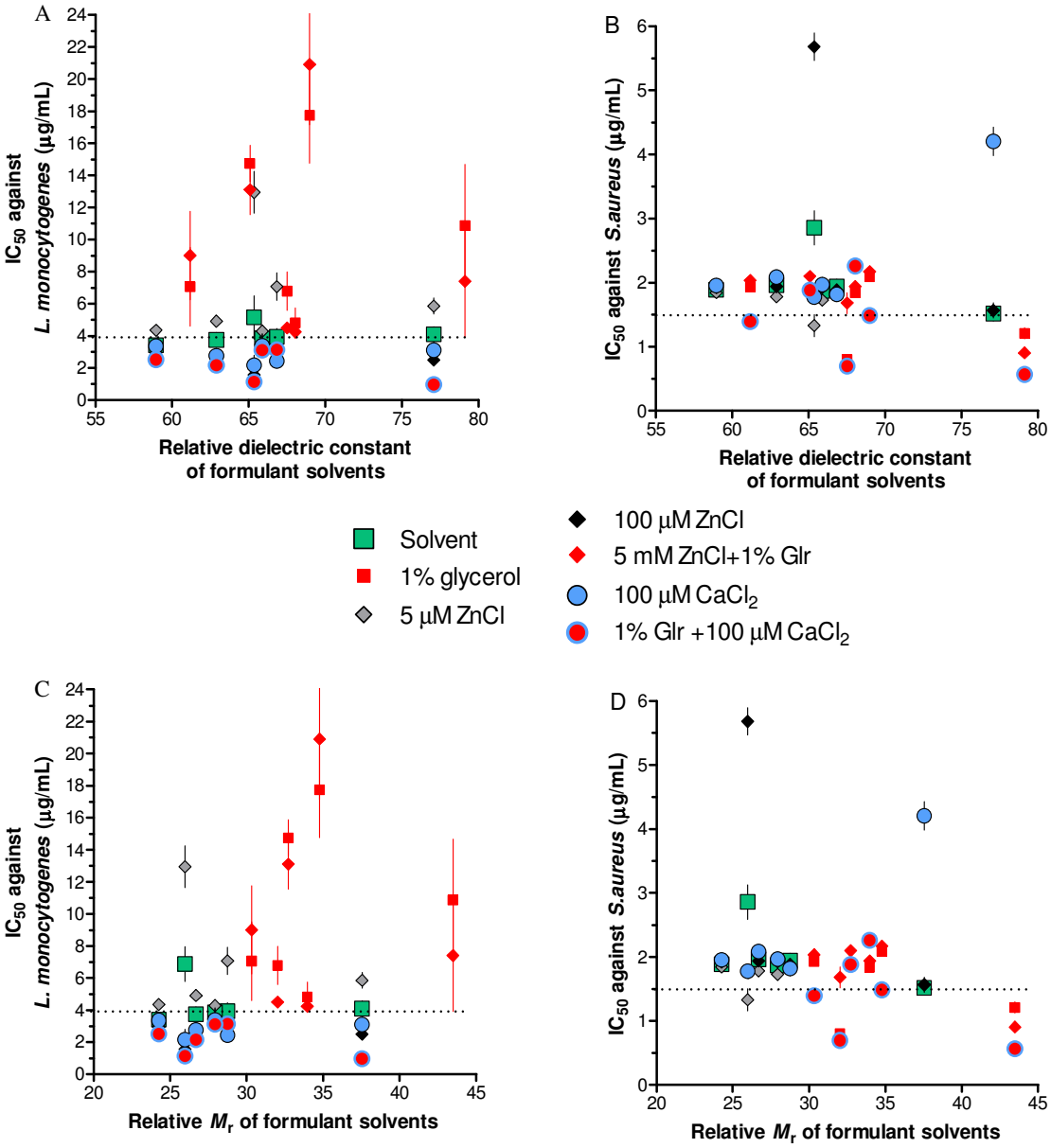

Figure 6.2 Comparative scatter plot of the influence of 1% Glr towards all the different Trc mix formulation solvents (ACN, EtOH, MeOH, IPA, TBA and PG) and conditions (1% Glr, 5 µM $ZnCl_2$, 1% Glr + 5 µM $ZnCl_2$, 100 µM $ZnCl_2$, 100 µM $CaCl_2$ and 1% Glr + 100 µM $CaCl_2$) on Trc mix antimicrobial IC_{50} values towards *L. monocytogenes* (A and C) and *S. aureus* (B and D), versus the dielectric constant and relative molecular weight of the formulations, respectively. Error bars represent the SD (n = 4-6). Refer to Table 3.1 for dielectric and relative M_r values used in calculations. Dotted line indicates arbitrary cut-off value from IC_{50} (horizontal) and relative M_r (vertical) by inspection of all solvent formulations.

6.2.3.1 Formulation influence on Trcs fluorescence and activity

The aim for Chapter 4 in this study was to evaluate and compare differences in the fluorescence properties of Trc mix alone in various solvent systems (ACN, EtOH, IPA, MeOH, TBA and PG) and in formulation with various additives (1% Glr, 5 µM $ZnCl_2$, 1% Glr + 5 µM $ZnCl_2$, 100 µM $ZnCl_2$, 100 µM $CaCl_2$ and 1% Glr + 100 µM $CaCl_2$.

Fluorescence results following the Trp residue(s) revealed the sensitivity of the Trcs to their local environment and how changes to peptide conformation/oligomerisation dictate the location of the Trp residue(s). Furthermore, polarity and the addition of additives resulted in clear observable changes to the fluorescence profile, confirming that the Trcs can have their conformation manipulated to find the most optimal operational concentration and conditions limiting aggregation but the formation of active peptide moieties, ideally amphipathic peptide dimer [12,13].

Assessment of the solvent-only influence at 50 µg/mL on the Trcs fluorescence revealed MeOH to result in the highest quenching, followed by ACN, EtOH and PG having similar responses then IPA and last TBA resulting in the highest fluorescence. Four of the six solvents induced a similar fluorescence over the peptide concentration range of 3.125 µg/mL and 6.25 µg/mL whereas ACN and EtOH lead to a similar fluorescence over the whole peptide concentration range tested. However, marked differences for each solvent group were observed at 12.5 µg/mL and above correlating to previously obtained critical micellular concentrations (CMC) [17]. This suggested that the observed quenching may be attributed to the peptide conformation which drives the environment of the Trp residue into either aromatic stacking or Trp-aromatic stacking induced FRET in a hydrophobic pocket. It has been shown that increased polarity will lead to an increase in expected quenching [14], which correlates to the observed results above. These results suggest that the more polar solvents would support oligomerization while less polar solvents may be effective in lowering the hydrophobic effect leading to larger oligomers/aggregates at higher concentrations.

Investigation into the influence of various additives in formulation with the Trcs revealed Trp dequenching induced by 5 µM $ZnCl_2$, 1% Glr, 100 µM $CaCl_2$ and 1% Glr + 5 µM $ZnCl_2$, whereas 100 µM $ZnCl_2$ and 1% Glr + 100 µM $CaCl_2$ resulted in quenching of the Trp residue. The observed Trp quenching by 100 µM $CaCl_2$ in 1% Glr may be attributed to the interaction between either Glr with the peptide and/or water due to increasing the availability of the hydroxyl groups. Although some quenching was observed in 100 µM $ZnCl_2$, it was not significant, suggesting that there could be an ideal additive concentration that has a stabilising effect on the peptide. The dequenching experienced by the Trcs in combination with 5 µM $ZnCl_2$ and 100 µM $CaCl_2$ can point towards the effect the electron deficient groups have towards the energy state within the Trp residue when it

undergoes excitation. TBA and EtOH formulations comprised of 100 µM $ZnCl_2$ and 100 µM $CaCl_2$ showed no quenching and slight dequenching respectively whereas all the formulations containing 1% Glr resulted in significant quenching. This quenching correlates to reasons described earlier in which 1% Glr introduces more OH groups leading to the competition of hydrogen bonding between the solvent and Glr, removing the hydrogen bonds between the peptide and solvent. This potentially may lead to more peptide oligomer interactions leading to large oligomer formation which in turn would lead to Trp aromatic stacking. Furthermore, two alternative factors may be at play namely: collisional quenching and static quenching. Collisional quenching may lead to interactions between the Trp fluorophore and the additive/quencher ionic molecule whereas static quenching may be due to complex formation thereby changing the ground and excited state energy levels [14]. The influence of PG formulations resulted in all conditions causing quenching of the Trp residue of the Trcs. This may be attributed to similarities between PG and 1% Glr with a higher concentration of OH group able to participate in hydrogen bonding with the solvent or peptide thereby increasing the amount of free water in the solution. This suggests that the increasing amount of hydrogen bonding may not limit oligomerisation of the peptide but rather result in an increased amount of free water that will drive the hydrophobic effect on the peptide, pushing Trp-aromatic stacking induced FRET in a hydrophobic pocket.

When the overall antibacterial activity was correlated with fluorescence yields no obvious trend could be deduced if all formulations are compared (Figure 6.3 A). However, when investigating and comparing the solvent specific conditions (Figure 6.3 B – D) a clear trend was identified. Fluorescence studies performed in this research followed the Trp residue and thus any biophysical changes observed could be linked to Trp as it was assumed to directly influence the activity. However, upon further evaluation, it can be observed that the role of Trp seems to not be directly responsible for peptide activity, but rather that Trp has more of a fundamental structural importance as seen in Figure 6.2 B-D. As the solvent system is changed, an increase in RFU is observed, however, there is no difference in the IC_{50} value as it remains constant from approximately 4400 ± 5000 RFU, followed by a sharp decrease or increase in IC_{50} once the RFU exceeds ± 5000. If Trp was more involved in activity, there would not be such a substantial change in the IC_{50} values when different solvents are introduced, however, as there is a clear fluctuation (Figure 6.1) in activity, even when additives are introduced, it can be suggested that Trp is more involved in structural stability. Furthermore, alternative amino acid residues such as Orn^9 or Lys^9 may be more important in activity and the observed changes in IC_{50} may be due to formulations forcing the cationic amid acid into a non-optimal orientation or conformation leading to decreased antimicrobial activity.

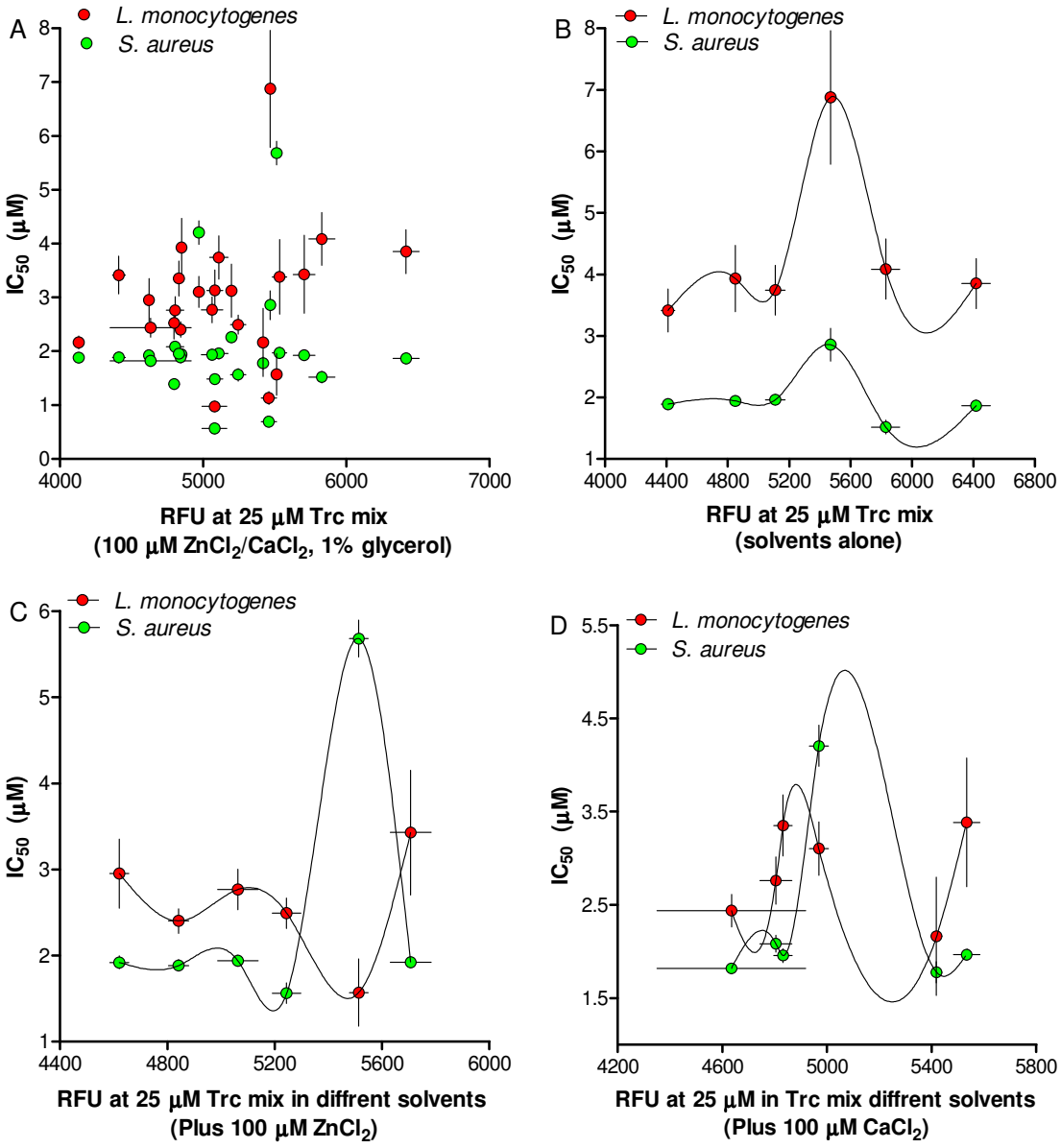

Figure 6.3 Comparative scatter plot of the influence of the different solvents systems (ACN, EtOH, MeOH, IPA, TBA and PG) alone and in formulation with additive conditions (1% Glr, 100 µM $ZnCl_2$, 100 µM $CaCl_2$ and 1% Glr + 100 µM $CaCl_2$) on Trc mix antimicrobial IC_{50} values towards *L. monocytogenes* (red) and *S. aureus* (green), versus the RFU of the respective formulation condition. Error bars represent the SEM of both the IC_{50} and conditions RFU with each data point representing the collection of 4 - 9 technical repeats.

Lastly, the distinct difference between $ZnCl_2$ and $CaCl_2$ may be linked to their ability to act as chaotropic agents. $CaCl_2$ may be more likely to incorporate itself into the peptide (further discussed later in this chapter in Figure 6.5) leading to a higher degree of structural disruption over $ZnCl_2$ resulting in the observed fluctuations of RFU for Trp. However, this will need to be further investigated to understand the interactions on a chemical/bonding level between the peptide and these

additives in solution and on surfaces. Therefore, it can be concluded that Trp has a much larger importance in peptide structural stability and conformation than activity, and that the peptides' activity and selectivity is dependent on other amino acid residues.

6.2.3.2 Oligomerisation of the tyrocidines in formulation

The objective of chapter 5 in this study was to evaluate and compare differences in the oligomerisation of Trc mix alone in various solvent systems (ACN, EtOH, IPA, MeOH, TBA and PG) and formulation with various additives (1% Glr, 5 µM $ZnCl_2$, 1% Glr + 5 µM $ZnCl_2$, 100 µM $ZnCl_2$, 100 µM $CaCl_2$ and 1% Glr + 100 µM $CaCl_2$). This was investigated utilising travelling-wave ion mobility (TWIM-MS).

It has been shown that the Trcs readily form extended oligomeric structures via non-covalent polar and hydrophobic interactions [12,13]. Furthermore, unwanted oligomerization of the Trcs may lead to masking of the important groups required for interaction with cellular targets, leading to steric hindrance, which ultimately decreases the peptides' antimicrobial activity. Furthermore, previous studies on the Trcs cyclodecapeptides have shown that the variable amino acids of the dipeptide unit play a large role in peptide oligomer formation.

The nature of the Trcs in having a strong degree of aggregation has been shown to be influenced by various aqueous environments, with the association being larger in water and less in low dielectric constant solvents[13,15]. Furthermore, overall peptide secondary structure and self-assembly can be further influenced by hydrophobic interactions within the aqueous environment and the amino acids of the dipeptide units at positions three and four [7,8]. CCS studies using TWIM-MS revealed a clear trend in conformational changes for TrcA, TrcB and TrcC with TrcA being more compact, TrcC being more relaxed whereas TrcB portrayed the average conformation behaviour across all tested solvents. TBA, EtOH and MeOH were dominant in driving a more compact TrcA peptide conformation whereas TrcC resulted in a more relaxed conformation for four of the solvents except for ACN and TBA. Conformational compactness for the different peptide analogues may be attributed to the amino acids at position three and four (TrcA: L-Phe^3-D-Phe^4; TrcB/B': L-Trp^3-D-Phe^4 and TrcC: L-Trp^3-D-Trp^4), with their role being more crucial in driving the peptide conformation in dimers compared to monomers [2,9].

Investigation into the monomeric and dimeric oligomer species revealed that for all formulations containing 1% Glr, there was an increase in the amount of doubly charged dimers with a loss in singly charged dimers, as determined via TWIM-MS. This suggests that Glr stabilizes hydrogen bonding and electrostatic and ionic interactions thereby decreasing the release of monomeric species. All 100 µM salt formulations showed a significant increase in doubly charged monomers suggesting that

at a high salt concentration, the salt may act as a chaotropic agent or induce a peptide conformational change leading to the disruption of larger oligomer formation. Furthermore, formulations with 100 µM salts for ACN, TBA, EtOH and IPA resulted in a significant decrease in singly charged monomers leading to an increase in doubly charged monomers, correlating to previously observed results. Furthermore, formulations with 1% Glr and 100 µM $CaCl_2$, except for PG, had an increase in doubly charged dimers and singly charged monomers but a decrease in doubly charged monomers. This further illustrates the nature of Glr to promote dimer formation via modulation of the hydrogen bonds and electrostatic interactions in formulation.

When the IMMS signal of the monomers and oligomers in Trc mix formulation was correlated with activity no discernible trend could be deduced (Figure 6.4: A, B). However, when the dimer signal alone was correlated some trends were found specifically when comparing solvent alone, 1% Glr (squares), 100 µM $CaCl_2$ (diamond) and 1% Glr + 100 µM $CaCl_2$ (square + diamonds) (Figure 6.4 C, D). Without any additives added, there is a low total ion signal of dimers present and most of the data points are clustered together (Figure 6.4: C, D). This suggests that in the solvent system alone, the peptide is potentially more prone to forming monomers and/or larger oligomeric structures but when exposed to the target cells, the larger oligomers may result in the release of the dimers to then illicit activity. Interestingly, the addition of 1% Glr has vastly different effects when looking at both targets IC_{50} but a similar effect when looking at the total ion signal of dimers (Figure 6.4). It can be observed that against *L. monocytogenes* the addition of Glr resulted in a decrease in activity (increased IC_{50}) but shifted to a higher total ion signal of dimers. Furthermore, when looking at *S. aureus* it can be observed that 1% Glr did not change the activity profile of the peptide but also resulted in an increased total ion signal of dimeric species. This finding correlates with and confirms the ability of *L. monocytogenes* to utilise Glr as a carbon source when under stress but this is not the case for *S. aureus* [21]. Additionally, Glr may disrupt higher order oligomerisation by competing for hydrogen bonds used by the peptide to form larger oligomers, thereby acting as a chaotropic agent, correlating to the earlier observations in Chapter 3 and Chapter 5. When in formulation with 100 µM $CaCl_2$ alone, the total ion signal for both target conditions reverts to being low however there is no substantial change in the activity profile when compared to the solvent alone. However, when the targets are exposed to peptide formulations made up of 1% Glr + 100 µM $CaCl_2$ a clear difference in total ion signal and activity is observed against both targets. These findings correlate with those summarised in this chapter and Chapters 3 and 5, confirming that the formulation with 1% Glr + 100 µM $CaCl_2$ results in the best relationship between the presence of dimers and interaction between the additive and peptide leading to the most optimal bioactivity.

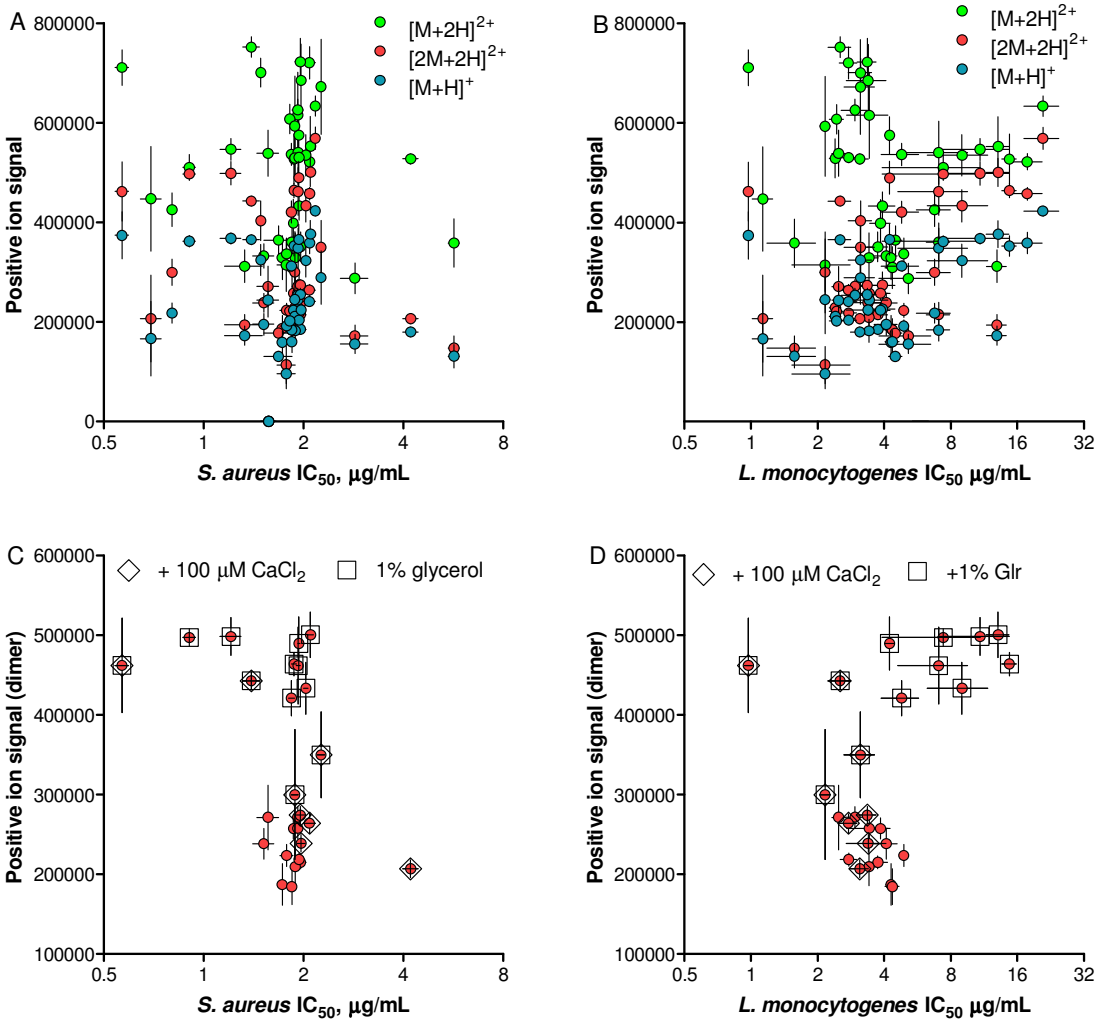

Figure 6.4 Comparative scatter plot of the influence of the different solvents systems (ACN, EtOH, MeOH, IPA, TBA and PG) alone using the total positive ion signal of singly charged monomers, doubly charged dimers and doubly charged monomers (A and B) and the doubly charged dimers in formulation with the specific additive conditions (1% Glr,100 µM $CaCl_2$ and 1% Glr + 100 µM $CaCl_2$) (C and D) on Trc mix against the antimicrobial IC_{50} values of *S. aureus* (A and C) and *L. monocytogenes* (B and D) . Error bars represent the SEM (n = 3) of both the IC_{50} and conditions RFU with each data point representing the collection of # technical repeats.

Considering the two most active formulations (Figure 6.1), both contained 100 µM $CaCl_2$.TWIM-MS results revealed a large, detected ion peak at 2.09 minutes (refer to Chapter 5, Figure 5.5 and Figure 5.6) for all 100 µM $CaCl_2$ peptide formulations, whereas formulations without 100 µM $CaCl_2$ revealed a small ion peak at the same time. These observations suggest the potential formation of a triply charged peptide-calcium complexes $[M+Ca+H]^{3+}$ as shown in Figure 6.5. Previous studies conducted by Loll *et al.* [18] and Munyuki *et al.* [19] showed that the Trcs form amphipathic β-sheets dimers where two β-turns are formed at the tight turns within the peptide serving as a potential anchoring site for the metal ion, as observed for Iturin A_2 [16]. However, as complex formation was

only observed for Ca^{2+} (ion radius 1.80 Å) and not Zn^{2+} (ion radius1.42 Å), it suggests that the atomic radius of the metal ion is important in being able to anchor at the β-turn site. Therefore, it is proposed that an optimal specific ion radius of >1.42 Å and ≤ 1.80 Å is required in order to form a highly stable complex, with Zn^{2+} being too small while Ca^{2+} is large enough to sit in the pocket to form stable electrostatic interactions (coordination bonds) with the carbonyl groups in the β-turn which can survive the harsh IM-MS conditions [7,8].

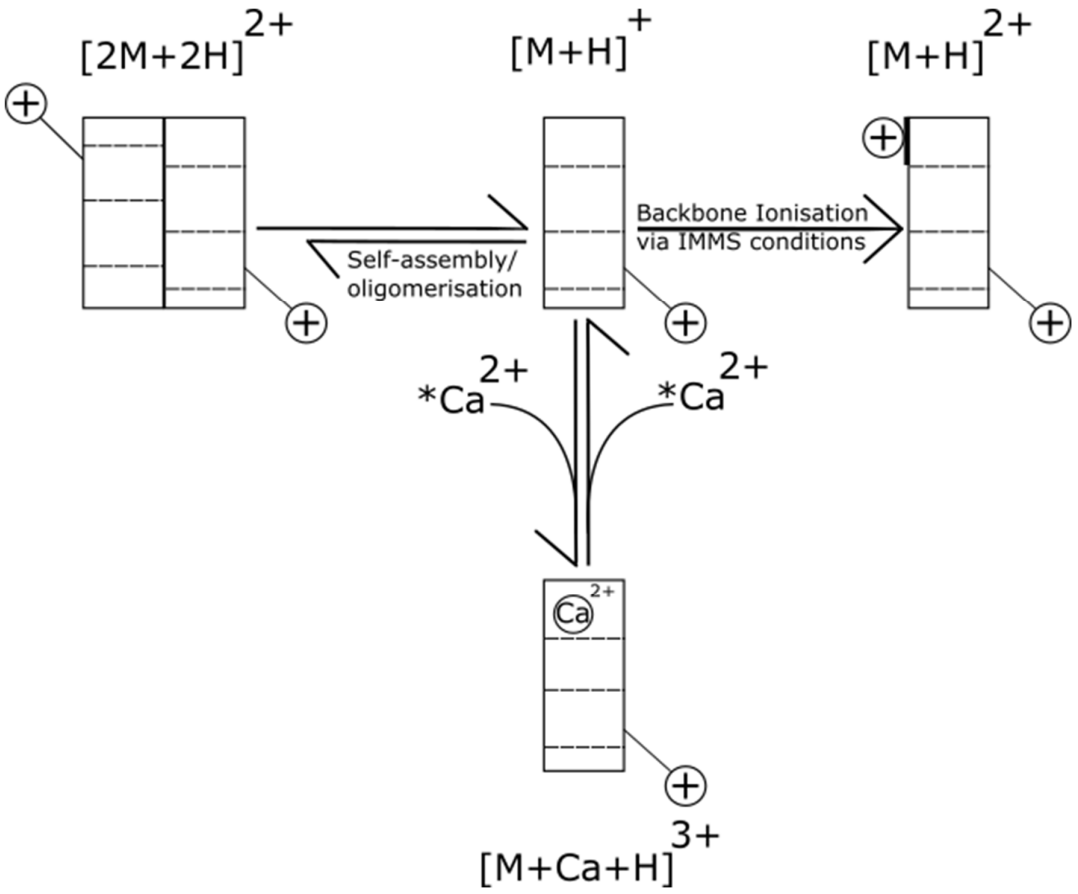

Figure 6.5 **S**chematic illustrating the dimeric $[2M+2H]^{2+}$ and monomeric $[M+H]^{+}$ species of the Trcs and the formation of the Trc-doubly charged monomer $[M+H]^{2+}$ and the triple charged Trc-metal complex $[M+Ca+H]^{3+}$. The schematic represents a working hypothesis as to the mechanisms for the Trc-metal complex structure formation. The dotted lines represent the intramolecular hydrogen bonds as described by Loll *et. al.* and the positive (+) signs represent the charge on the Trc. The * represents the metal ion which can be different depending on the metal-salt used in the formulation.

6.3 Future studies

This study provides insight into the influence various solvents and additives in formulations have on the antimicrobial activity of Trcs on treated solid surfaces. As this study only investigated the Trc mix, further investigation of the purified individual Trc analogues can be done with the solvents or additives used in this study. Furthermore, solvent percentage ranges (5% - 95%) can be tested to assess the impact varying solvent percentages have on the Trcs as well as testing different solvent

composition mixtures and ratios. Additionally, further biophysical analysis can be performed to investigate and focus on how different solvents and additives affect the Trcs structural changes and attempt to specifically identify what is responsible for driving the biophysical changes and linking that to observations in bioactivity. As this study only focused on using TWIM-MS and FS to elucidate the biophysical changes, other techniques that can be used but are not limited to are circular dichroism (CD) to investigate changes to the secondary structures, nuclear magnetic resonance (NMR) spectroscopy to study the interaction between the various solvents and/or additives and the Trcs, and attenuated total reflectance (ATR) Fourier transform infrared spectroscopy (FTIR) to study the peptide conformation on the solid surfaces. Although computational modelling was not included in this study and most computational models on the Trcs have looked at TrcA, TrcB, TpcC within only one to two solvent systems, future studies can investigate and build Trcs models using the solvent systems in this study. This will further assist in developing these formulations and understanding what makes a formulation the most optimal and why it is better from a bioactivity perspective.

Previously conducted research by the BIOPEP group and research members utilised SEM to obtain imagery of the Trcs and specific analogues (TpcC) on a surface. This provided initial insight into surface distribution and allowed for a deeper understanding of how the Trcs form structures on a surface. Presently, there is limited understanding of conformational landscape changes and structural transition of the Trcs on surfaces and computational models to explain this. Therefore, future studies for this specific avenue can utilise molecular dynamic simulations coupled with cryo-electron microscopy (cryo-EM) that can investigate fluid and short-lived changes in surface conformational states of the peptide which can be modelled to develop a deeper mechanical understanding of the peptide-surface relationship. Additionally, an electron probe micro-analyser (EPMA) can be used for sample imagery and chemical analysis along with its ability to use “spot” analysis for very small sample sizes resulting in the ability to detect small compositional variation in a sample’s texture context.

The antimicrobial activity performed in this study was only assessed towards two Gram-positive targets, *L, monocytogenes* and *S. aureus* because of their relevance to surface contamination. Future studies for peptide-treated surfaces can be expanded to assess activity towards Gram-negative bacteria such as *Escherichia coli*¸ as there are currently limited surface control methods for Gram-negative bacteria. Additionally, future studies can include assessing the formulations against various biofilm-forming pathogens, *L. monocytogenes and S. aureus* biofilm strains and *Candida albicans*, in the prevention of surface adhesion and biofilm formation. Furthermore, the solid surface assay used in this study is currently only optimised for bacterial targets, a preliminary study was performed, using the formulations in this study, in modifying this assay towards a fungal target *Botrytis cinerea,*

but requires further growth optimisation. Therefore, future studies can optimise the high throughput assay towards various fungal pathogens such as *Botrytis cinerea* and A*spergillus fumigatus*.

Lastly, as this study only investigated the treatment of a solid surface within the microtiter plate, future studies can investigate the ability of these formulations on various materials followed by bioactivity and biophysical studies. Previous studies on various carbohydrates and lipids in formulation with the Trcs showed promising activity, therefore future studies can add the best acting carbohydrates and lipids as additional additive(s) [17-19].

6.4 References

1. Vosloo, J.; Stander, M.; Leussa, A.; Spathelf, B.; Rautenbach, M. Manipulation of the tyrothricin production profile of *Bacillus aneurinolyticus*. *Microbiology* 2013, *159* (Pt_10), 2200-2211.
2. Vosloo, J.; Rautenbach, M. Following tyrothricin peptide production by *Brevibacillus parabrevis* with electrospray mass spectrometry. *Biochimie* 2020, *179*, 101-112.
3. Vogt, T.; Schinzel, S.; Bechinger, B. Biosynthesis of isotopically labeled gramicidins and tyrocidins by *Bacillus brevis*. *Journal of Biomolecular NMR* 2003, *26* (1), 1-11.
4. Sarges, R.; Witkop, B. Gramicidin A. IV. Primary sequence of valine and isoleucine gramicidin A. *Journal of the American Chemical Society* 1964, *86* (9), 1862-1863.
5. Troskie, A.; de Beer, A.; Vosloo, J.; Jacobs, K.; Rautenbach, M. Inhibition of agronomically relevant fungal phytopathogens by tyrocidines, cyclic antimicrobial peptides isolated from *Bacillus aneurinolyticus*. *Microbiology* 2014, *160* (9), 2089-2101.
6. van Rensburg, W.; Laubscher, W.; Rautenbach, M. High throughput method to determine the surface activity of antimicrobial polymeric materials. *MethodsX* 2021, *8*, 101593.
7. Loll, P.; Upton, E.; Nahoum, V.; Economou, N.; Cocklin, S. The high resolution structure of tyrocidine a reveals an amphipathic dimer. *Biochimica et Biophysica Acta (BBA) - Biomembranes* 2014, *1838* (5), 1199-1207.
8. Munyuki, G.; Jackson, G.; Venter, G.; Kövér, K.; Szilágyi, L.; Rautenbach, M.; Spathelf, B.; Bhattacharya, B.; van der Spoel, D. B-sheet structures and dimer models of the two major tyrocidines, antimicrobial peptides from *Bacillus aneurinolyticus*. *Biochemistry* 2013, *52* (44), 7798-7806.
9. Spathelf, B. Qualitative structure-activity relationship of the major tyrocidines, cyclic decapeptides from *Bacillus aneurinolyticus*. PhD thesis, Stellenbosch University, Department of Biochemistry: Stellenbosch, South Africa, 2010. http://scholar.sun.ac.za/handle/10019.1/4001
10. Leussa, N.-N.A. Characterisation of small cyclic peptides with anti listerial and antimalarial activity. PhD thesis, Stellenbosch University, Department of Biochemistry: Stellenbosch, South Africa.2014. http://scholar.sun.ac.za/handle/10019.1/86161.
11. van der Vossen, A.; van der Velde, I.; Smeets, O.; Postma, D.; Eckhardt, M.; Vermes, A.; Koch, B.; Vulto, A.; Hanff, L. Formulating a poorly water soluble drug into an oral solution suitable for paediatric patients; Lorazepam as a model drug. *European Journal of Pharmaceutical Sciences* 2017, *100*, 205-210.
12. Ruttenberg, M.; King, T.; Craig, L. The use of the tyrocidines for the study of conformation and aggregation behavior. *Journal of the American Chemical Society* 1965, *87* (18), 4196-4198.
13. Paradies, H. Aggregation Of tyrocidine in aqueous solutions. *Biochemical and Biophysical Research Communications* 1979, *88* (3), 810-817.
14. Lakowicz J. Principles of fluorescence spectroscopy. *Springer Science & Business Media*. 2013
15. Rautenbach, M.; Kumar, V.; Vosloo, J.; Masoudi, Y.; van Wyk, R.; Stander, M. Oligomerisation of tryptocidine C, a trp-rich cyclodecapeptide from the antimicrobial tyrothricin complex. *Biochimie* 2021, *181*, 123-133.
16. Rautenbach, M.; Swart, P.; van der Merwe, M. The interaction of analogues of the antimicrobial lipopeptide, Iturin A2 , with alkali metal ions. *Bioorganic & Medicinal Chemistry* 2000, *8* (11), 2539-2548.
17. Masoudi, Y.; van Rensburg, W.; Barnard-Jenkins, B.; Rautenbach, M. The influence of cellulose-type formulants on anti-candida activity of the tyrocidines. *Antibiotics* 2021, *10* (5), 597.
18. Van Wyk, R. Development of cyclodecapeptides from the tyrothricin complex as anticancer peptides. MSc thesis, Stellenbosch University, Department of Biochemistry: Stellenbosch, South Africa, 2019. https://scholar.sun.ac.za/handle/10019.1/105712
19. van Rensburg, W. The tyrocidines in the creation of antimicrobial cellulose and sterilising materials. PhD thesis, Stellenbosch University, Department of Biochemistry: Stellenbosch, South Africa, 2019. https://scholar.sun.ac.za/handle/10019.1/108461
20. Hermann, K.; Weaver, L. The shikimate pathway. *Annual Review of Plant Physiology and Plant Molecular Biology* 1999, *50* (1), 473-503
21. Joseph, B.; Mertins, S.; Stoll, R.; Schär, J.; Umesha, K.; Luo, Q.; Müller-Altrock, S.; Goebel, W. Glycerol metabolism and Prfa activity in *Listeria monocytogenes*. *Journal of Bacteriology* 2008, *190* (15), 5412-5430.